LOCKHEED MARTIN ENERGY RESEARCH LIBRARIES

3 4456 0515436 5

ORNL-4820

cy 2

CENTRAL RESEARCH LIBRARY

METALS and CERAMICS DIVISION

Annual Progress Report

Period Ending June 30, 1972

OAK RIDGE NATIONAL LABORATORY
CENTRAL RESEARCH LIBRARY
DOCUMENT COLLECTION

LIBRARY LOAN COPY

DO NOT TRANSFER TO ANOTHER PERSON
If you wish someone else to see this document, send in name with document and the library will arrange a loan.

UCN-7969
(3 3-67)

OAK RIDGE NATIONAL LABORATORY

OPERATED BY UNION CARBIDE CORPORATION • FOR THE U.S. ATOMIC ENERGY COMMISSION

Printed in the United States of America. Available from
National Technical Information Service
U.S. Department of Commerce
5285 Port Royal Road, Springfield, Virginia 22151
Price: Printed Copy $3.00; Microfiche $0.95

This report was prepared as an account of work sponsored by the United States Government. Neither the United States nor the United States Atomic Energy Commission, nor any of their employees, nor any of their contractors, subcontractors, or their employees, makes any warranty, express or implied, or assumes any legal liability or responsibility for the accuracy, completeness or usefulness of any information, apparatus, product or process disclosed, or represents that its use would not infringe privately owned rights.

ORNL-4820
UC-25 – Metals, Ceramics, and Materials

Contract No. W-7405-eng-26

METALS AND CERAMICS DIVISION ANNUAL PROGRESS REPORT

for Period Ending June 30, 1972

J. H Frye, Jr., Director
J. E. Cunningham, Associate Director

Section Heads

G. M. Adamson, Jr.
W. O. Harms
C. J. McHargue
P. Patriarca
J. R. Weir, Jr.

Compiled and Edited by Sigfred Peterson

SEPTEMBER 1972

OAK RIDGE NATIONAL LABORATORY
Oak Ridge, Tennessee 37830
operated by
UNION CARBIDE CORPORATION
for the
U.S. ATOMIC ENERGY COMMISSION

LOCKHEED MARTIN ENERGY RESEARCH LIBRARIES

3 4456 0515436 5

Reports previously issued in this series are as follows:

ORNL-28	Period Ending March 1, 1948
ORNL-69	Period Ending May 31, 1948
ORNL-407	Period Ending July 31, 1949
ORNL-511	Period Ending October 31, 1949
ORNL-583	Period Ending January 31, 1950
ORNL-754	Period Ending April 30, 1950
ORNL-827	Period Ending July 31, 1950
ORNL-910	Period Ending October 31, 1950
ORNL-987	Period Ending January 31, 1951
ORNL-1033	Period Ending April 30, 1951
ORNL-1108	Period Ending July 31, 1951
ORNL-1161	Period Ending October 31, 1951
ORNL-1267	Period Ending January 31, 1952
ORNL-1302	Period Ending April 30, 1952
ORNL-1366	Period Ending July 31, 1952
ORNL-1437	Period Ending October 31, 1952
ORNL-1503	Period Ending January 31, 1953
ORNL-1551	Period Ending April 10, 1953
ORNL-1625	Period Ending October 10, 1953
ORNL-1727	Period Ending April 10, 1954
ORNL-1875	Period Ending October 10, 1954
ORNL-1911	Period Ending April 10, 1955
ORNL-1988	Period Ending October 10, 1955
ORNL-2080	Period Ending April 10, 1956
ORNL-2217	Period Ending October 10, 1956
ORNL-2422	Period Ending October 10, 1957
ORNL-2632	Period Ending October 10, 1958
ORNL-2839	Period Ending September 1, 1959
ORNL-2988	Period Ending July 1, 1960
ORNL-3160	Period Ending May 31, 1961
ORNL-3313	Period Ending May 31, 1962
ORNL-3470	Period Ending May 31, 1963
ORNL-3670	Period Ending June 30, 1964
ORNL-3870	Period Ending June 30, 1965
ORNL-3970	Period Ending June 30, 1966
ORNL-4170	Period Ending June 30, 1967
ORNL-4370	Period Ending June 30, 1968
ORNL-4470	Period Ending June 30, 1969
ORNL-4570	Period Ending June 30, 1970
ORNL-4770	Period Ending June 30, 1971

Contents

SUMMARY xiii

PART I. FUNDAMENTAL PROGRAMS

1. CRYSTAL PHYSICS 1

Internal Centrifugal Zone Growth 1
Ternary Composites Through Directional Solidification 1
M-MO_x Binary and Ternary Eutectics 1
UO_2 Crystals 2

High-Temperature Solution Growth of Single Crystals 2
Single-Crystal Growth of CeO_2 Doped with ^{237}Np, ^{239}Pu, ^{243}Am, and ^{244}Cm 2
Melt Growth of $RbCaF_3$ and of $RbCaF_3$ Doped with ^{244}Cm 2
Crystal Growth of MgO from $Li_2O \cdot Na_2O \cdot 2B_2O_3$ 2
Single-Crystal Growth of $ThSiO_4$ Doped with Terbium 2
Epitaxial Growth of $LiLnMo_2O_8$ on Single Crystals of Ln_2GeMoO_8 3
Zero-Field Splittings of Cm^{3+} and Am^{2+} in Fluorite-Type Crystals 3
Formation and Stability of the Scheelite and Zircon Modifications of $ThGeO_4$ 3
Single-Crystal Growth and Several Optical Properties of $CaWO_4$ Doped with $^{243}Am^{3+}$ 3
EPR Investigations of Er^{3+}, YB^{3+}, and Gd^{3+} in Zircon-Structure Silicates 3
High-Temperature Solution Growth of Single-Crystal Plutonium Dioxide 4

Hydrothermal Studies 4
Growth and Crystal Morphology of Lead Sulfide in the Hydrothermal System PbS-RbOH-H_2O 4
Crystal Structure of a Rubidium Iron Feldspar 4

2. DEFORMATION OF CRYSTALLINE SOLIDS 5

Elastic Interaction of Prismatic Dislocation Loops with Point Defects Under Applied Stress 5

Elastic Interaction of a Point Defect with a Prismatic Dislocation Loop in Hexagonal Crystals 5

Displacement Fields of Straight Dislocations in Anisotropic Crystals 5

The Application of Atomic Potentials to the Heat of Mixing, the Lattice Parameter, and the Compressibility of Random Cubic Solutions 6

The Structure of Cu–16 at. % Al 6

Fracture Mechanism in Precipitation-Hardened Alloys 6

Precipitation Kinetics in Niobium-Hafnium Alloys 7

3. DIFFUSION IN SOLIDS 8

Tracer Self-Diffusion in Fe–17 wt % Cr–12 wt % Ni 8

Sectioning of Diffusion Specimens by Radio-Frequency Sputtering 8

Thermotransport of Cadmium and Thallium in Sodium and Potassium Chlorides 9

Diffusion of Hafnium in Ta–8 wt % W–2 wt % Hf and Ta–9.5 wt % W–2.5 wt % Hf–0.01 wt % C 9
Cation Self-Diffusion in Titanium Monoxide 9
Diffusion Under High Pressures 10

4. ELECTRON MICROSCOPY 11
Void Formation in Neutron-Irradiated Metals 11
Annealing of Voids in Aluminum 11
Effect of Structural Imperfections on Voids in Aluminum 11
The Role of Electron Microscopy in the Understanding of Neutron Irradiation-Produced Swelling 12
Electron Displacement Damage in Graphite and Aluminum 12
On the Question of Void Formation in Neutron-Irradiated Zirconium 12
High-Fluence Neutron Irradiation Damage in Cu–10 wt % Al and Copper 13
Structural Damage and Its Annealing Response in Neutron-Irradiated Magnesium 13
Radiation Damage and the Effects of Postirradiation Annealing in 1100 Aluminum 13
Swelling in Aluminum and Its Alloys 14
Transmutation-Produced Mg_2Si Precipitation in an Irradiated Al–2.5% Mg Alloy 14
Neutron Irradiation Damage in a Precipitation-Hardened Aluminum Alloy 14
Radiation-Induced Strengthening and Embrittlement in Aluminum 15
Electron Radiation Damage Near the Threshold Energy in Aluminum 15
Defects in Fast-Neutron-Irradiated Boron Carbide 15
Nucleation of Dislocation Loops in Solids Under Irradiation 15
Nucleation of Voids in Solids Containing Excess Vacancies, Interstitials, and Helium Atoms 16
Vacancies in Solid Solutions 16
Water Damage in Composites of Glass Fiber and Polyester Resin 16
Determination of the Energy Stored in Cold Worked Metals by Calorimetry 16
Work Hardening Theories Analyzed in Terms of Stored Energy Data 17
Techniques for Transmission Electron Microscopy of Micron-Size Particles of Ceramic Materials 17
Phase Analysis Studies of Reactor Materials 17
A General Program for Constructing Maps of Kikuchi and Kossel Lines 18

5. FUNDAMENTAL CERAMICS RESEARCH 19
Further Comments on the Deformation of Hyperstoichiometric Uranium Dioxide 19
Electron Microscopy of Polycrystalline Uranium Dioxide 19
Deformation of UO_2 Single Crystals 20
Boron Carbide Studies 20
Stoichiometry Changes in Molten Uranium Dioxide 20
High-Temperature Spectrometer 20
Absorption Spectrum of $Ca(AlCl_4)_2$:Ti(II) 21
Electronic Absorption Spectra of Platinum(II) Centers in Liquid Alkali Metal Chlorides 21
Raman Spectra of the Molten $AlCl_3$-$ZnCl_2$ System and Molten Cs_2ZnCl_4 21

6. FUNDAMENTAL PHYSICAL METALLURGY 22
The Diffusion of Point Defects Near a Prismatic Dislocation Loop 22
The Use of Computer Simulation to Index Complex Auger Electron Spectra 22
The Rolling Texture of Cu_3Au 22
The Behavior of Grain Boundaries During Recrystallization of Dilute Aluminum-Gold Alloys 23
The BCC (γ)-to-Tetragonal (γ°) Phase Transformation in Uranium-Niobium-Zirconium Alloys 24

7. PHYSICAL PROPERTY RESEARCH 25
Apparatus Development 25
Linear Heat Flow Apparatus 25
Radial Heat Flow Apparatus 25
Computerized Data Acquisition 26
Coefficient of Thermal Expansion Apparatus 26
Heat Transport in Metals 26
Tungsten 26
Transport Properties of Lead and Platinum 26
Heat Conduction in Alkali Halides 27
Related Topics 27
Physical Properties Conversions to IPTS-68 27
Powders Modeling 27
Electrical Resistivity Analysis with HEATING 3 27

8. SUPERCONDUCTING MATERIALS 28
Precipitates and Fluxoid Pinning in a Superconducting Nb-Hf Alloy 28
The Effects of Some *3d* and *4d* Solutes on the Superconductivity of Technetium 28
Critical Surface and Bulk Current Densities in the Mixed State of Type II Superconductors 29
Effects of Interstitial Oxygen on the Superconductivity of Niobium 29
Critical Current Densities in Sputter-Deposited Compounds with the A-15 Crystal Structure 29

9. SURFACE PHENOMENA 30
Oxidation of Uranium-Base Alloys 30
High-Temperature Oxidation of Uranium Alloys 30
The Mechanical Properties of Scales and Their Influence on High-Temperature Gas-Metal Reactions 30
Refractory Metal Oxidation 31
The Ignition of Tantalum-Base Alloys During Gaseous Oxidation 31
Impurity Distributions in Anoidic Films on Tantalum 31
Diffusion of Oxygen in Refractory Metals 31

10. THEORETICAL RESEARCH 32
Comments on the Coherent Potential Approximation for Dilute Alloys 32
Pressure-Induced Superconductivity in Cesium 32
Electronic Densities of States of Ag-Pd Alloys 32
First-Principles Calculation of the Optical Absorption in Diamond 33
A Combined Green's Function-Discrete Variational Method for Calculating the Electronic Structure of Crystal Compounds 33

11. X-RAY DIFFRACTION 34
Routine Analysis 34
Local Structural Order in BCC Alloys 34
The Short-Range Structure of Titanium and Zirconium BCC Solid Solutions 34
The Decomposition of Uranium-Base BCC Alloys 34
Local Atomic Arrangements in Ta-Mo and Ta-Nb BCC Alloys 35
Rapid Recording of Powder Diffraction Patterns with Si(Li) X-Ray Energy Analysis System: W and Cu Targets and Error Analysis 35
Crystal Structures of Unirradiated and Neutron-Irradiated Boron Carbides 36
X-Ray Fluorescence for Analysis of Trace Elements 36
A Unified Theory of Absolute Intensity Measurements in Small-Angle X-Ray Scattering 37
The Role of Soller Slits in Small-Angle Scattering Collimation Systems 37

PART II. FAST REACTOR TECHNOLOGY

12. ADVANCED FAST BREEDER REACTOR FUEL DEVELOPMENT 38
Irradiation Testing 38
Thermal Flux Tests 38
Fast Flux Tests 38
Fabrication of (U,Pu)N Fuel 39

13. COMPATIBILITY OF STEAM GENERATOR MATERIALS 40
Examination of Alco/BLH Steam Generator 40
Corrosion of Advanced Steam Generator Alloys 42
General Corrosion 42
Stress Corrosion 42

14. DEVLOPMENT OF FBR NEUTRON-ABSORBED MATERIALS 47
Irradiation Behavior of Boron Carbide 47
Microstructure of Boron Carbide after Fast-Neutron Irradiation 47
Evaluation of Fast-Reactor-Irradiated Boron Carbide Powders 49
Evaluation of Boron Carbide Pellets from EBR-II Higher Worth Control Rod 49
Evaluation of Boron Carbide Pellets from ORNL EBR-II Experiment X-099 49
Performance Modeling of Neutron Absorbers 50
Development of Vents 51
The Effect of Temperature on the Microstructure of Neutron-Irradiated Tantalum 52
Alternate Absorber Materials 53
Reactor Experiment Design and Fabrication 53

15. DEVELOPMENT OF FBR OXIDE FUELS 55
Development of Fabrication Processes 55
Irradiation Behavior 56
Fast Flux Irradiation Tests 56
Uninstrumented Thermal Flux Irradiations 56
ETR Instrumented Tests 58
Fuel-Cladding Mechanical Interaction Tests 58
Cladding Chemical Reactions 58

Analysis of Fuel Element Performance 61
Performance Model Development 61
Porosity, Actinide, and Oxygen Redistribution in Irradiated $(U,Pu)O_2$ 65
Analysis of ORR Instrumented Thermal Performance Tests 66
CASDAR: A Nuclear Data Manipulation Program 67

Chemical Modeling of Fuel-Cladding Attack in LMFBR Oxide Pins 68
Analysis of Intergranular Attack Data 68
Elimination of CO_2 and H_2O as Oxygen Transport Species in Mixed Oxide Fuel Pins 69

16. FABRICATION DEVELOPMENT OF FAST BREEDER REACTOR CLADDING 70

Biaxial Creep-Rupture of Stainless Steel Tubing with Electro-Discharge Machined Notches 70

Effects of Sharp Artificial Notches on Thin-Wall Type 316 Stainless Steel Tubing 71

17. JOINING OF STRUCTURAL MATERIALS 73

Stainless Steels 73
Heavy Section Weldment Evaluation 73
Properties of Stainless Steel Welds with Controlled Residual Elements 74
Filler Metal Development for Pipe Welding 74

Nickel-Rich Alloys 75
Inconel 718 75
Incoloy 800 75

Ferritic Steels 76
Stabilized Grades 76
Low-Carbon Grades 76
Tube-to-Tube-Sheet Welding Studies 77

18. MECHANICAL PROPERTIES OF ALLOYS IN REACTOR ENVIRONMENTS 79

Swelling of Austenitic Stainless Steel 79
Annealed Type 304 Stainless Steel 79
Annealed Type 316 Stainless Steel 80
Cold-Worked Type 316 Stainless Steel 80
Titanium-Modified Type 316 Stainless Steel 81

Mechanical Properties of Austenitic Stainless Steels 82
Type 316 Stainless Steel 82
Titanium-Modified Type 316 Stainless Steel 85

19. MECHANICAL PROPERTIES OF STRUCTURAL ALLOYS 86

Exploratory Tests on Type 304 Stainless Steel in Support of the High-Temperature Structural Design Methods for LMFBR Components Program 86

Heat-to-Heat Variations in the Mechanical Properties of Type 304 Stainless Steel 87

Mechanical Properties of Structural Materials for Steam Generators 88
Weldments 88
Base Metal 88

20. NONDESTRUCTIVE TEST DEVELOPMENT 91

Nondestructive Test Development for Steam Generators 91
Radiography 91
Liquid Penetrants 91
Eddy Currents 92
Ultrasonics 92

Electromagnetic Inspection Methods 93
Ultrasonic Inspection Methods 93
Frequency Analysis 93
Ultrasonic Imaging 94
Penetrating Radiation Inspection Methods 95

PART III. SPACE POWER TECHNOLOGY

21. CLADDING MATERIALS FOR SPACE ISOTOPIC HEAT SOURCES 96
New Platinum-Rhodium-Tungsten Alloys for Space Isotopic Heat Sources 96
Characterization of Pt-Rh-W Alloys 97
Characterization of Iridium 97

22. DEVELOPMENT OF URANIUM NITRIDE FUELS FOR NASA 98
Irradiation Testing of Uranium Nitride 98
UN Fabrication Studies 99

23. PHYSICAL METALLURGY OF REFRACTORY METALS 100
Embrittlement of T-111 Pioneer Fuel Capsules 100
Evaluation of Pioneer Test Capsules 100
Mechanical Properties and Structure of Internally Oxidized Ta–8% W–2% Hf (T-111) Alloy 101

24. TUNGSTEN METALLURGY 102
Fabrication of Experimental Tungsten Materials 102
The High-Temperature Creep Properties of Chemically Vapor Deposited Tungsten 102
Low-Stress Creep Testing of Tungsten 103
Creep Properties of W–3.8% ThO_2 103
Effect of Carburization on the Creep Properties of Tungsten Alloys 103
Radiation Damage to Refractory Metals as Related to Thermionic Applications 105
High-Temperature Fast-Neutron Irradiation of Tungsten Alloys 105

PART IV. REACTOR DEVELOPMENT SUPPORT

25. GAS-COOLED REACTOR PROGRAM 106
Coated Particles from Ion Exchange Resins 106
Resin Selection 106
Fuel Loading 107
Carbonization and Heat Treatment 107
Particle Design and Modeling 107
Analysis of Chemical Failure of Urania Fuel Particles in the HTGR 107
Fuel Element Fabrication Studies for HTGR Fuels 108
Carbonization 108
Warm Molding 108
Extrusion 108
Thermal Conductivity of Bonded HTGR Fuel Materials 109

HFIR Irradiation Testing of HTGR Fuels and Fuel Elements 110
Irradiation Performance of HTGR Fuel Sticks Bonded with Reference and Advanced Matrix Materials 110
Irradiation-Induced Dimensional Changes in Intrusion-Bonded Fuel Sticks 110
Performance of Coated Particles in HFIR Experiments 111
Gas-Cooled Fast Breeder Reactor Fuel Element Development 111
Thermal Reactor Experiments 112
Fast Reactor Experiments 112

26. HEAVY SECTION STEEL TECHNOLOGY 113
Characterization of Heavy Section Steel Plates 113
Hydrogen Technique for Generating Sharp Cracks in Low-Alloy High-Strength Steels 113
Static and Dynamic Fracture Toughness Tests on Precracked Charpy Specimens 114

27. MILITARY REACTOR FUEL ELEMENT PROCUREMENT ASSISTANCE 116

28. MOLTEN-SALT REACTOR PROGRAM 117
Intergranular Cracking of Structural Materials Exposed to Fuel Salt 117
Examination of Hastelloy N from the MSRE 117
Intergranular Corrosion of Hastelloy N 118
Intergranular Cracking of Materials Exposed to Several Fission Products and Sulfur 118
Effect of Tellurium on the Mechanical Properties of Several Alloys 119
Mechanical Properties of Hastelloy N Modified with Several Elements 119
Identification of Interaction Products of Tellurium with Structural Materials 119
Intergranular Cracking Studies 120
Further Studies of Hastelloy N 120
Development of a Titanium Modified Hastelloy N 121
Electron Microscope Studies 121
Fluoride Salt Corrosion 122
Corrosion of Hastelloy N in Steam 123
Graphite Studies 124
Reduction of Helium Permeability of Graphite by Pyrolytic Carbon Sealing 124
Characterization of Pyrolytic Carbon Sealants for Graphite 124
Helium Permeability Measurements on Various Grades of Graphite 125
Procurement of New Grades of Graphite 125
X-Ray Studies 125
Thermal Conductivity of Graphite 126
Irradiation of Graphite 126
Chemical Processing Materials 127
Construction of a Molybdenum Reductive-Extraction Test Stand 127
Fabrication Development of Molybdenum Components 127
Molybdenum Welding Development 128
Development of Techniques for Brazing Molybdenum 128
Corrosion of Structural Materials in Bismuth 129

29. THORIUM UTILIZATION 130
Thorium-Uranium Recycle Facility 130

Refabrication Development 131
Coating 131
Stick Fabrication 133

Refabrication Equipment Design 136

Commercial Recycle Plant Studies 137
Process Evaluation 137
Commercial Recycle Plant Conceptual Design 137

HTGR Recycle Fuels Irradiation 138
Large-Scale Irradiations 138
Capsule Irradiation Tests 139

PART V. THERMONUCLEAR AND TRANSURANIUM RESEARCH

30. CONTROLLED THERMONUCLEAR REACTOR PROGRAM 140

Neutron Radiation Damage 140
The Effect of Alloying and Purity on the Formation and Ordering of Voids in BCC Metals 141
Radiation Damage in Thermonuclear Reactor Primary Structures 140

Heavy-Ion Simulation of Radiation Damage 141
Preparations for Heavy-Ion Bombardments 141
The Temperature Dependence of Swelling in Pure Metals 141

Chemical Compatibility of Potential Blanket and First Wall Materials 141

31. TRANSURANIUM PROGRAM 142

Target Fabrication 142

HFIR Target Performance 143

Neutron Source Fabrication 143

Special Projects 143
Special Target 144
HFIR Rabbit 144
Special Source Fabrication 144

SRL Shipments 144

Development of Techniques for Nondestructive Determination of Thermal Conductivity of Target Pellets 144
Thermal Conductivity and DC Electrical Resistivity Calibration Experiment 145
Nondestructive Testing for Thermal Conductivity 145

PART VI. OTHER PROGRAM ACTIVITIES

32. ALUMINUM FUEL ELEMENT DEVELOPMENT 146

Irradiation Damage of UAl_x and U_3O_8 Fuel Dispersions 146

HFIR Fuel Element Production Assistance 146

Postirradiation Examination of HFIR Fuel Elements 100-I and 100-O 147

Materials Performance in HFIR Control Cylinders 147

Effect of Irradiation on Creep-Rupture of 5052 Aluminum Alloy at 50°C 148

33. FLAWS IN WELDS STUDIED BY AUTORADIOGRAPHY 149

34. FABRICATION OF PLUTONIUM TEST ELEMENT 151
Kernel Preparation 151
Coating 151
Fuel Stick Fabrication 152

35. DEVELOPMENT FOR THE LIGHT WATER BREEDER REACTOR 154
Conversion of Uranium Nitrate to Ceramic-Grade Oxide for the Light Water Breeder Reactor: Process Development 154
Fabrication of ThO_2-$^{233}UO_2$ Pellets 154
Fabrication of High-Purity $^{233}UO_2$ Pellets 155

36. GRAPHITE FABRICATION STUDIES FOR THE NAVAL ORDANCE LABORATORY 156

37. METALLOGRAPHY 157
Scanning Electron Microscopy 157
Microprobe Analysis 159
Epitaxial Ferromagnetic Etching 163
Examination of Failed Prosthetic Appliances 165
Metallographic Examination of the Alco/BLH Steam Generator 167
Alpha Autoradiography 167
Beta Autoradiography 168
Alpha Metallography Facility 170
Color Television Program 172

38. NASA T-111 Loop Studies 172

39. NERVA PROGRAM METALLURGICAL SUPPORT 175
The Gaseous Environment Inside a NERVA Reactor in Space 175
Friction of Graphite in Vacuum and Hydrogen 176

PRESENTATIONS AT TECHNICAL MEETINGS 178

PUBLICATIONS 186
Patents 197
Theses 197

AUTHOR INDEX 198

ORGANIZATION CHART 201

Summary

PART I. FUNDAMENTAL PROGRAMS

1. Crystal Physics

We report evidence of coupled growth in a ternary eutectic of metal oxides and a metal; steady-state morphology was observed for the three phases UO_2, MgO, and W. To obtain data for M-MO_x binary and ternary eutectics more completely, we have added the Bridgman technique using tungsten (or other refractory metal) crucibles heated by an electron beam. High-temperature solution growth, Bridgman, and Czochralski techniques were used to grow several different kinds of compound crystals, both undoped and doped with rare earths, actinides, and transuranic isotopes. Evidence is presented for oriented overgrowth of thin single-crystal layers of $LiLnMo_2O_8$ on large substrate crystals of Ln_2GeMoO_8. The system PbS-RbOH-H_2O has been investigated hydrothermally to determine the best conditions for cubic lead sulfide (galena) in steel vessels. The crystal structure of a rubidium iron feldspar, $RbFeSi_3O_8$, was determined.

2. Deformation of Crystalline Solids

Current work includes results on the displacements around dislocations and interaction of point defects and dislocation loops, including the effect of applied stress. The application of interatomic potentials was shown to lead to a very interesting concept of atom size in alloying. The effect of precipitate structure in niobium-hafnium alloys on the fracture properties and the superconductivity was studied.

3. Diffusion in Solids

Volume and grain boundary self-diffusion coefficients were determined for Fe–17 wt % Cr–12 wt % Ni over the range 600 to 1300°C. The use of an improved sectioning technique permitted the study of volume diffusion in this system in the low temperature range of practical applications. A radiofrequency sputtering technique was improved for the removal of very thin serial sections from diffusion specimens, allowing diffusion coefficients as low as 7×10^{-18} cm^2/sec to be measured. This technique will allow the annealing time of diffusion experiments to be greatly reduced from those necessary when coarser sectioning techniques are employed. Thermal diffusion of monovalent and divalent tracer impurities in sodium and potassium chlorides is being investigated in an effort to better understand the heat of transport in ionic systems. The ultimate aim of the study is a knowledge of thermotransport phenomena in ceramic materials under reactor conditions. The volume and short-curcuit diffusion of ^{181}Hf in Ta–8 wt % W–2 wt % Hf alloy is being studied. The investigation of ^{44}Ti diffusion in titanium monoxide (TiO_x) spanned the ranges of 1250 to 1555°C and x = 0.8 to 1.26. Results are examined in terms of published cation and anion vacancy concentrations. Research on atomic diffusion in refractory metals and alloys at high temperatures and pressures is being initiated.

4. Electron Microscopy

The formation of voids and an associated dislocation structure during elevated-temperature neutron irradiation in several high-purity metals and alloys are described, and the effects of postirradiation annealing on these defects are presented. The damage is extremely sensitive to microstructure and composition, and annealing behavior is complicated by the presence of the damage structure and transmutation products. The mechanical properties of commercially pure aluminum and the precipitation-hardened 6061 alloy are rationalized in terms of the irradiation-induced defect structure. Transmutation-produced silicon and the dislocation structure are shown to be the principal sources of the radiation hardening. The damage structure in boron carbide, which has a high cross section for the production of helium, also contains cavities, but unlike the voids found in irradiated metals these contain gas at a pressure higher than equilibrium. Theoretical descriptions are given for the nucleation of dislocation

loops during neutron irradiation and for the nucleation of voids in solids containing an excess of vacancies, interstitials, and helium atoms. An account is presented of the formation of cracks in fiber-reinforced resins by exposure to water. The single-step calorimetric procedure for the determination of the energy stored in metal crystals by plastic deformation is reviewed, and results are analyzed in terms of work hardening theories. Techniques are summarized for the preparation of specimens for transmission electron microscopy from ceramic particles 1 to 1000 μm in diameter and for analyzing precipitate structures in complex alloys. A computer program is described that allows construction of maps of Kikuchi and Kossel lines.

5. Fundamental Ceramics Research

Spectroscopic studies are reported for nickel-doped MgO crystals at high temperatures, titanium-doped $Ca(AlCl_4)_2$ crystals at low temperatures, and platinum(II) centers in liquid alkali metal chlorides. Redox equilibria of molten $UO_{2\pm x}$ were studied. Research was done on the significance of impurities in boron carbides. The system $AlCl_3$-$ZnCl_2$ was studied by Raman spectroscopy. Measurements of deformation parameters in single-crystal uranium dioxide indicate an interesting variation in behavior at 1000°C. Transmission electron micrographs of deformed polycrystalline uranium dioxide correlated with deformation characteristics.

6. Fundamental Physical Metallurgy

The nature of the diffusion of point defects near a prismatic dislocation loop was found, and the knowledge will be applied to radiation-induced void growth models. Computer simulation of Auger electron spectra aided in the interpretation of the complex experimental spectrum of powder-metallurgy tungsten. A stacking fault energy-texture reversal was observed in a rolled Cu_3Au order-disorder alloy. A grain boundary structure transformation was detected for migrating grain boundaries in a dilute aluminum-gold alloy. The bcc-to-tetragonal phase transformation in uranium alloys is being studied by x-ray diffraction.

7. Physical Property Research

Critical analyses of linear and radial heat flow techniques verified equipment modifications to obtain more accurate data. A computerized data acquisition system was used to measure several physical properties. A thermal expansion apparatus was tested. Electrical resistivity measurements on tungsten to 2600°K were analyzed. The lattice thermal resistivities of RbBr, RbCl, and RbI changed slope at the Debye temperatures.

8. Superconducting Materials

The relationship between superconducting fluxoid pinning and precipitate dispersion was investigated in Nb–38 at. % Hf. The critical current density showed a peak as a function of magnetic field, and a one-to-one correspondence was found between calculated fluxoid spacings at the field of the peak and average precipitate spacings obtained from electron microscopy. The effect on critical temperature of the addition of small amounts of Cr, Fe, Co, Ni, and Ru to technetium was studied. Our ac method for measuring critical current densities in bulk specimens was modified to allow the simultaneous measurement of critical surface current densities and to improve our measurement of the bulk critical current density. The effects of varying amounts of interstitial oxygen on the superconductivity of niobium was studied with measurements of critical temperature, low-temperature specific heat, and magnetization. A program to study critical current densities in sputter-deposited Nb-Al and Nb-Al-Ge with the A-15 crystal structure was started.

9. Surface Phenomena

We have continued studies of the oxidation of uranium alloys containing Nb, Zr, and Mo. The oxidation of these alloys is dominated by the very large stresses that develop in the oxide scale. Special attention was given to the role of the mechanical properties of both oxide scales and parent metals in the oxidation process, and the plasticity of the oxides and the creep rates of the alloys were measured. Vacancy diffusion as a stress-relief mechanism was investigated.

The influence of alloying elements such as tungsten and hafnium on the oxidation of tantalum was investigated. The extreme embrittlement of the alloys during oxidation and the stresses that lead to their eventual disintegration were characterized. A new simple, sensitive, and rapid method for determining the rate of oxygen diffusion in tantalum-base alloys was developed and tested successfully on tantalum; the method will be useful in our future studies of oxidizing systems in which oxygen solution effects play an important role.

10. Theoretical Research

We have continued to develop the coherent potential approximation (CPA) for calculating the one-electron states of disordered solids. We used it to calculate the electronic states of random substitutive Pd-Ag alloys across the whole range of concentration. This not only indicates the usefulness of the technique but also explains the origin of many of the physical properties of this and related alloy systems.

We have continued to develop the Korringa-Kohn-Rostoker (KKR) method for calculating the band structure of ordered solids and have coupled it with the discrete variational method (DVM) under investigation. This yields a very powerful tool for studying the one-electron states of ordered compounds.

The KKR method was used in connection with a new technique for calculating the electron-phonon interaction to study the superconductivity induced in cesium under pressure. The DVM method was used to calculate the optical absorption in diamond.

11. X-Ray Diffraction

We report results of theoretical and experimental studies of local structures in bcc alloys subject to displacive instabilities or to short-range chemical order. An energy-sensitive Si(Li) detector has been incorporated into a system to permit rapid recording of powder diffraction data. The errors and incident wavelength effects to be expected in such a system are described. X-ray diffraction effects from boron carbide crystals irradiated from 3 to 96% burnup at 54°C in HFIR are reported and compared with data obtained from ORR-irradiated crystals. We successfully incorporated pyrolytic graphite monochromators in an x-ray fluorescence analysis system designed to extend detectable limits to the range of parts per billion. Our studies of theoretical factors governing the conversion of relative intensities to an absolute scale in small-angle x-ray scattering measurements have been extended, and we have evaluated the effects of using Soller slits in these experiments.

PART II. FAST REACTOR TECHNOLOGY

12. Advanced Fast Breeder Reactor Fuel Development

Two capsules were placed in the ETR to determine the irradiation behavior of (U,Pu)N fuel. One was removed after a burnup of 5% FIMA at 30 kW/ft linear heat rating and is being examined at Los Alamos Scientific Laboratory (LASL). Radiography showed pellet cracking, but the fuel pins were dimensionally stable, and gamma scanning indicated a normal distribution of fission products.

We completed the fabrication of seven fuel pins, also containing (U,Pu)N pellets, for irradiation in EBR-II. Some difficulty was encountered in sodium bonding the pellets using ultrasonic vibration, which had previously proven satisfactory for UN pellets. The pins were shipped first to Battelle Columbus Laboratory, where a satisfactory bond was obtained by centrifugation, and then to LASL, who is now responsible for this program.

Work on the fabrication and characterization of mixed nitride fuel for the LMFBR was stopped at the end of FY 1972. We completed a report on the characterization of (U,Pu)N fuels to be irradiated in EBR-II and returned the residual materials from the nitride fuel development to AEC recovery centers.

13. Compatibility of Steam Generator Materials

Examination of the Alco/BLH steam generator after its failure at the Liquid Metal Engineering Center has revealed (1) fabrication difficulties associated with some tube-to-tube-sheet fillet welds, (2) lower tube sheet stress-corrosion cracks associated primarily with type 316 stainless steel sections and having at least three alternative explanations, (3) upper tube sheet stress-corrosion cracking caused by caustic formed in water-sodium reactions, (4) heavy corrosion of shell-side tube surfaces in the sodium vapor–argon gas space immediately below the top tube sheet, and (5) no evidence of significant general or stress-assisted corrosion for surfaces exposed exclusively to sodium. Our program to examine general and stress-assisted corrosion phenomena under steam environments at an operating power plant has continued with emphasis on chloride stress-corrosion cracking for wide ranges of temperatures, materials, and oxygen impurity contents.

14. Development of FBR Neutron-Absorber Materials

Boron carbide powders and pellets irradiated in the fast flux of the EBR-II were examined. Transmission electron microscopy revealed crystallographically oriented cavities with high strain fields. These are assumed to be helium-filled bubbles generated by the $^{10}B(n,\alpha)^{7}Li$ reaction. After irradiation above about 500°C, a denuded zone free of bubbles was observed adjacent to grain boundaries. However, at these tem-

peratures bubbles are concentrated in grain boundaries, on dislocations, and on stacking faults. Upon irradiation at about 750°C or upon postirradiation annealing at higher temperatures these bubbles coalesced, causing grain separations, reflected in pellet cracking and fragmentation. Lattice contractions and expansions were observed coincident with bubble formation. Upon postirradiation annealing the lattice parameters returned to their preirradiation values as the strain fields associated with the helium bubbles were relieved. Scanning electron microscopy of surfaces fractured after annealing reveals particles, which may be a result of lithium precipitation during the anneal.

Stainless steel and molybdenum disks were fabricated with controlled porosity by powder metallurgy for potential use as vents in boron-containing control rods. Methods were developed for joining these disks to stainless steel housings.

Tantalum irradiated in the EBR-II in the range 425 to 1050°C showed voids by transmission electron microscopy. Peak swelling of 2.4% was observed at 585°C with a void concentration of 1.9×10^{17} voids/cm^3.

Methods of fabricating tantalum borides, which are attractive because of their high reactivity worth, were developed. These materials have been characterized in preparation for testing in the EBR-II.

A materials variables irradiation testing program encompassing boron carbide, tantalum and its alloys, and tantalum borides is under way. This program consists of 21 capsules in three EBR-II subassemblies. One subassembly (X-099A) is presently at the EBR-II, and the others are scheduled for insertion in September and November.

15. Development of FBR Oxide Fuels

The oxide fuels development program was a five-year program to advance the technology of $(U,Pu)O_2$ as a fast breeder reactor fuel. The objectives were to establish the performance characteristics and limitations of $(U,Pu)O_2$ fuels fabricated by different processes, to obtain a fundamental understanding of the mechanisms involved in the irradiation behavior of fuel elements incorporating these fuels, to develop economical techniques to fabricate a product with optimized performance, and to develop analytical models sufficiently accurate to optimize experimental design and predict fuel element response to fast reactor conditions.

Previously developed processes for loading fuel pins by the Sphere-Pac process or making pellets from sol-gel precursor material and for adjusting fuel composition to meet specifications were used to prepare fuel and load fuel pins for irradiation tests. The ability to Sphere-Pac fuels to controlled densities of 81 to 84% of theoretical was demonstrated. The ability to fabricate pellets from sol-gel material was demonstrated, and techniques were developed for control of the various specified parameters, including density and stoichiometry.

The irradiation program has had as its objective the determination of in-reactor properties and performance of $(U,Pu)O_2$ fuel pins as functions of fabrication form, porosity distribution, stoichiometry, and irradiation condition. The program has included both fast and thermal flux irradiations and steady-state, cyclic, and transient power conditions.

The principal results were that Sphere-Pac fuels perform as well as pellet fuels, they exhibit better compatibility with cladding, and they have better fuel-cladding thermal conductance. In our fast flux tests in EBR-II, two Sphere-Pac $(U,Pu)O_2$ fuel pins were examined after achieving a peak burnup of 6% FIMA and had performed very satisfactorily. Three similar pins have continued irradiation in EBR-II and are now at a peak calculated burnup level of 8.1% FIMA. A 37-pin subassembly for EBR-II, consisting of 19 pins from ORNL and 18 from the Babcock and Wilcox Company, was irradiated to a peak burnup level of approximately 3.8% FIMA. It contains Sphere-Pac and pellet fuels derived from the sol-gel process and pellets and Vi-Pac shards processed from coprecipitated powders. One fuel pin containing $(U,Pu)O_2$ Sphere-Pac fuel was irradiated to 11.3% FIMA without any abnormal effect, but the peak cladding temperature was low (<400°C). The irradiation of two ETR instrumented capsules was completed with a calculated burnup of approximately 8% FIMA maximum.

A highly instrumented capsule was irradiated in the ORR to measure in-reactor axial extension of the fuel column and cladding and the internal gas pressure developed during operation under prototypic LMFBR power and temperature conditions. Almost daily power cycles simulated load-following conditions in a power reactor. Gas release was continuous as burnup increased at power and was not significantly changed by power transients. The fuel column grew as a result of thermal expansion during heatup, shortened during early constant power operation, probably because of creep or restructuring, and expanded slowly in accordance with expected fission product swelling.

When solution-treated type 316 stainless steel tubing was exposed to a controlled oxidation potential, matrix oxidation and intergranular attack were often localized in areas having discrete temperatures of operation. For example, localized increased attack was observed in the range 585 to 605°C out of the total temperature range

tested, 560 to 650°C. A greater change in wall thickness of the tubing used was indicated above 660°C. We postulate that this oxidation in specific temperature regimes is due to the morphology of the carbide present in the stainless steel. Additional work may explain observations on intergranular attack in $(U,Pu)O_2$ fuel pins clad with stainless steel.

We incorporated a sophisticated fuel-cladding gap conductance model in the FMODEL fuel performance code and also refined the model for thermal-gradient-induced redistribution of porosity and fuel components during irradiation of PuO_2 fuel. The principal modeling effort was detailed analysis of sensitivity of predicted fuel pin performance to uncertainties in physical and mechanical properties of the fuel and cladding. The uncertainties examined included thermal expansion of both fuel and cladding, fuel thermal conductivity, mechanical properties of fuel and cladding, and cladding swelling characteristics as a function of fast neutron fluence and temperature. A statistical analysis was done to further confirm that the central temperature (°C) of Sphere-Pac fuel under irradiation is always cooler than that in pellet fuel by 11.7 ± 1.2% at the 99% confidence level. Additional analyses included modeling of chemical attack between mixed oxide and stainless steel cladding and a thermodynamic study that showed that CO_2 and H_2O do not transport oxygen in mixed oxide fuel pins.

16. Fabrication Development of Fast Breeder Reactor Cladding

Two types of artificial defects in type 316 stainless steel tubing reduced creep strengths and ductility. Stress concentrations occur at the defects.

17. Joining of Structural Materials

We are studying the elevated-temperature properties of austenitic stainless steel weldments for application to LMFBR vessels and components, particularly piping. Included in the program are the shielded metal-arc, gas tungsten-arc, submerged-arc, gas metal-arc, and electroslag welding processes. The serious lack of long-term ductility in conventional weldments has led to the development of filler metals having improved strength and ductility.

We have participated in the preparation of a program plan to determine the weldability and properties of Inconel 718, an age-hardenable nickel-chromium alloy. Weld-metal fissuring in Incoloy 800 is intergranular and is probably related to large columnar grains. We developed a filler metal that has the nominal composition of Incoloy 800 but does not produce large columnar grains. The cracking propensity of this composition is reduced, and we are attempting further improvements to eliminate the problem.

Niobium-stabilized 2¼ Cr–1 Mo–½ Ni steels are prone to hot cracking during welding because a liquid phase is present in the heat-affected zone and, in multipass welds, in the weld metal. The presence of this phase, however, does not deleteriously affect the tensile and impact properties of the weldment. Hardness studies of the low-, medium-, and high-carbon 2¼ Cr–1 Mo steels showed that the base metal is the weakest zone in a weldment. We developed a technique to simulate the bore-side weld in a flat-plate configuration that will permit the preparation of specimens for mechanical properties and nondestructive testing. Moreover, we devised a double-torch technique that permits the simulation across an entire weldment of the overlap region in a weld.

18. Mechanical Properties of Alloys in Reactor Environments

Microstructural changes that occur as a result of fast neutron irradiation over a wide range of temperature and neutron fluence were studied in types 304 and 316 stainless steel. Of particular importance is the observation that preirradiation structure has a pronounced effect on void formation and swelling. Ductility is the most adversely affected mechanical property. The loss of ductility appears to result from a combination of matrix hardening and helium effects.

19. Mechanical Properties of Structural Alloys

Before the deformation behavior of type 304 stainless steel can be predicted under complicated loading conditions for reactor components, the creep law predicting strain under variable loads must be determined. Our tests to date support a strain-hardening rule for cumulative creep rather than a time-hardening rule.

In design, average mechanical property data are customarily used with minimum strength properties sometimes available. For the critical analyses of components operating in the creep range, it is necessary to validate those average properties and establish the expected heat-to-heat variation in creep properties. Thus far our effort has shown that the variation in creep properties at 593°C is greater than anticipated.

We are collecting mechanical property data for steam generator materials. Our program involves the Croloy and Incoloy 800 alloys, both wrought and weld metal.

To date, our work has been primarily directed toward determining the influence of carbon on the properties of $2\frac{1}{4}$ Cr–1 Mo alloy in the normalized and tempered condition. In general, the strength increases with carbon content.

20. Nondestructive Test Development

We are developing new methods, techniques, and equipment for nondestructively inspecting materials and components for the LMFBR, with emphasis on problems related to steam generators.

The primary problem being investigated for steam generators is the tube-to-tube-sheet welded joint. Studies have begun on radiography using a small-rod-anode x-ray unit. Preliminary techniques were examined for application of liquid penetrants with viewing by closed-circuit television. Computer design of optimum eddy-current coils for the tubular configuration is in progress. A prototype ultrasonic system was developed for quantitative recording of flaws in flat-weld simulations of the tubular joint.

We continued computer analysis of eddy-current test systems with emphasis on applied problems such as optimum design for reflection coils, reduction of noise and temperature drift, improved capability for measurement of thickness, and measurement of liquid level. The experimental program included construction of equipment to confirm and apply the above, including measurement of the degree of cold work in stainless steel.

Significant progress was made in the ability to characterize flaws of different configurations by ultrasonic frequency analysis. Improvements in the optical imaging system for ultrasound increased its frequency response and power and allowed studies of stainless steel welds by schlieren techniques. Preliminary studies were performed on interferometric and Bragg diffraction methods.

PART III. SPACE POWER TECHNOLOGY

21. Cladding Materials for Space Isotopic Heat Sources

Alloys of platinum with rhodium and tungsten, including modifications with small amounts of hafnium and titanium, were prepared in sufficient quantities for properties determinations. In toughness at 1316°C, Pt–30% Rh–8% W–1.0% Hf–0.2% Ti was superior to refractory materials such as iridium, TZM, and T-111. Forming studies have also been initiated. In general, the alloys continue to show great promise for use as container materials in space applications of isotopic power fuels.

22. Development of Uranium Nitride Fuels for NASA

Three capsules were irradiated throughout the year without serious difficulty. Neutron radiographs showed that the pins contained in the capsules were dimensionally stable although some pellet cracking occurred. Leakage of 10^{-5} of the fission product gas was detected in the blanket gas of two capsules. The principal operational difficulty was the failure of cladding thermocouples, which required the use of heat-generation measurements to control the capsules.

Two methods were developed to fabricate 85%-dense UN pellets that are thermally stable to 2300°C. One method involved preconditioning of UN powders before pressing and sintering; the second involved the use of $UN_{1.74}$ as starting material.

23. Physical Metallurgy of Refractory Alloys

The failure of T-111 containers of $^{238}PuO_2$ fuel in test Pioneer radioisotope thermoelectric generators was traced to oxygen contamination. Sources of the oxygen were identified and suggestions made for diminishing the problem. The rates of oxygen contamination, the degree of sensitivity, and mechanism for embrittlement were determined for T-111 under simulated operating and reentry situations. The mechanical properties of T-111 Pioneer test capsules were measured to determine the effectiveness of the engineering "fix" for this problem.

24. Tungsten Metallurgy

Experimental tungsten materials including CVD tungsten with controlled fluorine contents and tubing of arc cast tungsten and W–2% ThO_2 were fabricated for evaluation in the thermionic reactor program. Deposits of CVD tungsten containing 15 to 25 ppm F were significantly stronger in creep at 1650°C than deposits containing 5 to 10 ppm. We are testing CVD tungsten at stresses to produce 1% creep in 1000 to 50,000 hr using highly accurate optical strain measuring techniques. In creep rupture tests W–3.8% ThO_2 was stronger and more stable than W–2% ThO_2. The creep strength of tungsten tested in low-pressure CH_4 is lower at 1800°C but greater at 1650°C compared to material tested in vacuum.

A review of radiation damage to refractory metals as related to thermionic applications was completed. A high-temperature irradiation experiment on various tungsten materials was completed after achieving a peak fluence of 8×10^{21} neutrons/cm^2. Determination of the effect of irradiation temperature, fabrication processing, and alloying on the void formation and electrical properties began.

PART IV. REACTOR DEVELOPMENT SUPPORT

25. Gas-Cooled Reactor Program

Our primary objective is to develop and improve the coated-particle fuels currently specified for large high-temperature gas-cooled reactors (HTGRs). We prepared and characterized coated particles and simulated fuel elements and tested them to high fuel burnup and fast fluence. Uranium-loaded particles derived from ion-exchange resins can be substituted for the fissile particles in the fuel cycle. Such particles with stable coatings performed well to a burnup of 30 at. % and full HTGR fluence of 8×10^{21} neutrons/cm^2. Fuel sticks intrusion bonded with coal-tar pitch containing reference flake graphite and experimental filler materials survived irradiation to full fluence and burnup without coating failures and with only slight debonding. We developed and are testing fuel sticks prepared by molding and extrusion techniques that offer savings in fabrication costs and improved physical properties.

Our program also contributes to the development of fuel elements for a gas-cooled fast breeder reactor (GCFBR). Irradiation testing in the ORR of a new manifolded-vented fuel element design to an exposure of 53,000 MWd/ton was completed satisfactorily. We prepared the $(U,Pu)O_2$ fuel and fuel pin for the second test of a vented element and also prepared five fuel pins for irradiation testing in EBR-II.

26. Heavy Section Steel Technology

We continue to provide support to the Heavy Section Steel Technology Program and have expanded our studies to determine the tensile and impact properties of HSST plates 02 and 03. The hydrogen technique for generating sharp cracks has been applied to initiate controlled cracks in small scaled-down test vessels and large flawed tensile specimens and also for precracking fracture-toughness specimens.

A study was also initiated to determine the feasibility of using the simple Charpy-type specimen to determine the static and dynamic toughness parameters, K_{Ic} and K_{Id}, which are customarily determined by large compact tension specimens.

27. Military Reactor Fuel Element Procurement Assistance

Technical assistance was provided for procurement of the Type II fuel elements for the Army MH-1A reactor, including evaluation of fabricators and review of numerous documents.

28. Molten-Salt Reactor Program

All Hastelloy N surfaces exposed to fuel salt in the MSRE exhibited intergranular cracking, particularly after deformation at 25°C. We have not been able to produce these cracks under various corrosion conditions and have developed considerable evidence that they result from the diffusion of Te along the grain boundaries. The laboratory experiments show that cracking can be produced by Te. Several materials show better resistance to cracking by Te than Hastelloy N and offer encouragement that a resistant alloy can be found. In-reactor experiments will be required to confirm such resistance.

A modified Hastelloy N containing 2% Ti was evaluated rather completely and appears to have suitable resistance to embrittlement by thermal neutron irradiation. This alloy has been produced in 100-lb commercial quantities, and no obstacle to full commercial development is known.

Hastelloy N (standard and modified) shows excellent corrosion resistance in $LiF\text{-}BeF_2\text{-}ThF_4\text{-}UF_4$ and acceptable corrosion resistance in sodium fluoroborate. Compatibility with steam is excellent in unstressed Hastelloy N but unclear in the stressed state.

Studies of many graphites show that very strong grain boundaries that resist fracture during shearing deformation are required for good dimensional stability. Improvements in techniques and equipment have enabled the use of the scanning electron microscope (SEM) to determine that many failures of our pyrolytic carbon coatings during irradiation are due to flaws. Better coating methods have been developed with the aid of the SEM.

Chemical processing methods presently being developed for removing fission products from MSBR's currently use Bi-Li alloys. Molybdenum is compatible with these alloys and with fuel salt. The techniques for fabricating a test facility of Mo were developed, and assembly is starting. Compatibility tests have begun on graphite and T-111, and initial results indicate that these materials may also be usable.

29. Thorium Utilization

The objective of the Thorium Utilization Program is to demonstrate economic processes and techniques for

the Th-^{233}U fuel cycle for the high-temperature gas-cooled reactor. Fabrication processes and equipment are being developed to handle the highly radioactive recycle fuel, and the fuel materials of interest are being tested under irradiation. The program is to demonstrate recycle capabilities starting in 1977. The maintenance and improvement of the Thorium-Uranium Recycle Facility was continued. Process development emphasized refinement of techniques for deposition of pyrolytic carbon and silicon carbide and the slug injection process for bonding coated fuel particles with a carbonaceous matrix. Considerable effort was expended in developing techniques for inspection of fuel products at various stages in the process. Silicon carbide coatings can be applied in the prototype remote coater, and the variation in pyrolytic carbon coating layers was reduced. An automatic fuel stick machine, based on the slug injection process and having a capacity of 500 or more fuel sticks per day, was designed and fabricated. Equipment and systems diagrams were prepared for microsphere coating, fuel stick fabrication, and fuel element assembly in TURF. We commenced a comprehensive study of the process alternatives involved in the recycle of HTGR fuel. The processes of interest were identified in the areas of head-end processing, solvent extraction processing, fuel preparation, and fuel fabrication. The technical data for evaluation of 13 processes were prepared, including 8 types of fuel elements, 16 types of particles, and 68 types of fuel sticks. A computer code was developed to handle the data and calculate overall cost, considering processing options. In addition, a brief conceptual design study was made for a commercial recycle plant to determine general arrangement and space requirements.

The irradiation of the recycle test elements in the Peach Bottom Reactor and capsules in the Engineering Test Reactor continued. One RTE was removed for examination and use in head-end processing studies. Two capsules were removed from the ETR, and examination has just started.

PART V. THERMONUCLEAR AND TRANSURANIUM RESEARCH

30. Controlled Thermonuclear Reactor Program

Neutron damage in refractory metals and their alloys was studied. Swelling due to void formation was examined for Mo, Nb, V, and one alloy of each for irradiation temperatures of 400 to 800°C. Tensile tests on Mo and Mo–0.5% Ti irradiated at 425°C showed these to be brittle below 550°C at fast test speeds.

A program to simulate neutron damage by heavy-ion irradiation in accelerators was initiated. Alteration of the ORNL 6-MeV Van de Graaff was begun by the Physics Division staff. An experiment was inserted into ORR to provide information on the temperature dependence of void formation in Al, Ni, and V. Theoretical effort on the range and distribution of self-ions was provided by the Solid State Division.

A limited compatibility program involving refractory metals and lithium was initiated at midyear.

31. Transuranium Program

A total of 24 targets, all containing $(Am,Cm)O_2$ as the starting material, were fabricated for irradiation in the HFIR. During the year, 19 target rods were removed from the HFIR as scheduled and showed no cracks or unusual consequences of irradiation. Thus, incorporation of additional void volume assures adequate target performance for the design burnups, which reach as high as 85% of the starting actinide elements. We fabricated 28 sources containing a total of approximately 81 mg of ^{252}Cf. We prepared a special target for irradiation in HFIR, a HFIR rabbit containing ^{240}Pu, and two sources for study of the Mössbauer effect.

PART VI. OTHER PROGRAM ACTIVITIES

32. Aluminum Fuel Element Development

An irradiation experiment initiated last year designed to determine the effects of fuel plate materials and processing variables was evaluated. Swelling of aluminum-clad U_3O_8-Al and UAl_x-Al dispersions depended primarily upon the fission density and the effective void content of the fuel core.

We continued to assist the manufacture of HFIR fuel elements. The fuel plate rejection rate has been further reduced from 2.20% last year to 1.89%. Preliminary work is under way for the potential use of burned U_3O_8 in place of high-fired U_3O_8 and unclad 6061 aluminum in place of alclad 6061 in the manufacture of fuel plates. Preparations for the addition of Al_2O_3 to the filler section of fuel plates to increase void volume are under way.

Examination of spent HFIR fuel elements 100-I and 100-O containing burned U_3O_8 indicates that the fuel plates performed at least as well as plates containing the more expensive high-fired oxide. Heat treatments also revealed an improvement in the blistering temperature

of these plates over those fabricated with the high-fired oxide.

Postirradiation examination of HFIR control cylinders after 48,000 MWd use revealed a 3- to 5-mil surface oxide buildup and no degradation or metallographically detectable reaction in either the Ta-Al or Eu_2O_3-Al portions.

Aluminum alloy 5052, strengthened by the precipitation of Mg_2Si during irradiation, fractured intergranularly in creep tests at 50°C. Elongations of the failed specimens were about 1%.

33. Flaws in Welds Studied by Autoradiography

A heterogeneous distribution of base and filler metals was found in welds of Incoloy 800 with Inconel 625 made with ^{63}Ni-traced filler metals. Segregation can be revealed by ^{14}C and other isotopes.

34. Fabrication of Plutonium Test Element

Plutonium is potentially a very attractive fuel for high-temperature gas-cooled reactors, in which it would replace makeup ^{235}U that is required when operating on the ^{233}U-Th fuel cycle. We developed processes and materials for the plutonium test element that is being irradiated in the Peach Bottom Reactor and fabricated the plutonium-bearing fuel components for it. The fuel element contained fissile kernels of PuO_2 and ThO_2–25% PuO_2 prepared by sol-gel procedures. We applied successive layers of low-density isotropic carbon, high-density isotropic carbon, silicon carbide, and high-density isotropic carbon. Fabrication of fuel sticks by the slug injection process produced a coated particle body bound together by a carbonaceous binder.

35. Development for the Light Water Breeder Reactor

Development was completed on a process for converting uranyl nitrate solution to very pure ceramic grade UO_2 powder. About 300 $^{233}UO_2$-ThO_2 pellets and two matched sets of $^{233}UO_2$ pellets were fabricated to close tolerances.

36. Graphite Fabrication Studies for the Naval Ordnance Laboratory

Graphites developed for irradiation resistance have superior properties compared to conventional graphites and offer potential for improved nose-tip performance. A modification of these newer graphites for optimum thermal shock and ablation resistance is in progress.

37. Metallography

The scanning electron microscope has greatly extended our microscopic analysis capabilities, and the recent addition of the nondispersive x-ray attachment will be an added bonus in analytical studies, even in animal tissues. This instrument is designated for both unirradiated and irradiated samples and is a definite complement to the analytical utility of the shielded and unshielded electron microprobe analyzers. An international grand prize was received for a metallography entry in the use of magnetic etching. This development has been extended to the detection of strain-induced martensite in some types of stainless steel. Metallographic failure analysis of prosthetic appliances was explored. Considerable metallographic contributions were made in a cooperative post-test study of a sodium-heated steam generator. The utility of alpha and beta autoradiographic techniques was extended by the use of cellulose nitrate film, stripping film, and nuclear track emulsion. Work has continued in the alpha metallography facility in the study of plutonium-base fuels.

38. NASA T-111 Loop Studies

In a forced circulation loop that operated with lithium between 1200 and 1370°C, the tantalum alloy T-111 showed less than 1 mg/cm^2 mass transfer; principally hafnium was transferred. Ultimate and yield stresses of the alloy decreased with increasing exposure temperature; elongation was unaffected.

39. NERVA Program Metallurgical Support

The outgassing properties of graphite fuel elements were used to predict the environment inside a NERVA reactor during space flight, both before and after the reactor engine is fired. The coefficient of friction of graphite in vacuum and hydrogen varied reproducibly over a range from 0.03 to about 1.3. This has important implications for high-temperature gas-cooled graphite reactors.

Part I. Fundamental Programs

1. Crystal Physics

G. W. Clark

The growth of crystals of high-melting refractory materials is our central theme. Such suitable crystals are often difficult to obtain, and often very specific crystals (composition, phase, purity, perfection, size, etc.) are required to characterize physical properties uniquely or required in technical devices for their optimum operation. Hence, we are conducting a continuing program to provide crystals needed in research, to devise and improve methods of crystal growth, and to develop increased understanding of crystal growth processes and kinetics. Crystals are grown by several methods: by internal centrifugal zone growth, by temperature-gradient zone melting, from molten-salt solvents, from supercritical aqueous systems, and by the general Verneuil method. During this report period, our crystals were shared with at least 17 different researchers for such diverse investigations as: electron spin resonance; optical, defect, magnetic, and elastic properties; deformation; radiation damage and gas bubble migration; diffusion; field emission; and electronic oscillator quality. Also, we are investigating selected physical properties, both those related to the crystal growth process and those important for characterizing new compounds and eutectic structures.

INTERNAL CENTRIFUGAL ZONE GROWTH

Ternary Composites through Directional Solidification

G. W. Clark J. C. Wilson
B. F. Oliver[1]

We report metallographic evidence of ternary eutectic coupled growth, wherein three phases, $UO_{2.0}$-MgO-W, exhibit a steady-state morphology. Structural characteristics in this system indicate that it is a simple ternary eutectic system with virtually no terminal solid solubility of any of the three phases in the other phases. On a random transverse cut of ternary eutectic solid, to a very high degree, the three phases are observed to be in bulk contact. We believe this is as it should be, because local interface equilibrium demands that four condensed phases be in equilibrium at the solid-liquid interface. X-ray diffraction results show marked preferred orientation of the UO_2 and MgO and less prominent orientation of W. These diffraction data are support for the contention of steady-state coupled growth of the three-phase structure.

M-MO_x Binary and Ternary Eutectics

G. W. Clark J. C. Wilson
B. F. Oliver[1]

In studying the parameters determining growth and morphology of binary and ternary metal–metal oxide systems we turned from the ICZG method to the Bridgman technique using tungsten (or other refractory metal) crucibles heated by an electron beam. We thereby expect: (1) to avoid the difficulty of coupling rf power to high (electrical) resistivity oxides; (2) to measure more accurately the temperature gradients and growth velocities at the solid-liquid interface; and (3) to exercise closer control of the O/U ratio in the oxides, since it appears that the metal solubility in certain oxides depends strongly on O/U ratio.[2,3] In prototype

1. Consultant from the University of Tennessee.

2. R. E. Latta and R. E. Fryxell, *J. Nucl. Mater.* **35**, 195 (1970).

3. N. E. Grynkewich, J. A. Graves, and A. T. Chapman, paper presented at the 74th Annual Meeting of the American Ceramic Society, May 6–11, 1972, at Washington, D.C.; abstracted in *Amer. Ceram. Soc. Bull.* **51**, 393 (1972).

apparatus, 2400°C was reached over a 5-cm length of crucible. Extrapolation of the data indicates that we should reach 2700°C over the length of a 7.5-cm crucible.

UO_2 Crystals

J. C. Wilson G. W. Clark

Large UO_2 crystals, grown by the ICZG method, were supplied to eight different researchers, including three at ORNL. We contracted and supplied approximately 250 g of UO_2 crystals of 3.5, 17.5, and 35% enrichment for Argonne National Laboratory experiments.

HIGH-TEMPERATURE SOLUTION GROWTH OF SINGLE CRYSTALS

C. B. Finch G. W. Clark

Single-Crystal Growth of CeO_2 Doped with ^{237}Np, ^{239}Pu, ^{243}Am, and ^{244}Cm

C. B. Finch M. M. Abraham[4]

We grew CeO_2 single crystals as octahedra up to 4 mm on edge, each batch individually doped with ^{237}Np(1:60), ^{239}Pu(1:40), ^{243}Am(1:300), or ^{244}Cm (1:3000) (dopant:Ce atom ratio in solution in parentheses). The crystals were grown at 1150 to 1200°C from $Li_2O \cdot 2WO_3$ solvent, using a previously described thermal gradient technique.[5] The crystals are being subjected to electron paramagnetic resonance studies, which have thus far identified $^{239}Pu^{3+}$. While undoped CeO_2 grown by this technique is blue, the above transuranic dopings cause the following color changes in CeO_2: Np, black; Pu, dark amber; Am, reddish black; and Cm, greenish yellow.

Melt Growth of $RbCaF_3$ and of $RbCaF_3$ Doped with ^{244}Cm

C. B. Finch M. M. Abraham[4]

Single crystals of the cubic, congruently melting perovskite $RbCaF_3$ up to 1 × 2 cm were grown by the Bridgman and Czochralski methods. In the former method, an evacuated, sealed conical-bottom platinum ampul containing polycrystalline $RbCaF_3$ was dropped through a 20°/cm negative thermal gradient from 1200°C to room temperature. In the Czochralski method, the crystals were pulled from melts contained in an inductively heated platinum crucible under an atmosphere of dry, flowing argon. The latter method was also used to prepare $RbCaF_3$ crystals doped with ^{244}Cm (Cm:Ca atom ratio = 1:1700). Although curium-doped crystals emit a vivid red thermoluminescence and undergo gradual darkening due to radiation damage, electron paramagnetic resonance studies have as yet been unable to detect Cm^{3+}.

Crystal Growth of MgO from $Li_2O \cdot Na_2O \cdot 2B_2O_3$

C. B. Finch G. W. Clark

Crystals of MgO were grown as cubooctahedra up to 3 mm on edge from the high-temperature solvent $Li_2O \cdot Na_2O \cdot 2B_2O_3$ at 1300 to 1350°C. A thermal gradient method was used. The resulting crystals contain small amounts of Fe^{2+} and Cr^{3+} impurity (in spite of the use of high-purity starting materials). The crystals have a greenish yellow color and on uv excitation exhibit fluorescent emission due to Cr^{3+}. Attempts to dope MgO with Gd^{3+} by the above technique were unsuccessful; any incorporated Gd^{3+} was below limits of electron paramagnetic resonance detection (estimated at <10 ppm).

Single-Crystal Growth of $ThSiO_4$ Doped with Terbium

C. B. Finch

A previously described thermal gradient method[6] was used to prepare $ThSiO_4$ single crystals containing Tb^{4+}, Tb^{3+}, or both. The growth experiment was conducted at about 1150°C over a four-week period. The Tb:Th atom ratio in solution was 1:3, but we believe that considerably less than this was actually incorporated in the resulting $ThSiO_4$ crystals. Crystals of both modifications of $ThSiO_4$ resulted: the tetragonal zircon-type (thorite) and the monoclinic monazite-type (huttonite). The tegragonal is light brown and fluoresces only weakly under ultraviolet; the monoclinic is colorless and has a bright fluorescence (due to Tb^{3+}). The crystals are being studied to characterize the Tb^{4+} electron paramagnetic resonance spectra in zircon-type $ThSiO_4$.

4. Solid State Division.
5. C. B. Finch and G. W. Clark, *J. Appl. Phys.* **37**, 3910 (1966).
6. M. M. Abraham, G. W. Clark, C. B. Finch, R. W. Reynolds, and H. Zeldes, *J. Chem. Phys.* **50**, 2057–62 (1969).

Epitaxial Growth of $LiLnMo_2O_8$ on Single Crystals of Ln_2GeMoO_8 (ref. 7)

G. W. Clark L. A. Harris
C. B. Finch H. L. Yakel

Evidence is presented for oriented overgrowth of thin ($\leqslant 3$ μm) single-crystal layers of $LiLnMo_2O_8$ on large substrate crystals of Ln_2GeMoO_8 grown from $Li_2O \cdot 2MoO_3$ solutions containing dissolved lanthanide sesquioxides in contact with solid GeO_2 at 1050°C. Both substrates and epitaxial layers have a scheelite-type ($CaWO_4$) crystal structure, and axes of the two tetragonal unit cells are always parallel. Lattice parameters obtained from x-ray diffraction data and electron microprobe analyses support the conclusion that the layers are lithium lanthanide molybdates, $LiLnMo_2O_8$. Etching experiments indicate that the overgrowth is epitaxial rather than syntaxial. The solution chemistry probably responsible for the effect is described.

Zero-Field Splittings of Cm^{3+} and Am^{2+} in Fluorite-Type Crystals[8]

W. Kolbe[9] N. Edelstein[9]
C. B. Finch M. M. Abraham[4]

The Γ_6-Γ_8 energy level splittings were derived for Cm^{3+} and Am^{2+} in several fluorite-type crystals from measurements of the anisotropy of the g value of the Γ_6 state at 35 GHz. Anisotropy measurements were also made of the g value of the excited Γ_7 state for Cm^{3+} in $SrCl_2$, and the Γ_8-Γ_7 splitting was obtained.

Formation and Stability of the Scheelite and Zircon Modifications of $ThGeO_4$ (ref. 10)

L. A. Harris C. B. Finch

The formation conditions and relative stability of the two tetragonal modifications of $ThGeO_4$ (scheelite and zircon) in the range 750 to 1500°C and 1 atm were studied by x-ray diffraction. The growth of large zircon-type single crystals at 750 to 1400°C and the conversion of scheelite-type $ThGeO_4$ to zircon type in the presence of LiCl–40 at. % mineralizer argue that zircon-type $ThGeO_4$ is the more stable of the two forms in the range 750 to 1400°C. In absence of a mineralizer, scheelite-type $ThGeO_4$ formed at temperatures up to 1050°C, apparently as a metastable phase. The validity of single-crystal growth as a criterion of relative phase stability at a given temperature was reestablished.

Single-Crystal Growth and Several Optical Properties of $CaWO_4$ Doped with $^{243}Am^{3+}$ (ref. 11)

C. B. Finch G. W. Clark

Single-crystal boules of $CaWO_4$ doped with from 0.1 to 1.8 at. % $^{243}Am^{3+}$ were grown by the Czochralski (pulling) method. The crystals display strong fluorescent emission at 6950 Å (5100-Å excitation) and have fluorescence lifetimes between 50 and 80 (±15) μsec. None of the samples exhibited room-temperature laser action. Self-induced radiation damage results in a degradation of optical properties, observable within several days after crystal preparation.

EPR Investigations of Er^{3+}, Yb^{3+}, and Gd^{3+} in Zircon-Structure Silicates[8]

R. W. Reynolds[12] L. A. Boatner[12]
C. B. Finch M. M. Abraham[4]
A. Chatelain[13]

The electron paramagnetic resonance spectra of Er^{3+}, Yb^{3+}, and Gd^{3+} were observed in the host single crystals $ZrSiO_4$, $HfSiO_4$, and $ThSiO_4$, which we grew by a flux-gradient technique. For most systems, spectra were observed with both tetragonal and orthorhombic symmetry. The tetragonal spectra were characterized by a principal axis system that coincided with the principal crystallographic axes. The observed orthorhombic spectra were of two types. For Gd^{3+} in $ZrSiO_4$ and $HfSiO_4$, orthorhombic spectra due to eight inequivalent sites were observed and had principal axis systems that were not simply related to the host crystallographic axes. All other orthorhombic spectra resulted from four inequivalent sites whose z and x axes lay in {110} planes with equal angles between the crystal tetragonal symmetry axis (c axis) and each z axis. For both types of orthorhombic spectra, the corresponding EPR transitions from the different sites were superimposed with the applied magnetic field parallel to the c axis.

7. Submitted to *Journal of Crystal Growth.*
8. Submitted to *Journal of Chemical Physics.*
9. Lawrence Berkeley Laboratory.
10. Submitted to *American Mineralogist.*
11. Submitted to *Journal of Physics and Chemistry of Solids.*
12. Advanced Technology Center, Dallas, Tex.
13. Federal Institute of Technology, Lausanne, Switzerland.

High-Temperature Solution Growth of Single-Crystal Plutonium Dioxide[14]

C. B. Finch G. W. Clark

Macroscopic $^{239}PuO_2$ single crystals were grown from $Li_2O \cdot 2MoO_3$ solvent by a thermal gradient technique at 1270 to 1300°C. Polycrystalline PuO_2 nutrient, on the floor of a tall, tightly closed platinum vessel at 1300°C, underwent transport upwards through 7 cm of PuO_2-saturated solution, whose upper surface was maintained at about 1270°C. Two-week runs resulted in the growth of octahedral crystals up to 2 X 3 X 3 mm in size, which formed on platinum substrates in the upper solution regions at 1270 to 1280°C. The growth rate for good-quality PuO_2 was $\leqslant 1$ mm/week and approximates that previously reported for the isostructural compounds CeO_2, ThO_2, and NpO_2 from similar solvents in this temperature range. Spectrochemical, lattice parameter, and oxygen analysis data indicate that the crystals are of good purity (>99.9%) and are near stoichiometric ($PuO_{1.97 \pm 0.03}$).

HYDROTHERMAL STUDIES

Growth and Crystal Morphology of Lead Sulfide in the Hydrothermal System PbS-RbOH-H_2O (ref. 15)

O. C. Kopp[1] G. W. Clark

The system PbS-RbOH-H_2O was investigated hydrothermally to determine the best growth conditions for cubic lead sulfide (galena) in steel vessels. At low pressures (below 0.1 to 0.7 kilobar depending on the temperature), blades, needles, columns, etc., are formed, while at higher pressures (above 0.8 to 2 kilobars depending on the temperature), hoppered cubes are produced. Cubic to cubo-octahedral crystals are produced at intermediate pressures. Increasing the temperature of the growth zone, the pressure, and the RbOH concentration result in increased growth rates or rates of transportation. However, RbOH concentrations greater than 1 *N* cause extreme corrosion and vessel failure. An attempt is made to understand the chemical reactions taking place during the dissolution and recombination of lead sulfide in the nutrient and growth regions of the vessel.

Crystal Structure of a Rubidium Iron Feldspar[16]

G. D. Brunton[17] L. A. Harris
O. C. Kopp[1]

The compound $RbFeSi_3O_8$ is a synthetic hydrothermal intermediate microcline with Fe^{3+} substituting 38.9, 48.7, 10.2, and 11.0 at. % for silicon at the four tetrahedral positions in the order customarily used by crystallographers. Lattice parameters for the triclinic cell ($C\bar{1}$) are a_0 = 8.952, b_0 = 13.127, c_0 = 7.359 Å, α = 89.95°, β = 116.47°, and γ = 90.65° at 24°C. The calculated density is 3.032 g/cm^3. The Rb-O interatomic distances range from 3.033 to 3.348 Å. The average Si-O distances are 1.702, 1.734, 1.620, and 1.622 Å, respectively, for the same four positions. An asymmetrical ($C1$) structure was also refined, and the discrepancy factors $R(F_0^2)$ and $wR(F_0^2)$ for the two structures are not significantly different at the 0.01 level. The $C\bar{1}$ model is probably the correct structure because several of the Si-O distances in the $C1$ model are abnormally short, for example, Si(8)-O(12), 1.50 Å.

14. Abstract of *J. Cryst. Growth* **12**, 181–82 (1972).
15. Abstract of *J. Cryst. Growth* **11**, 336–40 (1971).
16. In press, *American Mineralogist*.
17. Reactor Chemistry Division.

2. Deformation of Crystalline Solids

R. O. Williams

Metals are most often used under conditions where resistance to deformation is of consideration. Consequently, alloys are normally used, and economic considerations require that we have adequate understanding of how specific alloys will perform under given conditions. Our work contributes to the overall understanding of the structures and properties of metals and alloys.

ELASTIC INTERACTION OF PRISMATIC DISLOCATION LOOPS WITH POINT DEFECTS UNDER APPLIED STRESS[1]

M. H. Yoo W. A. Coghlan

Based on the sphere-in-hole model for a point defect, the elastic interaction potential, the interaction force, and the drift direction were calculated analytically for a point defect near a circular prismatic dislocation loop in an elastically isotropic medium. A kinetic analysis for the transient stage of point defect segregation to a dislocation loop of Frank type was made by use of numerical integration techniques. The fraction, F, of available point defects migrated to Frank loops within time t may be given by

$$F(t) = K\rho(Dt/T)^n,$$

where ρ is the dislocation loop density, D is the diffusion coefficient for point defects, T is the absolute temperature, and K is a constant related to the shear modulus of the medium, the Burgers vector, the volume and the dilatation associated with a point defect, and the loop radius. The exponent, n, was 0.6 to 0.7 for the size effect interaction and 0.4 to 0.5 for vacancies by the modulus effect interaction. A uniform applied stress of magnitude 10^{-3} times the shear modulus applied normal to a Frank loop lowers the value of $F(t)$ by approximately 2% for the vacancy modulus effect. The power exponent is not altered by the applied stress.

ELASTIC INTERACTION OF A POINT DEFECT WITH A PRISMATIC DISLOCATION LOOP IN HEXAGONAL CRYSTALS[2]

M. H. Yoo S. M. Ohr[3]

Effects of elastic anisotropy on the interaction between an axially symmetric point defect and a prismatic dislocation loop in hexagonal crystals were investigated. The elastic interaction was affected significantly by the anisotropic elastic field of a loop. The most pronounced effects were found in zinc and graphite. Generally, effects of the point defect anisotropy were much more pronounced than those of the anisotropic elastic field of a loop. A point defect whose strain is greater in the **a** direction than in the **c** direction finds two centers of concentration (or depletion) at directly above and below a prismatic loop. The distance between the concentration center and the loop varies with the degree of anisotropy in the elastic self-fields of both the point defect and the prismatic loop.

DISPLACEMENT FIELDS OF STRAIGHT DISLOCATIONS IN ANISOTROPIC CRYSTALS[4]

M. H. Yoo B.T.M. Loh

The displacement fields of glissile dislocations of active slip systems in common crystal structures were analyzed in detail by taking account of elastic anisotropy. Each displacement component can be generally expressed in terms of 12 real coefficients. The cases for which analytic expressions of these

1. Summary of paper presented at the 1972 Spring Meeting of the Metallurgical Society of AIME, Boston, Mass., May 8–11, 1972.

2. Abstract of a paper to be published in *Journal of Applied Physics.*

3. Solid State Division.

4. Abstracted from *J. Appl. Phys.* **43**, 1373–79 (1972).

coefficients are possible are enumerated. An efficient method of numerical calculation for a general case is introduced, and numerical results for Cu, α-Fe, and Zn are given in polar diagrams. Bending, warping, and dimpling of lattice planes about the dislocation axes are discussed in terms of radial and angular dependencies of the displacement components normal to the Burgers vector. Choices of integration constants are described in accordance with symmetry properties about the dislocation axes.

THE APPLICATION OF ATOMIC POTENTIALS TO THE HEAT OF MIXING, THE LATTICE PARAMETER, AND THE COMPRESSIBILITY OF RANDOM CUBIC SOLUTIONS[5]

R. O. Williams

If the interactions between atoms are represented as interatomic potentials, then it follows that for random cubic solutions the compositional dependence of the heat of mixing, the lattice parameter, and the compressibility is expressible in terms of only three constants, which depend upon the interactions of unlike atoms. This formulation provides an interesting representation of strain energy and is directly applicable to alloys of greater complexity since only pair-wise interactions are required.

THE STRUCTURE OF Cu–16 at. % Al

R. O. Williams

The diffuse scattering data for an aluminum-copper alloy of Borie and Sparks[6] were reanalyzed by a least-squares fitting of the parameters. An advantage of this method is that individual values for the Warren-Cowley short-range-order parameters are directly obtained rather than the two-dimensional combinations obtained previously. Using those parameters, one can carry out a computer simulation of the structure. Figure 2.1 shows a stereo pair of such a simulation. While the general structure reasonably resembles the 200–211 tetrahedra proposed by Borie and Sparks, the arrangement is perhaps less regular than implied by their description and also shows elements of the structure Cu_3Au.

5. To be published in *Acta Metallurgica.*

6. B. Borie and C. J. Sparks, Jr., *Acta Crystallogr.* **17**, 827–35 (1964).

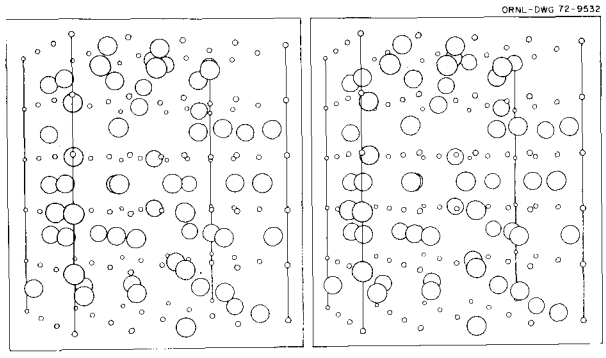

Fig. 2.1. A computer simulation of the structure of Cu–16 at. % Al. For clarity, only the aluminum atoms are shown.

FRACTURE MECHANISM IN PRECIPITATION-HARDENED ALLOYS[7]

R. W. Carpenter

Niobium and hafnium form a body centered cubic solid solution at elevated temperatures and at lower temperatures precipitate the hcp alpha phase, which is nearly pure hafnium. Investigation of the mechanical properties of these alloys has shown that elongation to fracture is small, typically 1 to 8% for alloys quenched from high temperature and aged within the two-phase region, and that an appreciable fraction of the fracture surface is intergranular. The occurrence of this type fracture is usually attributed to either the presence of a precipitate in the grain boundaries, the existence of a precipitate-free zone (PFZ) along grain boundaries, or both. The behavior has also been observed in several other alloy systems, all based on the fcc structure.[8–10] In the Nb-Hf system both exist, and the grain boundary precipitate is essentially α-Hf, which is a weak ductile material at room temperature. The critical question was whether there were strongly localized plastic strains in the grain boundary regions leading to localized ductile fractures, or whether the fracture is truly brittle

7. Abstracted from "Transmission and Scanning Electron Microscope Observations of Niobium-Hafnium Alloys," pp. 667–78 in *Electron Microscopy and Structure of Materials,* proceedings of the Fifth International Materials Symposium "The Structure and Properties of Materials – Techniques and Applications of Electron Microscopy," University of California, Berkeley, September 1971, ed. by G. Thomas, R. Fulrath, and R. Fisher, University of California Press, 1972.

8. R. W. Carpenter, *Acta Met.* **15**, 1297 (1967).

9. P.N.T. Unwin and G. C. Smith, *J. Inst. Metals* **97**, 299 (1969).

10. D. L. Douglass and T. Barbee, *J. Mater. Sci.* **4**, 121 (1969).

cleavage through a more or less continuous precipitate film. Direct observations of the fracture morphology on fractured grain boundary surfaces showed that the former case occurs; there is very localized ductile fracture in grain boundary regions. Why such a localized ductile fracture occurred at short total elongation when both the matrix grains and the precipitate are ductile materials is directly related to the difference in flow stress between the matrix (yield stress ≈ 140,000 psi) and precipitate (yield stress ≈ 35,000 psi). When plastic flow begins in such a system the weaker layer, which is thin, will yield first. But it will not be able to strain freely, since it is everywhere constrained by the much stronger unyielded matrix. The constraint leads to the development of a triaxial stress state in the grain boundary regions. The triaxial tension in the boundary (≈100,000 psi) leads to rapid growth of fracture nuclei once they are formed and results in very small overall strains before fracture.

PRECIPITATION KINETICS IN NIOBIUM-HAFNIUM ALLOYS

R. W. Carpenter

During the course of an investigation of some superconducting properties of Nb–38 at. % Hf alloys,[11] we observed that the size of metastable transition alpha precipitate obeys a cube-root time dependence law; that is, a simple coarsening process is occurring during which the precipitate composition is not changing. This observation was substantiated by measurement of the transition temperature on specimens isothermally aged to contain transition alpha; the transition temperature was constant after approximately 30 min of aging. Since transition alpha has a strained hcp lattice and exhibits strain contrast fringes when observed by transmission electron microscopy, it is at least partially coherent. Unfortunately the precipitate particles are too small to establish the degree of coherency and the configuration of misfit dislocations, which are almost certainly present in some regions of the interface. It is important to establish whether the degree of coherency is changing during isothermal aging, since such a change will surely affect the strain field contribution to fluxoid pinning, in addition to any changes in pinning behavior due to geometric changes in the precipitate dispersion. Since the matrix elastic strain associated with a coherent precipitate is a deterrent to its growth, one expects that if coherency is lost or reduced, a marked increase in coarsening rate will be observed. This event has been clearly observed in some other alloy systems such as nickel-silicon.[12] No deviation from the $t^{1/3}$ coarsening law was observed in the niobium-hafnium alloy, indicating that the degree of coherency is constant for very long aging times at 600°C (at least 1000 hr). Thus the contribution to fluxoid pinning due to strain field interaction (the "dielastic" contribution depends only on the geometry of the precipitate array and not on changes of the strain field due to changes in coherency.

11. C. C. Koch and R. W. Carpenter, "Precipitates and Fluxoid Pinning in a Superconducting Nb-Hf Alloy," *Phil. Mag.* **25**, 303–20 (1972).

12. R. K. Rastogi and A. J. Ardell, *Acta Met.* **19**, 321 (1971).

3. Diffusion in Solids

P. T. Carlson

The research interests of the Diffusion in Solids Group include the entire spectrum of atomic migration phenomena in crystalline materials. Our efforts concentrate primarily on the examination of diffusion rates under various conditions by the macroscopic redistribution of radioactive tracers in metals, alloys, and ceramics. Areas of study include effects of varying stoichiometries and vacancy concentrations on diffusion rates in ceramic materials, grain boundary and short-circuit diffusion mechanisms, thermal migration in ionic and ceramic substances, and the effects of high pressure on atomic transport processes.

TRACER SELF-DIFFUSION IN Fe–17 wt % Cr–12 wt % Ni

R. A. Perkins N. K. Tunali[1]
R. A. Padgett, Jr.

Volume and grain boundary self-diffusion are being investigated in the ternary alloy Fe–17 wt % Cr–12 wt % Ni for the radioactive tracers ^{59}Fe, ^{51}Cr, and ^{63}Ni. For the ^{59}Fe and ^{51}Cr tracers, conventional lathe and grinding techniques have been employed together with residual activity measurements to obtain volume diffusion coefficients above 1000°C and grain boundary diffusion coefficients in the range 600 to 1000°C. Sectioning by a radio-frequency sputtering technique and residual activity measurements are being used to study the volume diffusion of these two tracers in the range 600 to 1000°C. Volume diffusion coefficients for ^{63}Ni have been obtained through the use of the sputtering technique for annealing temperatures between 600 and 1250°C, and the values obtained agree well with those obtained from the grinding technique. The grain boundary diffusion contribution for this tracer was studied by grinding techniques and surface activity decrease measurements for the entire temperature range. The sputtering technique has been used to remove sections as thin as 150 Å and has yielded results that are in good agreement with those obtained from the more conventional sectioning techniques. A linear Arrhenius plot was obtained for ^{63}Ni volume diffusion coefficients for the entire temperature range, allowing the study of true volume diffusion down to 600°C, which approaches the temperature range of practical applications. Volume diffusion coefficients for ^{59}Fe also displayed a linear Arrhenius plot. The results obtained for ^{63}Ni are, for volume diffusion,

$$D_v = 8.8 \times 10^{-3} \exp(-60{,}000/RT)\ \mathrm{cm^2/sec}$$

and for grain boundary diffusion,

$$\delta D_{gb} = 3.7 \times 10^{-9} \exp(-31{,}500/RT)\ \mathrm{cm^2/sec},$$

where δ is the grain boundary width. The results for ^{59}Fe are

$$D_v = 0.20 \exp(-65{,}100/RT)\ \mathrm{cm^2/sec}$$

and

$$\delta D_{gb} = 2.0 \times 10^{-8} \exp(-35{,}000/RT)\ \mathrm{cm^3/sec}.$$

Preliminary results for ^{51}Cr diffusion indicate volume diffusion coefficients about double those of the ^{59}Fe diffusion over the entire temperature range.

SECTIONING OF DIFFUSION SPECIMENS BY RADIO-FREQUENCY SPUTTERING

R. A. Perkins R. A. Padgett, Jr.

A radio-frequency sputtering technique described in a previous report[2] has been improved for the removal of very thin serial sections from diffusion specimens. The equipment consists of an MRC sputtering module

1. Formerly on leave from Middle East Technical University, Ankara, Turkey.

2. D. M. Kroeger and E. W. Chandler, *Metals and Ceramics Div. Annu. Progr. Rep. June 30, 1971*, ORNL-4570, p. 14.

SM-8500, which has been modified to accept a ½-in.-diam specimen for the cathode and to include a turntable, which accommodates 18 planchets (substrates).

Material can be collected for 18 sections of a diffusion sample by rotation of the turntable so as to position each substrate in turn beneath the specimen. The sputtering rate has been rather insensitive to the gas pressure in the range 0.010 to 0.015 torr, although the importance of a high-purity gas cover has been observed. The rate has been observed to be linearly dependent on the forward current in the system from 10 to 35 μA, and fairly reproducible rates (±25%) could be obtained for various sputtering runs at a particular forward current setting. From recent experiments, we could remove fairly uniform section thicknesses within a particular sputtering run and attain a minimum thickness of 150 Å. Diffusion coefficients as low as 7×10^{-18} cm^2/sec have been measured. This technique will allow the annealing time of diffusion experiments to be greatly reduced from those times necessary when coarser sectioning techniques are employed, thus allowing diffusion to be studied at lower temperatures than previously possible.

THERMOTRANSPORT OF CADMIUM AND THALLIUM IN SODIUM AND POTASSIUM CHLORIDES

P. T. Carlson L C Manley, Jr.

The thermal diffusion of monovalent and divalent tracer impurities in single crystals of sodium and potassium chlorides is under investigation with the intent to gain a better understanding of the heat of transport in ionic systems. Ionic materials are convenient systems in which to study thermotransport because adequate literature exists on interatomic potentials, lattice energies, and formation energies of lattice defects.

Preliminary results have been obtained for the thermal diffusion of divalent ^{115m}Cd and monovalent ^{204}Tl tracer impurities in single crystals of high-purity NaCl and KCl respectively. Thin disks of the ionic crystals, doped with the appropriate radioactive tracer, were annealed in temperature gradients of up to 1000°C/cm under 2 atm argon and subsequently sectioned, and the activity of each section was counted with a multichannel analyzer. Since the water-soluble and brittle nature of the ionic material precluded the use of conventional grinding or lathe sectioning techniques, we developed a sectioning procedure that uses an American Optical rotary microtome to obtain sections about 1 μm thick. Results show that under the influence of a temperature gradient, thallium diffuses toward the lower temperatures in potassium chloride with an experimental heat of transport of 15,000 cal/mole. Cadmium preferentially migrates to the higher temperatures in sodium chloride; this indicates a negative heat of transport. Considerable difficulty has been encountered with regard to vapor transport of the tracer impurities out of the host material (a violation of the boundary conditions); consequently, the apparatus has been redesigned to attempt to decrease the amount of impurity lost in this manner. The information gained in this type of investigation will assist in our understanding of thermal transport in nuclear ceramic fuels under reactor conditions, since ionic forces contribute significantly to the interatomic forces present in ceramic materials.

DIFFUSION OF HAFNIUM IN Ta–8 wt % W–2 wt % Hf AND Ta–9.5 wt % W–2.5 wt % Hf–0.01 wt % C

P. T. Carlson R. A. Padgett, Jr.

We have initiated a new program with the intent to gain a better understanding of the diffusion processes in various tantalum-base alloys. Initial experiments are being performed to examine the tracer diffusion of ^{181}Hf in the ternary Ta–8 wt % W–2 wt % Hf alloy in the range 700 to 1500°C. Subsequent experiments are planned for diffusion in the quaternary Ta–9.5 wt % W–2.5 wt % Hf–0.01 wt % C alloy. Conventional sectioning and counting techniques are being used, as well as previously developed radio-frequency sputtering and anodizing-stripping techniques, to adequately describe the volume and short-circuit diffusion processes in these systems. Preliminary results for diffusion of ^{181}Hf in Ta–8 wt % W–2 wt % Hf alloy at 1300°C indicate volume diffusion coefficients on the order of 10^{-18} cm^2/sec, with significant contributions to the overall diffusion process from grain boundary and short-circuit paths.

CATION SELF-DIFFUSION IN TITANIUM MONOXIDE

T. S. Lundy R. A. Padgett, Jr.
M. D. Banus[3]

The investigation of ^{44}Ti diffusion in the high-temperature cubic NaCl structure of titanium monoxide

3. Lincoln Laboratory, Massachusetts Institute of Technology.

has been completed. The study spanned the ranges of 1250 to 1555°C and x = 0.8 to 1.26 in the formula TiO_x. It had been suggested at the beginning of this study that the extremely high cation vacancy concentrations of 6 to 24% over the stoichiometry range[4] in these specimens would result in unusually large diffusion coefficients for substitutional diffusion by a vacancy mechanism. Such high values were not observed; however, the diffusion coefficients for a particular temperature did increase approximately tenfold for increasing values of oxygen content.

4. See, for example, M. D. Banus and T. B. Reed, "Structural, Electrical and Magnetic Properties of Vacancy Stabilized Cubic 'TiO' and 'VO,' " pp. 488–520 in *The Chemistry of Extended Defects in Nonmetallic Solids,* ed. by L. Eyring and M. O'Keefe, North-Holland, Amsterdam and London, 1970.

DIFFUSION UNDER HIGH PRESSURES

P. T. Carlson T. S. Lundy

Measurement of diffusion coefficients in refractory metals at high temperatures and pressures is awaiting installation of equipment designed for operation up to 14 kilobars and 1500°C. The equipment is undergoing the final performance tests at the fabrication site, and we expect that installation will begin in the very near future. The initial experiments will concentrate on tracer diffusion in the refractory metals Nb, Ta, and W, so that precise penetration data can be obtained by the anodizing the stripping technique. Such data will yield accurate activation volumes, which can, in turn, be related to the atomic jumping process. In addition, the sensitive sectioning techniques will allow measurements of the effect of pressure on lattice and short-circuit diffusion processes in these systems.

4. Electron Microscopy

J. O. Stiegler

Since materials are often placed in service under conditions in which their microstructures are unstable, their mechanical and physical properties frequently change during use. We are using electron microscopy and related techniques to characterize microstructural changes that occur in several technologically important areas, and we are attempting to relate them to the corresponding variations in properties. Our effort is focused on the changes that occur during neutron irradiation at elevated temperatures, but we are also examining effects of plastic deformation and aging treatments in complex alloys. Work supported by the USAEC Division of Research and some studies that are primarily microstructural in nature are summarized in this chapter. Other contributions by members of the Electron Microscopy Group in support of other programs in the Division appear in Chaps. 2, 14, 18, 24, 28, and 30 of this report.

VOID FORMATION IN NEUTRON-IRRADIATED METALS[1]

J. O. Stiegler

The characteristics of void formation in high-purity metals are reviewed and summarized in terms of irradiation and material variables. Fluence, irradiation temperature, flux and spectral effects, and the role of impurities are discussed. Results are compared and contrasted with those for stainless steel and evaluated in terms of proposed mechanisms for the nucleation and growth of voids. Although general trends of behavior are established for most of the experimental variables, exceptions are invariably found. The observations indicate that details of the damage structure are sensitive to purity and structure.

ANNEALING OF VOIDS IN ALUMINUM[2]

A. Jostsons[3] E. L. Long, Jr. J. O. Stiegler
K. Farrell D. N. Braski[4]

The activation energy for annealing of voids in neutron-irradiated 1100 aluminum was 1.7 ± 0.2 eV from measurements of density recovery in bulk specimens, which is significantly higher than 1.3 eV, the activation energy for self-diffusion. Trapping of vacancies by neighboring voids as well as by transmutation-produced silicon can explain this apparent discrepancy. In high-purity aluminum containing a large volume of voids, significant void coarsening occurred during annealing. When electrolytically thinned foils were annealed, the vacancies from the shrinking voids piled up at preferred sites at the oxide-metal interface. Shrinkage rates for voids of a given size varied widely. No evidence was found for enhanced shrinkage of voids located on dislocations, nor is there any reason to believe that the voids may be hydrogen filled.

EFFECTS OF STRUCTURAL IMPERFECTIONS ON VOIDS IN ALUMINUM[5]

K. Farrell A. Wolfenden
J. T. Houston R. T. King
A. Jostsons[3]

Impurities, inclusions, dislocations, and grain boundaries are structural features that significantly influence the nature and distribution of voids in neutron-irradiated aluminum. Preinjected hydrogen and helium are shown to increase the nucleation of voids for a given fluence without changing the swelling, whereas substitutional-type impurities retard void nucleation. Accelerated void development is frequently noted in the

1. Abstracted from pp. 292–337 in *Radiation-Induced Voids in Metals* (Proc. Int. Conf. Albany, N.Y., June 9–11, 1971), ed. by J. W. Corbett and L. C. Ianniello, U.S. Atomic Energy Commission Office of Information Services, Oak Ridge, Tenn., 1972.

2. Ibid., pp. 363–75.

3. On attachment from Australian Atomic Energy Commission Research Establishment.

4. Isotopes Division.

5. Abstracted from pp. 376–85 in *Radiation-Induced Voids in Metals.*

immediate vicinity of inclusions, and in some cases large spherical shells of voids form around inclusions. Alongside grain boundaries are regions denuded of voids, and next to these are regions in which void formation is enhanced; at low irradiation temperatures these near-grain-boundary regions contain more voids than the grain interiors, but at high irradiation temperatures they contain very much larger voids than elsewhere. A microsturcture consisting of many fine precipitate particles and dislocations has a much improved resistance to void formation.

THE ROLE OF ELECTRON MICROSCOPY IN THE UNDERSTANDING OF NEUTRON IRRADIATION-PRODUCED SWELLING[6]

A. Wolfenden K. Farrell
J. O. Stiegler

The significant role played by transmission electron microscopy in the studies of radiation-induced swelling in nuclear reactor structural materials is reviewed. After a discussion of void formation in the swelling process, we deal with the effects of irradiation temperature, neutron fluence, and preexisting microstructure on the degree of swelling. Finally, some interesting features of void ordering and annealing are mentioned.

ELECTRON DISPLACEMENT DAMAGE IN GRAPHITE AND ALUMINUM[7]

S. M. Ohr[8] A. Wolfenden
T. S. Noggle[8]

High-voltage electron microscopes provide the possibility of studying the kinetics of the clustering of point defects resulting from the displacement of atoms by the electrons in the illuminating beam. We observed the formation of defect clusters in thin films of graphite and aluminum. These clusters nucleate randomly and grow to form loops observed throughout most of the film thickness.

In graphite, irradiation at 300 to 600°C with electrons of energies greater than 150 keV led to visible damage clusters, which indicates that the threshold energy for displacement of the carbon atoms in graphite is less than the reported value of 33 eV. The present work brackets the threshold energy between 26 and 32 eV. The damage clusters show contrast behavior consistent with interstitial-type dislocation loops and in dark field appear as black and white spots present in alternating layers parallel to the specimen surfaces. Detailed studies of this layered contrast indicate that it is due mainly to the stacking fault in the dislocation loops. Calculations are in progress using anisotropic elasticity theory applied to prismatic loops to obtain intensity profiles that can be compared with the experimental observations.

Defect clusters formed in 99.999+% aluminum foils after exposure to the electron beam. The threshold energy for observation of this damage in aluminum of this purity is between 16 and 20 eV. A Burgers vector analysis of these dislocation loops indicates that their vectors lie in either (111) or (110) planes. In 99% aluminum and in alloy 2024 (4.5% Cu, 1.5% Mg, 0.6% Mn, balance Al), no displacement damage due to the electron beam is observed. However, if the 99% aluminum specimens are first neutron irradiated, then subsequent electron bombardment in the microscope causes the further development of visible dislocation loops. These loops form preferentially at grain boundaries, precipitate particles, and grown-in dislocations and possibly mark the positions of preexisting defects that are initially too small to be resolved in the electron microscope. No electron displacement damage is seen in the 2024 alloy specimens whether neutron irradiated or not.

Discussion of these varied observations centers around the effects of purity and microstructure on the nucleation and growth of dislocation loops. The future potential of such experiments is pointed out.

ON THE QUESTION OF VOID FORMATION IN NEUTRON-IRRADIATED ZIRCONIUM[9]

A. Wolfenden K. Farrell

High-purity zirconium irradiated to a fluence of 3×10^{21} neutrons/cm^2 (>0.1 MeV) at 150 to 200°C or to 2×10^{21} neutrons/cm^2 at 550°C did not contain irradiation-induced voids. Neither did Zircaloy-2 irradiated to 2×10^{21} neutrons/cm^2 at 550°C. A dislocation structure is also absent from both materials. Reasons for the apparent resistance of zirconium to void formation are discussed. We point out that zirconium has a low cross section for helium production and that helium might influence the defect structure. In

6. Abstracted from pp. 984–95 in *Electron Microscopy and Structure of Materials* (Proc. Fifth Int. Materials Symposium, Univ. Calif., Berkeley, Sept. 13–17, 1971), ed. by G. Thomas, University of California Press, Berkeley, 1972.
7. Ibid., pp. 974–83.
8. Solid State Division.
9. Summary of *Scripta Met.* **6**, 127–30 (1972).

conclusion, we suggest that no voids are formed because of the absence of dislocation structure, because of a low helium content, or both.

HIGH-FLUENCE NEUTRON IRRADIATION DAMAGE IN Cu–10 wt % Al AND COPPER[10]

A. Wolfenden

Annealed specimens of Cu–10 wt % Al and high-purity copper were irradiated to a fast (>0.1 MeV) fluence of about 1.3×10^{22} neutrons/cm^2 at 175 ± 25°C. Transmission electron microscopy was used to examine the structural damage. The alloy showed uniformly distributed equiaxed and elongated voids. The voids, often associated with particles and dislocation tangles, were present in concentrations of about 10^{11}/cm^3 and had sizes up to about 3500 Å (equiaxed) or 4500 Å (elongated). Arrays of tangled dislocations and small dislocation loops were also observed in the irradiated alloy. The only radiation damage seen in the high-purity copper was a multitude of small dislocation loops. Explanations of these observations near the lower limit (about 0.3 times the absolute melting point) of the temperature range for void formation in fcc metals are offered in terms of differences in the starting microstructures of the specimens.

STRUCTURAL DAMAGE AND ITS ANNEALING RESPONSE IN NEUTRON-IRRADIATED MAGNESIUM[10]

A. Jostsons[3] K. Farrell

Transmission electron microscopy and immersion density techniques were used to characterize the nature and extent of radiation damage in zone refined and commercially pure magnesium irradiated to 1.7×10^{21} neutrons/cm^2 (>0.1 MeV) at about 75°C. Swelling from radiation-induced voids was 1.9 and 0.7%, respectively, for the high-purity and commercial magnesium. This difference was caused by larger voids in the zone refined material. The voids were not equiaxed, being bounded by $\{0001\}$, $\{10\bar{1}0\}$, and $\{10\bar{1}1\}$ and flattened in $\langle 0001 \rangle$, but the larger voids were more equiaxed. Clusters of voids formed in layers parallel to $\{0001\}$ planes. The irradiation-induced dislocation structure was also clustered parallel to the basal planes. This dislocation structure is deduced to consist of a complex tangle of $\frac{1}{6}\langle 20\bar{2}3 \rangle$ partial dislocations and their associated stacking faults.

During postirradiation annealing, voids began to anneal out in 1 hr at 150°C and were eliminated in 1 hr at 320°C. The smaller voids as well as voids near grain boundaries disappeared first. Slow annealing of voids near some grain boundaries suggested that not all grain boundaries are equally good sinks for vacancies. Voids also became more equiaxed during annealing. Stacking faults were eliminated before the voids disappeared, and the dislocations formed networks. Annealing at 500°C or higher caused the appearance of gas bubbles.

RADIATION DAMAGE AND THE EFFECTS OF POSTIRRADIATION ANNEALING IN 1100 ALUMINUM[11]

A. Jostsons[3] E. L. Long, Jr.

Transmission electron microscopy and immersion density measurements were used to characterize radiation damage and postirradiation annealing effects in annealed 1100 aluminum irradiated at 45°C in an aqueous environment to maximum fluences of 3.2×10^{22} neutrons/cm^2 (>0.1 MeV) and 3.1×10^{22} neutrons/cm^2 (thermal). Radiation-induced swelling from voids was first detected at 7×10^{21} neutrons/cm^2 and reached a value of 1.5% at 3.2×10^{22} neutrons/cm^2 with a void concentration of 1.8×10^{14}/cm^3. Transmutation-produced silicon, from thermal neutron reactions with ^{27}Al, formed fine precipitate particles at approximately 5×10^{15}/cm^3, uniformly distributed throughout the matrix.

Irradiation-induced swelling began to anneal out in 1 hr from 110 to 170°C, with complete elimination of voids between 300 and 350°C. Subsequent annealing at higher temperatures resulted in the growth of transmutation gas bubbles and renewed swelling. No helium loss was detected in 20-hr postirradiation anneals at 560°C. The activation energy for void annealing, determined from isochronal and isothermal density recovery measurements in the range 170 to 300°C, was in the range 1.8 to 2.0 eV. Void annealing occurred by the preferential elimination of all voids near grain boundaries as well as the smaller voids within grains. Significant void coarsening occurred within the grains before eventual elimination.

10. Abstract of a paper accepted for publication in *Radiation Effects.*

11. Abstract of a paper submitted to *Radiation Effects.*

SWELLING IN ALUMINUM AND ITS ALLOYS[12]

A. Jostsons[3] J. E. Ferguson[13]
E. L. Long, Jr. K. Farrell

Immersion density measurements and transmission electron microscopy were used to study neutron-induced swelling at temperatures in the range 45 to 60°C in high-purity aluminum and three aluminum-rich alloys commonly used in water-cooled reactors. Aluminum irradiated at these temperatures swells from two distinct effects: (1) radiation voids, which result from the preferred agglomeration of vacancies produced by displacement damage due to fast neutron bombardment, and (2) a silicon precipitate, which is produced by the agglomeration of the solid transmutation product from thermal neutron reactions with aluminum. Swelling due to radiation voids was derived from immersion density values corrected for the effects of silicon production during irradiation. Each material examined exhibited a threshold fluence before voids were detected. Taking 0.1% swelling as the limit of detection of voids in our immersion density measurements, the threshold fluences (>0.1 MeV) range from 2×10^{20} neutrons/cm^2 for 99.9999% Al to 4 to 5×10^{22} neutrons/cm^2 for an overaged 6061 alloy. The rate of swelling with increasing fluence depends on the material and in some cases decreases with increasing fluence. These observations demonstrate that void nucleation depends critically on the impurity content. The best swelling resistance was shown by the 6061 alloy, which contained a high density of dislocations and a coherent Mg_2Si precipitate before irradiation.

TRANSMUTATION-PRODUCED Mg_2Si PRECIPITATION IN AN IRRADIATED Al–2.5% Mg ALLOY[14]

A. Jostsons[3] R. T. King

Irradiation of aluminum alloys in the neutron flux of thermal reactors leads to the creation of clustered point defects from displacement damage and the generation of gaseous transmutation products from (n,p) and (n,α) reactions. These defects arise primarily from the fast neutron component of the reactor spectrum. The thermal neutron component, on the other hand, is responsible for the production of silicon by transmutation of aluminum through the $^{27}Al(n,\gamma)^{28}Al$, $^{28}Al \rightarrow {}^{28}Si + \beta^-$ reactions. Since the solubility of silicon in aluminum is generally very low, transmutation-produced silicon precipitate particles are produced eventually in irradiated aluminum alloys.

Our studies of irradiated specimens of the 5052 aluminum alloy (Al–2.5 wt % Mg) irradiated in HFIR at 55°C to neutron fluences in excess of 1×10^{22} neutrons/cm^2 (>0.1 MeV) and 3×10^{22} neutrons/cm^2 (thermal, <0.414 eV) have revealed a new phase transformation. The transmutation-produced silicon in this alloy combined with magnesium in solid solution to precipitate Mg_2Si, which is responsible for age hardening of the commercially important 6000 series of Al-Mg-Si alloys. The fine (≈40-Å-diam) irradiation-induced Mg_2Si precipitate is distributed uniformly throughout the matrix and on grain boundaries and is mainly responsible for one of the largest irradiation-induced strength increases reported for any aluminum-base alloy. The only vestiges of displacement damage are dislocation loops ($\approx 3 \times 10^{14}$ cm^{-3}); irradiation-induced voids have not been observed even in specimens irradiated in excess of 2×10^{22} neutrons/cm^2 (>0.1 MeV) at 55°C. This resistance to void formation is similar to that observed in commercial Al-Mg-Si alloys heat treated to give a high concentration of fine precipitate particles.

NEUTRON IRRADIATION DAMAGE IN A PRECIPITATION-HARDENED ALUMINUM ALLOY[15]

R. T. King A. Jostsons[3]
K. Farrell

A 6061 aluminum alloy target sleeve from the High Flux Isotope Reactor, originally in a precipitation-hardened condition, was examined for neutron radiation damage after exposure to a maximum fast fluence of 9.2×10^{22} neutrons/cm^2 (>0.1 MeV) and a thermal fluence of 1.2×10^{23} neutrons/cm^2 at 60°C. Voids and a transmutation-produced silicon precipitate caused about 1.1% internal swelling; a surface oxide scale contributed additional swelling. Irradiation-induced strength increases were measured at test temperatures in the range 25 to 200°C and are accounted for in terms of the observed silicon precipitate and an associated dislocation structure. There was also a loss of ductility,

12. Abstract of a paper to be presented at the Fall Meeting of The Metallurgical Society of AIME, Detroit, Oct. 18–21, 1972.
13. Operations Division.
14. Summary of *Scripta Met.* **6**, 447–51 (1972).
15. Abstracted from a paper presented at the Sixth International Symposium on the Effects of Radiation on Structural Materials, ASTM Annual Meeting, Los Angeles, June 26–28, 1972, to be published in the proceedings.

which was most severe at 200°C. The fracture mode remained transgranular over the range of test temperatures.

RADIATION-INDUCED STRENGTHENING AND EMBRITTLEMENT IN ALUMINUM[16]

K. Farrell R. T. King

Commercially pure aluminum (1100 grade) in the annealed condition was irradiated to fast fluences in the range 1 to 3 × 10^{22} neutrons/cm^2 (>0.1 MeV) and to similar thermal fluences at 40 to 55°C, and was then tensile tested at temperatures between 25 and 370°C. The irradiation more than doubled ultimate tensile strength and more than tripled flow stress. This strengthening is due to a fine precipitate of transmutation-produced silicon and an associated dislocation network. Relatively few voids are present and make only a minor contribution to strengthening. The work hardening exponent is severely reduced by irradiation, and there is a significant loss in ductility. At test temperatures below about 150°C, the fracture mode is transgranular. Above 200°C the fracture mode becomes predominantly intergranular, and ductility is further reduced. Intergranular fracture is shown to be associated with the growth and coalescence of cavities on the grain boundaries.

Unirradiated specimens containing cyclotron-injected helium show no hardening and no change in work hardening coefficient but display a loss in ductility at elevated temperatures. We conclude that helium is important in reducing ductility in these specimens and the irradiated ones, but the extent of the embrittlement depends on strength level and helium content.

ELECTRON RADIATION DAMAGE NEAR THE THRESHOLD ENERGY IN ALUMINUM[10]

A. Wolfenden

Foils of high-purity aluminum, both with and without preinjection of about 10 at. ppm He, were electron irradiated in the electron microscope operating in the range 150 to 200 kV. In the helium-doped aluminum, electron damage in the form of black spots was produced at 150 kV after about 90 min irradiation time. They showed contrast effects characteristic of dislocation loops. No such spotlike damage was observed at 150 kV in the uninjected aluminum for bombardment times over 4 hr. Damage was observed in both preinjected and uninjected specimens at 175 and 200 kV. Possible mechanisms for subthreshold damage were examined to see which account for the electron damage observed below the accepted threshold of about 170 kV for aluminum.

DEFECTS IN FAST-NEUTRON-IRRADIATED BORON CARBIDE[17]

A. Jostsons[3] C. K. H. DuBose

Boron carbide irradiated in a fast neutron flux to ^{10}B burnups up to 3% at temperatures in the range 450 to 750°C was studied by transmission electron microscopy. The damage structure is characterized by small cavities surrounded by strong strain fields. The cavity shape is markedly anisotropic, with the major facets predominantly parallel to the rhombohedral (111) plane. These defects exhibit the characteristics of gas-filled bubbles originating presumably from the transmutation reaction $^{10}B(n,\alpha)^7Li$. The strain fields suggest that the gas pressure exceeds the equilibrium pressure required to satisfy surface tension restraints. Within the range of variables studied, increasing irradiation temperature and burnup increase the size of these bubbles.

Intrinsic defects such as grain boundaries, stacking faults, and dislocations appear to act as preferred sites for nucleation of the helium bubbles. Numerous examples have been observed of the coalescence of gas bubbles on grain boundaries and on dislocations so that large cracks are opened up in the irradiated boron carbide.

Postirradiation annealing studies revealed that significant bubble growth does not occur until temperatures exceed about 1400°C. At these higher annealing temperatures, the thermal vacancy supply is adequate to compensate for the excess helium in the bubbles, and the strain fields are eliminated.

NUCLEATION OF DISLOCATION LOOPS IN SOLIDS UNDER IRRADIATION[18]

B. T. M. Loh

An expression for the nucleation of dislocation loops in solids under the coexistence of excess vacancies and

16. Abstract of a paper presented at the Annual Meeting of the American Nuclear Society, Las Vegas, Nev., June 18–22, 1972.

17. Summary of papers to be published in the *Journal of Nuclear Materials* and to be presented at the 18th Annual Meeting of the American Nuclear Society, Las Vegas, Nev., June 18–22, 1972.

18. Summary of *Scripta Met.* **5**, 1049–52 (1971).

interstitials can be obtained by a simple conversion of Katz and Wiedersich's formulation.[19] The conversion involves some proper exchanges of parameters. The only new complication encountered in the loop nucleation is the dependency of the dislocation line energy on the loop radius or the number of interstitials forming the loop. The possible effects of external stresses and gas atoms on loop formation are also discussed.

NUCLEATION OF VOIDS IN SOLIDS CONTAINING EXCESS VACANCIES, INTERSTITIALS, AND HELIUM ATOMS[20]

B. T. M. Loh

A homogeneous nucleation model is presented for void formation in solids containing excess vacancies, interstitials, and helium atoms. The reactions between void embryos and these diffusing species can be represented by pseudobinary kinetics. A steady-state nucleation rate is derived by assuming the existence of a saddle point in the energy surface of the formation of embryos. The result can be reduced to Katz and Wiedersich's[19] case in which no helium is present. A significant enhancement in nucleation rate by the presence of excess helium atoms is predicted.

VACANCIES IN SOLID SOLUTIONS

B. T. M. Loh

The triangle approximation of Kikuchi's cluster variation method has been used to study the thermodynamics of vacancies in binary solid solutions. The calculated results showed that the equilibrium concentrations of vacancies and solute-vacancy pairs depend not only on the commonly studied energy factor B, the interaction energy of forming a solute-vacancy pair, but also on the interaction energy of forming a solute-solvent pair, V. Similarly, the equilibrium distribution of divacancies depends not only on the commonly recognized interaction energy of forming a divacancy, E, but also on B and V. Comparing the results with those calculated from the pair approximation and several dilute solution approximations showed that the pair approximation is good for estimating the concentrations of vacancies and solute-vacancy pairs when V is close to zero. The dilute solution approximations are useful when the temperature is high, V is close to zero, and the values of B and solute concentration are low.

19. J. L. Katz and H. Wiedersich, *J. Chem. Phys.* **55**, 1414 (1971).

20. Abstract of a paper to be published in *Acta Metallurgica.*

WATER DAMAGE IN COMPOSITES OF GLASS FIBER AND POLYESTER RESIN[21]

K. H. G. Ashbee[22]

The nature of cracks produced in five cured polyester resins during exposure to water was studied by a combination of electron-optical techniques. General-purpose polyester resins and "E" and "C" glass fibers all contain water-soluble constituents, dissolution of which by diffused water can generate pockets of very high pressure. Interaction between such pockets of pressure and the elastic field resulting from resin shrinkage during water uptake creates internal resin cracks. By doping isophthalic resins with suitable inorganic salts, the controlled growth of such cracks has been developed into a method for the internal decoration of resins.

The progress of debonding caused by diffused water has been followed in several composite systems by (1) observing an interfacial load transfer index obtained from optical retardation measurements, (2) using fibers as wave guides for a laser beam, and (3) measuring the electrical conductivity at fiber-resin interfaces. Resin shrinkage is partially relieved by molecular orientation in the resin adjacent to fiber ends, and the structure of this orientation during debonding has been investigated by transmission electron microscopy. Resin shrinkage, after debonding is complete, eventually causes cracks to propagate across conical surfaces normal to polyester chain alignments near fiber ends.

DETERMINATION OF THE ENERGY STORED IN COLD WORKED METALS BY CALORIMETRY[23]

A. Wolfenden

The energy relations in the room-temperature tensile plastic deformation of single-crystal and polycrystalline metals have been determined with a single-step isoperibol calorimeter. The method uses the first law of thermodynamics to measure the stored energy as the difference between the mechanical work expended by

21. Abstracted from pp. 1205–22 in *Electron Microscopy and Structure of Materials* (Proc. Fifth Int. Materials Symposium, Univ. Calif., Berkeley, Sept. 13–17, 1971), ed. by G. Thomas, University of California Press, Berkeley, 1972.

22. On leave of absence from the H. H. Wills Physics Laboratory, University of Bristol, England.

23. Abstract of paper presented at the 5th Experimental Thermodynamics Conference, University of Lancaster, April 12–14, 1972; to be published in the Conference Abstracts Booklet.

the tensile machine in deforming the specimen and the energy evolved as heat in the specimen. Integration of the load-elongation curve gives the former term, while measurement of the temperature rise of the specimen during deformation allows the latter term to be calculated. Allowances are made for the elastic deformation of the specimen and machine and for the thermoelastic cooling of the system. The energy stored during deformation has been determined for copper, silver, and aluminum single crystals as a function of strain and crystal orientation, for polycrystalline copper and a gold-silver alloy as a function of strain, and for polycrystalline Cu_3Au as a function of degree of long-range order and strain. The single-crystal results have been used to elucidate theories of work hardening. The polycrystalline data have been compared with some from previous investigations and for the case of copper were in good agreement with those of Williams, obtained for similar specimens and test conditions.

WORK HARDENING THEORIES ANALYZED IN TERMS OF STORED ENERGY DATA[24]

A. Wolfenden

The widespread use of metals can be attributed to their high strength, which may be enhanced by plastic deformation through work hardening mechanisms. It is highly desirable to have a full understanding of all the changes in metallurgical structure produced during plastic deformation and their effects on the properties of the material. Since these changes are many and complex, most interpretations of the work hardening behavior of metals have centered around theoretical and experimental studies of the distribution and interactions of dislocations in single crystals. The experimental results of several recent stored energy investigations on silver, copper, and aluminum single crystals deformed in tension at room temperature and 78°K are used to analyze some modern work hardening theories. Allowances are made for the fact that both dislocations and point defects contribute to energy storage, whereas the theories of work hardening are concerned with dislocations only. The comparison of the theoretical estimates for the stored energy with the experimental data allows some important conclusions to be made about the work hardening theories.

24. Abstract of invited paper presented at the Symposium on Defect Interactions in Solids, May 9–13, 1972, at the Indian Institute of Science, Bangalore, India, to be published in the Proceedings.

TECHNIQUES FOR TRANSMISSION ELECTRON MICROSCOPY OF MICRON-SIZE PARTICLES OF CERAMIC MATERIALS

C. K. H. DuBose G. L. Copeland

Techniques have long been in service for thinning bulk materials for examination by transmission electron microscopy and for the direct viewing of submicron particles, but materials in the intermediate range have generally been inaccessible to examination. We have developed a technique to allow us to examine particles of ceramic materials in the range 1 to 1000 μm in diameter. The specimen, if larger than 20 μm in diameter, is first crushed to produce powders up to 20 μm; these are then blended with −100-mesh aluminum powder in proportions to yield 30 to 40 vol % of the powder particles in the composite. The powders are then loaded into a graphite die and hot pressed in vacuum at 630°C under 280 kg/cm^2 for 30 min. This results in complete densification of the composite. It is then treated as a petrographic specimen and mechanically ground to a thickness of 5 mils, after which it is further thinned by ion bombardment for electron transmission studies. Powder particles of boron carbide 20 μm or less in diameter have been routinely thinned by this technique. In addition, crushed ion exchange resins and pyrolytic carbon and silicon carbide coatings from fuel particles have been examined.

PHASE ANALYSIS STUDIES OF REACTOR MATERIALS

R. E. Gehlbach J. M. Leitnaker J. O. Stiegler
C. R. Brooks[25] J. E. Spriuell[25]

We are studying the precipitation processes in several reactor materials to determine the relationships between microstructure and mechanical properties. By understanding and predicting the role that precipitates produced by aging or irradiation have on properties, we hope to be able to control the initial microstructures to optimize properties of the materials in reactor service. The alloys under consideration include various modifications of Hastelloy N (Molten-Salt Program), type 316 stainless steel (LMFBR fuel cladding), and type 308 stainless steel weld metal in type 304 stainless steel (FFTF and LMFBR vessels). Several experimental alloys are also being studied.

25. Consultant from the University of Tennessee.

Identification and characterization of phases in these systems involve transmission electron microscopy, electron and x-ray diffraction analysis of individual and bulk precipitates, electron probe microanalysis, scanning electron microscopy, optical metallography, and selective etching techniques. High-voltage electron microscopy permits acquisition of high-quality electron diffraction patterns from extremely fine precipitates. We have modified our x-ray diffraction techniques to markedly improve phase detectability, peak resolution, and accuracy. X-ray data are now routinely computer processed, and we are working out computer iteration techniques to determine at least semiquantitatively the concentrations of various phases in a given sample. Correlation and modification of these techniques are permitting microstructural characterization to be approached on a more quantitative basis than before.

A GENERAL PROGRAM FOR CONSTRUCTING MAPS OF KIKUCHI AND KOSSEL LINES[26]

B. T. M. Loh K. H. G. Ashbee[22]

A FORTRAN program has been written for constructing stereographic or gnomonic projections of Kikuchi and Kossel lines and of crystallographic poles and directions. The orientation, solid angle, and magnification of any of these projections can each be varied as required. These projections permit the indexing of Kikuchi and Kossel lines and hence facilitate crystallographic analyses of the electron and x-ray diffraction patterns.

---

26. Abstract of ORNL-TM-3557 (September 1971).

5. Fundamental Ceramics Research

G. P. Smith

This program continues the previous programs on Fundamental and Physical Ceramics and Crystal Spectroscopy. Included are residual results from the former Spectroscopy of Ionic Media program.

FURTHER COMMENTS ON THE DEFORMATION OF HYPERSTOICHIOMETRIC URANIUM DIOXIDE[1]

C. S. Yust C. J. McHargue

The phenomenon of the change of slip system with addition of oxygen to the UO_2 lattice is discussed. A mechanism is proposed to account for both the change in slip system and modification of the dislocation substructure. The proposed mechanism attributes the observed changes to interaction between dislocations gliding on the {001}⟨110⟩ slip system and the oxygen defect clusters introduced by the presence of excess oxygen.

ELECTRON MICROSCOPY OF POLYCRYSTALLINE URANIUM DIOXIDE

C. S. Yust

The deformation of polycrystalline uranium dioxide is being studied in cooperation with J.T.A. Roberts of Argonne National Laboratory. The polycrystalline specimens were prepared and deformed at Argonne; the electron microscope samples were prepared and examined at Oak Ridge. Specimens deformed in four-point bending at temperatures ranging from 1000 to 1700°C at an outer fiber strain rate of 0.92/hr have been examined. In general, the structures observed correlate with the deformation response of the specimen; those specimens observed to be brittle show little dislocation content in the grains and little grain boundary structure, while those deformed in the plastic range show significant dislocation production in many, but not all, grains, as well as generation of grain boundary structure. A typical grain deformation structure is shown in Fig. 5.1, where dislocations are seen interacting with pores in the grain. The numerous pores are residual porosity remaining from the sintering process by which the specimens were prepared. This specimen had been deformed at 1450°C. A grain boundary structure observed in a specimen deformed at 1575°C is seen in Fig. 5.2. The linear features in the boundary are grain boundary dislocations and may be associated with grain boundary sliding. Detailed study of both the grain boundary and grain lattice deformation structures is in progress.

Fig. 5.1. Dislocation array in a deformed grain of polycrystalline uranium dioxide. At left center, a series of dislocations is moving through a region containing a void, while at lower left a set of dislocations appears to emerge from the grain boundary. 13,000×.

1. Abstract of paper submitted to the *Journal of the American Ceramic Society.*

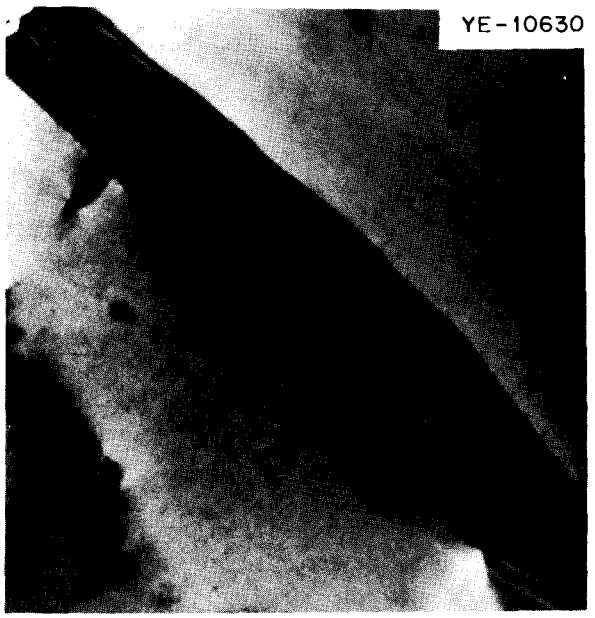

Fig. 5.2. Grain boundary features observed in deformed polycrystalline uranium dioxide. The distribution of the linear defects and their interaction with dislocations intersecting the boundary suggest that these features are grain boundary dislocations. The apparent thickness of the boundary arises from its oblique orientation in a specimen of finite thickness. 31,500×.

DEFORMATION OF UO_2 SINGLE CRYSTALS

C. S. Yust C. J. McHargue

Deformation data collected for both stoichiometric and hyperstoichiometric UO_2 single crystals have been analyzed in terms of the activation volume, which is derived from strain rate sensitivity and stress relaxation tests. In addition, the internal stress in the deforming crystal has been estimated by measurement of stress relaxation after a rapid, partial stress removal. The activation volume values agree excellently with those published[2] for polycrystalline UO_2 over the range of comparable shear stress values. In addition, since the activation volume is inversely related to the applied stress,[3] we analyzed plots of the reciprocal of the activation volume against applied stress and found that the effective stress, the difference between the applied stress and the internal stress, is minimized at about 1000°C. The independent estimation of the effective stress also indicates a minimization of the effective stress at 1000°C. The relative increase in the magnitude of the internal stresses at 1000°C suggests that dislocations interact among themselves or with other defects at this temperature and is consistent with increases in the critical resolved shear stress previously reported for UO_2 crystals in this temperature range.[4] We also observed that just above this temperature range the $\{111\}\langle 011\rangle$ slip system, which is active in hyperstoichiometric UO_2 crystals, reverts to the $\{001\}\langle 011\rangle$ slip system typical of stoichiometric crystals.

2. J.T.A. Roberts, *J. Nucl. Mater.* **38**, 35 (1971).
3. C. Y. Cheng, *Scripta Met.* **4**, 375 (1970).

BORON CARBIDE STUDIES

J. Brynestad R. A. Potter
L. D. Hulett[5]

Efforts are being made to prepare boron carbide specimens that are well characterized and of high purity. By electron spectroscopy and ion etching techniques we have preliminary evidence that oxygen may be present in solid solution in boron carbides.

STOICHIOMETRY CHANGES IN MOLTEN URANIUM DIOXIDE[6]

A. T. Chapman[7] J. Brynestad
J. C. Wilson G. W. Clark

Using induction heating we have been able to internally melt UO_2 samples under oxygen pressures that are controlled and monitored by the H_2/H_2O ratio while minimizing the influence of interfering side reactions. Both hyper- and hypostoichiometric compositions can be readily maintained in molten UO_2, and the change in liquid composition is far more sensitive to small changes in oxygen potential than equivalent stoichiometry variations in the solid. The implications of these data relative to improving single crystal growth from the melt are considered. In addition, the significance of these data to reactor technology is discussed.

HIGH-TEMPERATURE SPECTROMETER

C. R. Boston G. P. Smith

Preliminary measurements have now been made on the recently constructed high-temperature spec-

4. C. S. Yust and C. J. McHargue, *J. Nucl. Mater.* **31**, 121–37 (1969).
5. Analytical Chemistry Division.
6. Abstract of a paper presented at the 74th Annual Meeting of the American Ceramic Society, Washington, D.C., May 7–10, 1972.
7. Consultant from the Georgia Institute of Technology.

trometer. The sample was held inside a cylindrical tungsten susceptor, which in turn was surrounded by a water-cooled quartz jacket and finally by the coil of a 10-kW induction heating unit. The optical absorption spectrum of MgO doped with Ni(II) was measured at various temperatures up to 1600°C.

ABSORPTION SPECTRUM OF $Ca(AlCl_4)_2$:Ti(II)

C. R. Boston J. Brynestad
G. P. Smith

To determine the absorption spectrum of divalent titanium, single crystals of $Ca(AlCl_4)_2$ containing small concentrations of titanium were prepared. Preliminary measurements on the blue-green crystals indicate that the absorption spectrum at low temperatures is similar to that observed for $Ti(AlCl_4)_2$.

ELECTRONIC ABSORPTION SPECTRA OF PLATINUM(II) CENTERS IN LIQUID ALKALI METAL CHLORIDES[8]

G. N. Papatheodorou[9] G. P. Smith

The optical electronic absorption spectra of Pt(II) centers were measured in liquid CsCl, KCl, LiCl, and CsCl-LiCl and KCl-LiCl mixtures over substantial temperature ranges. In CsCl at 650 to 700°C and in the eutectic mixtures below about 400°C the spectrum is that expected for normal square-planar $PtCl_4^{2-}$ complex anions at elevated temperatures. In LiCl and the mixed solvents at elevated temperatures the spectrum is modified by a drawing together of the two spin-allowed bands. This effect is attributed to the polarization of $PtCl_4^{2-}$ by the outer shell of Li^+ ions.

RAMAN SPECTRA OF THE MOLTEN $AlCl_3$-$ZnCl_2$ SYSTEM AND MOLTEN Cs_2ZnCl_4 (ref. 10)

G. M. Begun[11] J. Brynestad
K. W. Fung[12] G. Mamantov[12]

"Evidence was obtained that no discrete complex ion species exist in the liquid system $AlCl_3$-$ZnCl_2$. The chloride acceptor strengths of $AlCl_3$ and $ZnCl_2$ appear to be comparable. Interactions between Al_2Cl_6 and $ZnCl_2$ result in a breaking up of the polynuclear, network-like $ZnCl_2$ structure."

---

8. Abstract of a paper to be submitted for publication.
9. Presently at the James Franck Institute of the University of Chicago.
10. Abstract from a paper, *Inorg. Nucl. Chem. Lett.* 8, 79 (1972).
11. Chemistry Division.
12. University of Tennessee.

6. Fundamental Physical Metallurgy

R. A. Vandermeer

Engineering materials are complex mixtures of perfection and imperfection. We seek to understand the nature and behavior of the defects such as grain boundaries and interfaces, impurity atoms, vacant lattice sites, dislocation configurations, ordered domains, and preferred grain orientations. By investigating the interaction of some of these defects with others in relatively simple, idealistic systems we extract knowledge that is applicable to the understanding of practical materials.

THE DIFFUSION OF POINT DEFECTS NEAR A PRISMATIC DISLOCATION LOOP[1]

W. A. Coghlan M. H. Yoo

Recent theories of irradiation-induced void growth are critically based on the hypothesis that dislocations are better sinks for interstitials than for vacancies. To investigate the origin of this bias, the steady-state concentration of point defects near a prismatic dislocation loop was calculated for point defect supersaturations as well as for thermal equilibrium point defect concentrations. The elastic interaction energy has been calculated by combining Eshelby's sphere-in-hole model and the finite loop solution for the dislocation's stress field. The stress-assisted diffusion of point defects has been treated by using a finite difference solution to the partial differential diffusion equation. This solution allows easy adjustment of boundary conditions and thereby easy application of the results to specific void growth models. We calculated the number of vacancies diffusing in aluminum to and from an interstitial loop with a radius 10 times the Burgers vector. The inclusion of the interaction between the dislocation stress field and a point defect substantially decreases the calculated shrinkage rate as compared to the case in which only concentration gradients control diffusion.

THE USE OF COMPUTER SIMULATION TO INDEX COMPLEX AUGER ELECTRON SPECTRA[2]

W. A. Coghlan

To gain a more thorough understanding of Auger processes and to aid in the interpretation of experimental spectra, Auger electron spectra were computer simulated by using a combination of experimental and theoretical information. Both the electron energy distribution and its more commonly measured first derivative were calculated for simple surfaces and surfaces containing several atomic species. We tried to demonstrate by simulation how secondary electron background, interactions of spectra from different elements, and changes in experimental parameters affect the observed spectra. Spectra have been simulated for a fractured powder-metallurgy tungsten specimen containing Fe, Ni, P, S, O, and C. Figure 6.1 compares these simulated spectra with experimental ones measured by R. E. Clausing of the Structure and Properties of Surfaces Group.

THE ROLLING TEXTURE OF Cu_3Au (ref. 3)

R. A. Vandermeer J. C. Ogle

The rolling texture of a Cu_3Au alloy was investigated by x-ray diffraction to determine what effects degree of long-range order, temperature, and amount of deformation have on texture development. At room temperature, independent of the degree of order, a texture

1. Summary of a paper presented at 1972 Spring Meeting of The Metallurgical Society of AIME, Boston, May 8–11, 1972.

2. Summary of a paper presented at 1971 Fall Meeting of The Metallurgical Society of AIME, Detroit, Oct. 18–21, 1971.

3. Summary of a paper presented at 1972 Spring Meeting of The Metallurgical Society of AIME, Boston, May 8–11, 1972. To be submitted to *Texture*.

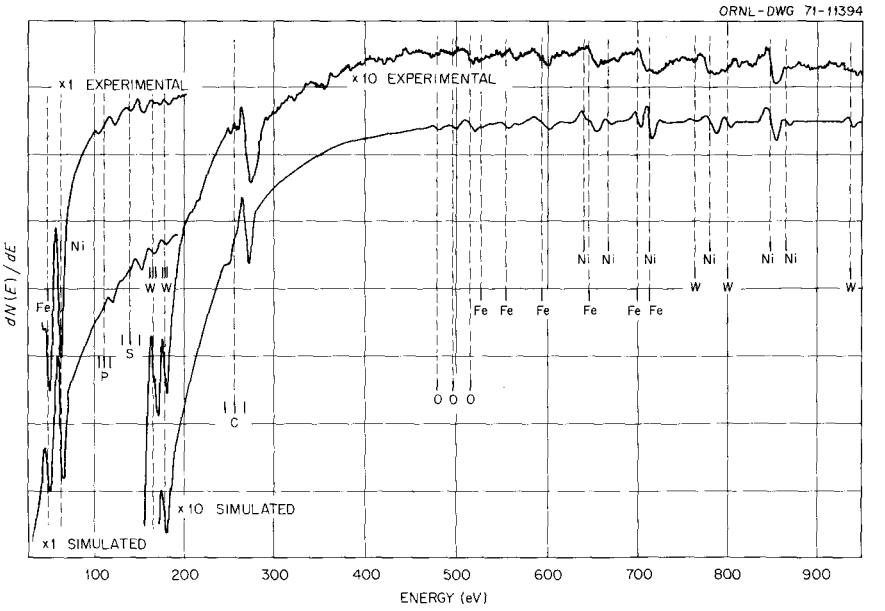

Fig. 6.1. Experimental and simulated Auger spectra for a surface containing W, Fe, Ni, P, S, O, and C.

that may be regarded as a "hybrid" of the prototype face-centered cubic textures of pure copper and 70/30 brass was developed. Upon being rolled at 77°K, however, the disordered alloy tended to be more "brasslike" than the ordered alloy. This result is explained if a stacking fault energy (SFE)–texture reversal analogous to that reported in wire-drawing low-SFE materials is also present for deformation by rolling. The lack of twinning (or another deformation mechanism, such as slip by partial dislocations) in the ordered alloy could be responsible for this turnaround behavior.

THE BEHAVIOR OF GRAIN BOUNDARIES DURING RECRYSTALLIZATION OF DILUTE ALUMINUM-GOLD ALLOYS[4]

R. A. Vandermeer

The main conclusions are:

1. The early stage characteristics of recrystallization in five gold-doped, zone-refined aluminum alloys cold-rolled 40% at 0°C conformed to a grain-edge-nucleated, growth-controlled phenomenological model for recrystallization.

2. The length, l, of the matrix grain boundary edges producing recrystallized colonies (groups of contiguous recrystallized grains strung out along these edges) depended on the penultimate grain size and was longer for larger grain sizes.

3. A modification of the original phenomenological model was proposed and incorporated colony lengthening as well as the usual colony thickening in the growth aspect of recrystallization.

4. The modified model accounts semiquantitatively for discrepancies that exist between the measured recrystallization parameter, k, and the expected one based on the original model when $l < 0.030$ cm.

5. The presence of an $AuAl_2$ precipitate due to aging did not materially alter either the number or the type of nucleation sites for recrystallization but did cause a 10^4-fold increase in grain boundary migration rate, a result that can be rationalized in terms of the solute-drag theory of boundary migration.

6. The activation energy for grain boundary migration in alloys containing greater than 3.4 ppm Au was 25,700 cal/mole and did not vary with the extent of recrystallization. This value was slightly less than that predicted for solute-controlled migration of a "tight" boundary.

7. In the 3.4-ppm alloy a transition in activation energy for boundary migration was observed and attributed to a grain boundary "structure" transformation. An excess vacancy concentration in the

4. Paper presented at 1971 Fall Meeting of The Metallurgical Society of AIME, Detroit, October 18–21, 1971; to be published in *The Nature and Behavior of Grain Boundaries*, ed. H. Hu, Plenum Publishing Corp., New York, July 1972.

boundary region was thought to control the transformation by changing the nature of the solute atom drag from a "porous" to "tight" condition.

8. A theory of vacancy-enhanced grain boundary migration, incorporating the impurity drag concepts, was proposed and used to analyze some of the experimental results.

THE BCC (γ) TO TETRAGONAL (γ°) PHASE TRANSFORMATION IN URANIUM-NIOBIUM-ZIRCONIUM ALLOYS[5]

R. A. Vandermeer

An x-ray diffraction study of the decomposition of the bcc phase in polycrystalline uranium containing nominally 7.5 wt % Nb and 2.5 wt % Zr on cooling from 800°C is in progress. The presence of weak, broad superlattice reflections in the as-quenched tetragonal phase has been interpreted in terms of an atom displacement ordering rather than chemical species ordering.

An intermediate stage in the γ to γ° transition was encountered. This structural state (γ^{s}) showed strong diffracted intensities at positions expected from a bcc structure reflective of the high-temperature phase, but with additional weak, broad diffraction maxima requiring a doubling of the cubic unit cell edges. Correlated ⟨100⟩ atom displacements from certain sites could explain the results. The relationship of the γ^{s} state to the γ° phase may be thought of as the *short*-range atom displacement ordering counterpart to the γ° phase analogous to the short- and long-range chemically ordered states encountered in alloys.

Increasing the quenching rate or the solute composition favors the formation of the γ^{s} state. Aging at low temperatures ($< 200°C$) tends to stabilize the γ° phase.

5. Summary of talk presented at conference on "The Local Structural Order and Decomposition of Ti, U, and Zr-Base BCC Solid Solutions" held at Cornell University, May 15–16, 1972.

7. Physical Property Research

D. L. McElroy

We are pursuing two complementary paths to obtain an improved theoretical and practical understanding of the physical properties of solids. First, we are developing independent, overlapping, and accurate techniques to determine thermal conductivity, λ; electrical resistivity, ρ; Seebeck coefficient, S; specific heat capacity, C_p; coefficient of thermal expansion, α; and total hemispherical emittance, ϵ, of selected solids from 4.2 to 2600°K. Second, we are critically examining experimental results to test theories, to obtain property estimations beyond the range of available measurements, to suggest means to control properties, and to provide better measurements. The data obtained by this research also provide needed input to other projects.

APPARATUS DEVELOPMENT

Critical analysis of equipment and comparison of results from different techniques are yielding better measurements.

Linear Heat Flow Apparatus

J. P. Moore

Analytical and experimental studies of a technique[1] for measuring λ, ρ, and S on small rods from 300 to 1000°K indicated means to reduce measurement uncertainties to under ±1.6%. The analytical heat balance analysis suggested better thermal grounding of specimen heater wires, use of more specimen temperature sensors to sense and fit thermal gradients, and improved thermal contact between the specimen and its heater. Temperature measurement errors were found during tests on chromium when the two wires of a thermocouple were not collinear because the specimen S is high with respect to that of the thermoelements. Knowledge of the wire separations allows a proper temperature measurement correction. Chapter 28 contains λ results on two irradiated graphites using this technique.

A modified linear heat flow apparatus[2] yielded λ results precise to ±0.2% from 80 to 380°K for a high-purity molybdenum sample. A second zone-refined molybdenum sample ($R_{273}/R_{4.2}$ = 4700) of larger cross-sectional area is under test to determine heat leaks.

Radial Heat Flow Apparatus

T. G. Godfrey

The accuracy of λ measurements of powders was improved by modifications that yielded less axial heat flow in a radial heat flow apparatus.[3] These modifications were first suggested by instrumented tests on an NaCl powder sample (backfill material for Nuclear Waste Repository containers). These experimental results were confirmed by a finite difference computer program[4] (HEATING-3) used to solve the three-dimensional heat-conduction representation of the instrumented tests. Measurements of λ using MgO powder,[3,5] a quasi standard, validated the system modifications and indicate a system accuracy that may be limited by bed packing variability but appears to be better than ±2% from 300 to 1100°K.

1. J. P. Moore, D. L. McElroy, and R. K. Williams, "A Technique for Determining Thermal and Electrical Conductivity and Seebeck Coefficient between 300 and 1000°K," paper prepared for submission to *Journal of Applied Physics.*

2. D. L. McElroy, *Metals and Ceramics Div. Annu. Progr. Rep. June 30, 1971,* ORNL-4770, pp. 22–25.

3. J. P. Moore, D. L. McElroy, and R. S. Graves, "Thermal Conductivity of a 58% Dense MgO Powder in Nitrogen" (abstract), p. 711 in *Thermal Conductivity, Proc. 7th Conf., Gaithersburg, Maryland, Nov. 13–16, 1967,* Nat. Bur. Stand. Spec. Publ. **302**, ed. by D. R. Flynn and B. A. Peavy, Jr., National Bureau of Standards, Washington, D.C., September 1968.

4. W. D. Turner and M. Siman-Tov, *HEATING 3 – an IBM 360 Heat Conduction Program,* ORNL-TM-3208 (February 1971).

5. H. W. Godbee, *Thermal Conductivity of Magnesia, Alumina, and Zirconia Powders in Air at Atmospheric Pressure from 200°F to 1500°F,* ORNL-3510 (April 1966).

Computerized Data Acquisition

T. G. Kollie

The ORNL-designed computer-operated data-acquisition system (CODAS) was interfaced with several apparatuses to obtain on-line and instantaneous computation of several properties. This system has a measurement uncertainty (±0.013%, ±0.4 μV) near that of many potentiometers and has a maximum data acquisition speed of 600 readings/sec.

A CODAS:absolute longitudinal λ apparatus yielded λ values on ThN within ±0.2% of potentiometrically determined values.[6] The CODAS:four-probe ρ system found wide time-saving applications. It was used to measure: (1) the room-temperature ρ of 220 calibration samples for eddy-current ρ methods, (2) ρ as a function of time during isothermal transformations in a U-Nb-Zr alloy to determine transformation kinetics, and (3) ρ as a function of temperature of Pt–26% Rh–8% W and Pt–8% W samples, which are possible new heater elements because of their inertness and low value of $(1/\rho)d\rho/dT$. Tests are in progress with a CODAS: expansion apparatus to control the apparatus and obtain length, temperature, and ρ data on the specimen.

Coefficient of Thermal Expansion Apparatus

T. G. Kollie W. M Ewing

A quartz differential dilatometer[7] designed to measure α yielded values for copper within 2% of reported literature values.[8] Each data point requires 4 to 8 hr for temperature stability; thus, use of CODAS on a 24-hr basis will treble data collection.

HEAT TRANSPORT IN METALS

Tungsten

R. K. Williams

Measurements of the electrical resistivity of a zone-refined tungsten sample between 1100 and 2500°K were completed. Analysis of ρ data obtained in helium and argon atmospheres showed that thermionic conduction had a slight (0.07%) effect on the ρ at 2500°K, and the results were corrected for this error. The new results were in good (0.2%) agreement with our previous studies on high-purity tungsten in the temperature overlap range, and the data define ρ from 80 to 2500°K. Analysis of the data indicates the following.

1. The *s-d* scattering formula,[9] which assumes that electrons in *d* states do not contribute to the conductivity, cannot account for the observed behavior.
2. At high temperatures, the nonlinearity of ρ can be attributed to thermal expansion effects.[10] Using data on the effect of pressure[11] to correct the data to constant volume produces a ρ:T curve that is within ±1.6% of linearity between 500 and 2500°K with a ρ intercept of $-3.5\ \mu\Omega$-cm. The problem of analyzing the behavior reduces to explaining the source of an intermediate temperature effect that can cause the observed intercept.
3. No evidence of high-temperature electron-electron resistivity was found.
4. Jones' proposed explanation[12] of the ρ curvature is inconsistent with the experimental electronic Lorenz function,[13] but a term of this type can partially explain the negative intercept.

Transport Properties of Lead and Platinum

J. P. Moore R. S. Graves

The absolute Seebeck coefficient of platinum (S_{Pt}) is used to obtain S values for other materials.[14] Recent values for S_{Pt} from 300 to 1200°K are more representative of reference grade platinum used for thermoelements.[15] From comparison tests with lead, we extended S_{Pt} to 80°K. This experiment yielded λ and ρ values for high-purity lead in the range 80 to 400°K. Although the ratio $\lambda\rho/T$ was within 1.5% of the

6. S. C. Weaver, *An Investigation of the Thermal Conductivity, Electrical Resistivity, and Thermoelectric Power of Thorium Nitride–Uranium Nitride Alloys,* Ph.D. dissertation, University of Tennessee, March 1972.
7. J. P. Moore and T. G. Kollie, *MSR Program Semiannu. Progr. Rep. Feb. 29, 1972,* ORNL-4782, in press.
8. R. K. Kirby and T. A. Hahn, NBS Standard Reference Material 736, November 1969.
9. A. H. Wilson, *Proc. Roy. Soc. (London) Ser. A* **167**, 580 (1938).
10. N. F. Mott and H. Jones, *The Theory of the Properties of Metals and Alloys,* Dover, London, 1936.
11. A. W. Lawson, "The Effect of Hydrostatic Pressure on the Electrical Resistivity of Metals," pp. 1–44 in *Progress in Metal Physics,* ed. by B. Chalmers, Butterworth, London, 1956.
12. H. Jones, "Theory of Electrical and Thermal Conductivity in Metals," pp. 227–315 in *Handbuch der Physik,* vol. XIX, ed. by S. Flügge, Springer-Verlag, Berlin, 1956.
13. R. K. Williams and W. Fulkerson, "Separation of the Electronic and Lattice Contributions to the Thermal Conductivity of Metals and Alloys," pp. 389–456 in *Thermal Conductivity, Proc. 8th Conf.,* ed. by C. Y. Ho and R. E. Taylor, Plenum Press, New York, 1969.
14. N. Cusack and P. Kendall, *Proc. Phys. Soc. (London)* **72**, 898–901 (1958).
15. M. J. Laubitz, *Can. J. Phys.* **47**, 2633–44 (1969).

Sommerfeld limit L_0, the behavior was unusual. Above 170°K, $\lambda\rho/T$ deviates negatively from L_0 rather than asymptotically approaching L_0, perhaps indicating an inelastic electron scattering mechanism.

HEAT CONDUCTION IN ALKALI HALIDES

J. P. Moore

Previous λ results[2] were clouded by the apparent presence of cesium in samples of RbI, RbCl, and RbBr. Thermal conductivity measurements made on a high-purity sample of RbBr and calculations based on Abeles' work[16] indicated that the measured cesium contents in the previous results were wrong. The chemical analysis errors were probably introduced by contamination in the sampling procedure. Thermal conductivity data on the four samples are being analyzed theoretically. The greatest problem in interpreting λ:T behavior is the presence of a linear region above θ_D similar to ones observed in silicon and ThO_2.

RELATED TOPICS

Physical Properties Conversions to IPTS-68

T. G. Kollie W. M. Ewing
T. G. Godfrey J. P. Moore

A method was derived to convert physical properties to the basis of the International Practical Temperature Scale of 1968 if the temperatures had been measured with Pt vs Pt–10% Rh and Pt vs Pt–13% Rh thermocouples and computed with the tables in NBS circular 561. The corrections to the physical property values are of the same order of magnitude (±1%) as state-of-the-art uncertainties in many physical property measurements.

16. B. Abeles, *Phys. Rev.* **131**, 1906 (1963).

In addition, Chromel vs constantan calibrations, which we normally use below 400°K, have been converted to IPTS-68, and programs have been written to permit platinum resistance thermometer use on IPTS-68 down to the boiling point of oxygen. All measurements now made in this laboratory are on the new temperature scale.

Powders Modeling

R. J. Dippennaar[17]

A model was derived to predict the effective λ of a system of solid spheres in a gas, with account being taken for solid-solid contact conduction, parallel and series solid-gas conduction, and radiation. The model predictions compare favorably with a variety of experimental results obtained on thoria microspheres in argon or helium from 400 to 1300°K and from 0.3 to 2.0 atm.

Electrical Resistivity Analysis with HEATING 3

T. G. Godfrey J. P. Moore R. S. Graves

A four-probe dc measurement of ρ appears simple. However, our experiences have shown nonuniform potentials and incorrect ρ values can result if samples have small length-to-diameter ratios, improper current lead placement, or insufficient spacing between the current leads and the voltage taps. The HEATING-3 heat conduction computer code[4] was used to model a four-probe ρ system to study these variables. This thermal simulation of an electrical system verified the sources of measurement difficulties and indicated means to obtain correct ρ values.

17. On assignment from the South Africa Atomic Energy Board.

8. Superconducting Materials

C. C. Koch D. M. Kroeger

We are studying the effects of metallurgical variables on the properties of superconducting materials. The most highly structure-sensitive superconducting property appears to be current-carrying capacity in an applied magnetic field; it is sensitive to mechanical strain, preferred orientation, fabrication and heat-treatment procedures, grain size, and the morphology, composition, and volume fraction of second-phase particles. Meaningful correlation of structure and properties requires detailed knowledge of both. Consequently, much of our effort is devoted to obtaining basic metallurgical information on phase diagrams, transformation kinetics and products, and the microstructures that result from them in systems based upon superconducting materials. The alloy systems of primary interest are those based on niobium and technetium.

C. C. Koch is spending a year on assignment at the Atomic Energy Research Establishment at Harwell, England. He is working on superconductivity with a group supervised by James Lee in the Process Technology Division. In August 1971, D. M. Kroeger, along with M. Strongin and W. Sampson of Brookhaven National Laboratory, toured four laboratories in the Soviet Union that are engaged in research in superconductivity. This trip was part of a program for exchange of technical specialists between the USAEC and the Soviet Union's State Committee for the Utilization of Atomic Energy. The corresponding Soviet team visited here in May 1972.

PRECIPITATES AND FLUXOID PINNING IN A SUPERCONDUCTING Nb-Hf ALLOY[1]

C. C. Koch R. W. Carpenter

The relationship between superconducting fluxoid pinning and precipitate dispersion was investigated in a high-field type II superconducting alloy. The alloy, Nb–38 at. % Hf, is a bcc solid solution above 1200°C; at lower temperatures the equilibrium structure is two-phase: bcc beta and hafnium-rich hcp alpha. The quenched alloy was aged at 600°C. The changes in microstructure during aging were examined by transmission electron microscopy. The attendant changes in superconducting properties – transition temperature (T_c) and critical flux gradient (dB/dr) – were measured by an ac susceptibility technique.

Precipitation at 600°C proceeded by the formation and growth of strained, partially coherent particles termed transition alpha, α_t, in the bcc matrix. Particle size measurements indicated that growth of α_t follows a $t^{1/3}$ coarsening law after times not longer than 0.5 hr. Transition temperature measurements substantiate this finding. Measurements of dB/dr showed little change from the quenched solution behavior for short aging times. This was attributed to the precipitate size being appreciably less than the calculated fluxoid core diameter. After longer times a broad peak in dB/dr developed at a particular value of external field, H. Following its initial appearance the peak moved to lower values of H with further particle growth. Comparison of calculated fluxoid spacing at peak field with average particle spacing calculated from measurements on micrographs indicated a one-to-one correspondence within the experimental limits. The point fluxoid pinning force was calculated approximately from the bulk pinning force, and the results are compared to theoretical predictions.

THE EFFECTS OF SOME 3*d* AND 4*d* SOLUTES ON THE SUPERCONDUCTIVITY OF TECHNETIUM[2]

C. C. Koch W. E. Gardner[3], M. J. Mortimer[3]

For many years there has been interest in the change in superconducting transition temperature (T_c) of an

1. Abstracted from *Phil. Mag.* **25**, 303–20 (1972).

2. Abstracted from a paper submitted for presentation at the Thirteenth International Conference on Low Temperature Physics, August 1972, Boulder, Colorado.

3. Atomic Energy Research Establishment, Harwell, England.

element produced by the addition of magnetic impurities. We have investigated the change of T_c of technetium with composition in alloys containing up to about 5 at. % of Cr, Fe, Co, Ni, or Ru. Technetium has two advantages as the superconducting solvent for studying the effects of such impurity atoms: all the "magnetic" 3*d* elements are extensively soluble in technetium, and the high T_c of technetium (7.8°K) is experimentally convenient. The results of this study were as follows: (1) the initial rate of decrease of T_c with small additions (≈1 at. %) of Co, Ni, and Ru was essentially identical when T_c was plotted against "average group number" (i.e., "rigid band" behavior); (2) the initial rate of decrease produced by iron additions was about 3 times that produced by Co, Ni, or Ru, which suggests that spin fluctuation effects are associated with the Fe sites; (3) in contrast to the behavior of V and Mo additions, which raised T_c, the addition of Cr significantly lowered T_c.

CRITICAL SURFACE AND BULK CURRENT DENSITIES IN THE MIXED STATE OF TYPE II SUPERCONDUCTORS[2]

D. M. Kroeger C. C. Koch W. A. Coghlan

The important materials parameters determining ac losses in type II superconductors in the mixed state are the critical current density, J_c, and ΔH, the increment by which the field at the surface of the specimen may be changed without affecting the internal distribution of flux. For metallurgical studies, measurement of J_c by the ac method developed by Bean is convenient, but surface currents as indicated by the observance of ΔH must be accounted for if the measurement of J_c is to be meaningful. Using the Bean-London constant critical current model and taking account of ΔH, we have calculated, without approximation, the third harmonic of the response of a coil wound around a cylinder as a function of the amplitude of an applied ac magnetic field. Experiments agree well with the calculation, indicating that meaningful measurements of both J_c and ΔH can be obtained in this manner.

EFFECTS OF INTERSTITIAL OXYGEN ON THE SUPERCONDUCTIVITY OF NIOBIUM

C. C. Koch J. O. Scarbrough D. M. Kroeger

Interstitial atoms such as oxygen alter the fundamental superconducting properties of elemental superconductors such as niobium and vanadium. DeSorbo concluded from calculations based on magnetization measurements that the decrease in T_c for niobium with increasing oxygen in solid solution was not due to changes in the density of electronic states at the Fermi level. We are experimentally investigating the influence of interstitial oxygen on the superconducting properties of niobium. We have measured the low-temperature specific heat, the critical temperature, and the magnetization on niobium specimens with interstitial oxygen contents ranging from 40 to 6000 ppm by weight. These results are being compared with various theoretical predictions for T_c.

CRITICAL CURRENT DENSITIES IN SPUTTER-DEPOSITED COMPOUNDS WITH THE A-15 CRYSTAL STRUCTURE

D. M. Kroeger J. O. Scarbrough

The highest known values of T_c and H_{c2} have been found among materials having the A-15 crystal structure. For commercial utilization of such materials it is necessary to find an economical method for producing composite conductors consisting of superconductor in intimate contact with copper or aluminum and having high critical current densities. We have begun a cooperative project with S. Dahlgren and R. Nelson of Battelle Northwest Laboratories to study the superconducting properties of sputtered Nb-Al and Nb-Al-Ge compounds having the A-15 structure. They have high sputtering rate capabilities, which allow them to produce specimens up to several mils in thickness. Thus the method has commercial potential. We are measuring critical current densities in these materials with the aim of optimizing J_c through heat treatments and variation of stoichiometry.

9. Surface Phenomena

J. V. Cathcart

The research of this group is directed primarily at achieving an understanding of the basic mechanisms involved in the oxidation of alloys. We have shown that the oxidation of alloys, even more than that of pure metals, results in the generation of large stresses, which in turn profoundly influence the course of oxidation. These results have led us to identify the mechanical properties of both oxide and parent metal as important parameters in many oxidation processes. We are also concerned with the various stress-generating and stress-relief processes that operate during oxidation; thus our research involves studies of diffusion modes, oxygen solution effects, the plasticity of oxides, vacancy diffusion, and grain boundary oxidation.

This work is divided between two general research projects. One involves the oxidation of a series of uranium-base alloys and the other a set of refractory alloys based on tantalum. Our interest in diffusion studies also continues in measurements of the diffusion rates of oxygen in these refractory alloys.

OXIDATION OF URANIUM-BASE ALLOYS

J. V. Cathcart R. E. Pawel
G. F. Petersen

Uranium and its alloys are excellent subjects for study in research dealing with the influence of stress on oxidation and of the role of oxide and metal mechanical properties in the oxidation process. During oxidation, material transport across the oxide scale occurs almost exclusively via anion diffusion. Thus one of the most effective stress-generating mechanisms, the formation of new oxide at a confined interface, is operative in these alloys. Furthermore, stress relief occurs in a variety of ways in both oxide and in the alloys themselves, and through a proper choice of experimental conditions one can frequently sort out the various mechanisms involved.

Alloys studied were a U-Nb-Zr-Si quaternary, a U-Nb-Zr ternary, and binary alloys of uranium with niobium, zirconium, and molybdenum. Phenomena investigated include the influence on oxide morphology of the relative free energies of formation of UO_2 and the oxides of alloying elements, the plastic deformation properties of oxide scales formed on the various alloys, the influence on oxide plasticity of minor alloying additions such as silicon, and vacancy flow as a stress-relief mechanism in the alloy. In conjunction with the Physical Metallurgy Group we also measured the creep and tensile properties of the U-Nb-Zr and U-Nb alloys between 750 and 900°C.

High-Temperature Oxidation of Uranium Alloys[1]

J. V. Cathcart R. E. Pawel
G. F. Petersen

The oxidation characteristics of U–16.6 at. %Nb–5.6 at. % Zr, U–21 at. % Nb, U–15 at. % Zr, and U–18 at. % Mo in the temperature range 700 to 1100°C are discussed. Stresses as large as 10^6 psi develop in the oxide scales on these alloys as oxidation proceeds, and these stresses lead to large increases in the lateral dimensions of the specimens. The morphology of the oxide scales is described, and a mechanism of stress generation is suggested. Several stress relief processes, including the plastic deformation of both oxide and metal, are discussed.

The Mechanical Properties of Scales and Their Influence on High-Temperature Gas-Metal Reactions[2]

J. V. Cathcart

Surface stresses between 10^5 and 10^6 psi are frequently generated during oxidation of metals, and several stress-generating mechanisms are discussed. The

1. Abstract of paper presented at the Fifth International Congress on Metallic Corrosion, Tokyo, Japan, 21–27 May, 1972. Paper to be published in the *Proceedings* of the conference.

2. Abstract of paper presented at the Symposium on High-Temperature Gas-Metal Reactions, the Metallurgical Society of AIME, Boston, May 8–11, 1972. Paper to be published in the *Proceedings* of the Symposium.

influence of such stresses on scale rupture, structure, and morphology, on diffusion rates within the scales, and on the shape change experienced by oxidation specimens is pointed out. Evidence for extensive high-temperature plasticity in oxides is cited, and the oxidation behavior of two uranium-base alloys is described by way of emphasizing the importance of the mechanical properties of scales in gas-metal reactions.

REFRACTORY METAL OXIDATION

R. E. Pawel

The addition of tungsten and hafnium to tantalum produces alloys with attractive high strength properties; furthermore, these same additions result in a substantial modification of the oxidation characteristics of tantalum. We are attempting to evaluate the roles of these alloying elements in the oxidation process. Alloys investigated include Ta–10 wt % W and two commercial alloys, T-111 (Ta–8 wt % W–2 wt % Hf) and T-222 (Ta–10 wt % W–2.5 wt % Hf–0.01 wt % C). The oxidation kinetics, oxide morphology, and generation of stress during the early stages of oxidation of the T-222 alloy have been examined from 500 to 800°C. Similar sets of experiments with the other alloys are in progress.

Typical "breakaway" oxidation kinetics was observed for all alloys at the lower temperatures, and all showed a resistance to breakaway above 700 or 750°C, although the time of breakaway and the temperature at which breakaway was suppressed were characteristic of the individual alloys. Determination of activation energies of oxidation and of stress generation in the pre-breakaway stage of oxidation indicated that the rate-determining step in the oxidation process for all these alloys was diffusion through the oxide scale, while the stress generation studied in our flexure measurements was related to strains in the surface layers of the alloys associated with the solution of oxygen in the substrate metal. These alloys are also subject to extreme embrittlement during oxidation, a process which in some instances leads to the disintegration and even ignition of the specimens.

The Ignition of Tantalum-Base Alloys during Gaseous Oxidation[3]

R. E. Pawel J. J. Campbell

An example of a unique form of catastrophic oxidation was found for the tantalum-base alloys Ta–10% W, T-111, and T-222, in which specimens ignited after prolonged oxidation at elevated temperatures. We characterized this behavior experimentally and propose a mechanism. The phenomenon is the final step in a sequence that involves oxygen penetration, severe grain-boundary embrittlement, and finally a sudden disintegration of the specimen causing violent ignition.

Impurity Distributions in Anodic Films on Tantalum[4]

R. E. Pawel J. P. Pemsler[5] C. A. Evans, Jr.[6]

Anodization of tantalum in electrolytes containing ions of phosphorus or flourine incorporated a quantity of these elements into the anodic film. While phosphorus was concentrated in the outer portions of such films, flourine was attracted to the oxide-metal interface. With an ion-microprobe mass spectrometer we examined the concentration profiles of these elements in films formed by a variety of anodization procedures. These experiments demonstrated the usefulness of the IMMS as a tool for such work and, in addition, furnished information on the characteristics of film growth and the distribution and movement of these impurities. The decrease in the adherence of the anodic films by flourine-rich layers at the oxide-metal interface was also described.

DIFFUSION OF OXYGEN IN REFRACTORY METALS

R. E. Pawel

We are testing the feasibility of using our flexure technique to determine oxygen diffusion rates in refractory metals and their alloys. When oxygen is allowed to diffuse into only one side of a thin specimen, the resulting dilation of the surface layers of the specimen causes the sample to flex, and for carefully controlled boundary conditions, a correspondence exists between the kinetics of this flexing process and the rate of oxygen diffusion.

We have applied this technique to the measurement of the diffusion coefficient of oxygen in tantalum at 800°C. Using only a single correlation point (the point of maximum flexure), five experiments yielded values of the diffusion coefficient ranging from 3.4 to 4.8 $\times 10^{-8}$ cm^2/sec. The average value, 4.3 $\times 10^{-8}$ cm^2/sec, agrees very well with that determined by conventional techniques (4.8 $\times 10^{-8}$ cm^2/sec). The success of these initial experiments indicates that we have a very sensitive, simple, and rapid method for the study of oxygen diffusion in systems where oxygen solution effects play an important role in the oxidation process.

3. Abstract of paper to be presented to the Electrochemical Society, Oct. 8–13, 1972, Miami Beach, Florida.
4. Abstracted from *J. Electrochem. Soc.* **119**, 24–29 (1972).
5. Ledgemont Laboratory, Kennecott Copper Corp.
6. Materials Research Laboratory, University of Illinois.

10. Theoretical Research

J. S. Faulkner

We have contributed significantly to the development of a number of techniques that are useful in theoretical solid state physics, particularly in areas that are most relevant within a materials science context. We use the Korringa-Kohn-Rostoker (KKR) method for band theory calculations on metals and metallic alloys, the discrete variational method (DVM) for band theory calculations on ionic and covalent compounds, and the coherent potential approximation (CPA) for treating disordered alloys and amorphous materials. We are continuing to develop and improve on these techniques and to use them to understand the physical properties of technologically interesting materials.

COMMENTS ON THE COHERENT POTENTIAL APPROXIMATION FOR DILUTE ALLOYS[1]

J. S. Faulkner

By simple algebraic manipulations we obtain a set of equations that are useful for discussing the CPA for alloys in the low concentration limit. These equations apply to an arbitrary set of nonoverlapping potentials. It is seen how the CPA approaches the same limit as the averaged-t approximation as the number of scatterers becomes very small for this most general case. The averaged-t approximation in its usual form for electrons diverges from the CPA for very low concentrations, but a similar approximation originally proposed for phonons diverges more slowly.

PRESSURE-INDUCED SUPERCONDUCTIVITY IN CESIUM[2]

G. M. Stocks G. D. Gaspari[3]
B. L. Gyorffy[3]

A theoretical attempt is made to understand the occurrence of superconductivity in cesium under pressure, assuming that electron-phonon coupling is the only source of pairing interaction. As was recently shown,[4] the d-resonances of the muffin tin crystal potential play a dominant role in determining the magnitude of the electron-phonon coupling constant. A band structure calculation by one of us,[5] using the self-consistent potential of Averill,[6] indicates that in cesium the Fermi energy, E_f, moves up toward the d resonance in the unoccupied part of the band when the metal is compressed. Using the result of this calculation we estimate the superconducting transition temperature, T_c, in bcc Cs at zero pressure and in fcc Cs at 43 kilobars. We find that as the pressure changes, T_c is greatly enhanced by E_f having moved closer to the resonance. In conclusion we discuss the possibility of observing superconductivity at 42 kilobars.

ELECTRONIC DENSITIES OF STATES OF Ag-Pd ALLOYS[7]

G. M. Stocks R. W. Williams[8]
J. S. Faulkner

Results of calculations of electronic densities of states functions for random substitutional Ag-Pd alloys are presented. The calculations are based on the coherent potential approximation and a model that has proved useful for discussing the Cu-Ni alloy system.[9] For low Pd concentrations the large separation in energy between the d-scattering resonances associated with Ag and Pd sites in Ag-Pd alloys results in the formation of an impurity d subband of approximately Lorentzian

1. Abstract of a paper presented at the March meeting of the American Physical Society, Atlantic City, N.J., Mar. 27–30, 1972.
2. Abstract of a paper to be presented at the Low Temperature Physics Conference, Boulder, Colo., Aug. 20–26, 1972.
3. Physics Department, Bristol University, Bristol, England.
4. G. D. Gaspari and B. L. Gyorffy, *Phys. Rev. Letters* **28**, 801 (1972).
5. G. M. Stocks, to be published.
6. F. W. Averill, *Phys. Rev.* **B4**, 3315 (1971).
7. Abstract of a paper to appear in the *Journal of Physics.*
8. Present address: University of Vermont, Burlington.
9. G. M. Stocks, R. W. Williams, and J. S. Faulkner, *Phys. Rev. Lett.* **26**, 253–56 (1971); *Phys. Rev.* **B4**, 4390–4405 (1971).

shape midway between the Ag *d*-band structure and the Fermi energy. As the Pd concentration is increased the Pd subband grows at the expense of the Ag subband and develops structure at approximately 50% Pd; at this concentration the high density of states part of the Pd *d* subband begins to intersect the Fermi energy. The calculated densities of states are discussed in the light of available experimental results of photoemission and low-temperature specific heat experiments.

FIRST-PRINCIPLES CALCULATION OF THE OPTICAL ABSORPTION IN DIAMOND[10]

A. R. Lubinsky[11] D. E. Ellis[11]
G. S. Painter

The optical absorption expressed as the imaginary part of the dielectric function, $\epsilon_2(\omega)$, was obtained from a first-principles energy band structure calculated without empirical adjustment. The use of k-dependent oscillator strengths improved the agreement with experiment compared to that obtained with averaged matrix elements. Although the structure in the low-energy region suggests inherent shortcomings in the energy band model, the one-electron theory, when implemented without further approximation, does give good agreement with experiment for the magnitude and position of the main peak and the general shape of $\epsilon_2(\omega)$ over a large energy range.

10. Abstract of a paper to appear in the *Physical Review*.
11. Physics Department, Northwestern University, Evanston, Ill. 60201.

A COMBINED GREEN'S FUNCTION–DISCRETE VARIATIONAL METHOD FOR CALCULATING THE ELECTRONIC STRUCTURE OF CRYSTAL COMPOUNDS[1]

G. S. Painter

The recently developed discrete variational method[12] (DVM) has been combined with the Korringa-Kohn-Rostoker method[13,14] (KKR) to form a flexible, efficient technique applicable to crystalline compounds. Solutions to the muffin-tin average of the full Hamiltonian are obtained from the KKR and used as basis functions for the DVM, which has the capability to use unrestricted basis sets and a wide class of operators in the Hamiltonian. A scheme has been developed to use KKR orbitals from several symmetry points in k-space to derive a basis at arbitrary wave vector, forming a precise, rapid interpolation procedure. At any stage, variational freedom can be increased by including other functions to extend the KKR basis.

12. D. E. Ellis and G. S. Painter, *Phys. Rev.* **B2**, 2887 (1970).
13. J. Korringa, *Physica* **13**, 392 (1947).
14. W. Kohn and N. Rostoker, *Phys. Rev.* **94**, 1111 (1954).

11. X-Ray Diffraction

B. S. Borie H. L. Yakel

Our laboratory maintains general capabilities in x-ray diffraction methods and theory, especially as they find application in metallurgical and ceramic research. We apply these abilities to assist other groups in their studies of materials, and to our own programs of basic research in fields where x-ray diffraction can make a major contribution.

In the latter areas, we report progress in the analysis of local structural order in bcc alloys, the use of energy-sensitive detectors in recording powder diffraction data, the correlation of x-ray diffraction data from neutron-irradiated boron carbides with likely structural damage, the development of x-ray fluorescence techniques suitable for trace element analysis, and the understanding of experimental and theoretical factors that affect small-angle x-ray scattering experiments.

ROUTINE ANALYSES

R. M. Steele H. L. Yakel

Routine diffraction experiments were performed on 730 samples during the reporting period. Results for those samples originating in the Metals and Ceramics Division are cited in other sections of this report.

The use of the stepping microdensitometer in the measurement of photographically recorded data has produced the sought advantages in time and labor, especially with the development of time-sharing computer programs to assist in final analysis of results.

LOCAL STRUCTURAL ORDER IN BCC ALLOYS

The Short-Range Structure of Titanium and Zirconium BCC Solid Solutions[1]

B. S. Borie

Under certain conditions, titanium-zirconium solid solutions that have partially transformed to the omega phase exhibit deviations from periodicity in their diffraction patterns. The primary characterisitcs of the diffraction pattern are: (1) There are two classes of Bragg maxima. Those common to both the omega phase and the parent bcc phase remain sharp and unshifted in reciprocal space. Those associated only with the omega phase are diffuse and shifted in either direction parallel to the omega c^* axis. (2) The broadening of the Bragg maxima is such that the diffuse scattering is mainly in planes whose normal is the omega c^* axis. (3) The sharp unshifted Bragg reflections exhibit a large Debye-Waller-like factor, so they decrease rapidly in intensity with distance from the origin in reciprocal space. This effect is not of thermal origin.

A model is proposed to account for these observations. The model consists of associating three subvariants with each omega-phase variant. The kinematic double sum computed with the model exhibits all of the properties of the experimentally observed intensity distribution. The magnitude of the peak shifts is controlled by the average dimensions of each subvariant, and the direction of the shifts depends on the nature of the interfaces between them.

The Decomposition of Uranium-Base BCC Alloys[1]

H. L. Yakel

The bcc (gamma) alloys in the U-Mo, U-Nb, and U-Nb-Zr systems decompose to equilibrium phases via a series of metastable intermediates. In analogy with bcc zirconium and titanium systems, these phases were once thought to be chemically ordered superstructures, but later work proved they were based principally on regular atom displacements.

The degree of distortion from the bcc structure decreases with increasing solute concentration in alloys quenched from the gamma phase field and increases as a

1. Summary of paper presented at the Conference on the Local Structural Order and Decomposition of Titanium, Uranium, and Zirconium-Base BCC Solid Solutions, Cornell University, Ithaca, New York, May 15–16, 1972.

given as-quenched structure is aged. At high solute contents a phase designated γ^s appears in as-quenched crystals; here atoms in the gamma structure are shifted by displacement waves traveling in $[100]_\gamma$ directions with nodes at $\{100\}_\gamma$ planes. The waves persist only over short distances in the lattice, and γ^s may be regarded as the displacement analog of a short-range chemically ordered structure. Aging γ^s or quenching alloys with less solute produces a phase designated γ°, the long-range-ordered displacement structure corresponding to γ^s. This intermediate has tetragonal symmetry, is isostructural with β-neptunium, and like γ^s shows no long-range chemical order.

Prolonged aging, aging at higher temperatures (300–500°C), or quenching alloys with still less solute produces a monoclinic structure called α'', closely related to α-uranium. If the alloy has passed through the γ° stage, the atom displacements in that phase favor 4 of the 12 possible α'' orientations; in addition, the $\gamma \rightarrow \gamma^s \rightarrow \gamma^\circ$ transition is stress sensitive, and the net result is a "memory" effect reminiscent of the titanium-nickel transformations. The γ^s, γ°, and α'' phases appear to form from the parent γ without compositional change in single grains.

The last metastable intermediate produced by decomposing uranium-base bcc alloys en route to equilibrium is an orthorhombic structure called α', which is still more closely related to the stable α-uranium phase. It forms from either γ° or α'' with rejection of solute into a metastable solute-rich bcc phase.

Atom displacements involved in the $\gamma \rightarrow \gamma^s \rightarrow \gamma^\circ$ transitions represent a new variant for the relaxation of a bcc alloy subject to elastic instabilities. They seem to be unique to uranium-base systems, and in particular to the uranium-rich ends of these systems. We note that whereas the displacements leading to omega-phase formation increase the coordination numbers of atoms from 8 to 11 or 14, those leading to γ^s or γ° decrease the number of closest neighbors from 8 to 4. This would seem to correlate with the 12-fold coordinations characteristic of stable hcp α-zirconium or α-titanium and the four closest neighbors found in stable α-uranium.

Local Atomic Arrangements in Ta-Mo and Ta-Nb BCC Alloys[2]

R. E. Predmore[3] R. J. Arsenault[3]
C. J. Sparks, Jr.

Both Ta-Mo and Ta-Nb binary phase diagrams show continuous bcc solid solutions. Tantalum-niobium alloys are known to show no solution hardening. Both kinds of atoms have the same 2.86-Å size, as determined from the distance of closest approach in their elemental cubic form. However, tantalum and molybdenum show a large hardness increase with addition of the other up to a broad maximum near 50 at. %. In this case, the molybdenum atom is 5% smaller. Short-range order was observed for the Ta-Mo alloys by diffuse x-ray scattering. The modeling of these results showed a strong preference for the solute atom to have unlike nearest neighbors. In addition, the distances between atom pairs also obtained from the x-ray diffuse scattering showed the Mo-Mo first neighbor atom pairs to be closer, whereas the Ta-Mo nearest neighbor pairs were separated further than calculated from the average lattice parameter. X-ray diffuse scattering from Ta-Nb alloys gave no evidence of short-range order nor of the atoms being displaced from the sites of the average structure.

RAPID RECORDING OF POWDER DIFFRACTION PATTERNS WITH Si(Li) X-RAY ENERGY ANALYSIS SYSTEM: W AND Cu TARGETS AND ERROR ANALYSIS[4]

C. J. Sparks, Jr. Dale A. Gedcke[5]

X-ray diffraction patterns using continuous radiation from copper and tungsten target x-ray tubes and detected with a lithium-doped silicon energy analysis system are presented. Errors casued by a misaligned diffractometer and x-ray penetration into the sample are shown to be more difficult to correct and larger in magnitude than errors arising from energy calibration. All these errors can be minimized by mixing a standard with the unknown sample.

The energy resolution of the detector influences the breadth of the diffraction peaks more strongly than the standard slit systems available with commercial diffractometers. Thus, to reduce the recording time and maintain the same standard deviation for the data, one should increase the sizes of the front and receiving slits, including the Soller slits. X-ray energy diffraction patterns can be recorded with standard deviations less than ±0.001 Å in the interplanar spacing with only 200

2. Contribution to *X-Ray Study on Strength and Deformation of Metals,* proceedings of the 1971 Conference on the Mechanical Behavior of Materials, Kyoto, Japan, August 1971.
3. Engineering Materials Group, University of Maryland.
4. Abstract of paper to be published in the proceedings of the 1971 Denver Conference on Applications of X-Ray Analysis, *Advances in X-Ray Analysis,* vol. 15.
5. ORTEC, Inc., Oak Ridge, Tenn. 37830.

sec measurement time using the standard diffractometer slit system. Copper targets are probably as useful as tungsten even though they give only about one-third the continuous intensity. Copper has fewer interfering characteristic lines, and its use permits convenient conversion to normal θ-scanning diffractometer operation.

CRYSTAL STRUCTURES OF UNIRRADIATED AND NEUTRON-IRRADIATED BORON CARBIDES

H. L. Yakel

Lattice parameters of unirradiated and irradiated boron carbides of interest to the FBR Neutron-Absorber Materials Program are summarized in Chap. 14.

Variations of lattice parameters with composition in samples prepared by solid-state reaction at 2000°C may be interpreted in terms of two regions around an ideal $B_{13}C_2$ (B_{12}·CBC) composition. At higher carbon contents, carbon substitutes for icosahedral boron atoms, expanding the rhombohedral a_0 parameter but leaving the rhombohedral angle unaffected. In the hypostoichiometric region, boron enters interstitial positions, leaving the rhombohedral a_0 parameter unchanged but increasing the angle α.

Of course, it is impossible to obtain boron-to-carbon ratios beyond 9 by filling interstitial sites only, so that an additional loss of carbon from some chains would have to be invoked if the chemical analyses reported in Chap. 14 for these samples are accepted. In any case, the validity of this hypothesis must be tested by density measurements.

We previously reported[6] irradiation of natural boron carbide crystals to 3, 28, and 96% ^{10}B burnups (1.7×10^{18}, 1.7×10^{19}, and 1.7×10^{20} neutrons/cm^2, >1 MeV, respectively) at 54°C. Results of experiments with these crystals follow.

Crystals irradiated to 96% ^{10}B burnup are seemingly metamict in that they retain morphology but give x-ray diffraction patterns characteristic of an amorphous structure. The measured densities of two such irradiated crystals were 1.78 and 1.84 g/m^3.

Crystals irradiated to 28% ^{10}B burnup give x-ray diffraction patterns with broad maxima at each reciprocal lattice point. Sharp components are not observed. The anisotropy of the lattice parameter changes is qualitatively similar to that observed for the ORR-irradiated crystals,[6] but quantitative differences in the relative expansions and contractions are evident.

Crystals irradiated to 3% ^{10}B burnup yield x-ray diffraction data resembling those from the ORR-irradiated crystals[6] in that each Bragg reflection has a sharp and a diffuse component. The artificial temperature factor affecting the former is less noticeable for the HFIR-irradiated crystals, however, and the diffuse maxima are less intense. Lattice parameter changes again show anisotropy, with the cell volume of the sharp maxima slightly expanded and that of the diffuse maxima slightly contracted relative to the probable unirradiated value.[7]

X-RAY FLUORESCENCE FOR ANALYSIS OF TRACE ELEMENTS[8]

C. J. Sparks, Jr. L. A. Harris

The selection of monochromatic radiation for excitation in x-ray fluorescence analysis as opposed to the use of white radiation reduced the background 10- to 100-fold, thus enhancing the signal-to-noise ratio. Molybdenum $K\alpha$ radiation has been monochromated with successive compression-annealed pyrolytic graphite monochromators until the spectral purity of the radiation is sufficient to contribute a negligible amount to the background. We then measured the contribution to the background from Mo $K\alpha$ x rays that do not give up all their energy inside the active volume of the lithium-doped silicon detector and hence give rise to pulses corresponding to lower energies. This detector and electronic background is added to the background from Mo $K\alpha$ radiation that undergoes photoelectric absorption in the specimen of interest, producing bremsstrahlung.

Knowing these background contributions, we can calculate the ultimate detectable limit that is permitted by the x-ray fluorescence analysis technique. In the more favorable cases of determining heavy-element concentrations in lighter element crystalline matrices, the detectable limit is below 50 parts per billion. Our present effort is to extend our measurements to cover a wider variety of elements in various matrices.

6. L. A. Harris and H. L. Yakel, *Metals and Ceramics Div. Annu. Progr. Rep. June 30, 1971*, ORNL-4770, p. 36.

7. Crystals employed here were not characterized by individual estimations of lattice parameters and densities before irradiation. Subsequent measurements have proven that the Norton boron carbide crystals available to us are not homogeneous with respect to these properties. Statements about detailed parameter changes produced by irradiation of such crystals must therefore await experiments in which individual preliminary characterizations are made.

8. Funded by the National Science Foundation.

A UNIFIED THEORY OF ABSOLUTE INTENSITY MEASUREMENTS IN SMALL-ANGLE X-RAY SCATTERING[9]

R. W. Hendricks

A general equation relating the intensity (in electron units) scattered at small angles by a sample to the power received by the x-ray detector in a small-angle collimation system is developed. The equation includes the effects of a nonuniform incident beam and a nonuniformly sensitive detector. The theoretical bases for various experimental methods of measurement of the power in the incident beam are discussed. These include primary methods, such as ionization chambers and attenuation by multiple foils or mechanical devices, and secondary methods, which involve the measurement of scattering from standards such as gases, liquids, or amorphous scatterers for which the scattering may also be computed in absolute units.

9. Abstract of paper accepted for publication in the *Journal of Applied Crystallography.*

THE ROLE OF SOLLER SLITS IN SMALL-ANGLE SCATTERING COLLIMATION SYSTEMS[9]

R. W. Hendricks

In small-angle x-ray scattering (SAXS) the effects of angular divergences in the incident and scattered beams are accounted for by the introduction of weighting functions. Some SAXS collimation systems use Soller slits immediately in front of the receiving slit. Up to now, no proposed theory allows the quantitative evaluation of an "effective" slit-length weighting function for small-angle diffractometers that make use of Soller slits. Hence, correct collimation corrections could not be performed on data gathered with this type of collimation. In this communication the necessary theory is developed and illustrated with an example. Disadvantages connected with the use of Soller slits in SAXS experiments are discussed.

Part II. Fast Reactor Technology

12. Advanced Fast Breeder Reactor Fuel Development

J. L. Scott

The goals of this program are to investigate the properties and behavior of those uranium- and plutonium-base ceramic fuels that we term conductors – such as the mononitrides, carbonitrides, and monocarbides – and to compare their potential as liquid-metal fast breeder reactor (LMFBR) fuel with that of $(U,Pu)O_2$, which by comparison is an insulator. Since the thermal conductivity of the ceramic conductors is about ten times that of $(U,Pu)O_2$, one could theoretically operate a conductor at ten times the power density with the same central temperature. In practice, heat transfer limitations, thermal stresses in the cladding, and high rates of swelling at high temperatures limit the power density to about two or three times that of $(U,Pu)O_2$ – still a challenging improvement. Additionally, the margins for transient overpower are much higher in the ceramic conductors than in $(U,Pu)O_2$.

To evaluate the true potential of these fuels, we need to define the structures, composition, and quality control required to achieve 150,000 MWd/metric ton at peak linear heat ratings of 30 to 50 kW/ft. We must also demonstrate the possibility of a low-cost fuel cycle for manufacturing fuel with the needed properties. Our work is oriented primarily toward demonstrating the irradiation performance of (U,Pu)N at high burnups and high heat ratings. Therefore, much of our effort is devoted to fabricating and characterizing fuel for irradiation testing.

Other work on nitride fuels is reported in Chap. 22.

IRRADIATION TESTING

T. N. Washburn

Thermal Flux Tests

The initial series of irradiation tests are two noninstrumented capsules of four pins each in the ETR. These "screening" tests are to determine the performance of nitride fuel synthesized from metal. The peak linear heat rating is 30 kW/ft to burnups of 50,000 and 100,000 MWd/metric ton. The fuel is cold-pressed and sintered pellets with densities from 86 to 91% of theoretical, and the fuel pins have a 0.010-in. radial gap between the fuel pellet and cladding, filled with NaK-19 to enhance heat transfer.

Capsules 43-N1 and 43-N2 were inserted into ETR in December 1970; 43-N1 continues in irradiation, and 43-N2 was removed from the reactor in January 1972 after achieving a burnup level of about 5% fissions per initial actinide metal atom (FIMA). Capsule 43-N2 is currently in postirradiation examination at Los Alamos Scientific Laboratory (LASL). Betatron radiographs of the irradiated capsule showed the only significant change from the preirradiation neutron radiograph to be numerous cracked pellets in each fuel pin, an entirely expected condition from operation at 30 kW/ft linear heat rate. Gamma scanning, both for gross activity and for several radionuclides of interest, revealed only normal fission product distribution. Diameters of the fuel pins showed negligible deviations from preirradiation values. All information obtained to date indicates that the fuel pins performed very satisfactorily.

The postirradiation examination of capsule 43-N2 will be continued at LASL in FY 1973, and technical responsibility for capsule 43-N1, which is still being irradiated, was transferred to LASL on June 30, 1972.

Fast Flux Tests

E. J. Manthos T. N. Washburn

Fabrication was completed on seven unencapsulated fuel pins, five for testing in EBR-II and two as spares or replacements. Test parameters and description of these

fuel pins were previously reported.[1] All aspects of the fabrication were satisfactory except that the sodium bond between the fuel pellets and cladding showed evidence, by eddy-current testing, of voids in excess of the established $^1/_{16}$-in.-diam. standard. The sodium bonding was performed by ultrasonic vibration, which had proven to be satisfactory for bonding UN fuel pellets in both development pins and two UN-fueled dummy pins loaded at the same time as the (U,Pu)N fuel pins. We were not able to establish why there was a difference in the quality of sodium bond with (U,Pu)N instead of UN pellets. Since this program was being phased out, the pins were shipped to Battelle Columbus Laboratory for bonding by their established centrifuging technique. After centrifuging, the bond quality was satisfactory, and the fuel pins were shipped to LASL, who has been assigned responsibility for this program.

FABRICATION OF (U,Pu)N FUEL

E. S. Bomar

This program was terminated, and work during this period was limited to writing the results of examinations to characterize fuel pellets for EBR-II irradiation tests and to disposing of the residual fuel materials.

We had residual fuel in three forms: arc-cast uranium-plutonium ingots, sintered pellets, and powder. Since the powder is pyrophoric, it was necessary to convert it to a stable form before shipping to a recovery point. On the assumption that the nitride powder would oxidize readily, we treated several batches in argon plus oxygen or air mixtures at temperatures to 750°C. The results varied from one batch of powder to another and ranged from complete oxidization in some instances to only superficial oxidation in others. Since use of the available furnaces did not assure the formation of a stable oxide powder, we therefore dissolved the nitride powders in nitric acid. About 1.5 kg of nitride powder was treated in this manner. All of the residual fuel materials were then shipped to recovery sites.

1. E. J. Manthos, M. K. Preston, and J. H. Erwin, *Metals and Ceramics Div. Annu. Progr. Rep. June 30, 1971*, ORNL-4770, p. 61.

13. Compatibility of Steam Generator Materials

P. Patriarca J. R. Weir, Jr.

Two programs are under way to investigate the behavior of steam generator materials under potential service conditions in an LMFBR heat transport system. One program concerns the post-test examination of a failed sodium-to-steam steam generator, and the second involves the corrosion testing of representative materials in steam, with and without chloride and caustic as contaminants.

EXAMINATION OF ALCO/BLH STEAM GENERATOR

J. H. DeVan G. M. Slaughter

We have investigated the chemical and metallurgical condition of the Alco/BLH steam generator[1] following its removal from the Sodium Components Test Installation at the Liquid Metal Engineering Center. Our examination centered around the upper tube sheet, which was the site of three tube failures, and the lower tube sheet, which was extensively cracked.

Our preliminary findings[2] can be summarized as follows:

1. The Alco/BLH steam generator was fabricated with procedures adequate to obtain good quality of construction. However, numerous tube-to-tube-sheet fillet welds exhibited small weld cracks, and the weld throat thickness was marginal (Fig. 13.1).

2. Cracks in the lower tube sheet are almost totally confined to type 316 stainless steel sections and appear to have been caused by stress corrosion. As shown in Fig. 13.2, one system of cracks linked several tube crevices that had contained sodium with a small opening into the water side of the tube sheet. Another system of cracks appeared to enter from the air side of the tube sheet and to connect with the former crack system.

3. Tube leaks in the upper tube sheet were caused by caustic stress-corrosion cracking, which initiated in the sodium-filled tube crevices. We believe that the stress-corrosion conditions were set up by leakage of water into the tube crevices through defective tube-to-tube-sheet fillet welds.

4. Our examination revealed heavy corrosion of shell-side tube surfaces in the sodium vapor–argon gas space immediately below the top tube sheet. The corrosion was associated with the collection of sodium-steam reaction products (Fig. 13.3) and consumed up to 0.040 in. of the type 316 stainless steel surfaces.

5. Steam generator surfaces that had been exposed to liquid sodium showed no evidence of either general or stress-assisted corrosion.

Referring to Fig. 13.2, there are at least three alternative explanations for the onset of stress-corrosion conditions in the lower tube sheet. The water side of the tube sheet was protected by a $\frac{3}{8}$-in.-thick Inconel

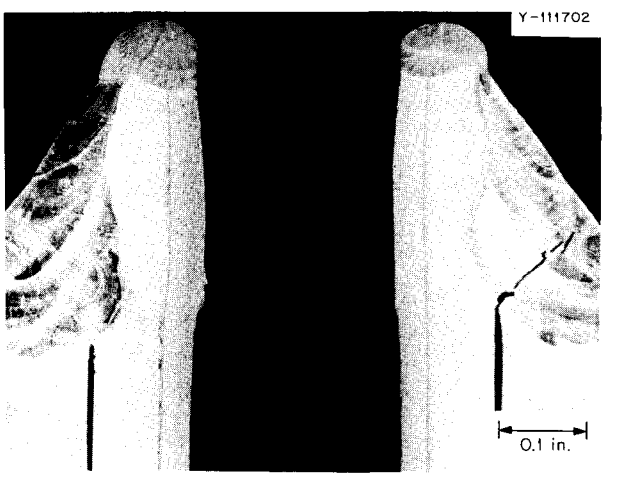

Fig. 13.1. Tube-to-tube-sheet weld in upper tube sheet, showing weld-bead cracking. 8.5×. Etchant: hydrochloric and nitric acids. Reduced 34%.

1. G. M. Slaughter, R. H. Jones, J. H. DeVan, and P. Patriarca, *Metals and Ceramics Div. Annu. Progr. Rep. June 30, 1971*, ORNL-4770, pp. 97–98.

2. G. M. Slaughter, J. H. DeVan, and R. H. Jones, "Post-Test Examination of the LMEC Alco/BLH Steam Generator," *Trans. Amer. Nucl. Soc.* **14**, 787–88 (1971).

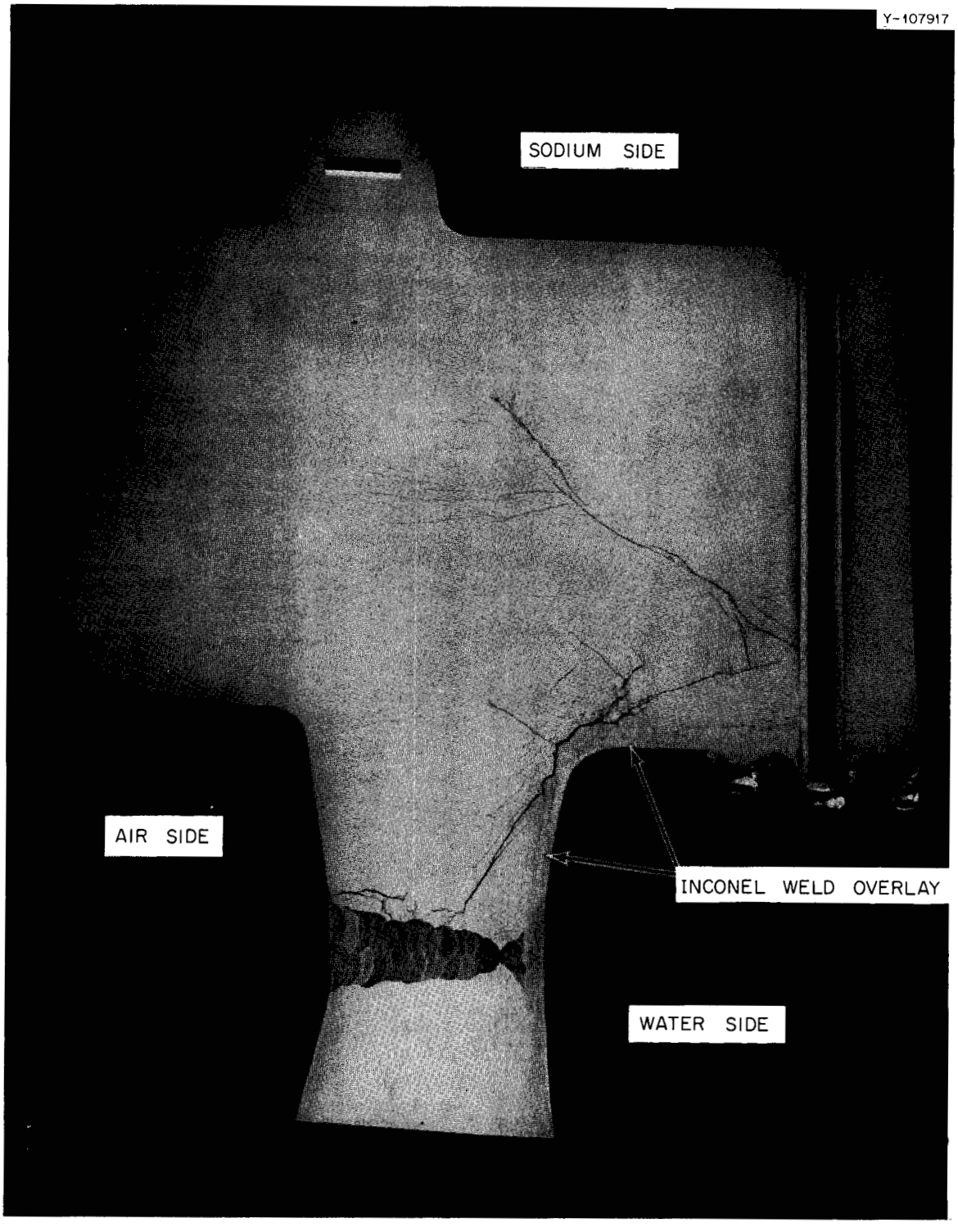

Fig. 13.2. Cross section along radius plane of lower tube sheet of Alco/BLH steam generator. Note system of stress-corrosion cracks, which interconnect tube crevices with the outside surface of tube sheet.

Fig. 13.3. Corrosion products observed in argon cover gas region in Alco/BLH steam generator, formed by reaction of steam with condensed sodium.

weld overlay, and water reached the crack networks through a small hole in this overlay. Assuming that the overlay was cracked at this point before operation, chloride impurities may have induced both the system of cracks that ran to the air side of the tube sheet and those leading to the sodium-filled crevices. Alternatively, as in the case of the top tube sheet, defects in the tube-to-tube-sheet fillet welds may have provided a path for water to reach the tube crevices. In this case, caustic cracking would have proceeded from the crevices to the Inconel overlay and thence toward the air side of the tube sheet. Thirdly, cracking may have originated at the air side of the steam generator as a consequence of chloride impurities and moisture contained in the thermal insulation surrounding the generator. The cracking patterns are such that none of these explanations can be disregarded.

CORROSION OF ADVANCED STEAM GENERATOR ALLOYS

J. P. Hammond G. M. Slaughter

This program concerns the corrosion behavior of steam generator alloys in steam, primarily as weldments. The actual testing is performed under subcontract by Southern Nuclear Engineering, Inc., at the Bartow Plant of Florida Power Corporation. It includes two areas of investigation: (1) general corrosion (uniform scaling, including pitting and localized attack at fusion lines) at 480, 595, and 650°C (900, 1100, and 1200°F) and (2) stress-corrosion cracking (induced by chloride or caustic as contaminants) at 282 to 595°C (540 to 1100°F).

General Corrosion

The general corrosion specimens of similar- and dissimilar-alloy weldments examined at 595 and 650°C for advanced gas-cooled reactor applications[3] were removed from tests after exposures to 23,000 hr, and the test loop was reconditioned to enable tests at 480 and 595°C on materials of special interest for LMFBR application. The findings of the former investigation, which included exposures to 16,000 hr, were promulgated.[4] The study of materials for LMFBR use includes specimens of Incoloy 800, Super 12 Cr (HT-9), 2¼ Cr–1 Mo steel, and various intermediate and highly alloyed ferritic steels, in both ground and electropolished surface conditions. These materials are being studied by the weight-loss and weight-gain methods, making determinations at intervals to 12,000 hr.

Stress Corrosion

Chloride. During the past year, runs 6 and 7 were completed and run 8 begun in the chloride-injection corrosion loop. All of these runs were conducted under identical cyclic operating conditions (20 ppm O_2 injected continuously and 10 ppm NaCl added during the saturation phase of cycling only). Because large numbers of specimens and such a wide variety of materials were represented, studies were made to establish more precisely the environmental conditions that prevailed as a function of time and location within

3. J. P. Hammond, *Metals and Ceramics Div. Annu. Progr. Rep. June 30, 1971*, ORNL-4770, pp. 90–94.

4. J. P. Hammond, "Corrosion of Nickel Base Alloy Weldments in Steam at 1100 and 1200°F (595 and 650°C)," paper presented at American Welding Society 52nd Annual Meeting, San Francisco, April 26–30, 1971 (submitted for publication).

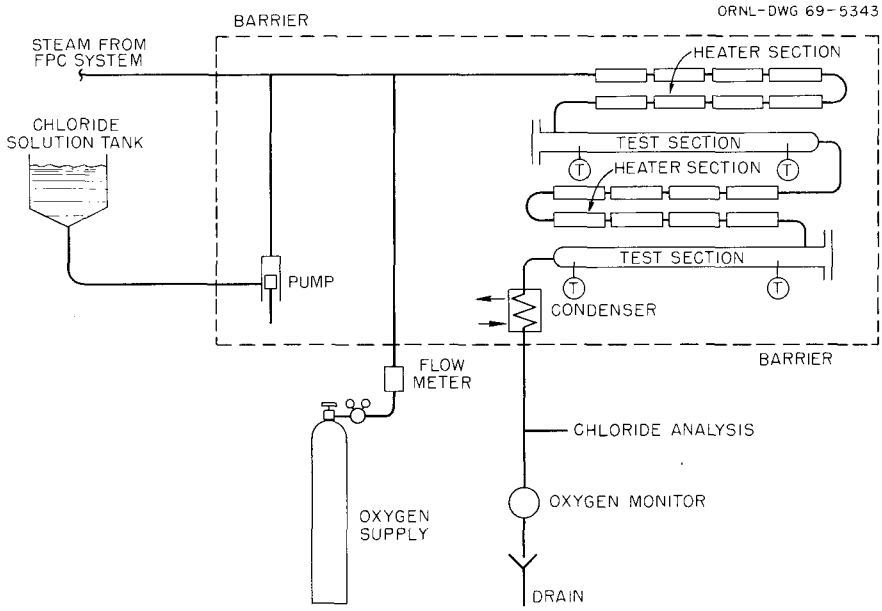

Fig. 13.4. Chloride and oxygen additive loop, schematic.

the test autoclaves. To more closely simulate steam generator components, a stress-corrosion test employing a tubular specimen was developed to complement the present U-bend test.

Environmental analyses. The objectives of the environmental analyses were to (1) determine the amount and location of moisture in the test autoclaves as a function of time during test, (2) establish water levels accumulating in the bottom of the autoclaves, and (3) assess the chloride concentrations in the saturated steam and accumulated water. The experimental procedures and detailed findings of these analyses were reported earlier.[5] The findings are summarized below along with information on the loop operating conditions.

A schematic of the chloride-injection steam corrosion loop is reproduced in Fig. 13.4. Operating conditions of the loop during runs 6 through 8, for which the analyses were made, were as follows:

Test cycles	Three per week between superheated and saturated conditions
Saturation periods	24 hr each, followed by 24 hr at superheat (except 48 hr on weekends)
Superheat temperature	427°C (800°F)
Steam-saturation temperature	282°C (540°C)
Oxygen content (continuous)	20 ppm
Sodium chloride content (during saturation phase of cycle only)	10 ppm
Steam flow (at saturation temperature)	100 lb/hr
Loop pressure	900 psig

The oxygen and chloride contents were deliberately maintained at high levels to permit evaluation of material behavior under off-design conditions and to permit a screening study in which failures would occur in reasonable times. Subsequent tests will be designed to incorporate test conditions of decreasing severity.

Several conclusions were reached by these analyses. The amount of moisture formed during the saturation phase of the cycling averaged about 25%. However, because the velocity of the steam flow in the autoclaves (devoid of specimens) was very low (≈2 fps), this moisture manifested itself largely as water that collected at the bottom of the autoclaves (1.9-in.-ID pipes) and flowed on through the loop. This water begins to collect just as the autoclaves reach the saturation temperature and rises parabolically to a final depth of about 0.090 in. The stressed regions of the U-bend test specimens, when mounted in an upright orientation, are $^1/_{16}$ in. above the bottom of the autoclaves and become wetted by the accumulated water within the first hour after the autoclaves reach the saturation temperature. The analysis revealed that little moisture and very little of the chloride contaminant reside in the saturated steam above the water level. Although the water at the

5. J. P. Hammond, *Fuels and Materials Development Program Quart. Progr. Rep. March 31, 1972,* ORNL-TM-3797, pp. 129–37.

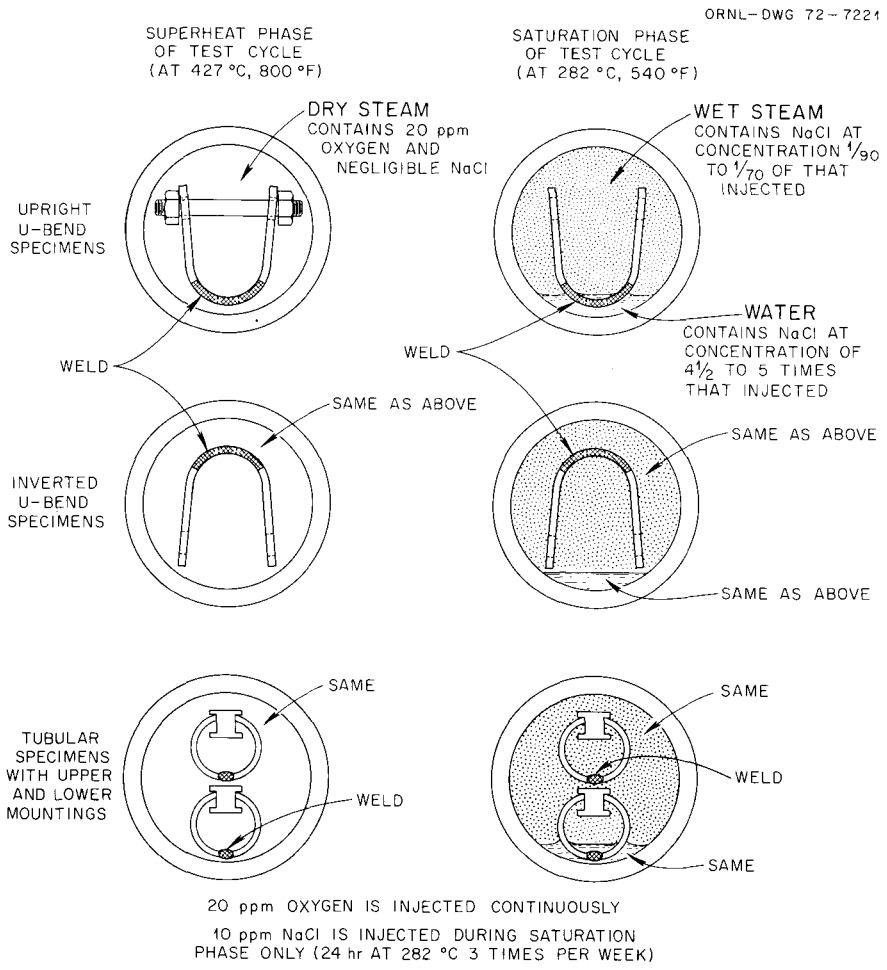

Fig. 13.5. Test specimens and environmental conditions for cyclic stress-corrosion tests. The loop operates at 900 psi.

bottom of the autoclaves contained 44 to 50 ppm NaCl, the saturated steam above contained only 0.11 to 0.14 ppm NaCl. Negligible NaCl was found in the superheated steam.

Figure 13.5 shows schematically the environmental conditions found in the autoclaves during test and illustrates the type of specimens being used and their orientations within the autoclaves. The tubular specimens are stressed by springing the slitted pieces outward while mounting them on an I-shaped rail; thus their stressed region (at the weld) is diametrically opposite from the mounting rail.

The time dependence of the moisture concentration was very similar for the upper and lower autoclaves.[5] From this we conclude that specimens see similar environments whether exposed in different autoclaves or in different axial positions in the same autoclave.

Corrosion test results. Test results on samples examined in runs 6 through 8 as U-bend specimens in the upright position (see Fig. 13.5) are summarized in Table 13.1. Of the three specimen surface conditions examined (ground, annealed, and pickled), grinding on a 100-mesh belt gave greatest susceptibility to cracking. Incoloy 800 welded with Inconel 82, although not as susceptible as type 304 stainless steel welded with type 308, was definitely susceptible to cracking, as were a host of other stainless steel and high-nickel alloys. However, the Incoloy 800 weldment was only moderately susceptible. Inconel 625 joined with itself and Inconel 601 base metal along with a group of nonwelded ferritic materials displayed a seeming immunity to cracking. Of the ferritic materials, 26 Cr–1 Mo steel was an unexpected exception to nonsusceptibility.

Table 13.1. Chloride stress-corrosion results on stainless steels, high-nickel alloys, and ferritic alloy steels[a]

Base metal	Filler metal	Failure frequency[b]			Crack size	Location[c]
		G	A	P		
Type 304 SS	Type 308 SS	3 of 3	3 of 3	3 of 3	Large	B into W
18-18-2 SS	18-18-2 SS	3 of 3	3 of 3		Large	B and W
Hastelloy X	Hastelloy X	6 of 6	1 of 6	0 of 3	Large	B through W
Hastelloy N	Hastelloy N	2 of 2	2 of 2		Large	B and W
IN 102	IN 102	6 of 6	3 of 6		Medium	B into W
Incoloy 800	Inconel 82	6 of 6	4 of 6	1 of 6	Medium	B into FL
Inconel 600	Inconel 82	3 of 6	0 of 6	0 of 3	Medium	B into FL
Inconel 625	Inconel 625	0 of 6	0 of 6	0 of 3		
Inconel 601	No weld	0 of 6	0 of 6			
Hastelloy C	No weld	0 of 3	0 of 3			
Hastelloy G	No weld	0 of 3	0 of 3			
$2\frac{1}{4}$ Cr–1 Mo steel	No weld	0 of 3	0 of 3			
$2\frac{1}{4}$ Cr–1 Mo, Ni, Nb (HT 8 × 6) steel	No weld	0 of 3	0 of 3			
5 Cr–$\frac{1}{2}$ Mo steel	No weld	0 of 3	0 of 3			
9 Cr–1 Mo steel	No weld	0 of 3	0 of 3			
12 Cr steel	No weld	0 of 3	0 of 3			
12 Cr steel	12 Cr steel	0 of 6	0 of 6	0 of 3		
12 Cr–1 Mo, Ni, W, V (HT-9) steel	No weld	0 of 3	0 of 3			
26 Cr–1 Mo steel	No weld	3 of 3	3 of 3		Large	B

[a]Welds were prepared by the gas tungsten-arc process; the duration of test was 12 to 16 weeks.

[b]For surface conditions indicated by G, ground on 100-mesh belt; A, ground and annealed; P, ground, annealed, and pickled.

[c]W = weld deposit, B = base metal, FL = fusion line.

Figure 13.6 illustrates failed U-bend specimens in Incoloy 800 welded with Inconel 82 and the microstructural characteristics of the cracks that formed. The cracks in this weldment and various of the other failed weldments of Table 13.1 were usually intergranular; generally they initiated alongside the root pass and progressed along the heat-affected zone. Occasionally cracks propagated into the weld deposits, but never to any appreciable extent in the case of the Incoloy 800 weldment made with Inconel 82.

The testing of materials as inverted U-bend and tubular specimens (Fig. 13.5) is presently under way. Preliminary indications are that for some materials, type 304 stainless steel welded with type 308 and Hastelloy N welded with itself included, the test environment above the water level may be more severe than that below. It should be noted that while the amount of chloride present here was exceedingly low, specimens tested many cycles may be subject to significantly higher concentrations as a result of chloride accumulation.

Caustic. Southern Nuclear Engineering, Inc., recently completed fabrication of an Inconel 625 corrosion loop for investigating stress corrosion in steam with caustic as the contaminant. Tests in this loop are scheduled to begin in October 1972.

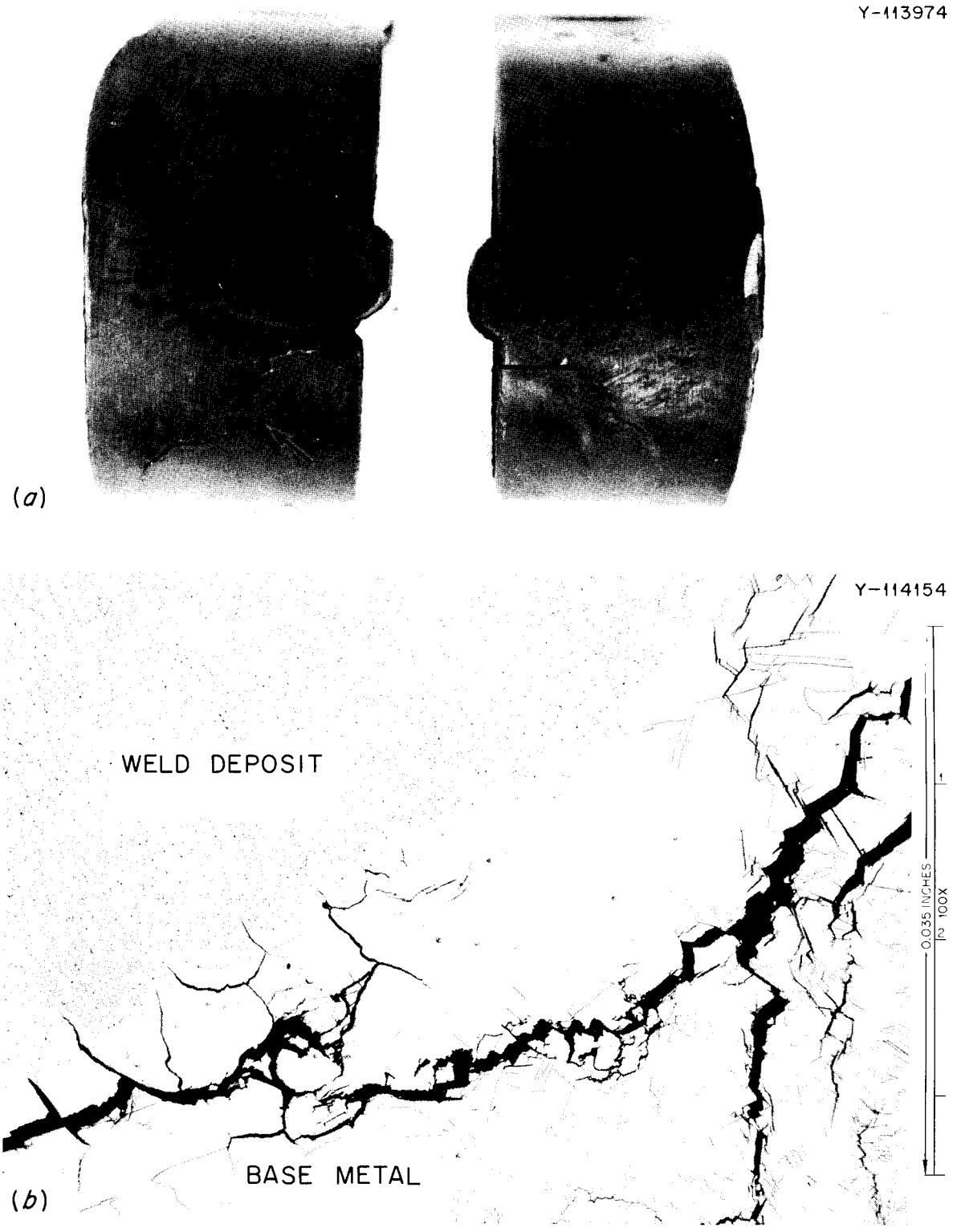

Fig. 13.6. Characteristics of chloride stress corrosion in Incoloy 800 welded with Inconel 82. (*a*) U-bend specimens after failure. (*b*) Microstructural features of cracks at arrow on *a*. Etched with H_2O_2-HCl mixture. Cracks here tend to be intergranular when in the heat-affected zone, but transgranular in the fine-grained material beyond.

14. Development of FBR Neutron-Absorber Materials

R. G. Donnelly W. R. Martin

Boron carbide is planned for control and shim rods for the FTR and demonstration LMFBR. Tantalum is also considered for the demonstration reactor. However, more data are required on the fast-reactor-irradiation behavior of these materials to assure safe and reliable performance for the desired service time. The solid swelling, gas release, and compatibility of boron carbide during irradiation are three of the principal problems. Principal problems with tantalum alloys are lower reactivity worth, solid swelling, compatibility, high after-heat, and stability of mechanical properties during irradiation. Some borides and rare-earth oxides have more reactivity worth per unit volume than tantalum but lack sufficient characterization and irradiation experience to warrant consideration at this time.

The purposes of this program are (1) to determine the irradiation performance of boron carbide and tantalum under expected operating conditions in the FTR and demonstration LMFBR and determine how materials and operating variations affect this performance, (2) to develop vent materials so that helium generated during irradiation of boron carbide may be safely and reliably released to the coolant, and (3) to investigate alternate materials that have possible advantages over boron carbide and tantalum for fast-reactor service and to provide sufficient pertinent data for an evaluation of their performance in service.

IRRADIATION BEHAVIOR OF BORON CARBIDE

Microstructure of Boron Carbide after Fast-Neutron Irradiation[1]

A. Jostsons[2] C. K. H. DuBose

Transmission electron microscopy has been used to investigate the nature of defect clusters produced in boron carbide by fast-neutron irradiation. Ion milling was used to prepare specimens from pellets of Argonne National Laboratory "higher worth" control rod irradiated in row 5 of EBR-II at an estimated temperature of 500°C to a burnup of 1.7% of ^{10}B (5470 MWd).

The defect clusters, shown imaged in diffraction contrast in Fig. 14.1*a*, superficially resembled the vacancy and interstitial dislocation loops formed in neutron-irradiated metals at temperatures below about 0.3 of their absolute melting temperatures. The defect clusters in boron carbide were not prismatic dislocation loops because the size of their images did not change on reversing the sign of the diffraction vector. Under absorption contrast conditions the defects appeared as narrow bright bands surrounded by dark Fresnel fringes in the under-focus condition (Fig. 14.1*b*) and as dark bands surrounded by light Fresnel fringes in the over-focus condition (Fig. 14.1*c*). This demonstrates unambiguously, according to the image calculations of Rühle,[3] that the defects are small cavities. The lobes of dark contrast in the diffraction image indicated that the lattice surrounding the defects is highly strained, but image overlap prevented determination of the sign of the strain. For this irradiation condition the cavities were present in a concentration of about $10^{16}/cm^3$. They were ribbon-like, with the largest face most frequently parallel to the trace of the (111) plane and less frequently to traces of {100} and {110}, indexed on the rhombohedral unit cell. The largest dimension of the cavities ranged between 30 and 200 Å.

The lattice strains around the cavities were eliminated by annealing at or above 1450°C. Annealing also reduced the concentration of cavities but increased their average size.

These cavities are in sharp contrast to the voids found in irradiated metals, which shrink and disappear on annealing and have no noticeable strain fields around them. We conclude that in boron carbide irradiated near

1. Summary of a paper accepted for publication in *Journal of Nuclear Materials.*

2. On attachment from the Australian Atomic Energy Commission, Research Establishment, Lucas Heights, N.S.W.

3. M. R. Rühle, "Transmission Electron Microscopy of Radiation-Induced Defects," p. 255 in *Radiation-Induced Voids in Metals,* ed. by James W. Corbett and L. C. Ianniello, USAEC Office of Information Services, Oak Ridge (1972).

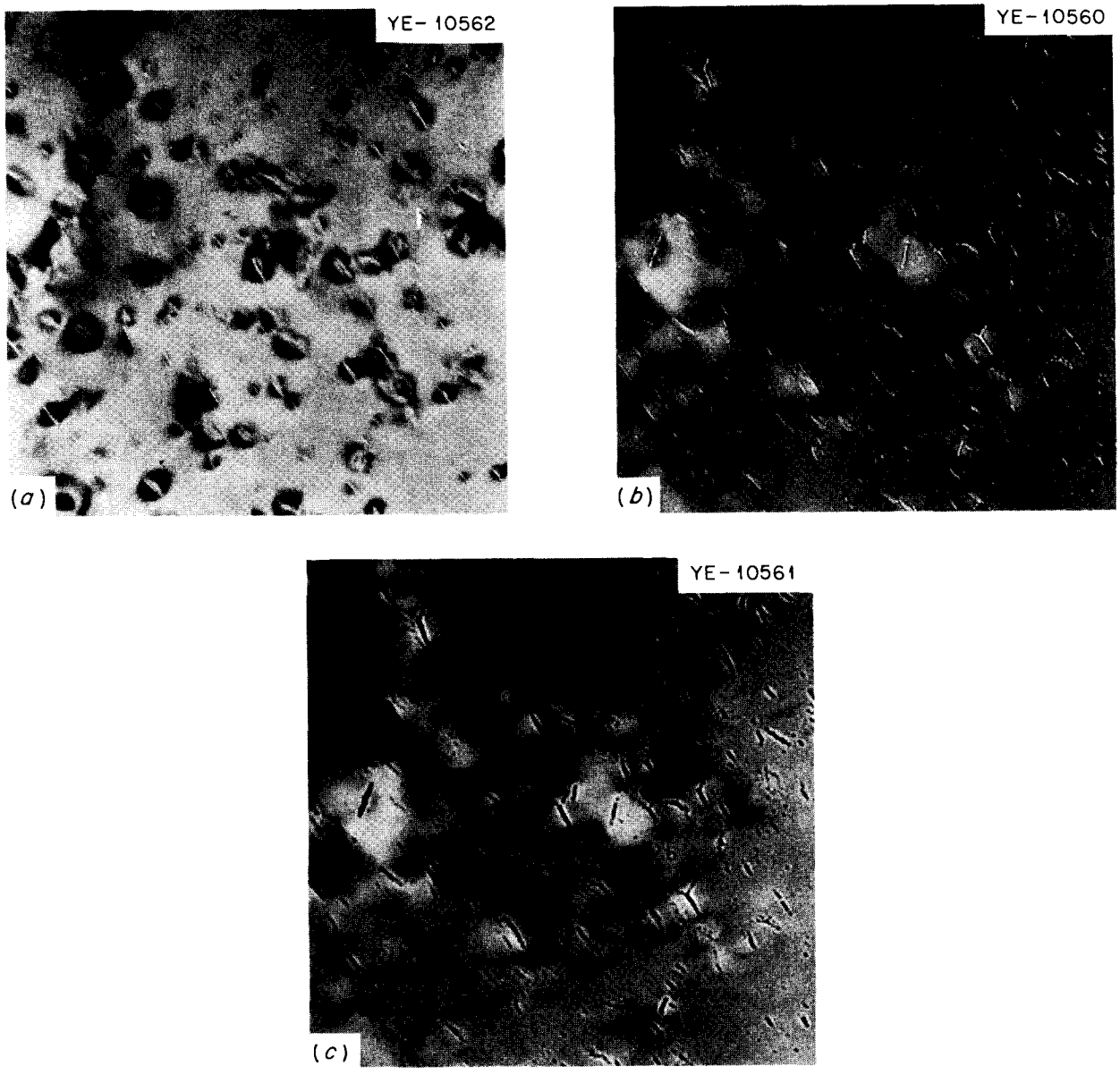

Fig. 14.1. Transmission electron micrographs illustrating the defect structure in neutron-irradiated boron carbide. (*a*) Bright-field two-beam condition. Bright field absorption contrast with (*b*) under-focused and (*c*) over-focused. This specimen had been annealed 1 hr at 1150°C. Similar but smaller defects were present as irradiated. 100,000×.

500°C the cavities probably contain helium at a pressure too high to balance the surface tension restraint. This is the source of the lattice strain. Upon annealing, the cavities grow into equilibrium bubbles, thereby eliminating the strain. According to Speight[4] such behavior is possible under conditions of high gas content if the diffusion coefficient of the gas atoms is much higher than the vacancy diffusion coefficient.

These observations indicate that the helium atoms do not remain dissolved in the open boron carbide lattice and that gas release will be limited by trapping of helium in the cavities.

4. M. V. Speight, *Met. Sci. J.* **2**, 73 (1968).

Evaluation of Fast-Reactor-Irradiated Boron Carbide Powders[5]

G. L. Copeland H. L. Yakel
C. K. H. DuBose

Boron carbide powders were irradiated by Hanford Engineering Development Laboratory in EBR-II to burnups of 3.7 and 4.8% of ^{10}B (7.7 and 10 $\times$ 10^{20} $n,\alpha/cm^3$) at 730 and 650°C, respectively. We examined the powders by transmission electron microscopy and x-ray diffraction as irradiated and after annealing for 1 hr at temperatures from 700 to 1900°C. As-irradiated powders contained platelike or ribbon-like cavities accompanied by complex strain fields. Previously examined powders irradiated in a thermal-spectrum reactor showed uniform black-spot damage resulting from defects too small for resolution.[6] The unit cell volume had decreased about 0.4% by a decrease in the rhombohedral *a* parameter with only a small change in the angle α. After annealing at 1450°C for 1 hr, the lattice parameters had returned essentially to the unirradiated values. The cavities had grown to slab-shaped bubbles, and the strain fields had essentially disappeared. At higher annealing temperatures the bubbles became more equiaxed.

Evaluation of Boron Carbide Pellets from EBR-II Higher Worth Control Rod

G. L. Copeland H. L. Yakel

We have examined capsules G and H from the EBR-II Higher Worth Control Rod. These capsules contained natural boron carbide pellets hot pressed to an average 95% of theoretical density. Each capsule contained 14 pellets about 0.54 in. in diameter by about 1 in. long. The assembly was irradiated at 500°C for 5468 MWd in row 5 of EBR-II, resulting in burnup ranging from about 1 to 1.7% ^{10}B depletion (2.1 to 3.6 $\times$ 10^{20} $n,\alpha/cm^3$). Plenum gas analysis of capsule H indicated that less than 2% of the helium generated had been released to the plenum during irradiation. Visually the pellets appeared to be in excellent condition. Average volume swelling (determined by dimensional measurements) of the pellets during irradiation was 0.28 and 0.38% for capsules G and H, respectively. Metallography revealed some microcracking, primarily in the interface between graphite inclusions and the boron carbide and along adjacent grain boundaries.

The lattice parameters as determined by x-ray diffraction after irradiation showed a unit cell volume increase of about 0.3% through an increase in the rhombohedral *a* parameter and a slight decrease in the angle α. This is in contrast to the powders described above, which decreased in the unit cell volume. After annealing, the lattice parameters behaved similarly. With increasing annealing temperature, *a* first increased and then decreased to the unirradiated value, whereas α first decreased and then increased to the unirradiated value. The unit cell volume decreased uniformly and returned to the unirradiated value after annealing at about 1300°C.

Transmission electron microscopy revealed bubbles within the grains similar to those in the powders but smaller. A denuded zone free of bubbles was observed adjacent to grain boundaries. Bubbles on the grain boundaries were so few and small that they were found only after grain boundary bubbles had been observed in the X-099 pellets described below. After annealing at 1400°C or greater, the bubbles became very apparent and coalesced similarly to those in the X-099 pellets. In addition, during annealing, bubbles grew within the grains similarly to those in the powders. This results in overall swelling of the material. Pellets annealed 1 hr at 1025, 1475, and 1900°C swelled 0.45, 1.23, and 10.8% in volume, respectively. During the 1475°C anneal 29% of the retained helium was released.

Evaluation of Boron Carbide Pellets from ORNL EBR-II Experiment X-099

G. L. Copeland A. Jostsons[2]

We are examining six pins containing natural boron carbide pellets that had been irradiated for 9700 MWd in row 7 of EBR-II. The results to date on swelling and gas release measurements are shown in Table 14.1. The swelling is higher than anticipated in the O-5 pins and lower than expected in the O-9 and O-10 pins. The gas release is higher than expected for the low-temperature pins and relatively insensitive to temperature (if the pins operated near their design temperatures). The denser pellets released more gas in each case. The most significant result is the severe cracking and lamellar fragmentation observed in pellets in O-9T and O-10T (higher density, higher temperature). Both high- and low-density pellets in O-10 showed radial cracking also. Weakening and separation of the grain boundaries due to gas bubble precipitation and coalescence are thought

5. Modified abstract from ORNL-TM-3729 (May 1972).
6. G. L. Copeland, C. K. H. DuBose, and D. N. Braski, *Metals and Ceramics Div. Annu. Progr. Rep. June 30, 1971*, ORNL-4770, p. 103.

Table 14.1. Summary of data from boron carbide EBR-II test X-099 (as of June 12, 1972)

Pin	Boron-to-carbon ratio	Pellet density (% of theoretical)	Calculated irradiation temperature[a] (°C)	Volume change[b] (%)	Helium released during irradiation[c] (% of total)	Burnup based on total helium		Comments
						Percent ^{10}B	$n,\alpha/cm^3$	
							$\times 10^{20}$	
O-5T	3.8	99	430	2.64	49.3	2.71	5.68	No cracks
O-5B	3.8	90	430	3.29	31.4	3.10	6.50	No cracks
O-9T	3.8	99	750	0.53	40.8	2.75	5.78	No cracks in 6, 7, 8; extensive lamellar cracks in 1–5; no radial cracks
O-9B	3.8	90	750	0.15	34.3	3.01	6.32	No cracks
O-10T	4.2	99	750	1.71	55.4	2.78	5.89	Lamellar and radial cracks; extensive in 1–5
O-10B	4.2	90	750	0.76	49.2	3.06	6.48	Radial cracks; no lamellar

[a]Based on gamma heating values for EBR-II as of about March 1972.
[b]Average of eight pellets except for O-9T (pellets 6, 7, 8) and O-10T (pellets 5, 6, 7, 8). Sum of twice the percentage diameter change and the length change.
[c]Based on plenum puncture plus vacuum fusion for retained helium.

to be responsible for the cracking. This same mechanism is operating in the lower temperature, lower density pellets and would probably lead to cracking in these pellets at higher burnups.

The high concentrations of bubbles on the grain boundaries are revealed by transmission electron microscopy. These bubbles coalesce, leaving regions of the grain boundaries completely separated. Within the grains, the bubbles have the flat anisotropic shapes with strain fields similar to previous observations. Figure 14.2 shows bubble coalescence at a grain boundary triple point where two of the boundaries are at an angle to the foil. The third boundary is perpendicular to the foil and appears to be almost completely separated. The top grain has contrast to show the strain fields, the contrast shows the bubbles in the right grain, and both are out of contrast in the lower grain. The denuded zone is about 0.2 μm wide, compared to the about 0.15 μm in the EBR-II Higher Worth Control Rod pellets. The bubbles are also strongly attracted to dislocations and stacking faults. If the preferred growth direction of the bubbles lines up with the dislocation or stacking fault direction, these bubbles line up to form extended cracks.

Scanning electron microscopy of surfaces fractured after vacuum annealing at 1600°C for 1 hr reveals a precipitate that was not observed as irradiated and may be a lithium compound, as indicated in Chap. 37 of this report. Nuclear magnetic resonance studies of as-irradiated boron carbide have given tentative evidence that the lithium is present as ions randomly distributed on interstitial sites. The lithium may precipitate during the anneal and then form compounds when exposed to the atmosphere on the fracture surface.

PERFORMANCE MODELING OF NEUTRON ABSORBERS[7]

F. J. Homan

A computer code to predict the performance of fast-reactor control rods was developed and used to analyze the integrated behavior of a FTR-type control rod in row 2 of EBR-II. In particular, the influence of the ^{10}B enrichment and solid reaction product swelling have been considered. Control rod claddings are predicted to begin rapid plastic strain very shortly after the fabricated gap between the absorber pellets and the cladding has closed. This strain is due to high contact pressure, which develops with continued pellet swelling. Models for helium gas bubble swelling and release are presented; they suggest minimum swelling from this source at about 1000°C.

7. Abstract of paper presented at the American Nuclear Society Meeting, Richland, Wash., April 24–27, 1972.

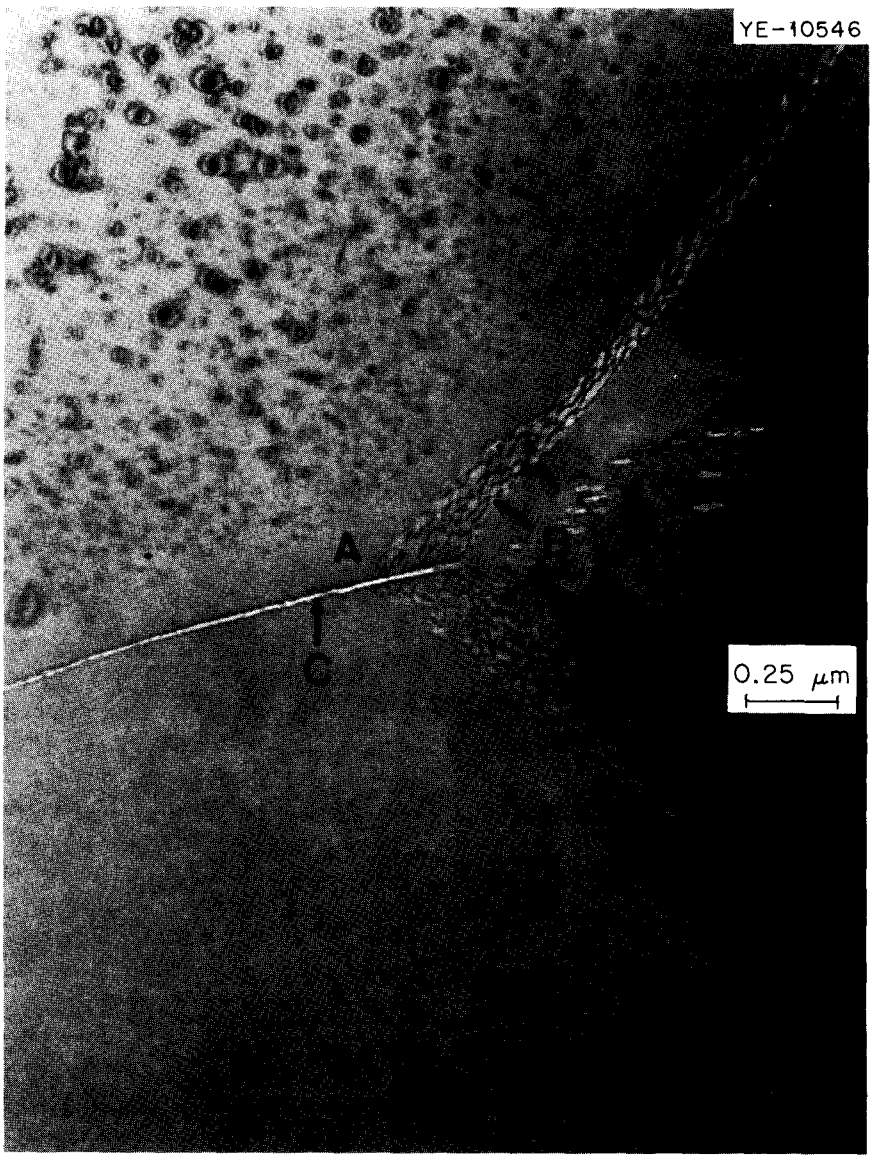

Fig. 14.2. Transmission electron micrograph of irradiated boron carbide showing (A) area adjacent to grain boundary, which is free of bubbles (denuded zone); (B) helium bubble coalescence on grain boundaries; and (C) edge view of grain boundary, indicating virtual separation of the grains. 50,000×.

DEVELOPMENT OF VENTS

J. I. Federer

Control rods for the Fast Test Reactor (FTR) consist of boron carbide pellets sealed in a stainless steel container. These rods are limited in life by helium generated from the $^{10}B(n,\alpha)^{7}Li$ reaction. The pressure of helium generated would eventually cause swelling of the stainless steel container, forcing removal of the rods from the reactor before the ^{10}B has been used most efficiently. The purpose of this task is to develop a venting device to release helium from such absorber elements into the sodium coolant. The basic requirements of helium vents in this application are: (1) a helium leak rate approximately equal to the release rate from boron carbide so as to minimize differential pressure across the vent, (2) compatibility with sodium at about 600°C, (3) no intrusion of sodium into the element due to hydraulic or capillary forces. Important elements of this task include fabrication of porous disks, bonding disks to holders, and characterization of vent assemblies.

Stainless steel and molybdenum disks have been cold pressed and sintered. After sintering, helium leak rates are determined with a calibrated helium leak detector. We are striving to obtain helium leak rates of 10^{-4} to 10^{-3} std cm^3/sec, a range that brackets recent data on helium release from boron carbide. However, vents having larger leak rates than 10^{-3} std cm^3/sec might also be used.

Sintered disks evidently have more porosity around the edges than elsewhere since a slight reduction in the diameter by machining substantially decreases the leak rate in most cases. We are attempting to minimize edge porosity by using a special die punch that densifies the edges of pressed disks about 10% more than the central region. We have also observed that the porosity is unevenly distributed. Flow generally occurs over about one-third of the total area of a disk face. This behavior is attributed to the difficulty in leveling the powder in the die before pressing.

Porous disks having the desired leak rates in the sintered condition must be bonded to a holder such as a tube to form a vent assembly. Bonding by electron-beam welding, brazing, and swaging has been tried. Welding is preferred to brazing, since the latter method introduces materials that may be less resistant to sodium corrosion than the disk and holder. The welded and brazed joints are qualitatively tested by observing the location of helium bubbles in alcohol placed on one side of the disk.

For type 316 stainless steel disks, sintering at 1200°C for 8 hr produced helium leak rates in the range 10^{-4} to 10^{-3} std cm^3/sec with a differential pressure of 1 atm across the disk. Mechanical sealing of these disks in stainless steel tubes to form vent assemblies has been unsuccessful and electron-beam welding only moderately successful. However, brazing with Nicrobraz 50 alloy at 1025°C has consistently produced leak-tight joints.

Molybdenum disks require sintering at 1600°C for 4 hr. However, attempts to braze these disks to type 304 stainless steel tubes with a variety of alloys were unsuccessful. This difficulty was overcome by substituting type 430 stainless steel, which has a coefficient of thermal expansion more closely matching that of the molybdenum.

Our plans include testing of vent assemblies in sodium, fabrication and characterization of vent assemblies with ceramic porous disks, and chemical vapor deposition of porous materials.

THE EFFECT OF TEMPERATURE ON THE MICROSTRUCTURE OF NEUTRON-IRRADIATED TANTALUM[8]

F. W. Wiffen

Fully recrystallized unalloyed tantalum irradiated in EBR-II to 2.5 to 4.4 × 10^{22} neutrons/cm^2 (>0.1 MeV) at 425, 585, 790, and 950 to 1050°C was examined by transmission electron microscopy to characterize the damage microstructure. The microstructure produced by irradiation at 425°C contained primarily a very high density of small "black spots," which could not be identified but were likely dislocation loops. There was no tendency for these loops to cluster, and no voids were identified in the sample. The damage was similar to that found at 450°C at one-eighth the fluence.[9] The samples irradiated at the higher temperatures all contained voids. Void concentrations were determined from sample thicknesses measured stereographically, and void sizes were measured on a particle size analyzer. The void parameters given in Table 14.2 show that trends established in other metals are also seen in tantalum. Within the temperature range of void formation the void concentration decreased and the average void size increased with increasing temperature. Void-denuded zones adjacent to grain boundaries were quite narrow in the specimens, only a few hundred angstroms in width. These narrow denuded zones were usually bordered by zones with higher than average void concentrations. The data in Table 14.2 show that the

8. Revised from summary of talk published in *Trans. Amer. Nucl. Soc.* **14**, 603 (1971).

9. G. L. Kulcinski and B. Mastel, "Microstructure of High-Temperature Neutron-Irradiated Tantalum and Molybdenum," *J. Appl. Phys.* **41**, 4752 (1970).

Table 14.2. Void parameters for neutron-irradiated tantalum

Irradiation temperature (°C)	Fluence[a] (neutrons/cm^2)	Void parameters		
		Concentration (voids/cm^3)	Average diameter (Å)	Volume fraction (%)
	× 10^{22}	× 10^{15}		
425	2.5	0		
585	2.5	190	61	2.4
790	2.5	6.1	117	0.65
950–1050	4.4	≤0.3[b]	130	≤0.03[b]

[a]>0.1 MeV.
[b]Void concentration locally variable. These are upper limits.

temperature range for maximum swelling of irradiated tantalum falls somewhere between 450 and 750°C and can be expected to be in the range 500 to 650°C. These results also show that the lower temperature limit for void formation is between 450 and 550°C and suggest that the upper temperature limit, at the fluence reported here, is probably not very much above 1000°C. These limits on the "temperature window" in which voids form are in close agreement with the limits 500 to 1000°C for void formation calculated by the Bullough-Perrin model,[10] using an activation energy of self-diffusion of 4.78 eV and a vacancy migration energy of 1.25 eV.

The voids in the sample irradiated at 585°C were partially ordered on a bcc superlattice, which was parallel to the bcc metal lattice and had a superlattice parameter of 205 Å. Voids occupied 80% of the superlattice points. The voids in the 790 and 1000°C specimens were not ordered, but they tended to be clustered in the specimen irradiated at 790°C.

The dislocation and loop structures in all samples were partially obscured by deformation during thinning and handling and have not yet been analyzed in detail.

ALTERNATE ABSORBER MATERIALS

M. M. Martin

Our objective is to characterize promising materials other than boron carbide and tantalum alloys for which there are now insufficient data to permit consideration of their use in fast-reactor control systems. Work was concentrated on the tantalum borides but recently has been expanded to include europium sesquioxide. Factors considered are reactivity worth, fabricability, irradiation performance, and compatibility with cladding and coolant.

We have fabricated and characterized pellets of three tantalum borides for irradiation at 500°C in EBR-II. One is a multiphase Ta-TaB_x cermet containing 3.6 wt % B in which the boron is enriched to 40 at. % ^{10}B. The others are hexagonal TaB_2 of both stoichiometric (2.00) and hypostoichiometric (1.75) compositions. All of these materials have a reactivity worth slightly better than B_4C containing natural boron.

REACTOR EXPERIMENT DESIGN AND FABRICATION

T. N. Washburn E. J. Manthos
J. W. Woods D. A. Dyslin[11]

The capsules for irradiation testing in EBR-II are listed in Table 14.3. Test series 1, subassembly X-099A, is scheduled to begin irradiation in August 1972 and contains three capsules (O-6, O-7, and O-8) previously irradiated in this subassembly, two capsules (O-12 and O-13) designed and fabricated this year, and two capsules (BTA-7 and -8) fabricated at HEDL. These latter two capsules had end fittings that are no longer standard at EBR-II, and a standard subassembly was modified to accept these two capsules.

The seven capsules for test series 2α were designed and fabricated during FY 1972, and irradiation in EBR-II is scheduled to begin in late August. Capsule O-27 contains test specimens from HEDL capsule B-58, which was disassembled at ORNL to modify the specimen holders to use our standard spacer hardware. These changes were made to reduce the level of uncertainty in calculating specimen temperature.

We began design and fabrication of the seven capsules for test series 2β. Capsule O-23 is funded by NASA and is a high-temperature (1200°C) test of the performance of boron carbide.

10. R. Bullough, personal communication, June 1971.

11. General Engineering Division.

Table 14.3. Neutron absorber irradiation experiments

Test series	Subassembly	Capsule	Control material[a]	Design temperature (°C)
1	X-099A	O-6	$B_{4.5}C$ and $B_{4.5}C$	430
		O-7	$B_{4.5}C$ and $B_{4.5}C$	430
		O-8	$B_{3.8}C$ and $B_{3.8}C$	430
		O-12	Ta alloys	400–900
		O-13	Ta alloys	400–750
		BTA-7[b]	Ta	700–1250
		BTA-8[b]	Ta	700–1250
2α	X-164	O-14	$B_{4.0}C$ + B and $B_{4.5}C$	430
		O-15	$B_{6.5}C$ and $B_{4.0}C$	430
		O-16	$B_{6.5}C$ and $B_{4.0}C$	700
		O-17	$B_{6.5}C$ and $B_{4.0}C$	850
		O-18	TaB_2 and $B_{4.0}C$	500–430
		O-20	Ta_2*B and TaB_2	500
		O-27[c]	Ta alloys	400–900
2β	X-1*yy*	O-19[d]	B_4C+Na and irradiated $B_{3.8}C$	430
		O-21	*$B_{6.5}C$ and *B_4C	700
		O-22	*$B_{6.5}C$ and *B_4C + compatibility	700
		O-23	*$B_{6.5}C$ and *B_4C	1200
		O-24	*$B_{6.5}C$ and *B_4C	700
		O-25	*$B_{6.5}C$ and *B_4C + compatibility	700
		O-26[d]	$B_{3.8}C$ and $B_{4.2}C$ (irradiated)	430 and 750

[a]Asterisk indicates that isotopic content of boron differs from naturally occurring content of 19.8% ^{10}B.

[b]Capsules supplied by HEDL.

[c]O-27 is reencapsulation of HEDL's B-58.

[d]O-26 and O-19B are reconstitution of pellets from X-099 after irradiation.

15. Development of FBR Oxide Fuels

A. L. Lotts F. J. Homan

The oxide fuels development program was a five-year program conducted to advance the technology of $(U,Pu)O_2$ as an LMFBR fuel. Funding for this program was terminated on June 30, 1972. The program emphasized determination of the properties and performance of sol-gel-derived oxide fuels fabricated by the Sphere-Pac and pelletizing techniques. The performance of these fuels was compared with that of other fuels, such as pellets from mechanically blended or coprecipitated oxide. The main objectives of the oxide fuels development program were:

1. to establish the performance characteristics and limitations of $(U,Pu)O_2$ fuels fabricated by different processes,
2. to obtain a fundamental understanding of the mechanisms involved in the irradiation behavior of fuel elements incorporating these fuels,
3. to develop fabrication techniques that provide both economy and a product with optimized performance, and
4. to develop analytical models sufficiently accurate to optimize experimental design and to predict fuel element response to LMFBR conditions.

These objectives were met through a program that included fabrication of fuel with different structures, characterization of these structures by out-of-reactor methods, and irradiation under a variety of conditions. The program emphasized irradiation testing, postirradiation examination of the various fuel structures, and evaluation of the results in terms of performance models.

Since a number of irradiation tests were still in progress when the program was terminated, responsibility for these tests was turned over to other USAEC contractors. Accordingly, all documentation, quality assurance work, and archive specimens have been transferred.

DEVELOPMENT OF FABRICATION PROCESSES

J. D. Sease R. A. Bradley

The objective of our $(U,Pu)O_2$ fabrication program was to develop processes by which mixed oxide fuel of controlled density and stoichiometry can be fabricated for irradiation tests. A large portion of this work has been the development of Sphere-Pac and sol-gel pellet fabrication techniques. The Sphere-Pac process, which uses low-energy vibration to infiltrate a close-packed bed of coarse microspheres (420 to 600 μm) with fine microspheres (<44 μm), has been used to load a number of fuel pins for irradiation tests to smear densities 82 to 84% of theoretical.[1] During the past year we prepared the fuel and loaded the fuel pins for two instrumented ETR capsules and for two irradiation experiments on the Gas-Cooled Fast Breeder Reactor program.

We fabricated the fuel pins for two instrumented capsules (ORNL 43-125 and 43-126) for in situ measurement of fission gas release. The irradiation experiment is described in more detail later. Each fuel pin contains approximately 20 in. of mixed oxide fuel. One contains $U_{0.75}Pu_{0.25}O_{1.97}$ pellets fabricated by WADCO from mechanically mixed powders. The other was loaded by the Sphere-Pac process with $U_{0.73}Pu_{0.27}O_{1.97}$ coarse microspheres and UO_2 fine microspheres to yield a nominal fuel bed of composition $U_{0.80}Pu_{0.20}O_{1.98}$. The smear densities of both the Sphere-Pac and the pellet pins are 83.5 ± 1.0% of theoretical.

Five replacement fuel pins were fabricated for the GCFBR F-1 irradiation experiment described in Chap. 25 of this report. These fuel pins contained both solid and annular $(U,Pu)O_2$ pellets with densities 87 and 92%

1. R. A. Bradley, W. J. Lackey, and J. D. Sease, *Metals and Ceramics Div. Annu. Progr. Rep. June 30, 1971*, ORNL-4770, pp. 38–39.

of theoretical and oxygen-to-metal ratios of 1.94 and 1.98. The preparation of the sol-gel powder[2] and the fabrication of the pellets[3] have been described previously.

Fuel for the GCFBR GB-10 capsule, also described in Chap. 25, was fabricated and loaded into the fuel pin. It contains 8.8 in. of nominally 87.5%-dense dished-end $U_{0.88}Pu_{0.12}O_{1.97}$ pellets, with the uranium containing 9% ^{235}U.

IRRADIATION BEHAVIOR

F. J. Homan T. N. Washburn

The irradiation testing portion of the FBR Oxide Fuels Program has been directed at determining the in-reactor properties and performance of $(U,Pu)O_2$ fuel pins as functions of fabrication form, porosity distribution, stoichiometry, and irradiation conditions. The program included both fast and thermal flux irradiations and steady-state, cyclic, and transient power conditions. Our irradiation program has shown that Sphere-Pac fuels exhibit better cladding-fuel compatibility and thermal conductance than pellet fuels. In all other respects, pellet and Sphere-Pac fuels perform similarly.

Fast Flux Irradiation Tests

A. R. Olsen

The ORNL oxide fuels irradiation in the EBR-II consisted of two series of tests. The five encapsulated Series I pins[4] all contained Sphere-Pac (^{235}U–20% Pu)O_2. Series II included 53 unencapsulated pins.[5] We fabricated 19 of the pins inserted in the first 37-pin subassembly and one replacement pin. The Babcock and Wilcox Company (B&W) fabricated 33 pins, 18 for the initial subassembly loading and 15 replacements. The ORNL pins contained Sphere-Pac and pellet fuels all derived from a sol-gel process. The B&W pins contain sol-gel-derived Sphere-Pac fuels or pellets and Vi-Pac shards processed from coprecipitated powders. These tests emphasized the effects of fuel form and void distribution on the release of fission gas, fission product redistribution, and mechanical and chemical interactions of fuel and cladding. Linear heat rates were 14 to 16 kW/ft, peak cladding temperatures from 550 to 650°C, and burnup levels up to 13% fissions per initial actinide metal atom (FIMA).

Two pins from the Series I group were examined after a peak burnup of 6% FIMA. The results have been discussed previously,[6,7] and a final report is in preparation.[8] The remaining three pins were irradiated for an additional 5200 MWd of EBR-II operation to a peak calculated burnup level of 8.1% FIMA. The nondestructive interim examination of the pins indicated no abnormal behavior, and they are being inserted for continued irradiation.

The unencapsulated Series II pins were irradiated in subassembly X112 for 10,600 MWd of EBR-II operation. The lead pin peak burnup is approximately 3.8% FIMA. Argonne National Laboratory will assume responsibility for these experiments on July 1, 1972. All replacement pins and the necessary quality assurance documentation have been shipped to the EBR-II project.

Uninstrumented Thermal Flux Irradiations

A. R. Olsen

We have irradiated 11 capsules in this series, six to provide preliminary performance data on sol-gel Sphere-Pac fuels and five, two of which are still under irradiation, to provide short-cooled irradiated fuel for reprocessing studies. The detailed description, purpose, scope, conditions of irradiation, and some results have been reported previously.[9] The results of the tests irradiated for performance analysis have been presented,[10] and a topical report is in preparation.

---

2. R. A. Bradley and J. D. Sease, *Gas-Cooled Reactor Program Semiannu. Progr. Rep. Sept. 30, 1970,* ORNL-4637, p. 49.

3. J. D. Sease and R. A. Bradley, *Fuels and Materials Development Program Quart. Progr. Rep. Sept. 30, 1971,* ORNL-TM-3550, pp. 4–6.

4. A. R. Olsen, *Experiment Description and Hazards Evaluation for the Series I ORNL Oxide Fuels Irradiation in EBR-II,* ORNL-TM-2635 (April 1970).

5. A. R. Olsen et al., *Preirradiation Data for ORNL Series II and B&W Oxide Fuel Tests in EBR-II,* ORNL-TM-3446 (November 1971).

6. A. R. Olsen, *Metals and Ceramics Div. Annu. Progr. Rep. June 30, 1971,* ORNL-4770, pp. 45–47.

7. A. R. Olsen, "Sol-Gel Sphere-Pac $(U,Pu)O_2$ Fuel Performance in EBR II Irradiation Tests," *Trans. Amer. Nucl. Soc.* **14**(2), 596–97 (October 1971).

8. A. R. Olsen, *Sol-Gel Sphere-Pac $(U,Pu)O_2$ Fuel Performance to Intermediate Burnup Levels in a Fast Flux Environment,* report in preparation.

9. A. R. Olsen and D. R. Cuneo, *Metals and Ceramics Div. Annu. Progr. Rep. June 30, 1970,* ORNL-4570, pp. 53–55.

10. A. R. Olsen, C. M. Cox, and R. B. Fitts, *Trans. Amer. Nucl. Soc.* **12**, 605–6 (1969); A. R. Olsen, ibid. **13**, 32–33 (1970), and **15**, 181–82 (1972).

R-59489

43-113-1, 8.8 kW/ft, 8.6% FIMA

43-113-4, 9.6 kW/ft, 9.7% FIMA

Fig. 15.1. Comparative microstructures of $U_{0.85}Pu_{0.15}O_{1.98}$ fuel pins. As polished.

The examination of the last performance data capsule was completed. The peak burnup achieved in a $^{238}U_{0.85}Pu_{0.15}O_{1.97}$ fuel pin was 11.3% FIMA while the comparison 20%-enriched UO_2 pin reached 13.8% FIMA. This difference reflects the difference in initial percentages of fissonable isotopes (15 vs 20%). The linear heat rate in each pin decreased with fissile depletion, with the maximum rate of change occurring in the $(U,Pu)O_2$ fuel pin with the highest heat rate and highest burnup; the initial heat rate of 14.7 kW/ft fell to approximately 6 kW/ft at the end of life even though the capsule was moved to a higher flux position in the reactor during its irradiation. The pin with the highest initial maximum heat rate had the lowest integrated

fission gas release (61%). The rationalization of this behavior involves the extended operation at low linear heat rate because of rapid fissile depletion.

The metallographic examination of these pins confirmed the data on restructuring derived from the early lower burnup tests.[11] The extent of columnar grain growth was defined by the peak linear heat rates early in life and did not change, although the radius of the more or less solid core of fuel increased significantly by the more time-dependent sintering processes. This can be seen in Fig. 15.1 where the sintering is defined by the circumferential cracks.

The third reprocessing capsule (43-118) was discharged from the reactor late in May, and the last capsule (43-123) was inserted in the same location. The processing studies on the first two capsules in this series have been reported elsewhere.[12]

ETR Instrumented Tests

A. R. Olsen R. A. Buhl

The ETR instrumented tests are designed to determine the performance of mixed oxide fuel under simulated LMFBR design operating conditions. The first two capsules (43-120 and 43-121) were irradiated to investigate fuel swelling and fuel-cladding chemical interactions of Sphere-Pac and pellet $(U,Pu)O_2$ fuels. Each capsule contains four fuel pins, with two thermocouples at the axial midplane of each pin.

Both capsules have completed their irradiation. Capsule 43-121 was discharged in January and 43-120 in May, both with a calculated burnup of approximately 8% FIMA. Details of the irradiation have been reported elsewhere.[13] Capsule 43-121 has been examined incompletely, and capsule 43-120 is in storage in the ETR pool pending a decision on where it is to be examined.

The second set of tests in this series consists of three instrumented capsules, each designed to measure fission gas pressure during testing and each containing one fuel pin with a 20-in.-long column of fuel. One capsule contains FTR-type pellets of the highest permissible density (94% of theoretical), the second contains FTR pellets of the lowest permissible density (88% of theoretical), and the third contains a packed bed of Sphere-Pac U-Fines fuel. In the latter fuel, all the plutonium is contained in the coarse fraction (approx 400 μm diam), and a fine fraction (<44 μm diam) of depleted UO_2 is infiltrated into the coarse bed. These capsules have been partially assembled.

Fuel-Cladding Mechanical Interaction Tests

B. Fleischer R. L. Senn[14]
R. B. Fitts

The MINT-1 capsule was fabricated and put into operation. The purpose of this test was to measure fuel column and cladding length changes and fission gas release under prototype FTR power and temperature conditions. It operated from in November 1971 to June 1972, including 32 power cycles, six of which were less than 10 kW/ft during startup. The fuel element operated for 15,800 kWhr, achieving an estimated burnup of 1.7% FIMA. A typical power cycle above 10 kW/ft consisted of a slow heatup ($\approx$1.5 to 3 hr) to operating power, hold at power overnight or over the weekend, then rapid cooldown (less than 2 min) by continuous retraction of the capsule to the minimum power position.

The most significant outcome of the experiment is the gas release behavior. The gas release was continuous with increasing burnup at power and not significantly changed by power transients. This behavior, shown graphically in Fig. 15.2, contrasts with that observed by other investigators,[15,16] who found very little gas release at power and significant gas release during power cycling. The reason for the disparity between these results is not evident. Our gas release measurements have shown a total gas release of approximately 56% over the life of the test. This quantity is within the range expected for 1.7% FIMA in the operating level of 13 to 17 kW/ft based on ANL data.[17]

11. A. R. Olsen, R. B. Fitts, and W. J. Lackey, "In-Reactor Restructuring Temperatures and Kinetics for $(U,Pu)O_2$," pp. 579–602 in *Proc. Conf. Fast Reactor Fuel Element Technology,* ed. by Ruth Farmakes, American Nuclear Society, Hinsdale, Ill., 1971.

12. J. H. Goode, *Chem. Technol. Div. Annu. Progr. Rep. Mar. 31, 1972,* ORNL-4794, pp. 27–29.

13. A. R. Olsen and R. A. Buhl, *Fuels and Materials Development Program Quart. Progr. Rep. Sept. 30, 1971,* ORNL-TM-3550, pp. 15–17; ibid., *Dec. 31, 1971,* ORNL-TM-3703, pp. 10–11; ibid., *Mar. 31, 1972,* ORNL-TM-3797, pp. 8–17.

14. Reactor Division.

15. T. B. Burley and M. D. Freshly, *Trans. Amer. Nucl. Soc.* **11**(1), 106–7 (1968).

16. M. J. Motley, R. DesHaies, and J. R. MacEwan, *Trans. Amer. Nucl. Soc.* 8(2), 424–25 (1965).

17. J. D. B. Lambert et al., "Performance of Mixed-Oxide Fuel Elements – ANL Experience," pp. 517–53 in *Proc. Conf. Fast Reactor Fuel Element Technology,* ed. by Ruth Farmakes, American Nuclear Society, Hinsdale, Ill., 1971.

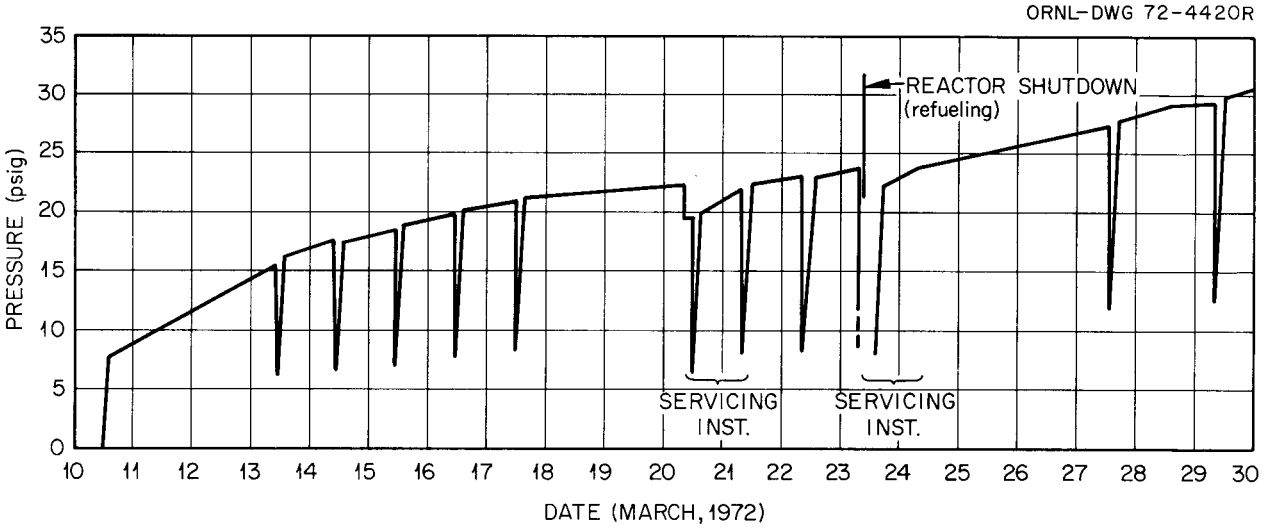

Fig. 15.2. MINT-1 fuel element internal pressure.

Fuel column length change measurements using the motion transducer are shown in Fig. 15.3. These measurements indicate that (1) the fuel column grew as a result of thermal expansion during heatup, (2) shortened during early constant power operation, probably because of creep or restructuring, and (3) expanded slowly as expected from fission product swelling.

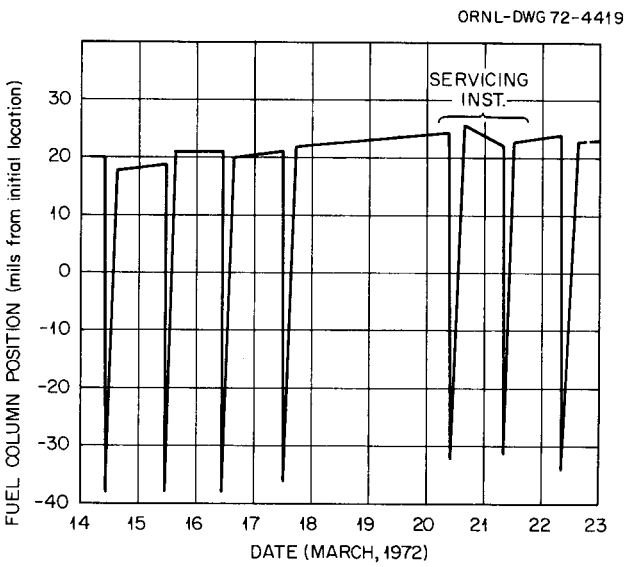

Fig. 15.3. MINT-1 fuel column behavior.

Cladding Chemical Reactions

A. R. Olsen J. M. Leitnaker
R. A. Buhl

Chemical interactions between oxide fuels, fission products, and cladding materials[18] have been recognized as a potential limiting factor to the operating conditions and attainable burnup. The fact that oxidation of the cladding is the primary reaction has also been established.[19,20] Two types of oxidation have been seen:

1. a general or matrix oxidation, with the buildup of a significant surface oxide layer and a more or less uniform reduction in wall thickness, and
2. an intergranular attack, which is often only in localized areas but which proceeds to significant depths, sometimes greater than 50% of the 0.016-in. tube wall thickness.

The intergranular attack, which usually shows some fission products such as cesium in the grain boundaries, is the source of greatest concern.

In a series of experiments, solution-treated type 316 stainless steel tubing was exposed to flowing Ar–4% H_2 with controlled moisture contents of 4000 or 40 ppm of H_2O to control the oxidation potential. A temperature gradient was maintained along each 10-in.-long

18. R. B. Fitts, A. R. Olsen, C. M. Cox, and E. L. Long, Jr., *Metals and Ceramics Div. Annu. Progr. Rep. June 30, 1971*, ORNL-4770, pp. 57–59.

19. R. B. Fitts, E. L. Long, Jr., and J. M. Leitnaker, "Observations of Fuel-Cladding Chemical Interactions as Applied to GCBR Fuel Rods," pp. 431–58 in *Proc. Conf. Fast Reactor Fuel Element Technology*, ed. by Ruth Farmakes, American Nuclear Society, Hinsdale, Ill., 1971.

20. J. M. Leitnaker, J. P. DeLuca, and R. B. Fitts, "Influence of Burnup on Reactivity of Oxide Fuel with Cladding," *Trans. Amer. Nucl. Soc.* **14**, 177 (1971).

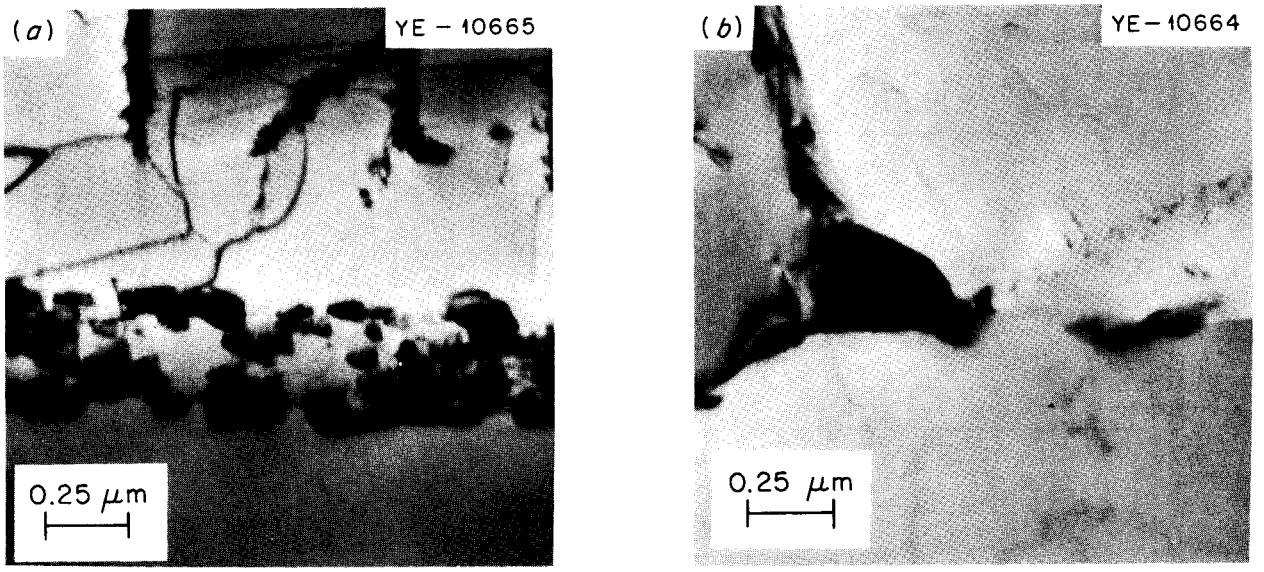

Fig. 15.4. Morphology of precipitates in stainless steel tubing heated in Ar–4% H_2–4000 ppm H_2O for 500 hr. (*a*) 615°C region; (*b*) 650°C region.

tube. Two gradients were used: 450 to 650°C or 500 to 710°C. In all, nine tubes have been tested in three groups of three tubes each. The entire length of each tube was nondestructively inspected for wall thickness with an eddy-current technique.[21] Two tests were conducted for 500 hr each and one for 1000 hr. All nine tubes showed an apparent wall thickness reduction, which was localized in the 560 to 650°C range with the maximum change at 585 to 605°C. In the 1000-hr test with the higher oxygen potential a second and greater change in wall thickness was indicated above 660°C. Standard metallographic examinations of the two 500-hr tests show no significant change in the geometric wall thickness. Although there are other metallographic differences, the most pronounced observation is the distinct increased sensitivity to etching (glyceria regia at room temperature) of all six sections cut from the 600°C region. The grain boundaries are most rapidly attacked; this effect is less on sections from higher or lower temperature regions.

Thinned sections from one tube in the 500-hr test with 4000 ppm H_2O have been examined by transmission electron microscopy. These samples, one from the 650°C region and one from the 615°C region, showed only $M_{23}C_6$ precipitates in the structure. However, the morphology of these precipitates is distinctly different, as shown in Fig. 15.4, with thin sheetlike precipitate covering most of the grain boundary in the lower temperature section and thicker, separated, agglomerated precipitate in the higher temperature section. This observation is in excellent agreement with the findings of Stickler and Vinckier.[22] These same authors report a maximum in intergranular embrittlement after exposure to Strauss solution for samples heat treated in the range 565 to 650°C. In another experiment in a dry environment, Pickering, Beck, and Fontana[23] report on corrosion tests in the range 93 to 760°C with NaCl with and without the presence of oxygen. Oxygen was required for both matrix and intergranular attack. Also, the reaction occurred most rapidly with $M_{23}C_6$ compounds. The salt led to the production of Na_2CrO_4 instead of a protective chromic oxide. Matrix attack producing of large amounts of surface scale occurred only at 704 to 760°C, whereas intergranular attack was very pronounced at 593°C.

21. C. V. Dodd and W. A. Simpson, Jr., *Thickness Measurements Using Eddy-Current Techniques,* ORNL-TM-3712 (March 1972).

22. R. Stickler and A. Vinckier, "Morphology of Grain-Boundary Carbides and Its Influence on Intergranular Corrosion of 304 Stainless Steel," *Trans. Amer. Soc. Metals* **54,** 362–80 (1961).

23. H. W. Pickering, F. H. Beck, and M. G. Fontana, "Rapid Intergranular Oxidation of 18-8 Stainless Steels by Oxygen and Dry Sodium Chloride at Elevated Temperatures," *Trans. Amer. Soc. Metals* **53,** 793–803 (1961).

Thus the work of others on intergranular corrosion may help explain our nondestructive test results in stainless steel heat treated in a pure oxidizing atmosphere. The postulated reaction for the apparent wall thickness reduction measured by the eddy-current technique is the formation of thin intergranular oxide layers where the thin interconnected sheets of $M_{23}C_6$ are formed near 600°C. Agglomerated carbide at higher temperatures does not provide a continuous path, so less penetration occurs until the matrix oxidation rate increases and a thicker continuous carbide precipitate is formed at the highest temperatures of our tests. The intergranular oxides would electrically insulate the grains and increase the resistivity, thus causing an apparent reduction in wall thickness.

The presence of fission product cesium in the grain boundaries of intergranularly attacked cladding on irradiated oxide fuel pins may also be the result of the formation of Cs, Cr, and O_2 compounds by removal of carbon from the $M_{23}C_6$ precipitate as CO. This would yield a surface area relatively free of carbide, as we have noted in some of our high-temperature tensile tests of previously heat treated type 316 stainless steel.[24] The postulated reactions require additional experimental proof. The known effects of neutron irradiation on carbide precipitation kinetics[25,26] may lower the temperature range.

ANALYSIS OF FUEL ELEMENT PERFORMANCE

F. J. Homan

The data derived from irradiation testing of oxide fuels from both the ORNL program and experimental programs at other sites have been used to develop analytical models for predicting and evaluating the performance of LMFBR fuel pins. The models are both theoretical and empirical and have emphasized the thermal, chemical, and mechanical performance of the fuel elements, particularly during startups, power cycles, and transients. This work includes direct support of the irradiation testing program in terms of optimizing experimental designs, interpreting results, and extrapolating these results to LMFBR conditions.

24. J. M. Leitnaker and H. Mateer, *Fuels and Materials Development Program Quart. Progr. Rep. Mar. 31, 1972,* ORNL-TM-3797, pp. 92–96.

25. T. T. Claudson, R. W. Barker, and R. L. Fish, "The Effects of Fast Flux Irradiation on the Mechanical Properties and Dimensional Stability of Stainless Steel," *Nucl. Appl. Technol.* 9, 10–23 (1970).

26. P. J. Barton, *Some Observations on the Structure and Tensile Properties of AISI Type 316 Steel as a Function of Fast Reactor Irradiation Temperature,* AERE-R-6435 (June 1970).

Performance Model Development

F. J. Homan

Development of the FMODEL code[27] during this reporting period was limited primarily to updating the individual models included in the code to reflect recent experimental data and the incorporation of a sophisticated gap conductance model.[28–30] The newly incorporated gap conductance model replaces the model used formerly, where the code user had to specify the gap conductance for each time period of interest. This model considers conductance across an open gap and across a gap that has closed so that the fuel contacts the cladding. It also considers the burnup-dependent changes in the composition and thermal conductivity of the gas phase due to the introduction of fission gases into the plenum. Accommodation theory is also applied where the size of the gap is of the same order of magnitude as the mean free path of the gas species.

The major modeling effort during this reporting period has been in the area of sensitivity analysis. The sensitivity of predicted fuel pin performance to uncertainties in physical and mechanical properties of the fuel and cladding were investigated in detail. In addition, the influence of the manner of employment of individual phenomenological models within the integrated fuel performance model was analyzed. The purpose of the sensitivity work is to gain understanding of the influence of individual material properties on the overall performance of fuel pins. In particular, it is desirable to know where uncertainty associated with a given property is sufficiently large to cause concern for the fuel pin performance. One of the objectives of the modeling work is to identify areas in which experimental study needs intensification.

The influence of uncertainties in thermal expansion of both fuel and cladding on pins with small fabricated gaps was considered using the FMODEL code.[31] Uncertainty was defined by comparing property measurements published for nominally similar materials and

27. F. J. Homan, *Metals and Ceramics Div. Annu. Progr. Rep. June 30, 1971,* ORNL-4770, pp. 52–54.

28. C. M. Cox and R. L. Diamond, *LMFBR Fuel Cycle Studies Progr. Rep. July 1971, No. 29,* ORNL-TM-3534, p. 55 (limited distribution).

29. C. M. Cox, F. J. Homan, and R. L. Diamond, *LMFBR Fuel Cycle Studies Progr. Rep. August 1971, No. 30,* ORNL-TM-3571, pp. 38–39.

30. C. M. Cox, F. J. Homan, and R. L. Diamond, *LMFBR Fuel Cycle Studies Progr. Rep. February 1972, No. 36,* ORNL-TM-3759, pp. 42–53 (limited distribution).

31. F. J. Homan, *A Parametric Analysis of Fuel-Cladding Mechanical Interactions,* ORNL-TM-3508 (August 1971).

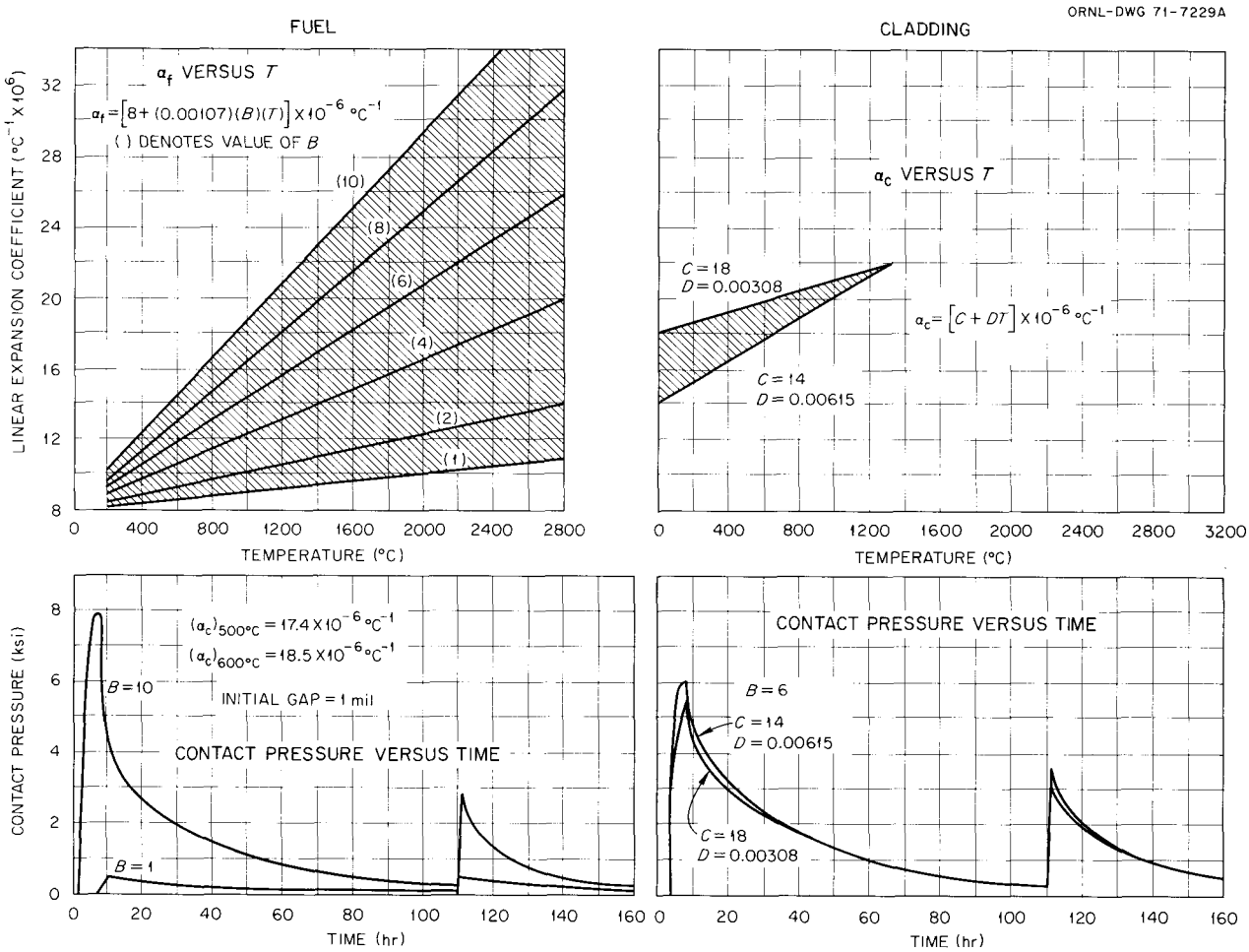

Fig. 15.5. Influence of uncertainty in fuel and cladding thermal expansion characteristics on mechanical interaction.

using the range of values as a measure of uncertainty. Then, using property data from the outer boundaries of the envelope of values so defined, performance was predicted with FMODEL, and the spread in predicted behavior used as a measure of the influence of uncertainty for that particular property. Using this technique we demonstrated that the uncertainty in cladding thermal expansion values was of little consequence; however, the uncertainty in fuel thermal expansion was of considerable importance in predicting the amount of mechanical interaction that would occur during the startup of a fuel pin with a small initial fuel-cladding gap.[31] This comparison is shown in Fig. 15.5. Also, the magnitude of this influence diminishes with increasing fabricated gap size.[31] From this analysis we concluded that additional experimental work is necessary to adequately characterize the thermal expansion characteristics of mixed oxide fuel, especially over the range of stoichiometries and compositions of interest for LMFBR.

The sensitivity of predicted performance to uncertainty in fuel thermal conductivity properties was also analyzed.[32] Thermal conductivity of mixed oxide fuels is influenced by a number of variables, including stoichiometry, density, temperature, burnup, plutonium content, and the shape and distribution of fabricated porosity. This last variable, the shape and distribution of fabricated porosity, is very influential as shown in Fig. 15.6, so the uncertainty related to this variable alone was investigated.[32] The study revealed a substantial impact on both the heat rate to melting and the mechanical interaction between fuel and cladding during startup of a small-gap, LMFBR-type fuel pin.

32. F. J. Homan, *LMFBR Fuel Cycle Studies Progr. Rep. September 1971, No. 31,* ORNL-TM-3614, pp. 42–46.

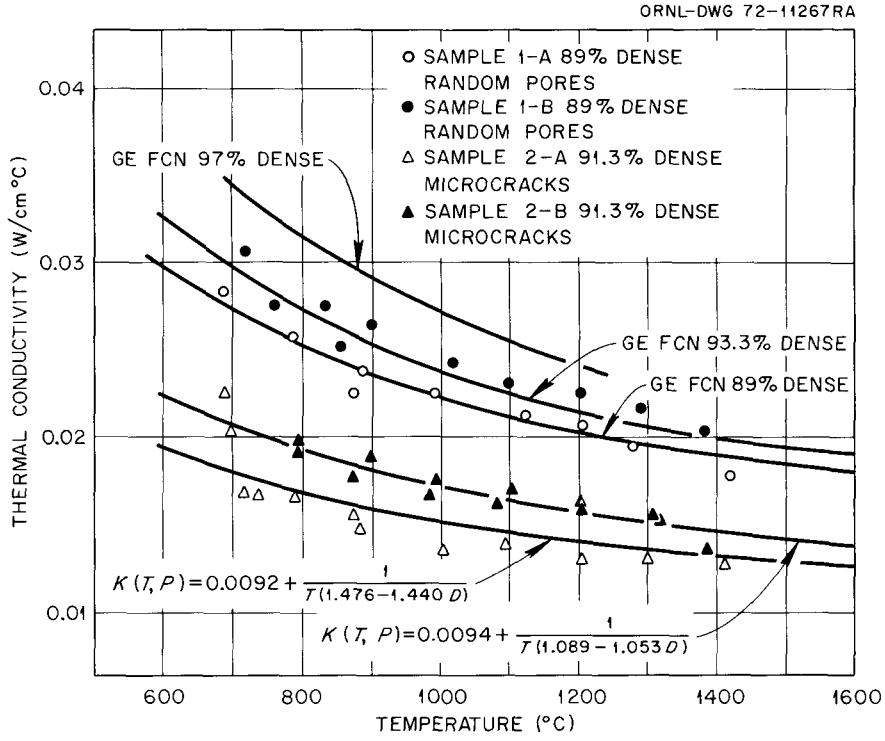

Fig. 15.6. Effects of pore morphology on thermal conductivity of UO_2–25% PuO_2 pellets sintered to about 90% of theoretical density.

This influence is shown in Fig. 15.7. The conclusions drawn in this case are somewhat different from those in the thermal expansion case, for a substantial body of information exists pertaining to thermal conductivity properties of mixed oxide fuels. However, it is important that the thermal conductivity properties of a given batch of fuel be carefully related to its microstructure and composition and that changes in these characteristics during irradiation be carefully taken into account[33] when the behavior of this fuel is modeled.

Studies of the influence of uncertainty in a given material property are fairly straightforward. Similar techniques can be employed to investigate effects that are postulated but not yet understood quantitatively. For example, the currently available equations to describe cladding swelling indicate a dependence on temperature and fast-neutron fluence. However, a stress effect has been postulated for some time[34,35] because of the differences noted between diametral expansion of the cladding, postirradiation immersion density measurements, and predicted behavior for a number of experimental pins using the temperature-fluence swelling correlations. Understanding the stress influence on void swelling in cladding materials is obviously needed to predict accurately how a fuel pin will behave in reactor.

As indicated earlier, the existing cladding swelling correlations describe swelling as a function of fast-neutron fluence and temperature. Given the fact that neutron fluence is relatively constant but a substantial temperature gradient exists across the cladding thickness, the question arises as to how to employ the swelling correlations. Should they be applied at one cladding node to represent the average cladding temperature, and thus the average volume change, or should they be applied at several nodes through the cladding to bring in the influence of differential swelling due to the temperature gradient? The predicted mechanical behavior of the cladding depends strongly on which alternative is selected, as can be seen in Fig. 15.8. In this figure the curve labeled "normal swelling" was calculated by applying the temperature-fluence cladding

33. W. J. Lackey, F. J. Homan, and A. R. Olsen, *Porosity and Actinide Redistribution during Irradiation of* $(U,Pu)O_2$, ORNL-TM-3762 (June 1971).

34. A. Boltax, T. P. Soffa, and A. Biancheria, *Trans. Amer. Nucl. Soc.* **14**, 631 (1971).

35. F. A. Garner et al., "The Effect of Stress on Radiation-Induced Void Growth," p. 841 in *Radiation-Induced Voids in Metals* (Proc. Intern. Conf., Albany, New York, June 9–11, 1971), ed. by J. W. Corbett and L. C. Ianiello, USAEC Office of Information Service, Oak Ridge, Tenn., 1972.

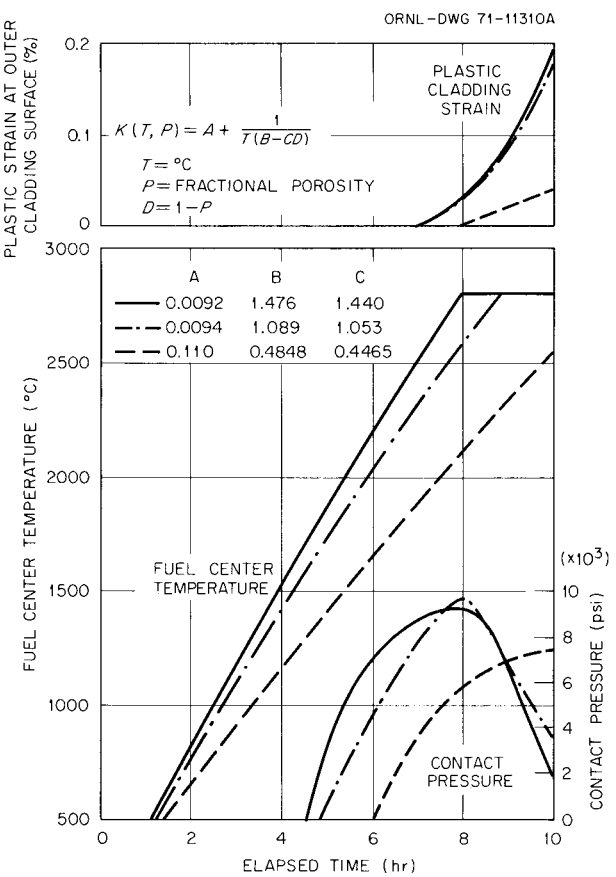

Fig. 15.7. Influence of fuel thermal conductivity on fuel pin performance during startup.

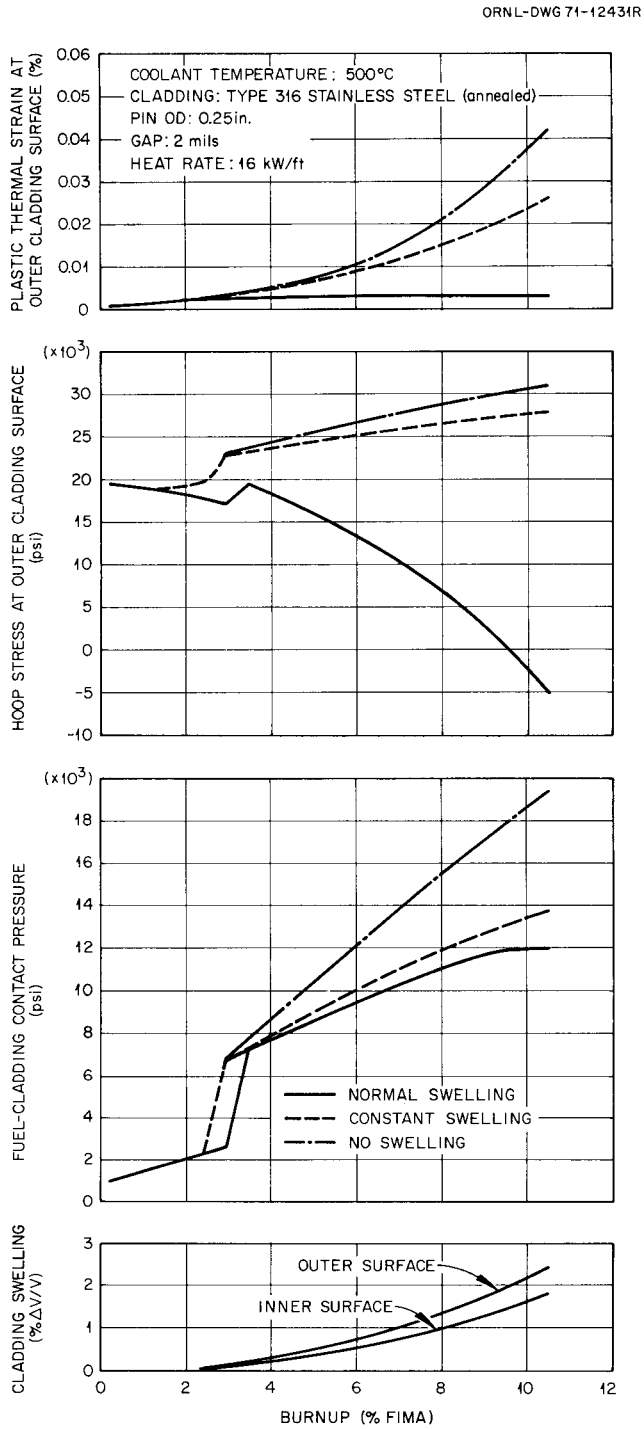

Fig. 15.8. Influence of method of application of cladding swelling equation on predicted mechanical behavior of cladding.

swelling correlation to each of six radial nodes spaced through the cladding wall. The curve labeled "constant swelling" was calculated by applying the correlation at only one node and assuming that cladding swelling is constant through the wall. The "no swelling" curve was calculated by assuming that the cladding does not swell because of irradiation and is shown merely for comparison. It is easily seen that the calculated cladding stresses and strains are strongly influenced by which cladding swelling assumptions are used in the calculations, indicating the need for more complete understanding of this phenomenon to achieve reliable performance predictions.

If swelling is calculated at several radial nodes throughout the cladding wall a swelling gradient is produced and causes stresses analogous to thermal stresses. Depending upon the location of the cladding temperatures with respect to the peak swelling temperatures, these stresses may either add to or subtract from the stresses due to internal pressurization. As with the thermal stresses, the stresses due to differential swelling across the cladding wall are relaxed with creep, but at high neutron exposures, where the temperature-fluence correlations predict very high cladding swelling rates,

very high stresses are calculated. The temperature-fluence correlations do not include stress effects, however, and if one side of the cladding is swelling more rapidly than the other, this side will be placed into compression and the other side into tension. It is intuitively appealing that cladding placed in tension will swell faster at the same temperature and neutron exposure than unstressed cladding, and theoretical calculations support this intuition.[32] The net effect is to reduce the swelling gradient and therefore the stresses caused thereby. If the converse is also true, and compressive stresses retard the swelling rate (also intuitively appealing), then the effect is more pronounced and the stresses due to swelling gradients are further reduced. The need for quantitative understanding of the stress influence on cladding swelling in order to achieve realistic behavior predictions in operating fuel pins is described in detail.[36]

Porosity, Actinide, and Oxygen Redistribution in Irradiated $(U,Pu)O_2$

W. J. Lackey F. J. Homan
A. R. Olsen

Thermal-gradient-induced redistribution of porosity and fuel components during irradiation of $(U,Pu)O_2$ will sufficiently alter the radial heat-generation profile,[37] fuel conductivity,[38–40] melting point,[41,42] oxygen activity,[43,44] and mechanical properties to significantly influence fuel pin performance. Accordingly, we have measured radial porosity and actinide profiles of irradiated fuel pins. Further, analytical models, which should prove useful in design and analysis of LMFBR fuels, were developed for predicting radial profiles of porosity, Pu:(U + Pu), and oxygen. These models have been incorporated into FMODEL, permitting determination of the consequences of fuel component redistribution on the thermal and mechanical performance of $(U,Pu)O_2$ fuel pins.

The interrelated porosity and actinide redistribution models are kinetic and based on the evaporation-condensation mechanism. An axial segment of the fuel pin of unit length is divided into 30 radial increments. After calculation of the radial temperature profile, it and the overall oxygen-to-metal ratio of the fuel are used to calculate the oxygen-to-metal distribution according to a previously proposed irreversible thermodynamic approach.[45] Next, the porosity of each of the radial increments at the end of a short time period is determined from knowledge of the initial porosity and calculation[46] of the movement of pores (or equivalently material) into and out of each radial increment. Similarly, since the initial Pu:(U + Pu) ratio for each radial increment and the amount of fuel transported into and out of each increment are known, the Pu:(U + Pu) ratio of each increment at the end of the time period can be calculated if the composition of the transported vapor is known. This composition was calculated[47] by equilibrium thermodynamics as a function of the temperature, oxygen-to-metal ratio, and Pu:(U + Pu) ratio of the solid fuel. Repeating the calculations for a series of time periods spanning the irradiation time can give the porosity, actinide, and oxygen radial profiles at any desired time.

Experimentally measured porosity and Pu:(U + Pu) radial profiles for a $U_{0.85}Pu_{0.15}O_{2.00}$ fuel pin clad with ¼-in.-OD stainless steel are shown to compare favorably with predicted profiles in Fig. 15.9. This Sphere-Pac fuel pin was irradiated in the ETR at a linear heat rate of 13.6 kW/ft to a burnup of 0.7% FIMA. The columnar grain region is considerably more porous than previously generally believed. We have observed the same to be true for pins irradiated in a fast-neutron flux. In the present case, the calculated fuel center

36. F. J. Homan, *LMFBR Fuel Cycle Studies Progr. Rep. October 1971, No. 32,* ORNL-TM-3624, pp. 46–64 (limited distribution).

37. W. T. Sha, P. R. Huebotter, and R. K. Lo, *Trans. Amer. Nucl. Soc.* **14,** 183–84 (1971).

38. R. L. Gibby, *J. Nucl. Mater.* **38,** 163–77 (1971).

39. R. L. Gibby, *The Effect of Oxygen Stoichiometry on the Thermal Diffusivity and Conductivity of* $U_{0.75}Pu_{0.25}O_{2-x}$, BNWL-727 (January 1969).

40. General Electric Breeder Reactor Development Operation, *Sodium-Cooled Reactors, Fast Ceramic Reactor Development Program,* GEAP-10028-35 (September 1970), pp. 44–49.

41. W. L. Lyon and W. E. Baily, *J. Nucl. Mater.* **22,** 332–39 (1967).

42. E. A. Aitken and S. K. Evans, *A Thermodynamic Data Program Involving Plutonia and Urania at High Temperatures, Quart. Rep. No. 4,* GEAP-5672 (1968).

43. J. A. Christensen, "Transport Processes in Oxide Nuclear Fuels," pp. 109–25 in *Ceramic Nuclear Fuels International Symposium, May 3–8, 1969, Washington, D.C.,* American Nuclear Society, Hinsdale, Ill., 1969; also BNWL-1202.

44. E. A. Aitken and S. K. Evans, "Thermodynamic Behavior of Plutonium Oxide Systems in a Temperature Gradient," pp. 772–80 in *Plutonium 1970 and Other Actinides, Nucl. Met.* **17,** (Part 2), The Metallurgical Society of AIME, New York, 1970.

45. General Electric Breeder Reactor Development Operation, *Sodium-Cooled Reactors, Fast Ceramic Reactor Development Program,* GEAP-10028-37 (March 1971), pp. 38–40.

46. F. J. Homan, *Fuels and Materials Development Program Quart. Progr. Rep. Dec. 31, 1970,* ORNL-TM-3300, pp. 33–39.

47. W. J. Lackey, A. R. Olsen, and D. K. Bates, *Fuels and Materials Development Program Quart. Progr. Rep. Dec. 31, 1970,* ORNL-TM-3300, pp. 33–39.

temperature was 9.6% (200°C) higher when based on the observed porosity distribution rather than the previously generally assumed three-zone porosity distribution model. This work has been described.[48]

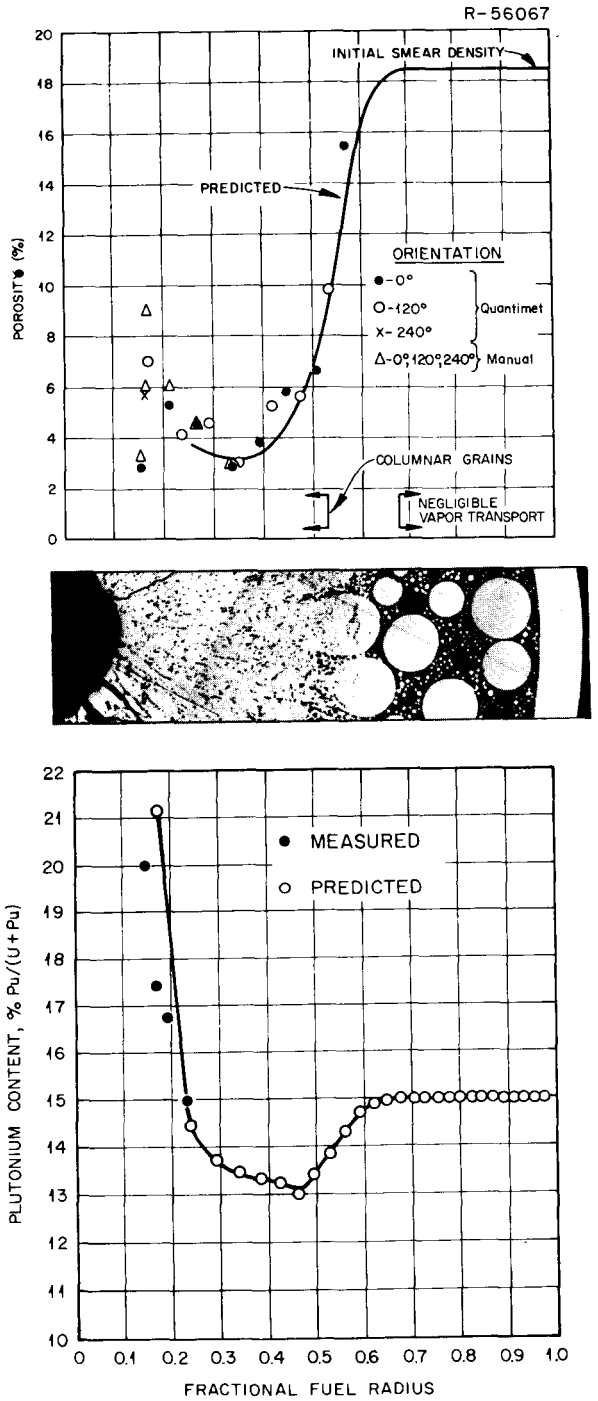

Fig. 15.9. Comparison of measured and predicted porosity and Pu:(U + Pu) profiles.

Analysis of ORR Instrumented Thermal Performance Tests

R. B. Fitts F. L. Miller[49]

Two type 304 stainless-steel-clad $(U,Pu)O_{1.99}$ fuel pins, one containing pellet fuel and the other Sphere-Pac fuel, were irradiated[50–52] in the third thermal performance test capsule, SG-3, in the Oak Ridge Research Reactor. In each pin the fuel smear density was 82% of theoretical, and the burnup achieved was about 0.5% FIMA. The goal of this irradiation test was to compare and quantify the relationship between center-line temperatures and average heat generation rates within the two fuel pins. The final detailed analysis of the thermometry data has been carried out and reported during the past year.[53]

Data from the SG-3 capsule were obtained from 12 thermocouples at the midlength of each fuel pin. The fuel and cladding temperatures and the heat flow from the fuel pins were monitored. The method of data analysis consisted of iteration of two steps. First, low-order polynomials were fitted by least squares to functions of the measured temperatures (e.g., center-line temperatures vs the average from the cladding thermocouples). Then deviations or differences from the fitted line were plotted against time, and patterns in these deviations were investigated. The polynomial used to describe the data was finally revised to better represent the data.

The above technique permitted a statistically valid definition of the differences in behavior of the two fuel pins, leading to the following observations.

1. Under the same conditions of steady-state heat generation rate and cladding temperature, the central temperature (°C) in the Sphere-Pac fuel is always cooler than that in the pellet fuel by 11.7 ± 1.2% at the 99% confidence level (see Fig. 15.10).

---

48. W. J. Lackey, F. J. Homan, and A. R. Olsen, *Porosity and Actinide Redistribution during Irradiation of* $(U,Pu)O_2$, ORNL-TM-3762 (June 1971).

49. Mathematics Division.

50. R. B. Fitts et al., *Trans. Amer. Nucl. Soc.* **13**, 549–50 (1970).

51. A. R. Olsen, R. B. Fitts, and W. J. Lackey, "In-Reactor Restructuring Temperatures and Kinetics for $(U,Pu)O_2$," pp. 579–602 in *Proc. Conf. Fast Reactor Fuel Element Technology*, ed. by Ruth Farmakes, American Nuclear Society, Hinsdale, Ill., 1971.

52. R. B. Fitts, *Metals and Ceramics Div. Annu. Progr. Rep. June 30, 1971*, ORNL-4770, pp. 50–51.

53. R. B. Fitts and F. L. Miller, *Trans. Amer. Nucl. Soc.* **15**(1), 180 (1972).

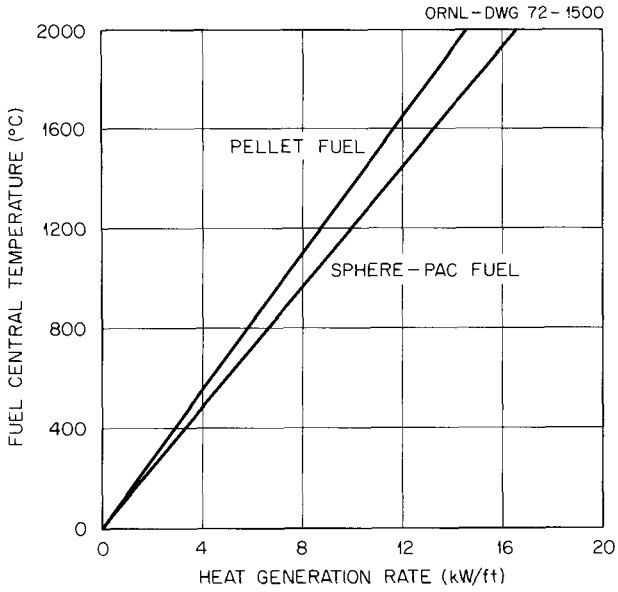

Fig. 15.10. Relationship between central temperature and heat rating for Sphere-Pac and pellet fuel pins in capsule test SG-3. The Sphere-Pac fuel is always 11.7 ± 1.2% cooler than the pellet fuel at the 99% confidence level.

2. Power cycling significantly affects fuel pin central temperature. In both fuel pins the central temperature at 8 to 16 kW/ft was about 250°C higher upon initial return to power after a reactor shutdown than it was at the same heat rate during steady-state operation. The duration of this fluctuation (several hours) was a function of the operating conditions and fuel form; the pellet fuel required the longer recovery time.

3. The effect of time at temperature on the temperature in the Sphere-Pac fuel pin was not significant, but small decreases in the heat generation rate were required to maintain a given pellet fuel temperature, indicating a slow worsening of heat transfer in the pellet fuel pin.

CASDAR: A Nuclear Data Manipulation Program

J. D. Jenkins[54] G. W. Cunningham[49]

A computer program, CASDAR[55] (Cross Sections and Spectra Direct Access Retrieval), has been completed and conveniently manipulated the large amounts of nuclear data used in fuel depletion and radiation damage calculations. The program contains an extensive library of neutron cross section data culled from a number of sources[56–58] and a library of neutron spectra for a number of reactors used as irradiation facilities. In addition, neutron spectrum information for specific experimental configurations as calculated by a number of reactor physics design codes[59–61] can be conveniently input to the program. These data can be used to provide spectrum-averaged effective cross sections.

The program interfaces with the depletion program ORIGEN,[62] which is designed to calculate the isotopic history of fuel and cladding materials during and after irradiation. CASDAR will provide on demand a properly spectrum-averaged neutron cross section library for ORIGEN using either one of its precalculated and stored library spectra or an input spectrum for a specific experimental facility.

In addition, the program can provide other types of data needed for the design and interpretation of irradiation experiments. For example, the program will provide on request spectrum-averaged damage cross sections, few-group averaged cross sections, calculated reaction rates for dosimeter evaluation, and plots of neutron cross sections and spectra. All of this information is available from the precalculated and stored data in the CASDAR library. Thus the program provides the materials scientist with convenient access to nuclear data and reactor spectra in a form directly applicable to the design and interpretation of his experiments and relieves him of the onus of calculating this information for himself.

54. Reactor Division.

55. J. D. Jenkins and G. W. Cunningham, *CASDAR, a Cross Section and Spectrum Direct Access Retrieval System for Nuclear Data Manipulation,* report in preparation.

56. H. C. Honeck, *Specifications for an Evaluated Nuclear Data File for Reactor Applications,* BNL-50066 (May 1966), revised by S. Pearlstein, Brookhaven National Laboratory, July 1967.

57. G. D. Joanou and J. S. Dudek, *GAM-II: A B_3 Code for the Calculation of Fast-Neutron Spectra and Associated Multigroup Constants,* GA-4265 (1963).

58. W. E. Alley, R. W. Gell, and R. M. Lessler, *Semiempirical Neutron Induced Reaction Cross Sections,* UCRL-50484 (August 1968).

59. W. W. Engle, Jr., *A User's Manual for ANISN,* K-1693 (March 1967).

60. N. M. Greene and C. W. Craven, Jr., *XSDRN: A Discrete Ordinates Spectral Averaging Code,* ORNL-TM-2500 (July 1969).

61. T. B. Fowler and D. R. Vondy, *Nuclear Reactor Core Analysis Code: CITATION,* ORNL-TM-2496 (July 1969).

62. M. J. Bell, *ORIGEN: The ORNL Isotope Generation and Depletion Code,* ORNL-4628, to be published.

CHEMICAL MODELING OF FUEL-CLADDING ATTACK IN LMFBR OXIDE PINS

Our goal in this program has been to understand the chemical attack that occurs between $(U,Pu)O_2$ and stainless steel cladding.

Analysis of Intergranular Attack Data

J. M. Leitnaker F. J. Homan

Since intergranular attack (IGA) seems potentially of greatest concern to LMFBR cladding, we analyzed much of the available data on this phenomenon. Out-of-reactor IGA of type 316 stainless steel by Ar–4% H_2–4000 ppm H_2O in the range 948 to 1190°K (ref. 63) obeys the rate equation[64]

$$\log_{10} \text{IGA (cm/hr)} = 4816/T(^\circ\text{K}) - 1.3129 .$$

In comparison, for a well-characterized thermal reactor experiment, GE pin B3C, which contained $(U,Pu)O_2$ with starting oxygen-to-metal ratio (O/M) of 2.00 clad with type 347 stainless steel, available data[64,65] in the range 821 to 1043°K fit the equation

$$\log_{10} \text{IGA (cm/hr)} = -4666/T(^\circ\text{K}) - 1.080 .$$

We compare these data in Fig. 15.11. Other in-reactor IGA data of less well-known temperatures and with starting O/M between 1.94 and 2.00 fall suggestively near these parallel lines; these data are shown in Fig. 15.12. Note that the IGA rate appears to drop as the O/M decreases.

In marked contrast to the above results, Sphere-Pac fuels made from sol-gel-derived $(U,Pu)O_2$ with starting O/M of 2.00 show no IGA. These data are shown in Fig. 15.13 as limits of experimental observations, 5×10^{-4} cm on IGA. The data seem to imply that the rate-limiting IGA mechanism is similar in all cases except Sphere-Pac fuel pins, in which a blocking mechanism occurs.

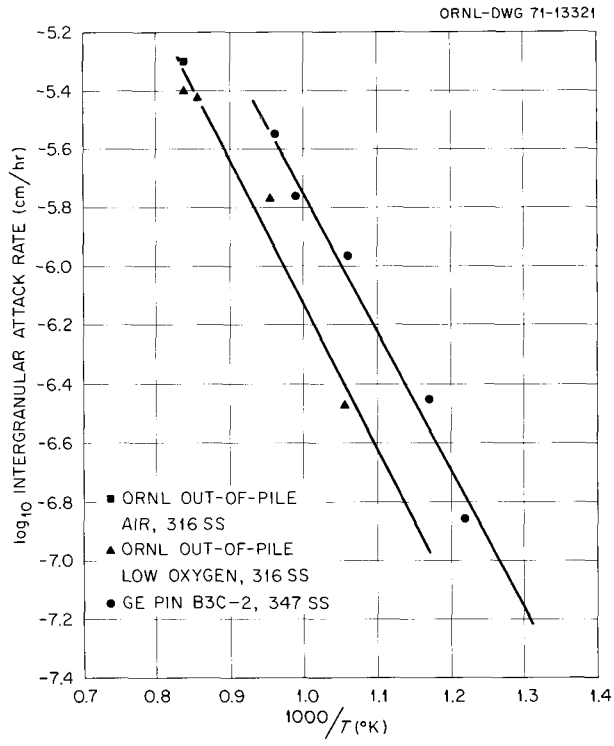

Fig. 15.11. Intergranular attack rates in stainless steel.

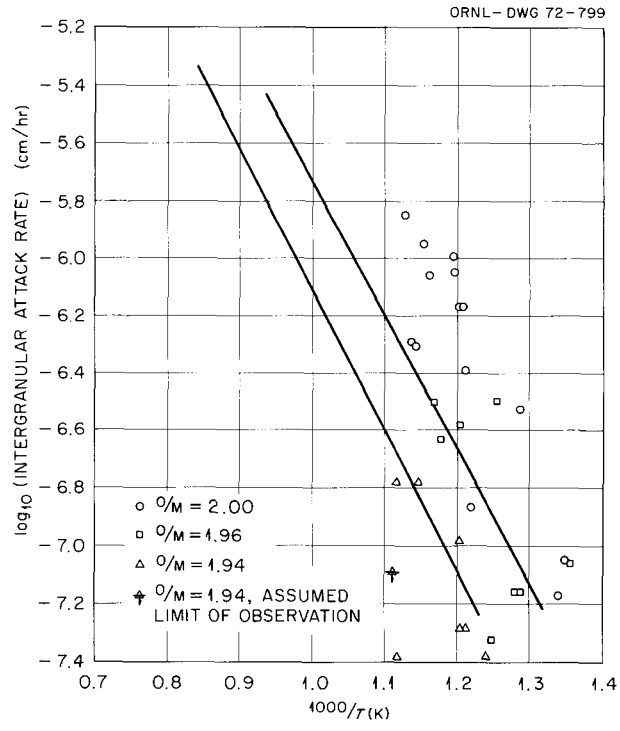

Fig. 15.12. Influence of fuel oxygen-to-metal ratio on cladding intergranular attack rates. Reference lines from Fig. 15.11.

63. R. B. Fitts, E. L. Long, Jr., and J. M. Leitnaker, "Observations of Fuel-Cladding Chemical Interactions as Applied to GCBR Fuel Rods," pp. 431–58 in *Proc. Conf. Fast Reactor Fuel Element Technology,* ed. by Ruth Farmakes, American Nuclear Society, Hinsdale, Ill., 1971.

64. J. M. Leitnaker and R. E. Adams, *LMFBR Fuel Cycle Studies Progr. Rep. November 1971, No. 33,* ORNL-TM-3663, pp. 40–47 (limited distribution).

65. K. E. Gregoire, P. E. Novak, and R. E. Murata, *Failed Fuel Performance in Naturally Convecting Liquid Metal Coolant,* GEAP-13620 (June 1970).

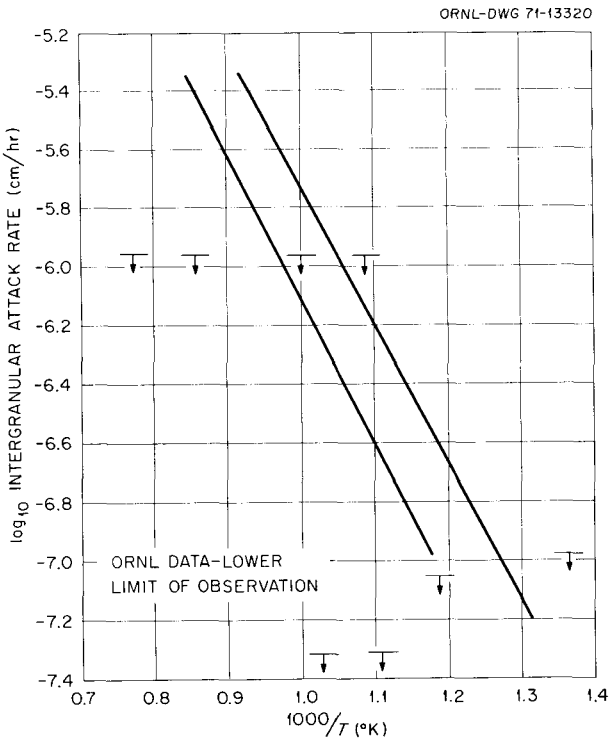

Fig. 15.13. Limit of intergranular attack rate on sol-gel-derived Sphere-Pac mixed oxide fuel. Reference lines from Fig. 15.11.

Elimination of CO_2 and H_2O as Oxygen Transport Species in Mixed Oxide Fuel Pins[66]

J. M. Leitnaker K. E. Spear[67]

Thermodynamic and kinetic calculations show that both CO_2 and H_2O do not transport oxygen in typical near-stoichiometric LMFBR mixed oxide fuel.[68] Thus, current gas-phase transport theories[69,70] do not correctly describe the oxygen distribution mechanism in such a pin. A method for measurement of the oxygen potential across an oxide fuel pin involving determination of Mo and MoO_2 concentrations is possible and may serve as a basis to establish the actual mechanism.[68]

66. Submitted to Journal of Nuclear Materials; also ORNL-TM-3849 (June 1972).

67. Consultant from Materials Research Laboratory, Pennsylvania State University, University Park, Pa. 16802.

68. J. M. Leitnaker, *Fuels and Materials Development Program Quart. Progr. Rep. Dec. 31, 1971,* ORNL-TM-3703, pp. 13–18.

69. M. H. Rand and L. E. J. Roberts, "Thermodynamics and Nuclear Engineering," pp. 3–31 in *Thermodynamics,* vol. I, International Atomic Energy Agency, Vienna, 1968.

70. M. H. Rand and T. L. Markin, "Some Thermodynamic Aspects of $(U,Pu)O_2$ Solid Solutions and Their Use as Nuclear Fuels," pp. 637–50 in *Thermodynamics of Nuclear Materials,* International Atomic Energy Agency, Vienna, 1968.

16. Fabrication Development for Fast Breeder Reactor Cladding

W. R. Martin A. C. Schaffhauser

The goals of this program are consistent with the need for high-quality but economical tubing for the FBR. For this reporting period, our efforts have been directed toward testing the effects of surface defects on the mechanical properties of type 316 stainless steel.

BIAXIAL CREEP-RUPTURE OF STAINLESS STEEL TUBING WITH ELECTRO-DISCHARGE MACHINED NOTCHES

R. T. King K. V. Cook
G. A. Reimann

The biaxial stress-rupture properties of annealed and 20%-cold-worked type 316 stainless steel tubing at 650°C have been investigated by testing internally pressurized tubes. Electro-discharge machined notches were made in the sufaces of 0.635-cm-diam X 0.041-cm-wall-thickness tubes, and they were always located on the thinnest segment of the wall. The effects of nominal notch depths equivalent to 10, 33, and 66% of the wall thickness and notch lengths of 0.076 and 0.635 cm were systematically explored as a function of applied stress. After machining, the notches were about 0.006 cm wide.

The test stresses produced rupture times varying from about 1 to 1000 hr. Under these conditions, all notched tubes that failed in the gage length of the specimen failed at the notch. Metallographic studies consistently showed accelerated deformation and intergranular cracking beneath the notches. This behavior was observed for both annealed and cold-worked tubing, regardless of whether the notches were located on the inside or outside surface of the tube.

The circumferential strains and rupture times of notched tubes and un-notched control specimens were compared. Notched tubes exhibited shorter rupture times and less circumferential strain, and the degradation of properties increased with increasing notch depth. Long notches had significantly greater effect upon the rupture life and circumferential strain than short notches because of the smaller constraint to deformation under a long notch. Within the limits of experimental error, there was no distinguishable difference between locating a given notch on the inner or outer surface of a tube. Generally, the effects of a given notch geometry were less severe in annealed tubing than in the cold-worked tubing.

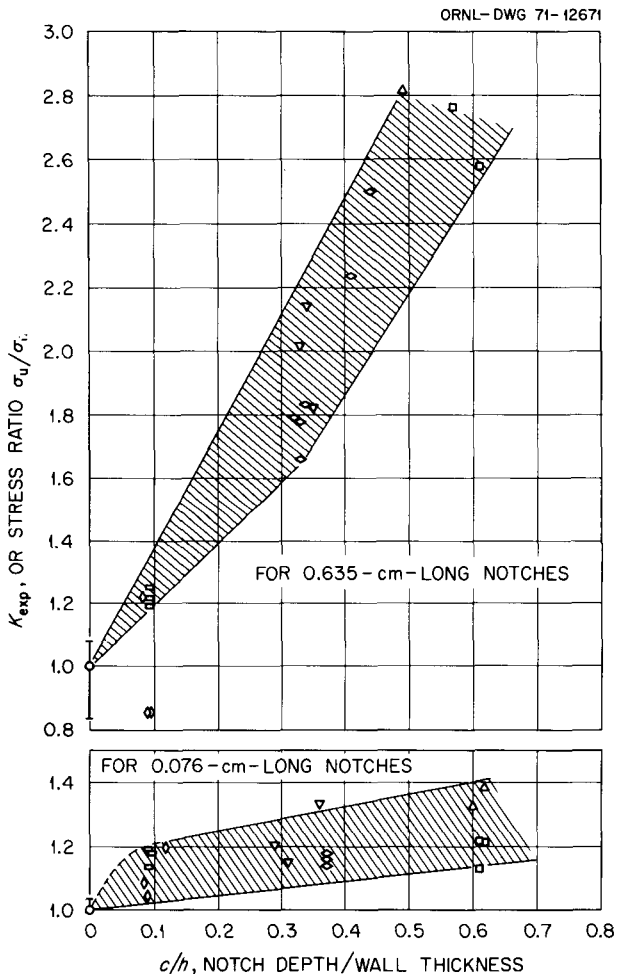

Fig. 16.1. Ratio of control specimen stress (σ_u) to notched specimen stress (σ_n) to cause failure after the same time for cold-worked type 316 stainless steel tubing at 650°C.

The results are not unique to the materials employed in this experiment. An abbreviated series of tests on tubing fabricated from another heat of type 316 stainless steel produced similar results.

There are several theoretical treatments of the stresses present near notches and cracks in elastic materials, but the rupture times for these tests do not correlate well with any such stresses. Such agreement would be fortuitous, in view of the involved time-dependent plastic flow processes under these notches. An interim analysis based on steady-state creep and a strain-limited fracture criterion have been developed and applied to the data to interpret these results. The analysis provides an internally consistent explanation of the observations.

A significant conclusion is that a simple design allowance for defects in cold-worked tubing based on the remaining cross-sectional area beneath the defect is not sufficient. A notch whose depth equals 10% of the wall thickness may require about a 20% reduction in stress to produce rupture in a given time. The ratio of stresses required to cause an un-notched tube (σ_u) and a notched tube (σ_n) to fail in a given time is a measure of the design stress concentration allowance that should be made for various ratios of notch depth to wall thickness. The specific results for 20%-cold-worked tubing are shown in Fig. 16.1.

EFFECTS OF SHARP ARTIFICIAL NOTCHES ON THIN-WALL TYPE 316 STAINLESS STEEL TUBING

R. T. King K. V. Cook
G. A. Reimann

Techniques have been developed for fabricating drawn tubing containing sharp artificial notches (about 0.0001 in. wide) parallel to the tube axis.[1] Sharp notches having 0.0005-, 0.0012-, and 0.0036-cm nominal depths and 0.63-cm lengths have been produced in 20%-cold-drawn type 316 stainless steel tubing. Sets of tubes were then tested in biaxial creep at 650°C over a range of stresses selected to produce rupture times ranging from about 10 to nearly 1000 hr.

The results of these tests show that sharp notches produce effects on tubing rupture life and ductility similar to those produced by electro-discharge machined notches (see above). Because of the stress concentrating effect of the nothces, more rapid defor-ation occurs beneath the notches than elsewhere in the tube (Fig. 16.2). Almost all of the tubes bearing deeper

1. K. V. Cook, G. A. Reimann, and R. W. McClung, *Metals and Ceramics Div. Annu. Progr. Rep. June 30, 1971,* ORNL-4770, p. 80.

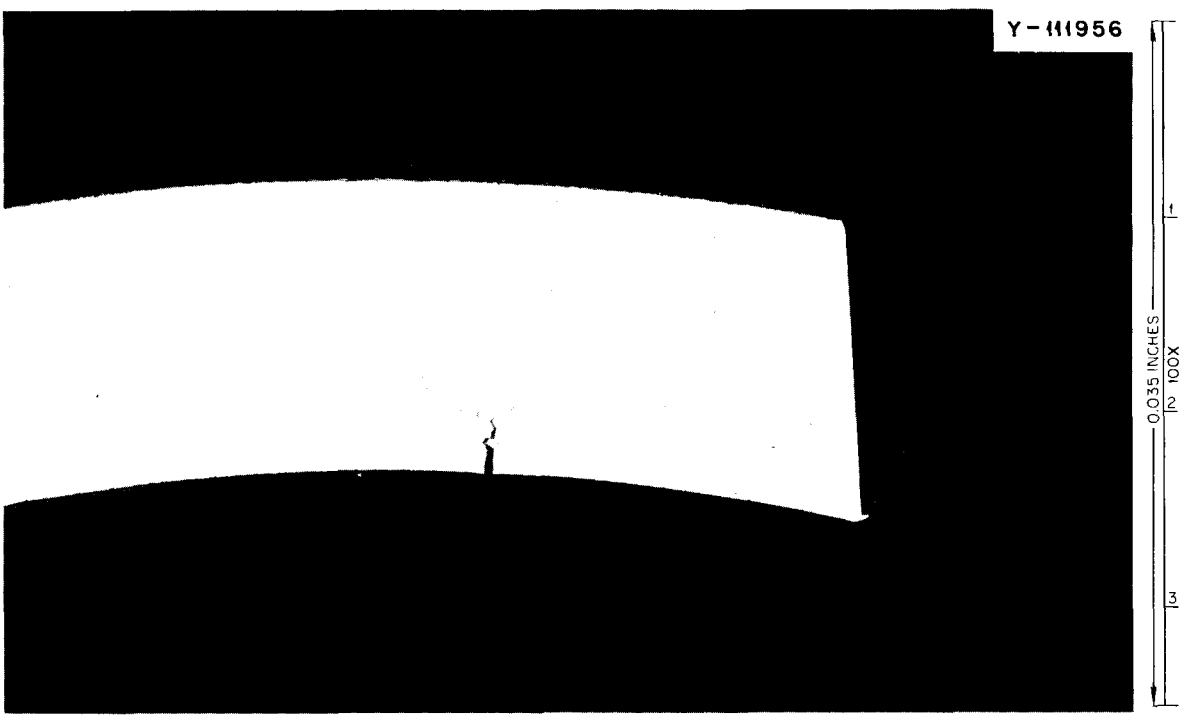

Fig. 16.2. Typical cross section of specimen tested with deep sharp notch. Test interrupted before failure occurred.

notches failed at the notches, whereas several tubes bearing 0.0005-cm-deep notches did not fail at the notches, and the effect of increasing notch depth was to reduce rupture time and ductility. A report concerning the analysis of the results is being prepared.

17. Joining of Structural Materials

G. M. Slaughter

The LMFBR welding development program is concentrated on three types of materials: austenitic stainless steels, nickel-rich alloys such as Incoloy 800 and Inconel 718, and ferritic steels.

STAINLESS STEELS

G. M. Goodwin N. C. Cole R. G. Berggren

We are studying the effect of chemical composition, welding process, and variables within a process on the behavior of weldments in austenitic stainless steels at 370 to 650°C for application to LMFBR vessels and components. Included in the program are the shielded metal-arc, gas tungsten-arc, submerged-arc, gas metal-arc, and electroslag welding processes. Section sizes range from ½ in., typical of LMFBR piping wall thicknesses, to 2⅜ in., representative of a typical LMFBR vessel wall. The information generated in these programs has pointed out a serious lack of long-term, elevated-temperature ductility in conventional austenitic stainless steel weldments and has been influential in the selection of a "controlled residual element" (CRE) filler metal having superior strength and ductility for use in the Fast Flux Test Facility vessel.[1] Piping welds are currently under intensive study.

Heavy Section Weldment Evaluation

We continued the evaluation of 36 heavy section (≥ 1 in. thick) weldments prepared using the shielded metal-arc, submerged-arc, gas metal-arc, and electroslag welding processes.

The study of the shielded metal-arc process has concentrated on the effects of minor compositional variations of the weld deposit produced by altering the electrode coating composition. We produced 23 welds in 1-in.-thick type 304 stainless steel plate, all conforming to the AWS-ASTM composition specifications for type 308 stainless steel filler metal. The series was composed of three welds of nominally identical composition made with different type electrode coatings, and 20 welds with intentional variations in the amounts of B, P, Si, S, C, and Ti in the deposit. Approximately 100 specimens from the weldments were creep tested at 650°C for times up to 5000 hr. Based on the single effects of each of the above elements, an optimized composition containing boron, phosphorus, and ferrotitanium was developed. These special "controlled residual element" (CRE) electrodes yield welds with excellent high-temperature strength properties and, as shown in Fig. 17.1, superior high-temperature creep ductility.

Eleven submerged-arc welds were produced in both 1- and 2-in.-thick plates. The object was to study the variability in elevated temperature properties attributable to flux composition and to the energy input used during welding. Only commercially available fluxes were investigated, and for these fluxes other variables,

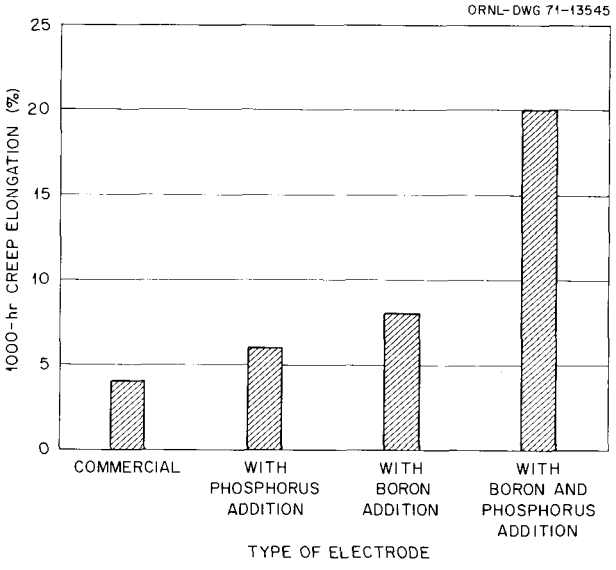

Fig. 17.1. Effect of residual elements on the ductility of type 304 stainless steel shielded metal-arc welds at 650°C.

1. G. M. Goodwin, N. C. Binkley, N. C. Cole, and R. G. Berggren, *Metals and Ceramics Div. Annu. Progr. Rep. June 30, 1971*, ORNL-4720, pp. 82–85.

particularly deposit composition, far outweighed the effect of flux formulation. Increasing heat input had a significant effect of decreasing strength and increasing ductility, but the effect was small by comparison with other variables.

Two electroslag weldments are being studied. Both are in 4-in.-thick material, with one weld joining two type 304 stainless steel plate sections and the other between two type CF8 stainless steel castings. Creep data have been collected for both base materials and the weld deposits. In general, the weld deposits are weaker than either the wrought or cast base material but have comparable ductility. The electroslag welds are slightly weaker but of greater ductility than the submerged-arc welds, presumably at least in part because of the heat input effect mentioned above. Two gas metal-arc welds produced with different shielding gas mixtures are being examined.

We have procured approximately 42 lin ft of weldment in $2\frac{3}{8}$-in.-thick plate for a detailed study discussed below. The welds are made in plate from two of the five FFTF vessel heats and electrodes from 7 of the 11 batches used to date in fabrication of the vessel.

Properties of Stainless Steel Welds with Controlled Residual Elements

R. T. King G. M. Goodwin J. O. Stiegler

We are investigating the structure and properties of CRE double-U-joint test weldments similar to those in the FFTF vessel to obtain design data and an understanding of properties. The test weldments join $2\frac{3}{8}$-in.-thick sections of type 304 stainless steel plate. Tensile and creep specimens have been prepared from different depths within the weld. Specimens oriented parallel to the welding direction (longitudinal), perpendicular to the welding direction (transverse), and perpendicular to the plate surfaces have been prepared with a 0.25-in.-diam × 1.25-in.-long gage section.

The CRE weld metal specimens from near the surface of the test weldments are generally weaker and more ductile than those from nearer the center of the weldments in tensile tests from 25 to 649°C. Hardness indentation profiles also showed increasing hardness from the surface to the center of the welds. This variation in short-time mechanical properties may be related to localized variations in the microstructure of the weld with an unknown contribution from chemical segregation effects. Near the surface of the weld, about 10^{10} straight dislocation lines/cm^2 and a few small loops exist; in the same region, relatively few carbide precipitate particles are found on austenite-ferrite interfaces. Toward the center of the weld, the loop and dislocation line densities increase, and most dislocations are involved in a well-defined cell structure. Also, the austenite-ferrite interfaces are decorated with carbide precipitate particles.

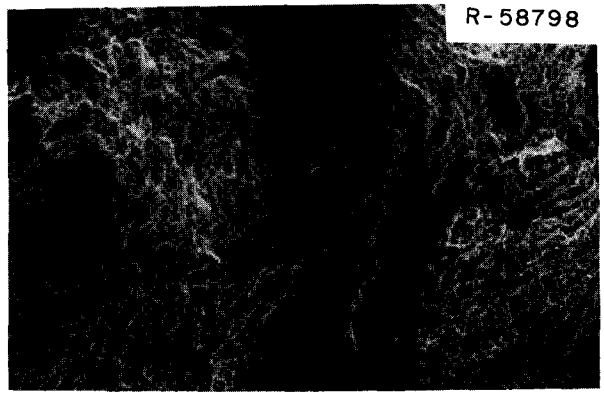

Fig. 17.2. Fracture surface of a controlled residual element weld specimen tested at 565°C. Inclusion particles are embedded in the fracture surface. 130×.

Transverse tensile specimens always fractured in the weld metal rather than in the base metal or heat-affected zones. Anisotropic deformation occurred in both longitudinal and transverse specimens, and the directions of the principal axis of anisotropy probably coincide with the local substructural orientation, which changes from point to point in the weld cross section.

The creep properties showed similar variations through the weld thickness to those observed in tensile tests. In one series of tests, weld metal from near the surface had a minimum creep rate nearly 1000 times greater than did similar specimens from near the weld center. The fracture surfaces of creep-rupture specimens were covered with shear dimples, which are normally associated with ductile fractures in metals. Figure 17.2 shows the fracture surface of a specimen that failed at 565°C after 2780 hr at 33,000 psi; ductile tearing occurred but is related to the local substructure only in isolated areas. Creep specimens exhibited ductility in excess of 15% for all tests completed to date. Although there is some tendency for the ductility to decrease with increasing rupture time (Fig. 17.3), the ductility of the CRE welds is considerably higher than that reported for conventional type 308 stainless steel weld metal.

Filler Metal Development for Pipe Welding

We are studying the properties of welds in $\frac{1}{2}$-in.-thick wrought types 304 and 316 stainless steel for application to LMFBR piping systems. In addition to

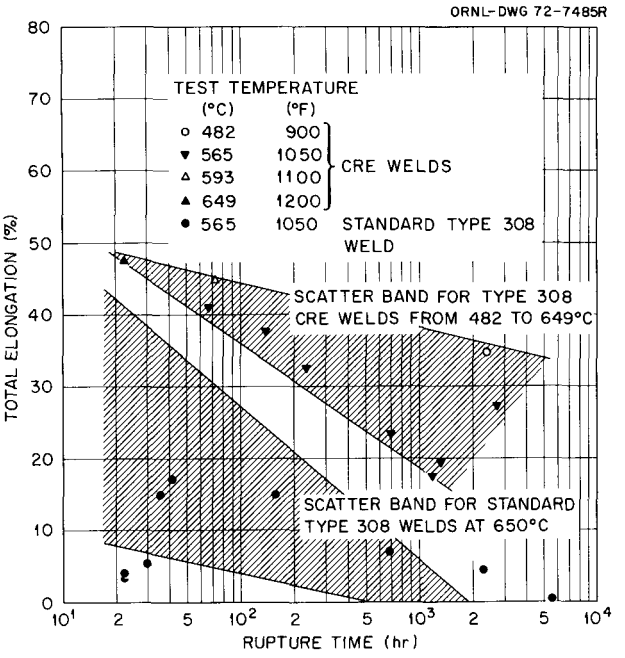

Fig. 17.3. Ductility in creep-rupture tests of type 308 stainless steel welds.

determining the elevated-temperature mechanical properties of conventional filler metals used with the shielded metal-arc and gas tungsten-arc processes, we are attempting to develop improved filler metals for types 304 and 316 stainless steel using essentially the same approach as was outlined in the heavy-section weldment study described above. Automated orbital welding equipment will be used to apply the information obtained to the production and evaluation of actual pipe welds in typical LMFBR piping up to and including 28 in. in diameter.

To date, 34 weldments, each approximately 10 in. long, have been produced in ½-in.-thick wrought types 304 and 316 stainless steel. Welds were made with the gas tungsten-arc and shielded metal-arc processes and conventional types 308, 316, and 16 Cr–8 Ni–2 Mo stainless steel filler metals, in addition to ten experimental tungsten-arc filler wires and 16 experimental batches of shielded metal-arc electrodes. As anticipated, the type 316 stainless steel weldments (including type 16 Cr–8 Ni–2 Mo stainless steel filler metal) exhibit greater strength than any of the type 308 stainless steel welds, but the ductility values obtained to date indicate a reduction in long-term creep ductility similar to that noted for type 304 stainless steel heavy section weldments. Our present plans emphasize the development of "controlled residual element" compositions for type 316 stainless steel weldments for direct application to the FFTF hot-leg piping.

NICKEL-RICH ALLOYS

D. A. Canonico

Inconel 718

We have assisted Aerojet Nuclear Corporation in preparing a program plan for the study of Inconel 718, an age-hardenable high nickel alloy. Our interest is associated with the effect of welding on the mechanical properties, in particular ductility, of postweld-heat-treated components. The aim of this program is to obtain ASME Code approval for Inconel 718.

Incoloy 800

Incoloy 800, an Fe-Ni-Cr alloy, is being considered for the construction of LMFBR steam generators. The weldability of this alloy without filler-metal additions is marginal, and current practices usually require the use of Inconel 82 filler metal. Inconel 82 is a Ni-Cr-Fe alloy whose physical and mechanical properties are quite unlike those of Incoloy 800. The study of the effect of various minor elements on the weldability of Incoloy 800 has provided an insight into their effect on cracking sensitivity.

We have continued[2] our studies on several experimental Incoloy 800 (Fe–32.5% Ni–21% Cr) compositions prepared in the Melting and Fabrication Laboratory at ORNL. Hot-ductility studies have shown that 0.08% C in the presence of 0.38% Ti slightly impairs the recovery of ductility after a thermal excursion simulating that experienced in the heat-affected zone of a weld. Adding nominally 0.015% S to an experimental alloy of a similar composition caused a distinct loss in the alloy's ability to recover ductility. This is in contrast to the ductility recovery observed when similar sulfur and titanium levels, without carbon, were investigated. Apparently, the carbon combines with the titanium, thereby negating its ability to immunize the Incoloy 800 against the deleterious effects of sulfur.

The use of experimental Incoloy 800 alloys as filler metals has provided additional information regarding the effect of the minor elements on weldability. A filler metal with high titanium (≈0.60%), medium carbon (≈0.04%), low sulfur (<0.010%), and medium phosphorus (≈0.015%) produced a weld metal with the least fissuring propensity. Furthermore, our studies have shown that the weld metal fissures were intergranular.

2. D. A. Canonico, *Metals and Ceramics Div. Annu. Progr. Rep. June 30, 1971*, ORNL-4770, pp. 128–29.

Welds made with the commercial 82T filler metal and the experimental Incoloy 800 filler metals showed a dramatic difference in microstructure.

The 82T welds exhibited a cellular microstructure, whereas the experimental Incoloy 800 filler metal welds contained large columnar grains epitaxially growing from the base metal. Reducing the grain size of the heat-affected zone at the fusion line did not affect the weld metal microstructure. Much of the cracking sensitivity exhibited by the Incoloy 800-type filler metals is attributed to the solidification morphology of the experimental weld metal. Thus our efforts to eliminate the cracking problems with Incoloy 800 weld metal have been somewhat successful. We have produced weld microstructures similar to those seen in welds made with Inconel 82 filler metal. A slight propensity toward cracking prevails, however, and our alloy development studies will continue on a limited basis.

FERRITIC STEELS

D. A. Canonico

Stabilized Grades

The investigation of the stabilized ferritic steels has concentrated on the niobium-stabilized 2¼ Cr–1 Mo–½ Ni low-alloy grade. The effort is directed toward the determination of the basic weldability of this alloy. Our previous[3] studies showed that it is prone to hot cracking when welded under highly restrained conditions. The cracks can be sealed by backfilling with a eutectic of Fe_2Nb and δ-iron.

We made a number of gas tungsten-arc welds in ¼- and ½-in.-thick plates from two heats of niobium-stabilized steel. The filler metal employed was prepared from the base metals, and the welds were fully restrained. The niobium-to-carbon ratios for the two heats were 11 and 13. Table 17.1 contains the chemical composition of the heats studied. All weldments satisfactorily passed room-temperature bend tests around a 2*T* radius mandrel (*T* = base-metal thickness). Metallographic studies of the welds showed the boundaries of the large austenite grains in the heat-affected zone to be outlined with the eutectic phase. Further, islands of the eutectic are visible in the heat-affected zone when viewed at a magnification of 500X.

Tensile tests in the as-welded condition showed the welds to have excellent strength and ductility, both at room temperature and 565°C (1050°F). Table 17.2 contains the results of the tensile tests. Charpy V-notch properties of the welds in both the as-welded and postweld heat-treated conditions were obtained at +40°F. The postweld heat treatment did not improve the weld metal toughness, but it did tend to normalize the impact properties at about 55 ft-lb. The as-welded values ranged from 42 to 111 ft-lb.

A metallographic study of the initiation site for fracture (at the root of the machined notch) showed considerable plastic deformation. The grain boundary film seen in the heat-affected zone of the base metal and in the weld metal, which was previously identified as a eutectic between Fe_2Nb and δ-iron, was not brittle. Indeed, it is capable of a great degree of deformation and has proven to be tough.

In summary, the niobium-stabilized 2¼ Cr–1 Mo–½ Ni low-alloy steel has a sensitivity toward microfissuring during welding due to the formation of a liquid phase at 1370°C (2500°F). However, the completed weld does not exhibit a degradation of toughness at room temperature.

Low-Carbon Grades

The study of the low-carbon 2¼ Cr–1 Mo steels is directed toward the assessment of the effect of carbon content on the mechanical properties of weldments. These properties will serve as a guide in the selection of the optimum carbon level to be used in the fabrication of steam generators for demonstration plants.

3. D. A. Canonico and N. C. Binkley, *Metals and Ceramics Div. Annu. Progr. Rep. June 30, 1971*, ORNL-4770, pp. 85–88.

Table 17.1. Chemical compositions of niobium-stabilized steel plate used in this study

Heat	Composition (wt %)[a]								
	C	Si	Mn	P	S	Cr	Ni	Mo	Nb
403150	0.09	0.27	0.48	0.017	0.004	2.36	0.60	0.97	0.98
450543	0.08	0.35	0.46	0.011	0.005	2.18	0.54	0.94	1.08

[a]Balance, Fe.

Table 17.2. Results of tensile tests on welds in the niobium-stabilized $2\frac{1}{4}$ Cr–1 Mo–$\frac{1}{2}$ Ni steel

Heat (base metal and filler metal)	Test thickness (in.)	Test temperature (°C)	Strength (psi)		Ductility (%)	
			Yield (0.2% offset)	Ultimate	Elongation	Reduction in area
403150	0.25	Room	61,700	85,700	13	77
403150	0.5	Room	64,400	80,000	18	76
450543	0.25	Room	65,400	86,200	15	75.5
450543	0.5	Room	57,100	74,100	15.6	76.1
403150	0.25	565	45,200	51,000	12.2	76
403150	0.5	565	41,800	44,600	14.2	80.7
450543	0.25	565	44,100	50,400	10	80
450543	0.5	565	35,400	40,100	16.8	80.0

Table 17.3. Results of hardness traverses on welds with varying carbon contents

Carbon content (%)	Condition	Diamond pyramid hardness number				
		Heat-affected zone		Weld metal		Base metal
		Last pass	Early pass	Last pass	Early pass	
0.003	As welded	166–239	165–177	242–266	152–180	129–135
0.035	As welded	163–225	180–210	291–307	205–275	127–145
	Stress relieved	135–176	126–142	203–211	164–196	115–117
0.11	As welded	238–264	234–312	361–394	256–361	177–194
	Stress relieved	205–228	190–218	223–234	199–228	180–192

Welds have been made with parameters identical to those previously reported.[4] These were made in $\frac{1}{2}$-in.-thick plates that had been normalized at 930°C for 1 hr and tempered at 705°C for 1 hr. These weldments were sectioned to provide transverse specimens for the mechanical property studies.

Hardness traverses through the weld metal, heat-affected zone, and base metal were conducted on weldments of all three carbon levels. These data are presented for the as-welded and welded-and-stress-relieved conditions in Table 17.3. In the as-welded condition, the base metal is evidently the softest zone regardless of carbon content. This is also true after a 705°C postweld heat treatment for welds made with the medium (0.035%) and high (0.11%) carbon materials. Insufficient material was available to obtain postweld heat treatment data for the low-carbon welds.

This investigation has been handicapped by a lack of commercial steel. However, we received in late June 1972 a commercial heat of low-carbon (0.027% C) $2\frac{1}{4}$ Cr–1 Mo steel. This material will be used in future weldability and mechanical properties studies.

4. D. A. Canonico and N. C. Binkley, *Metals and Ceramics Div. Annu. Progr. Rep. June 30, 1971*, ORNL-4770, p. 86.

Tube-to-Tube-Sheet Welding Studies

D. A. Canonico

The adequate evaluation of the mechanical properties of tube-to-tube-sheet welds is handicapped by the geometric configuration of the weld. In an effort to overcome this problem, we have developed a simulated bore-side tube weld using flat plates. This technique permits the machining of flat specimens for mechanical property testing and nondestructive test development. We have also developed a double-torch technique that will allow the simulation across an entire weldment of that area that may be most critical in a tube-to-tube-sheet weld, namely the weld overlap region. Figure 17.4 is a sketch showing the simulated specimen configuration for the tube-to-tube-sheet weld.

ORNL-DWG 71-9023

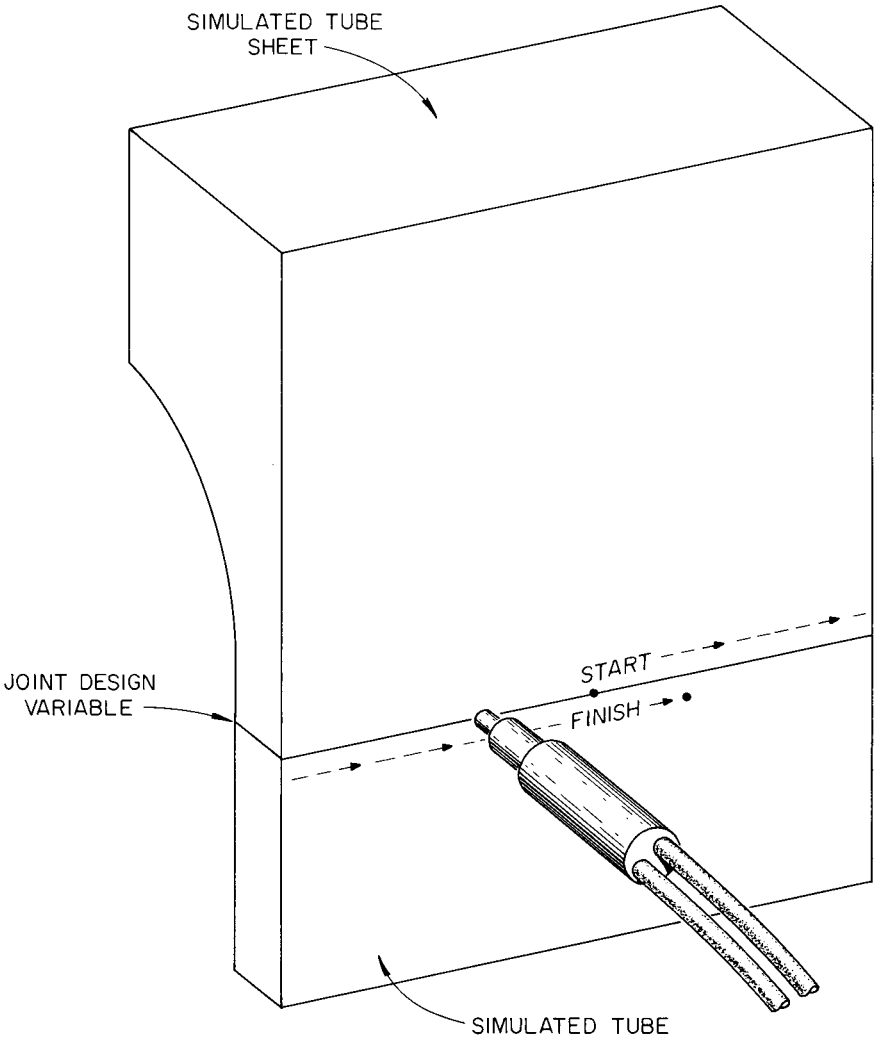

Fig. 17.4. Specimen configuration to simulate bore-side welds.

18. Mechanical Properties of Alloys in Reactor Environments

W. R. Martin H. E. McCoy, Jr.

Type 316 stainless steel will be used for fuel element cladding and fuel subassembly ducts in the FTR and possibly in future liquid metal fast breeder reactors. In these applications the alloy will operate in the range 350 to 750°C for times of several thousand hours. This alloy is unstable, and such thermal exposure will cause the precipitation of carbides (primarily $M_{23}C_6$) and intermetallic phases such as sigma, chi, and eta or Laves. In addition, voids and a dislocation structure will be formed by the precipitation of irradiation-produced vacancies and interstitials at temperatures in the range 350 to 650°C, and helium bubbles will be formed at higher irradiation temperatures. To reduce the swelling caused by the void-dislocation structure, the alloy will probably be used in the cold-worked condition, but a cold-worked structure will significantly alter the kinetics of the carbide and sigma precipitation reactions, in general by shifting the time-temperature-precipitation curves to shorter times and lower temperatures. In addition, irradiation may alter the precipitation kinetics and phase stability. The purpose of this program is to relate these complex microstructural changes to the deformation and fracture characteristics of the irradiated alloy and thus predict behavior under service conditions. Additional work is directed towards the development of alloys, such as the titanium-modified type 316 stainless steel, that exhibit improved resistance to radiation damage, particularly embrittlement.

SWELLING OF AUSTENITIC STAINLESS STEEL

J. O. Stiegler E. E. Bloom

Our studies of irradiation-induced defect structures in annealed specimens of type 304 stainless steel were extended into the fluence range above 10^{23} neutrons/cm^2 (>0.1 MeV) through examination of control and safety rod thimbles removed from EBR-II. Although void concentrations were observed to saturate, no limitation to void growth was found, and volume changes as high as 11% were measured for irradiation to a fluence of 1.7×10^{23} neutrons/cm^2 at 420°C. Our first experimental subassemblies containing type 316 stainless steel were returned from EBR-II. Specimens irradiated in the annealed and several cold-worked states were examined along with some modified by the addition of 0.23% Ti. Significant observations of defect structures and swelling in these steels are summarized below; mechanical properties measured on the same or equivalent specimens are reported in the following section.

Annealed Type 304 Stainless Steel

Work[1] during the past year established that void concentrations reach limiting or saturation values but that the concentration at saturation and the fluence at which saturation occurs are temperature dependent. For example, at 370°C, voids were first observed at a fluence of about 10^{21} neutrons/cm^2. The concentration increased with increasing fluence until it reached a limiting value of 1.5×10^{16} voids/cm^3 at a fluence of 1×10^{23} neutrons/cm^2. At 590°C, void nucleation occurred only in the narrow fluence interval between about 1.5 and 3×10^{22} neutrons/cm^2, and the limiting concentration was less than 2×10^{14} voids/cm^3. During the time in which voids were nucleated, the mean void diameter increased slowly, as less than the $1/6$ power of fluence. Limited results indicated that after saturation in the void concentration the mean diameter increased more rapidly, so that the rate of swelling changed little, if any. Especially at the higher irradiation temperatures, some heat-to-heat variations were evident in the numbers and sizes of voids, but the swelling was not significantly affected.

From comparison of the observations with predictions derived from models we were able to conclude that homogeneous nucleation and nucleation in displacement spikes, in overlapping spikes, or at pre-existing sites were unlikely to be major sources of the voids

1. E. E. Bloom, J. O. Stiegler, and C. J. McHargue, "Radiation Damage in Annealed Type 304 Stainless Steel," *Radiation Effects* (to be published).

Table 18.1. Comparison of void concentration and size distribution in annealed stainless steel: types 304,[a] 316, and 316 + 0.23% Ti

Stainless steel type	Irradiation temperature (°C)	Fluence >0.1 MeV (neutrons/cm^2)	Concentration (voids/cm^3)	Mean void diameter (Å)	Volume swelling (%)
		$\times 10^{22}$			
304	450	1.9	1.3×10^{15}	178	0.54
316	450	1.9	6.9×10^{13}	236	0.06
316 + 0.23% Ti	450	1.9	6.8×10^{14}	172	0.20
304	515	2.3	7.3×10^{14}	218	0.63
316	510	1.5	1.8×10^{13}	337	0.05
316 + 0.23% Ti	515	2.3	1.8×10^{13}	313	0.04
304	580	1.9	1.7×10^{13}	258	0.26
316	580	1.9	1×10^{13}	666	0.21
316 + 0.23% Ti	580	1.9	$\approx 10^{12}$		<0.02

[a]Values for type 304 stainless steel were calculated with the empirical equations of Brager et al., *Met. Trans.* **2**, 1893 (1971).

in neutron-irradiated stainless steel. Models for nucleation on helium bubbles or in displacement spikes stabilized by helium atoms did not disagree in any way with the experimental observations.

Since the threshold fluence for void formation increased with increasing irradiation temperature, the shape of the swelling vs temperature curve changed with increasing fluence. The temperature of maximum swelling increased with increasing fluence, and the curves extended to higher temperatures. We concluded that data obtained at a low fluence cannot be simply scaled up to predict behavior at higher fluences.

Annealed Type 316 Stainless Steel[2]

The defect structures found in type 316 stainless steel are qualitatively similar to but quantitatively different from those observed in type 304. Voids were observed for irradiation between 450 and 590°C, with the concentration decreasing and the mean size increasing with increasing irradiation temperature. For fluences of about 2×10^{22} neutrons/cm^2, void concentrations were less than $^1/_{10}$ that in type 304. Sizes were somewhat larger in the type 316, but not enough to overcome the reduced concentration, so that the overall swelling was significantly less. The difference was greater at the lower irradiation temperatures, as can be seen from the statistics given in Table 18.1. Similar behavior was found for the dislocation structure. However, precipitation reactions appeared to be enhanced in the type 316 material, although there was no obvious change in either type or morphology of precipitate particle. The range of defect structures produced in type 316 stainless steel for irradiation at 590°C is illustrated in Fig. 18.1, where voids, Frank loops, dislocation lines, $M_{23}C_6$ particles, and an unidentified ribbon-like precipitate are all present. The microstructural changes produced by irradiation between 450 and 580°C are described quantitatively.

Cold-Worked Type 316 Stainless Steel[2]

Prior deformation of 20% by cold working produced significant modifications in the microstructures of type 316 stainless steel irradiated to a fluence of about 2×10^{22} neutrons/cm^2 at temperatures between 450 and 800°C by suppressing the formation of voids and enhancing and changing the development of precipitate particles. Voids were found only in isolated recovered areas of a specimen irradiated at 580°C. No interstitial loops or structure that could be attributed to the displaced atoms was detected in any of the specimens. Partial recrystallization was observed in specimens irradiated above 680°C, but recrystallization was not complete in a specimen irradiated at a temperature that rose from 735°C at the start of the irradiation to 795°C at the finish. A 10-hr treatment at 750°C was sufficient

2. Summarized from E. E. Bloom and J. O. Stiegler, "Effect of Irradiation on the Microstructure and Creep-Rupture Properties of Type 316 Stainless Steel," paper presented at the 6th International Symposium on the Effects of Radiation on Structural Materials, ASTM Annual Meeting, Los Angeles, June 26–28, 1972 (to be published in the Proceedings).

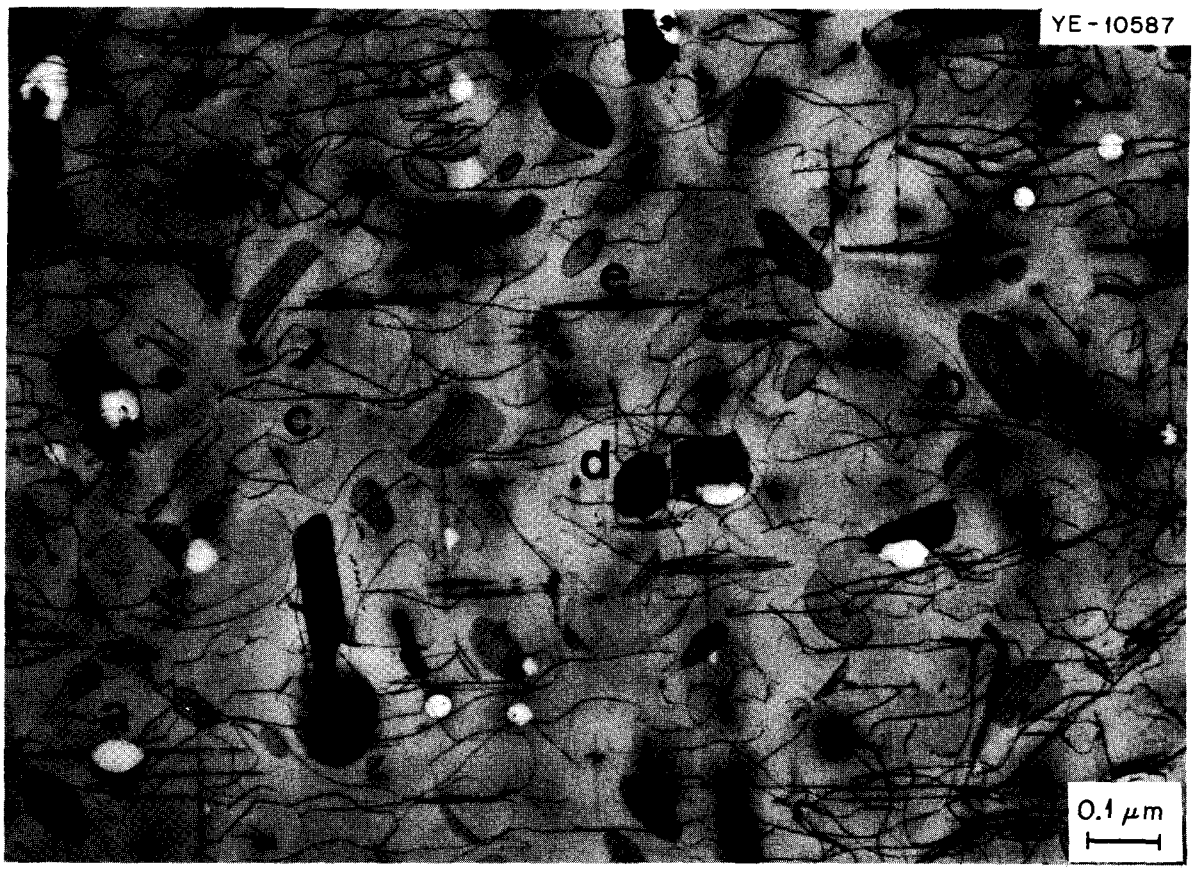

Fig. 18.1. Transmission electron micrograph illustrating the defect structures formed in type 316 stainless steel irradiated in EBR-II to a fluence of 2 × 10^{22} neutrons/cm^2 at 580°C. Features indicated are (*a*) voids, (*b*) Frank loops, (*c*) dislocation lines, (*d*) $M_{23}C_6$ particles, and (*e*) unidentified ribbon-like precipitate.

to cause complete recrystallization in the laboratory. Helium bubbles were found on grain boundaries of the irradiated specimens and may have inhibited recrystallization. Specimens that recrystallized also developed sigma-phase precipitates, usually at triple grain junctions. At the lower irradiation temperatures, $M_{23}C_6$ and Laves phase particles formed, usually in association with the stacking fault bands.

Void formation was also suppressed in a specimen deformed 10% before irradiation at 590°C to a fluence of 2.3 × 10^{22} neutrons/cm^2 and in one deformed 50% before exposure to 1.5 × 10^{22} neutrons/cm^2 at 640°C. In the former, small $M_{23}C_6$ and Laves phase precipitates formed, again in association with the stacking fault bands. In the latter, massive precipitate particles, as yet unidentified, were found.

Titanium-Modified Type 316 Stainless Steel

The addition of 0.23% Ti to type 316 stainless steel produced a steel having radiation damage characteristics different from types 304 and 316 stainless steels.[3,4] This further illustrates our contention that the damage introduced into stainless steels by fast neutron irradiation is extremely sensitive to composition. When irradiated at a low temperature (450°C) to a fluence of about 2 × 10^{22} neutrons/cm^2 the titanium-modified steel showed void concentrations midway between types 304 and 316 (see Table 18.1). At higher temperatures (515°C) it swelled less than either of the other two, and at 580°C it showed no measurable swelling at all, in contrast to 0.26 and 0.21% in types 304 and 316, respectively. These observations suggest that the small addition of titanium changes the temperature dependence of the swelling by decreasing the

3. H. R. Brager et al., *Met. Trans.* 2, 1893 (1971).

4. E. E. Bloom, "Nucleation and Growth of Voids in Stainless Steels during Fast Neutron Irradiation," pp. 1–29 in *Radiation-Induced Voids in Metals* (Proc. Int. Conf. Albany, N.Y., June 9–11, 1971), ed. by J. W. Corbett and L. C. Ianniello, U.S. Atomic Energy Commission Office of Information Services, Oak Ridge, Tenn., 1972.

temperature of maximum swelling. Alternatively, it may act by increasing the threshold fluence for void formation.

MECHANICAL PROPERTIES OF AUSTENITIC STAINLESS STEELS

E. E. Bloom D. Fahr J. O. Stiegler

To predict the behavior of austenitic stainless steels under LMFBR service conditions the relationships between microstructure and properties must be known. In initial studies, annealed and cold-worked type 316 stainless steel were irradiated at temperatures of interest to LMFBR's to a maximum fluence of 2.7×10^{22} neutrons/cm^2 (>0.1 MeV). The postirradiation tensile and creep-rupture properties were related to the irradiation-produced microstructure. Future irradiations will extend the fluence to about 2×10^{23} neutrons/cm^2, near the peak fluence for LMFBR components.

Type 316 Stainless Steel[2]

The most pronounced effect of neutron irradiation was a significant reduction in rupture life and ductility. For irradiation in the annealed condition, the rupture life was decreased by a factor of 3 or less in the range 550 to 700°C. At 750°C the rupture life was reduced 10- to 100-fold, with the effect being greater at the higher stress levels. The creep rates and stress dependency of the creep rate were not significantly affected by irradiation in the range 550 to 700°C. The creep rate was, however, markedly increased at 750°C.

For specimens irradiated in the cold-worked condition, the changes in creep-rupture properties were more complex. The rupture life appeared to increase and creep rates to decrease at 550°C, while at 600°C the opposite trend was observed. At 700 and 750°C the limited data suggested a decreased rupture life and increased creep rate at high stress levels with the effect becoming less and possibly reversing at lower stress levels.

Creep strain at the beginning of tertiary creep and total creep elongation for the unirradiated and irradiated conditions are shown in Fig. 18.2. For irradiation in the annealed condition, the specimens were less ductile at all temperatures in the range 550 to 750°C. For cold-worked material, the ductility after irradiation was reduced at 550 to 650°C but was increased sharply and equaled or exceeded the as-cold-worked values at 700 and 750°C. This latter effect appeared to be related to recovery and recrystallization during irradiation.

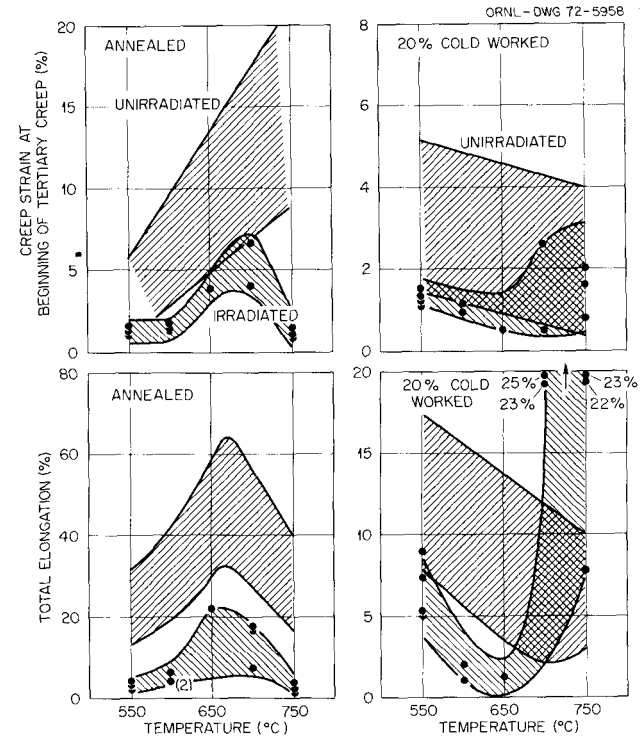

Fig. 18.2. Effect of irradiation on the creep-rupture ductility of type 316 stainless steel.

Longitudinal sections of samples irradiated in the annealed condition and tested to failure at 550, 650, and 750°C are shown in Fig. 18.3. At each temperature, extensive cracking occurred on grain boundaries approximately normal to the applied load. Cracks such as those shown in Fig. 18.3 were not localized to the region of the fracture but were found along the entire gage section. At 550 and 600°C a crack, particularly in a region removed from the fracture, was not wedge shaped but rather had nearly constant width from one triple point to another. Many of those boundaries normal to the applied load contained isolated cavities. Often a string of cavities extended from the tip of a grain boundary crack. At the higher temperature of 650°C, most of the cracks were wedge shaped, but again we observed small cavities on many of the grain boundaries. At the highest temperature, 750°C, the cracks were obviously formed by the linking of grain boundary cavities.

Scanning microscopy showed that at least two types of fracture occurred in the samples irradiated in the annealed condition and tested at 550 and 600°C. A portion of the fracture was completely integranular, as shown in Fig. 18.4*a*. Other regions of the fracture consisted of areas of integranular fracture surrounded

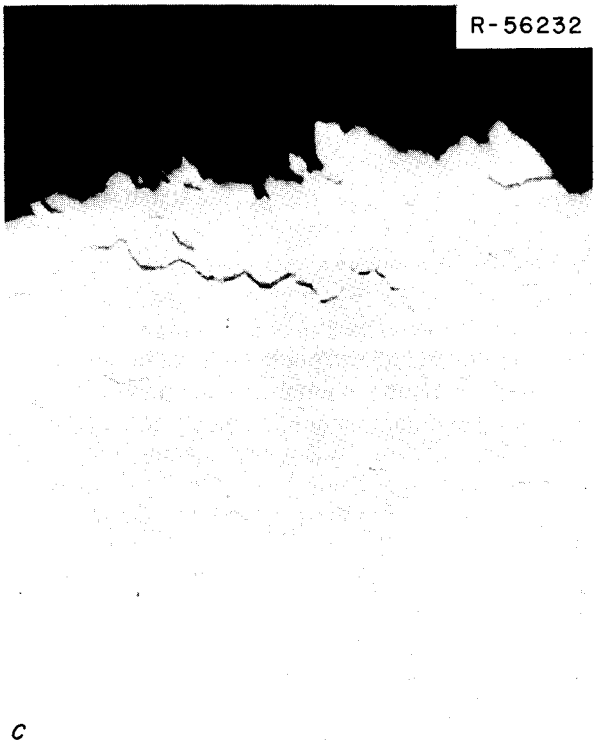

Fig. 18.3. Creep-rupture fractures of type 316 stainless steel irradiated in the annealed condition. 100×. (*a*) Irradiated at 580°C, 2.7 × 10^{22} neutrons/cm^2; tested at 550°C, 45,000 psi. (*b*) Irradiated at 630°C, 2.3 × 10^{22} neutrons/cm^2; tested at 650°C, 25,000 psi. (*c*) Irradiated between 735 and 795°C, 2.7 × 10^{22} neutrons/cm^2; tested at 750°C, 7500 psi.

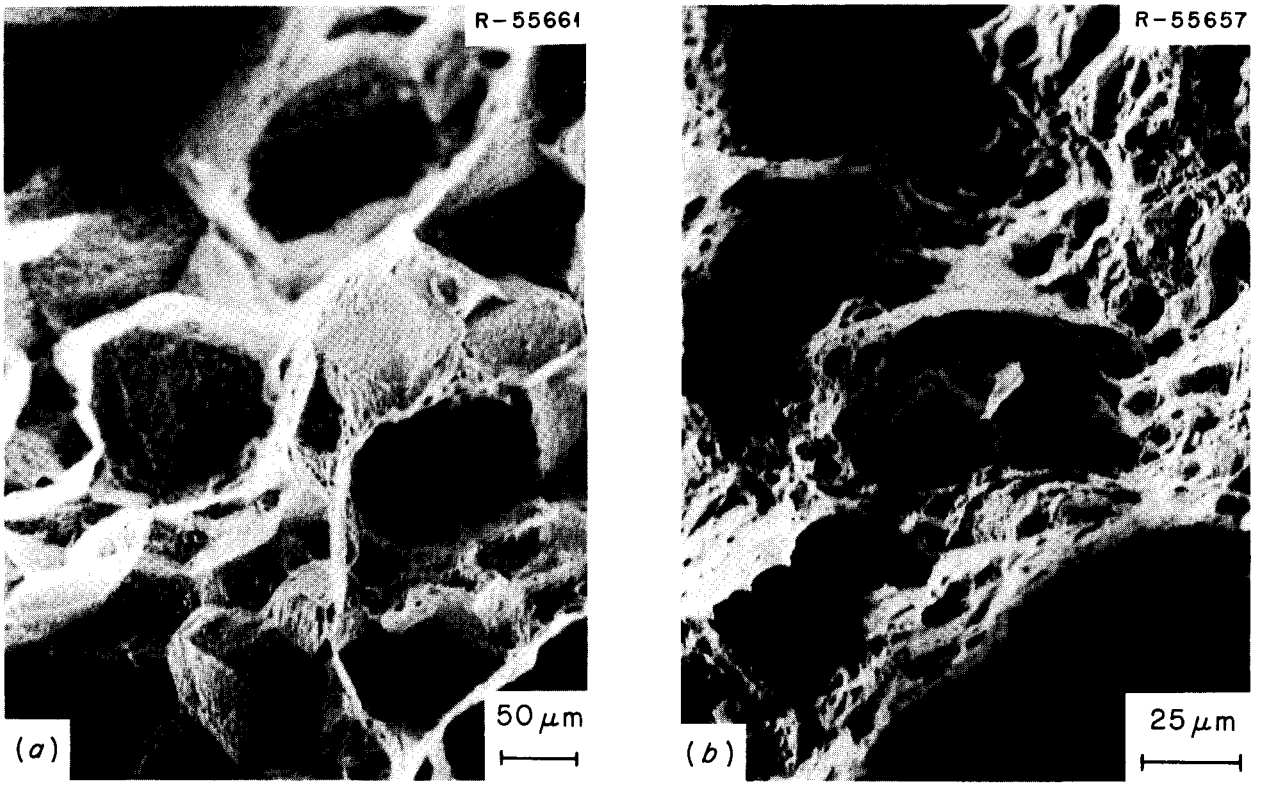

Fig. 18.4. Scanning electron micrographs of fracture in type 316 stainless steel irradiated at 580°C to 1.9 × 10^{22} neutrons/cm^2 and tested at 550°C and 45,000 psi. (*a*) Area of intergranular fracture. (*b*) Area of inter- and transgranular fracture.

by ductile transgranular fracture Fig. 18.4*b*. The failure was apparently initiated by the formation of grain boundary cracks, which propagated and eventually reduced the effective cross section of the specimen. The final separation then occurred by the linking of these cracks at a higher strain rate with considerable transgraunlar fracture.

For samples irradiated in the 20%-cold-worked condition and then tested in the range 550 to 650°C, the grain boundary cracks were fewer than in the companion samples irradiated in the annealed condition. The cracks were generally narrower in the cold-worked specimens than in the annealed specimens, and the percentage of intergranular fracture was much larger. Such observations suggest strongly that the strength of the matrix is important in crack initiation, propagation, or both. At 750°C, extensive sigma-phase precipitation was apparent, and cavities were usually associated with the sigma particles. The sigma phase particles were never fractured; the cavities and cracks were located at the particle-matrix interface.

These results suggest that at all temperatures, grain boundary cracks formed by the stress-induced growth and linking of grain boundary cavities. We believe that helium bubbles serve as cavity nuclei and stress-induced growth occurs by the vacancy-diffusion mechanism proposed by Speight and Harris.[5] Propagation of these cracks depended upon the flow stress of the matrix. At the lower irradiation temperatures, which resulted in high flow stresses, cracks were narrow and extended large distances (often across several triple grain junctions), possibly as a result of increased cavity growth rates near the leading edge of a crack due to stress concentration at the crack tip. At slightly higher temperatures, this stress concentration was apparently reduced by plastic deformation, and the crack propagation was sufficiently reduced to allow grain boundary sliding and matrix deformation. At the highest temperatures, cavity growth rates were sufficiently rapid to reduce the rupture life a factor of about 100.

5. M. V. Speight and J. E. Harris, *Metal Sci. J.* **1**, 83 (1967).

Table 18.2. Postirradiation tensile properties of annealed type 316 + 0.23% Ti stainless steel

Irradiation temperature (°C)	Fluence >0.1 MeV (neutrons/cm^2)	Test temperature (°C)	Stress (psi)		Total elongation (%)	Reduction in area (%)
			Yield	Ultimate tensile		
	$\times 10^{22}$					
465	1.2	450	44,400	82,200	35.4	30.3
510	0	500	21,200	84,500	47.8	58.8
	1.5	500	35,100	78,300	31.9	50.6
630	0	600	19,700	80,400	34.7	42.8
	1.2	600	31,200	56,600	29.8	56.7

Table 18.3. Postirradiation creep-rupture properties of annealed type 316 + 0.23% Ti stainless steel

Irradiation temperature (°C)	Fluence >0.1 MeV (neutrons/cm^2)	Test temperature (°C)	Stress (psi)	Rupture life (hr)	Creep rate (%/hr)	Total elongation (%)
	$\times 10^{22}$					
580	2.3	550	55,000	252.9	0.031	17.1
580	2.7	550	45,000	1930.0	0.0036	19.9
580	2.7	550	45,000	(452.4)[a]	(0.0026)[a]	(3.6)[a]
580	1.5	600	50,000	184.7	0.01	10.1
580	2.3	600	40,000	535.8	0.01	18.1
580	1.9	600	40,000	(199.4)	(0.008)	(3.4)
610	1.9	650	35,000	55.8		35.6
630	2.3	650	25,000	1590.3	0.01	28.2
630	2.3	650	25,000	(346.6)	(0.03)	(21.6)
870	2.7	750	7,500	>3600		>6.5
835	4.4	750	7,500	642.0	0.02	25.8
825	4.4	(750)	7,500	(105.3)	(0.018)	(3.3)

[a]Values in parentheses are typical results for type 316 stainless steel irradiated and tested at the same conditions as the titanium-modified alloy.

Titanium-Modified Type 316 Stainless Steel[6]

Thermal reactor irradiation experiments on four heats of vacuum-melted type 316 stainless steel containing 0.23, 0.33, 0.46, and 0.60% Ti demonstrated that 0.2 to 0.3% Ti resulted in maximum ductility for irradiation and test conditions that produced helium embrittlement. Specimens of the heat containing 0.23% Ti were irradiated in the EBR-II at temperatures in the range 450 to 850°C to maximum fast neutron fluences of 2.7 $\times$ 10^{22} neutrons/cm^2 (>0.1 MeV). Postirradiation examination included tensile and creep-rupture tests, which are summarized in Tables 18.2 and 18.3. The increase in tensile yield strength was a result of the void-dislocation-precipitate structure produced during irradiation. The decrease in ultimate tensile strength at the higher irradiation temperatures appears to result from the precipitation of carbon and is a result of thermal history rather than irradiation per se. The postirradiation creep properties compared favorably with those of standard type 316 stainless steel irradiated in the same experiment. Postirradiation ductilities were significantly higher than those of the standard alloy.

6. Summarized from E. E. Bloom and J. O. Stiegler, "Effect of Irradiation on Titanium-Modified Type 316 Stainless Steel," presented at the Annual Meeting of the American Nuclear Society, Las Vegas, Nev., June 18–22, 1972.

19. Mechanical Properties of Structural Alloys

W. R. Martin H. E. McCoy, Jr.

The use of structural materials in nuclear reactors at progressively higher temperatures requires that we improve design methods to ensure dependable and safe operation of such systems. The design methods program involves the procurement of machanical property data under various possible service conditions and the development of analytical methods for using these materials properties to design complex structures. ORNL is currently active in both of these areas, but we will be concerned here with only the mechanical properties information.

Although many of the methods that will be developed will be universally applicable for high-temperature design, the current work is concerned primarily with LMFBR's. The materials being studied include types 304 and 316 stainless steel and Croloys.

EXPLORATORY TESTS ON TYPE 304 STAINLESS STEEL IN SUPPORT OF THE HIGH-TEMPERATURE STRUCTURAL DESIGN METHODS FOR LMFBR COMPONENTS PROGRAM

R. W. Swindeman

We have been creep testing two heats of type 304 stainless steel over the range 538 to 649°C and for times extending to 5000 hr. The purpose is to collect basic data for use in the interpretation of the mechanical response of stainless steel under more complicated loading conditions, such as would be experienced by an LMFBR high-temperature component during its service life.

After a graphical analysis of our creep curves, we conclude that none of the more popular strain-time formulations perfectly model the mechanical behavior of either heat. However, the Garofalo[1] expression for metals appears to be a fair approximation to the observed behavior. This equation may be written:

$$\epsilon = \epsilon_e + \epsilon_p + \epsilon_t(1 - e^{-rt}) + \dot{\epsilon}_{min} t \ ,$$

where ϵ is the total strain, t is time, ϵ_e is the elastic component, ϵ_p is the plastic component, $\dot{\epsilon}_{min}$ is the minimum or linear creep rate after transient creep has been exhausted, ϵ_t is the final transient creep component, and r describes the rate of approach to ϵ_t. One of the problems with this equation at stresses and temperatures typical of conditions where type 304 stainless steel is commonly used is that ϵ_t, r, and $\dot{\epsilon}_{min}$ are difficult to obtain, because the time required to exhaust primary creep extends beyond our available test data. Some typical data are shown in Fig. 19.1.

We have begun testing under more complicated loading conditions. For example, a number of step load tests were performed under conditions where primary creep prevailed. Most tests were run for 300- to 500-hr intervals between load changes. The results for both heats were similar and revealed several interesting features. For example, when measurable creep occurred, the plastic yield stress was increased. The creep rate at the higher stress, however, generally correlated with the constant-load creep rate compared on the basis of creep strain rather than the total strain or time under stress. Our results tended to validate the strain-hardening rule for cumulative creep. Decreases in loads did not result in any appreciable creep recovery. Hence, it appears that the microstructures developed during creep at temperatures in the range 538 to 649°C must be fairly stable, at least for materials that are initially fully annealed.

Included in our test matrix are relaxation, compressive creep, cyclic creep, and superimposed creep and cyclic plasticity tests. Our available results are too preliminary to allow complete validation of any general laws or constitutive equations governing material behavior.

1. F. Garofalo et al., "Strain-Time, Rate-Stress, and Rate-Temperature Relations during Large Deformations in Creep," pp. 1–31 in *Joint International Conference on Creep,* The Institute of Mechanical Engineers, London, 1963.

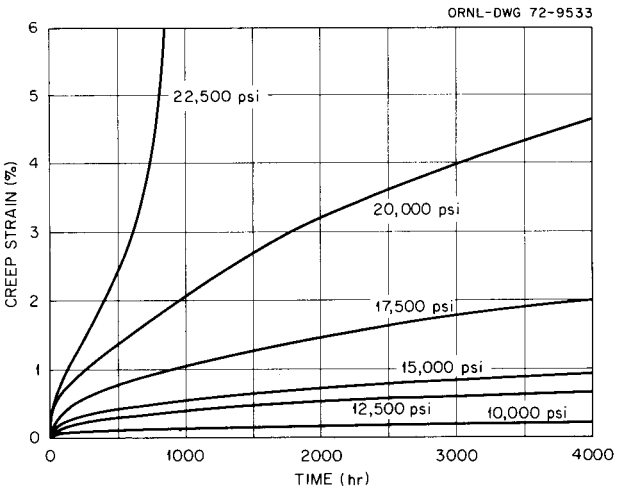

Fig. 19.1. Creep curves at 593°C for type 304 stainless steel. These curves show the long times during which primary creep dominates. Heat 9T2796 reannealed at 1093°C.

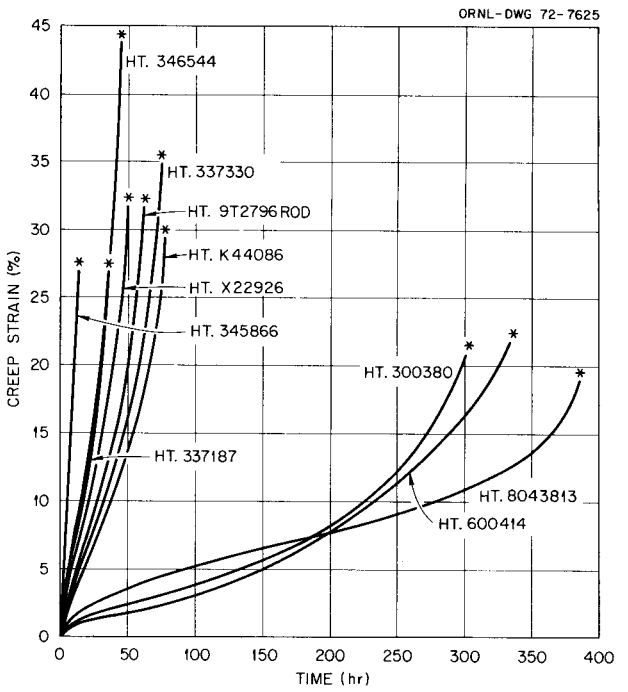

Fig. 19.2. Comparison of creep curves at 649°C and 25,000 psi for ten heats of type 304 stainless steel.

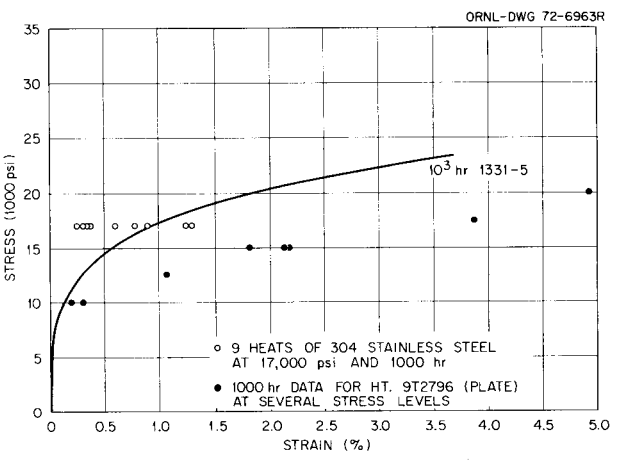

Fig. 19.3. Comparison of creep results with an isochronous stress-strain curve per code case 1331-5 at 1100°F for several heats of type 304 stainless steel.

HEAT-TO-HEAT VARIATIONS IN THE MECHANICAL PROPERTIES OF TYPE 304 STAINLESS STEEL

R. D. Waddell, Jr.

A study of the heat-to-heat variation of the mechanical properties of austenitic stainless steels began this year and now involves 17 heats of type 304 stainless steel. The heats selected for study encompass a fairly wide range of compositions and have been involved in some five or six additional programs.[2]

Tensile properties for several heats of type 304 stainless steel at room temperature, 427, 593, and 649°C, in both the as-received and reannealed conditions, have been determined.[2] We are also collecting creep and stress-rupture data at 538, 593, and 649°C. Figure 19.2 shows the wide range of variation in creep behavior for ten heats of type 304 stainless steel at 649°C and 25,000 psi stress. Similar curves for tests at 593°C and 30,000 and 35,000 psi have been reported.[2]

Figure 19.3 shows how nine heats in the as-received condition and heat 9T2796 (plate) in the reannealed condition compare with an isochronous stress-strain curve as taken from ASME code case 1331-5. The nine heats in the as-received condition compare favorably with the 1331-5 curve, but the reference heat, 9T2796 in the reannealed condition, falls considerably below the 1000-hr curve. We are also conducting a series of ten tests on one heat (X22926) in the reannealed condition at 593°C and 35,000 psi to ascertain what variation one might expect to find within one heat due to test methods, etc. The results of these tests to date indicate these variations to be small compared to the variation between heats.

2. R. W. Swindeman and R. D. Waddell, Jr., *Fuels and Materials Development Program Quart. Progr. Rep. Mar. 31, 1972,* ORNL-TM-3797, pp. 185–203.

MECHANICAL PROPERTIES OF STRUCTURAL MATERIALS FOR STEAM GENERATORS

R. L. Klueh

The steam generator for the LMFBR demonstration plant will probably be constructed of a ferritic steel or Incoloy 800. The mechanical properties program on steam generator materials comprises a determination of the important properties of welds and base metals as required by RDT and ASME elevated-temperature design requirements. Properties are to be measured for base metal and weld metal of 2¼% Cr–1% Mo steel (Croloy) and Incoloy 800 and to a limited extent on stabilized 2¼% Cr–1% Mo steel and high-chromium ferritic stainless steels. During the reporting period, all of the mechanical property effort was on the unstabilized 2¼% Cr–1% Mo steels.

A potential problem with the use of standard 2¼% Cr–1% Mo steel, which is allowed a maximum of 0.15% C (it usually contains about 0.1%), is the transfer of carbon by flowing sodium from the ferritic steel to the austenitic stainless steel of the intermediate heat exchanger. Such a transfer could lower the strength of the Croloy and embrittle the stainless steel. One possible remedy is to decrease the carbon level of the Croloy to near the solid solubility limit.

We are studying the mechanical properties of base metal and welds from laboratory heats of 2¼% Cr–1% Mo with three carbon levels, designated low, medium, and high (the high-carbon material is typical of a 2¼% Cr–1% Mo steel, ASTM A213-T-22 and ASTM A387 grade D). Weld metal and transverse weldment specimens were made from ½-in. plates (0.003, 0.035, and 0.110% C) that had been normalized 1 hr at 927°C and tempered for 1 hr at 704°C before welding. Base metal properties for normalized and tempered material (1 hr at 927°C, 1 hr at 704°C) were determined from specimens taken from ⅞-in. rods (0.009, 0.030, and 0.120% C). A 1-in. plate of commercial Croloy (0.135% C) is also being factored into the program.

Weldments

The tensile properties of all weld metal and transverse weld specimens were determined at room temperature and 565°C. For the weld metal the yield and tensile stresses increased with increasing carbon content and decreased after tempering for 1 hr at 704°C (the largest effect of tempering was in the high-carbon alloy). The uniform strain values range from 3 to 12% and the total strains from 8 to 20%, with little systematic variation; reductions of area are quite large, indicating low uniform elongation but high local strains at fracture.

The tensile properties of the transverse weld specimens also show increasing strength with increasing carbon content, although the difference is small at 565°C; strength values decrease and ductility values increase with tempering. Although the strength values are all below those for the weld metal, there is little difference in the ductility parameters. Fractures occurred in the base metal.

We collected creep-rupture data for weld metal and transverse welds of the modified carbon steels at 565°C and have begun tests at 510°C. Creep-rupture curves and minimum creep rates at 565°C are given in Figs. 19.4 and 19.5 for tempered weld metal and transverse welds, respectively. Examination of Fig. 19.5*a* shows little difference in the stress-rupture properties for the low- and medium-carbon steels for the transverse welds (only one curve is given for both materials). There appear to be separate curves for the three weld metals (Fig. 19.4*a*), although the difference for the low- and medium-carbon steels is small (Fig. 19.4*b*). A stress-rupture curve for annealed weld metal, taken from Smith's compilation of elevated-temperature properties for standard Croloy,[3] is also shown. The weld metal data for the high-carbon alloy seem to lie on this curve.

In all cases, the weld metal curves of Fig. 19.4 fall above those for the transverse welds of Fig. 19.5. Examination of the failures of the transverse welds by light microscopy and comparison of the failed specimens with macroetched specimens of similarly welded materials indicated that the failures occurred in the base metal that was unaffected by welding. Limited data on base metal taken from the plates on which the welds were made verified this conclusion.

Base Metal

Specimens from the ⅞-in.-diam rod with variable carbon content and the 1-in. plate of standard Croloy were tensile tested in the range 25 to 565°C. The data have been compared with a scatter band from Smith's compilation.[3] The results for the high-carbon rod and the standard Croloy plate – both comparable to the materials in Smith's compilation – fall at the top of Smith's scatter band for yield and tensile strength and just below the elongation band. The low- and medium-carbon steels have similar properties that fall just below the scatter band for yield and tensile strength and at the upper end of the scatter band for elongation.

Creep-rupture data for the three steels (⅞-in. rod) with different carbon contents and the 1-in. plate of commercial Croloy were determined at 565°C, and tests at 510°C began. Creep-rupture curves for 565°C are given in Fig. 19.6*a* along with a curve for normalized

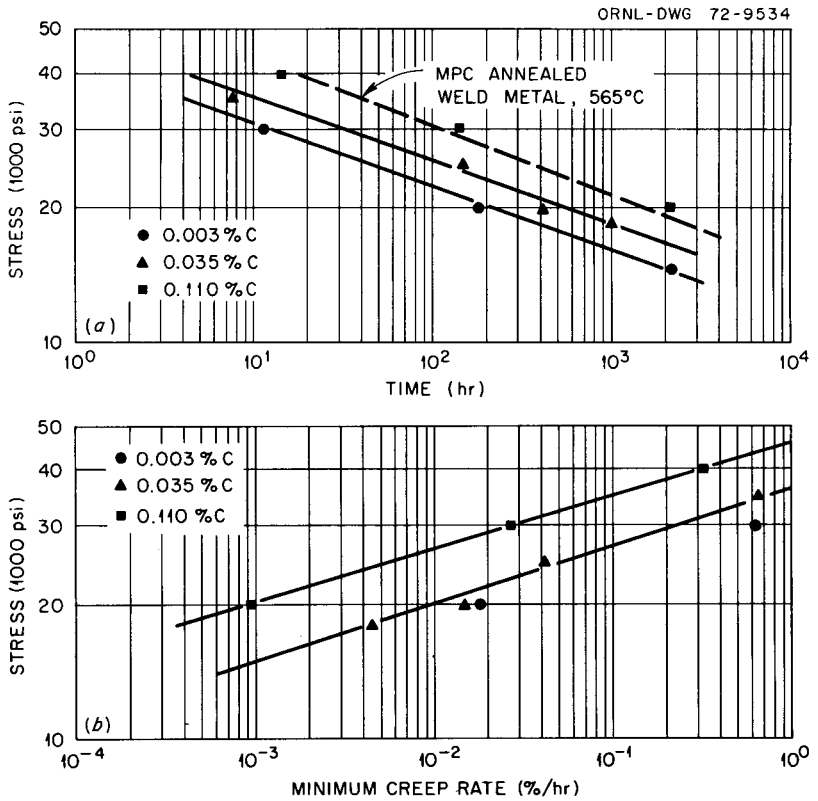

Fig. 19.4. Creep-rupture properties of tempered $2^1/_4$% Cr–1% Mo weld metal at 565°C. (*a*) Rupture life. (*b*) Minimum creep rate.

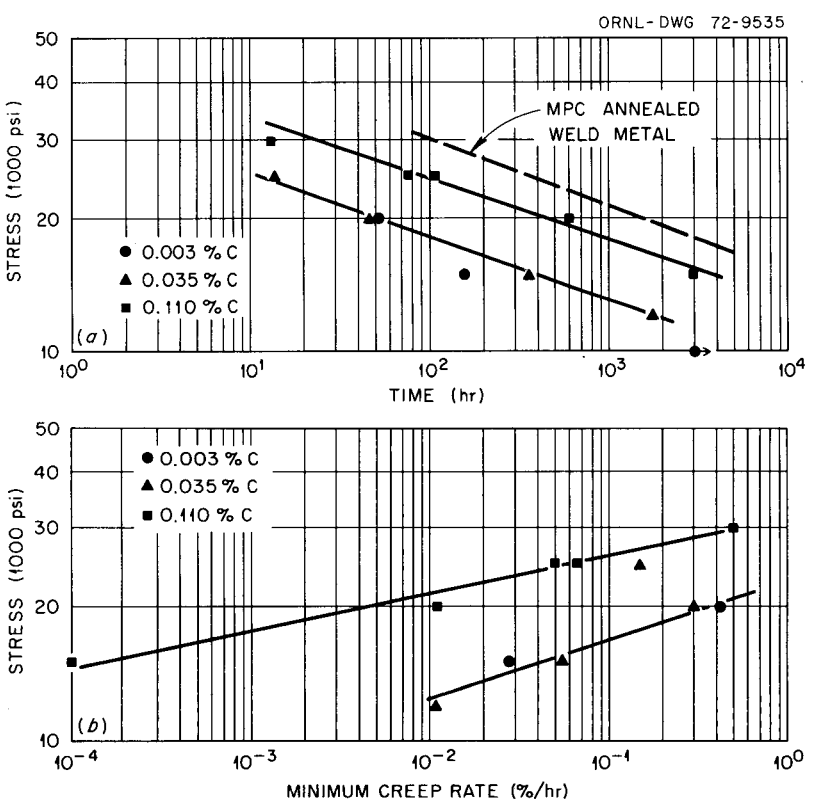

Fig. 19.5. Creep-rupture properties of tempered (after welding) $2^1/_4$% Cr–1% Mo transverse welds at 565°C. (*a*) Rupture life. (*b*) Minimum creep rate.

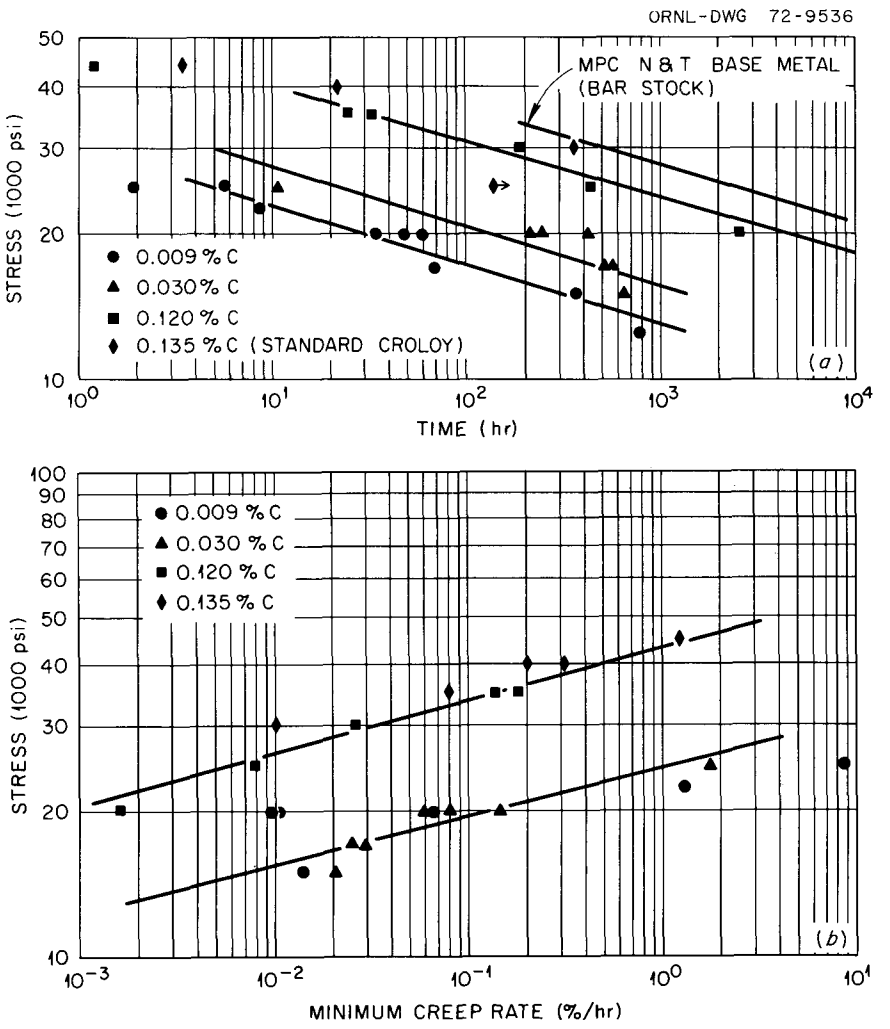

Fig. 19.6. Creep-rupture properties of normalized and tempered $2^1/_4$% Cr–1% Mo steel at 565°C. (*a*) Rupture life. (*b*) Minimum creep rate.

and tempered bar taken from Smith.[3] Figure 19.6*b* gives minimum creep rates as a function of stress at 565°C (Smith has only two minimum creep rate data points at 565°C, both in agreement with the data for the high-carbon rod and standard Croloy plate).

In general, the strength increases with increasing carbon, although the low- and medium-carbon steels again show similar properties, especially the rate data in Fig. 19.6*b*. Likewise, the high-carbon rod and 1-in. plate have similar properties at 565°C.

3. G. V. Smith, *An Evaluation of the Elevated Temperature Tensile and Creep-Rupture Properties of $2^1/_4$% Cr–1% Mo Steel,* to be published by the American Society for Testing and Materials, Philadelphia.

20. Nondestructive Test Development

R. W. McClung

This program is designed to develop new and improved methods of examining materials and components for the Liquid Metal Fast Breeder Reactor (LMFBR). To achieve this, we study the pertinent physical phenomena, develop instrumentation and other equipment, devise application techniques, and design and fabricate reference standards. Among the methods being studied are electromagnetic induction, ultrasonics, and penetrating radiation. Special emphasis is being given to developing techniques for inspection problems related to steam generators.

NONDESTRUCTIVE TEST DEVELOPMENT FOR STEAM GENERATORS

R. W. McClung

We began a development program to solve specific problems of nondestructive testing of steam generators for LMFBR. The inspection of bore-side tube-to-tube-sheet joints is emphasized, although other problems such as in-place inspection of tubing will also receive attention.

Radiography

B. E. Foster R. W. McClung

We began an investigation of the availability and capability of radiographic equipment (x-ray tubes, isotopic sources) for inspection of the bore-side weld. In conjunction with other European travel, Roentgen Technische Dienst in Rotterdam, Holland, was visited to see and discuss the small-diameter, long-rod-anode x-ray tube developed there.[1]

We borrowed a small-rod-anode x-ray tube and generator from the Los Alamos Scientific Laboratory (LASL). Measuring the focal spot of the x-ray tube, we demonstrated that the beam was out of focus and the focal spot was much larger than desired. Extensive effort was devoted to developing techniques to achieve and assure proper alignment and focusing.[2]

For initial evaluation of this rod-anode tube, a preliminary standard was fabricated from a stainless steel tube 0.625 in. OD with 0.100 in. wall. We used the Electro-Discharge Machining (EDM) technique to put flat-bottom holes (0.002 in. diam × 0.002 in. deep, 0.005 in. diam × 0.005 in. deep, and 0.010 in. diam × 0.005 in. deep) in the inner surface of the wall.

Penetrameters are being fabricated from stainless steel with thicknesses from 0.001 to 0.010 in., each with 0.005, 0.010, and 0.020-in.-diam holes. These penetrameters can be placed on the outer and inner wall of the tubing for radiography and system evaluation.

We are also fabricating a film loading-and-clamp mechanism to support the film around the tubing and facilitate loading and unloading the film. Appropriate radioisotopic sources are being acquired.

Liquid Penetrants

K. V. Cook B. E. Foster

We are developing techniques for liquid-penetrant inspection of the tube-to-tube-sheet weld joints. We have developed preliminary hardware for penetrant application and removal, for scanning tubing bores, and for coupling closed-circuit television to the borescope.[3] Because of limited illumination[4] with fluorescent penetrants, we have selected a red-dye visible penetrant. This improved the lighting problem, but slightly brighter illumination than that from our available borescope is desirable. We are investigating new, commercially available borescope systems.

1. R. W. McClung and B. E. Foster, *Fuels and Materials Development Program Quart. Progr. Rep. Dec. 31, 1971*, ORNL-TM-3703, pp. 177–78.

2. B. E. Foster and R. W. McClung, *Fuels and Materials Development Program Quart. Progr. Rep.* Mar. *31, 1972*, ORNL-TM-3797, pp. 180–81.

3. K. V. Cook and B. E. Foster, *Fuels and Materials Development Program Quart. Progr. Rep. Dec. 31, 1971*, ORNL-TM-3703, pp. 178–79.

4. K. V. Cook and B. E. Foster, *Fuels and Materials Development Program Quart. Progr. Rep. Mar. 31, 1972*, ORNL-TM-3797, p. 181.

Eddy Currents

C. V. Dodd W. A. Simpson

We are continuing our investigations into the design of an eddy-current system for the detection of defects in tubular sections.[5,6] This is the first stage of studies for the inspection of tube-to-tube-sheet joints and the in-place inspection of tubing. In the initial phase we considered two approaches. The first employed a dual encircling-coil bridge system, which was designed to be operated in an unbalanced mode. This configuration provides maximum rejection of diametral and conductivity variations, but it has the inherent disadvantage of low sensitivity to surface defects. The second design used a reflection-type encircling coil. This system is similar to a balanced bridge configuration in its rejection of diametral changes, but it has slightly greater sensitivity than the dual encircling-coil system to deep defects, vastly greater sensitivity to surface defects, and less sensitivity to drifts in the driving circuit elements. A prototype coil of this design was ordered and tested. It exhibited good sensitivity to defects, but the response to diametral changes was somewhat higher than we had hoped. This was not unexpected, since the rejection of diametral changes is achieved in this design merely by placing the pickup coils close together, thereby minimizing the response to changes that occur over distances larger than the coil separation.

To improve the rejection of diametral changes, we have begun the study of a reflection-type encircling coil whose pickups are operated in an unbalanced mode. This configuration will have additional diametral rejection, and we hope that it will retain the advantages of the reflection-type coil system.

Ultrasonics

K. V. Cook H. L. Whaley

Ultrasonic methods also offer a strong potential for the examination of the tube-to-tube-sheet weldments. The first work is being conducted on flat weld specimens that simulate typical joint configurations to determine optimum test parameters. Methods of introducing calibration notches have been established[7] and used to develop preliminary scanning techniques.

An *x-y-z* plan view recording system, which permits continuous, simultaneous, quantitative recording of the analog amplitude of discontinuities as well as their coordinates within the specimen, has been completed and is operational.

ORNL-DWG 72-9537

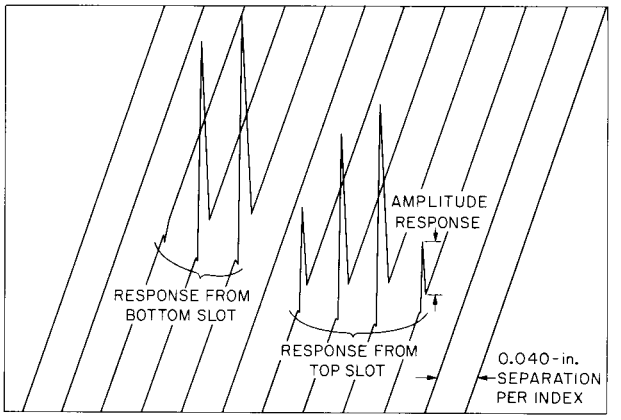

Fig. 20.1. Plan view recording of the ultrasonic response from two circular slots in Croloy $2\frac{1}{2}$ Cr–1% Mo. The specimen is scanned parallel to the slots at 0.040-in. intervals. The recorder is so operated that the traces are diagonal to prevent overlap of the peaks in successive traces.

Figure 20.1 is a plan view recording made on a $\frac{1}{8}$-in.-thick flat plate (Croloy, $2\frac{1}{4}$ Cr–1 Mo) that contains two circular slots. The depths of the slots (0.026 and 0.039 in.) are greater than will be required for weld inspection but were made large to facilitate equipment development. This recording was made to illustrate the capabilities of the *x-y-z* recording system that we have assembled. The scan direction, parallel to the notches, produces a skewed *y* axis trace. After each index along the *x* axis (each index is perpendicular to the weld), another parallel scan line is produced. If a flaw or notch is detected by the ultrasonic instrumentation, a sudden pen deflection along the *y* axis is produced that is proportional to the size of the discontinuity detected. Since this analog response appears to produce a third direction, we refer to it as a y' or *z* response. Displays such as this should be very beneficial in our weld inspection development work and reduce the number of recordings required.

5. C. V. Dodd and W. A. Simpson, *Fuels and Materials Development Program Quart. Progr. Rep. Dec. 31, 1971,* ORNL-TM-3703, pp. 179–80.

6. C. V. Dodd and W. A. Simpson, *Fuels and Materials Development Program Quart. Progr. Rep. Mar. 31, 1972,* ORNL-TM-3797, pp. 181–83.

7. K. V. Cook and H. L. Whaley, *Fuels and Materials Development Program Quart. Progr. Rep. Mar. 31, 1972,* ORNL-TM-3797, pp. 182–84.

ELECTROMAGNETIC INSPECTION METHODS

C. V. Dodd W. A. Simpson C. C. Cheng[8]
W. E. Deeds[8] J. H. Smith[9] C. W. Nestor[10]

We continued both theoretical and experimental research and development of electromagnetic inspection methods. We are preparing a report;[11] the abstract follows.

This report contains the theoretical analysis and computer programs for reflection-type coils above multiple layered conductors. The performance of the coils when connected to phase-sensitive eddy-current instrumentation can be evaluated. The programs calculate the effects of defects or variations in either conductivity or thickness for multiple conductors, all in the presence of lift-off variations. In addition, program options are included that allow the study of the design of the coil, the study of the effects of small variations or drifts of all the coil, conductor, and instrument parameters, and the effect of the instrument transmitting and receiving impedance on the problem. Examples are given of the use of the programs for the design of eddy-current tests with reflection-type coils.

We applied our computer programs to design a series of probes for a wide range of eddy-current problems. These probes have been constructed and tested. We also applied our computer programs to the design of a series of attenuators to match these coils at various frequencies. These attenuators reduce both the system noise and the effects of temperature variations on the coil.

We completed a report on thickness measurements.[12] It discusses the results of recent computer-based and experimental studies related to the design of optimum test conditions for measuring both the thickness of a single conductor and the thickness of one conductor clad on another. The various graphs in the report provide insight on the effects on thickness measurement of such variables as frequency, coil size, specimen conductivity, coil-to-conductor spacing, and coil resistance, allowing simple design of optimum test parameters and prediction of attainable results.

We completed the computer design, construction, and testing of a new system for measuring the changes in permeability produced in type 316 stainless steel tubing by various degrees of cold working.[13,14] In application to specimens from various suppliers, we demonstrated that within a batch, the error is about ±0.25% of the cold work. Recalibration will be necessary for different vendors and heats.

Under separate funding, we completed the design and testing of an induction probe to measure the level of molten bismuth in a chemical processing system. The probe will measure the level over a $13\frac{5}{8}$-in. range with a resolution of 10 mils. The average temperature coefficient of the probe is less than 8 mils/°C level change over a range of 550 to 700°C. The probe has a zero temperature coefficient from 600 to 625°C. There is excellent agreement between the calculated and experimental probe sensitivity and temperature coefficient. The associated phase-sensitive instrumentation can be adjusted to give direct level readings to within ±0.01 in.

We completed both the ac and dc measurements on 13 different conductors. A statistical analysis on the measurements gave an estimated accuracy of the conductivity of ±0.1%.

We improved the modular phase-sensitive eddy-current instrument. The temperature coefficient of the measurements of phase shift is now less than 0.01°/°C. The chassis of the instrument was revised to allow multiple frequency measurements with analog computer corrections of variable parameters. Also, the instrument can make differential magnitude measurements. This allows highly accurate lift-off measurements to be made over a very wide range of lift-off.

ULTRASONIC INSPECTION METHODS

H. L. Whaley K. V. Cook Laszlo Adler[8]

Frequency Analysis

We continued studying the frequency effects in ultrasonic testing by means of spectral analysis, with emphasis on the use of frequency analysis for the

8. Consultant from the University of Tennessee.
9. On assignment from UCN Y-12 Plant, Oak Ridge.
10. Mathematics Division.
11. C. V. Dodd, C. C. Cheng, J. H. Smith, and W. E. Deeds, *The Analysis of Reflection-Type Coils for Eddy-Current Testing,* report in preparation.
12. C. V. Dodd and W. A. Simpson, Jr., *Thickness Measurements Using Eddy-Current Techniques,* ORNL-TM-3712 (March 1972); also presented at the Spring Conference of the American Society for Nondestructive Testing, Los Angeles, March 15, 1972.
13. C. V. Dodd and W. A. Simpson, *Metals and Ceramics Division Annu. Progr. Rep. June 30, 1971,* ORNL-4770, pp. 100–101.
14. C. V. Dodd et al., *Fuels and Materials Development Program Quart. Progr. Rep. Sept. 30, 1971,* ORNL-TM-3550, pp. 168–69.

characterization of flaws. Several papers[15–19] on this work have been prepared. The following two abstracts briefly describe the approach and some of the accomplishments:

A new method was developed for the characterization (determination of the size and orientation) of a reflector by ultrasonic spectral analysis. This technique can be used to determine nondestructively the nature of flaws detected in a material by means of ultrasonic examination. It is shown that it is feasible to characterize a flaw by this technique in spite of its composition (i.e., crack, void, or inclusion) or shape and without the need for a calibration standard. This technique is free of several limitations inherent in techniques based on amplitude. The results presented here are based on a series of reflection experiments in which the ends of solid rods immersed in water and machined discontinuities in metal samples were used as reflectors. Broad-band ultrasonic pulses were analyzed after reflection from the interface of interest. A physical and analytical model was developed based on an interference mechanism that results from the superposition of spherical wavelets emitted from opposing extremes of the reflector, This model explains very well the experimentally observed spectral variations in terms of size and three-dimensional angular orientation of the reflector, distance between the transducer and reflector, and displacement of the reflector from the axis of the transducer for a flat reflector of any composition. Based on this technique, a detailed procedure can be outlined for characterizing a randomly oriented natural flaw in a plate. The feasibility and practicalityof using this technique to test various materials and in automated testing systems were considered.[15]

In an earlier paper, we have shown that the frequency analysis of a broad-band ultrasonic echo may be used to determine the size and orientation of flat circular reflectors. A single transducer was used as both source and receiver. The one-transducer is not completely satisfactory for the case of discontinuities having both random shape and orientation. Recently, we have used a second transducer to receive ultrasonic pulses scattered by a reflector. Defects in materials were simulated by irregularly shaped metal shims suspended with random orientation in water. The received frequency spectrum when analyzed shows characteristic maxima and minima, which depend on the shape, size, and orientation of the reflectors. A model – which assumes an interference pattern formation of the scattered spherical wavelets at the receiver – relates the spacing between frequency maxima and the positions of the two transducers to the size and orientation of the "discontinuities." The measurement and the analysis are greatly simplified with the use of the second transducer, and size determination of the discontinuities can usually be made within 10–20%.[19]

We continued development of the two-transducer method[20] for ultrasonic frequency analysis because of its much greater simplicity for determining the size of a randomly oriented reflector (or flaw). An initial problem was encountered when the reflector was oriented to allow specular reflections to reach the receiving transducer. A method for avoiding this type of reflected energy was adopted. We wrote a computer program that determines the size of a randomly oriented reflector from the spectral data obtained by the two-transducer method. Practical guidelines for obtaining optimum data by this technique were developed. The instruments used in this system were consolidated into a mobile rack mount to conserve space, simplify operation, and allow the system to be used conveniently at various places in the laboratory.[21] Only two coaxial cable connections are required now to include the capabilities of frequency analysis in any ultrasonic test at any location in the laboratory. This mobile system was "debugged" by collecting detailed spectral data on reflections from a number of irregularly shaped and oriented brass shims. Computer analysis of these data yielded good determinations of the sizes of the reflectors. This would not have been possible with the one-transducer method. We can apparently tell the difference between spherical and cylindrical reflectors by the two-transducer method. The analysis of machined notches in metal blocks by the two-transducer and one-transducer methods indicates that notch (or crack) depth can be determined by spectral analysis of ultrasonic energy scattered from the notch. A physical model has been developed to describe the observed spectral variations. Spectra obtained with notches and side-drilled reference holes are also being compared.

Ultrasonic Imaging

We improved the ability of the schlieren system to effectively image ultrasound at higher frequences (10 to

15. H. L. Whaley and L. Adler, "Flaw Characterization by Ultrasonic Frequency Analysis," *Mater. Eval.* **25**, 182–88, 192 (1971).

16. H. L. Whaley and L. Adler, "A New Approach to the Old Problem of Determining Flaw Size," *Int. J. Fract. Mech.* 8, 112–13 (1972).

17. L. Adler and H. L. Whaley, "Interference Effect in a Multifrequency Ultrasonic Pulse Echo and Its Application to Flaw Characterization," *J. Acoust. Soc. Amer.* **51**, part 2, 881–87 (1972).

18. H. L. Whaley and L. Adler, "Determining the Size of Flaws in Materials," *Instrum. Contr. Syst.* **44**,98–102 (1971).

19. L. Adler and H. L. Whaley "Advantages of a Two-Transducer Technique for Ultrasonic Frequency Analysis," presented at 83rd meeting of the Acoustical Society of America, April 18–21, 1972, Buffalo, N.Y.; submitted for publication in *Journal of the Acoustical Society of America.*

20. H. L. Whaley, K. V. Cook, and L. Adler, *Fuels and Materials Development Quart. Progr. Rep. Dec. 31, 1971,* ORNL-TM-3703, p. 185.

21. H. L. Whaley, K. V. Cook, and L. Adler, *Fuels and Materials Development Program Quart. Progr. Rep. Mar. 31, 1972,* ORNL-TM-3797, pp. 173–77.

20 MHz).[22] A second radio-frequency oscillator was obtained and modified for high-power applications, in which the transducers must be driven with large amplitude. The schlieren inspection of the stainless steel weld samples was completed.[22] Several test configurations were employed at various ultrasonic frequencies to determine optimum conditions. These tests were recorded on video tape. Effects of known defect areas in the welds on the propagation of ultrasound in the specimens were observed, but interpretation was difficult. The optical table and equipment reserved for prototype optical systems were used to construct an experimental interferometric system for imaging ultrasound.[23] This method was successful in forming an image of the ultrasonic beam, but the optical system could not provide the stability necessary to maintain a setup. The same optical table and equipment were used to construct a Bragg diffraction imaging system. Necessary mechanical fixtures were designed and built, and rudimentary images of objects placed in the path of the ultrasound were obtained. Design of a larger, more versatile, sensitive, and stable system was undertaken. A pulsed laser and all other necessary optical components for this system have been ordered. We built and tested 1- and 2-in.^{2} transducers for use with this system. Additional mechanical fixturing for this system has also been designed and built.

PENETRATING RADIATION INSPECTION METHODS

B. E. Foster S. D. Snyder

We continued our development of a closed-circuit television (CCTV) system[24-26] for enhancing and interpreting radiographs. Tests were conducted to optimize the settings of the various controls for system response and sensitivity. A radiograph on a high-resolution plate of 400-mesh screen has been used as a standard for assessing resolution capability of the system. With an optical magnification of only 2.3X, we were able to image a crack or break in a single 30-μm-diam wire of the 400-mesh screen. The 2.3X optical magnification results in a total image enlargement of 40X when combined with the 17.5X from the Vidicon mosaic to the monitor screen.

The system allows selection of one or more of the 500 lines of video on the monitor for closer examiation as well as any section of any of the lines. This selected region can be recorded on a strip chart or *x-y* recorder for further study. Any area of the image on the monitor screen can be selected and shaded (darkened or lightened) for more contrast and more comfortable viewing. This effect is quite similar to the split-screen viewing on a home television receiver, except in that case, the studio is using multiple cameras rather than a single camera.

The system is presently being applied to an intriguing problem on the heater bundle of the Fuel Failure Mockup (FFM). The engineering concern is possible movement of the heater elements during operation. The heater bundle was radiographed with a ^{60}Co source at conditions of (1) no load, (2) elevated temperature, and (3) flowing sodium. We are using the CCTV system to enlarge and enhance the region of interest on the radiograph. By selecting a portion of the proper scan line from the television raster we can produce an *x-y* recording from which we can measure the dimensions between a peripheral element and the surrounding clamp. Preliminary results are promising, with dimensional variations readily observable. We are calibrating the system to allow determination of accuracy and precision of the measurements.

---

22. H. L. Whaley, K. V. Cook, and L. Adler, *Fuels and Materials Development Program Quart. Progr. Rep. Sept. 30, 1971*, ORNL-TM-3550, pp. 171–72.
23. K. V. Cook, H. L. Whaley, and L. Adler, *Fuels and Materials Development Program Quart. Progr. Rep. Dec. 31, 1971*, ORNL-TM-3703, p. 186.
24. B. E. Foster and S. D. Snyder, *Fuels and Materials Development Program Quart. Progr. Rep. Sept. 30, 1971*, ORNL-TM-3550, pp. 173–74.
25. B. E. Foster and S. D. Snyder, *Fuels and Materials Development Program Quart. Progr. Rep. Dec. 31, 1971*, ORNL-TM-3703, p. 187.
26. B. E. Foster and S. D. Snyder, *Fuels and Materials Development Program Quart. Progr. Rep. Mar. 31, 1972*, ORNL-TM-3797, pp. 177-79.

Part III. Space Power Technology

21. Cladding Materials for Space Isotopic Heat Sources

R. G. Donnelly

The purpose of this program is to develop high-melting, oxidation resistant alloys for space applications of isotopic heat source capsules operating between 900 and 1300°C. This requires alloys exhibiting superior performance under operational, abort, reentry, earth impact, and postimpact conditions. Potential applications are as fuel containment materials in $^{238}PuO_2$- and $^{244}Cm_2O_3$-fueled thermoelectric generators, such as the Multihundred Watt (MHW) generator now under development and advanced versions of the SNAP-19 generator as used aboard the Pioneer space probe.

NEW PLATINUM-RHODIUM-TUNGSTEN ALLOYS FOR SPACE ISOTOPIC HEAT SOURCES[1]

H. Inouye C. T. Liu
R. G. Donnelly

Multiple layers of refractory alloys clad with a platinum-rhodium alloy are now used as the capsulating materials for the fuel in isotopic heat sources. In this design one alloy compensates for the shortcomings of another. This method was developed because no single alloy of current manufacture can meet the severe service and safety requirements of thermoelectric generators for space power. However, improvements in oxidation resistance and compatibility with heat source environment over those obtainable with the refractory alloy components in such capsule assemblies are desired. The conventional platinum-rhodium alloy cladding, although possessing excellent fabricability and oxidation resistance, lacks the desired mechanical strength and high melting temperatures. Our program objective has been to develop fabricable alloys with better strength, oxidation resistance, compatibility, and melting temperatures.

The new platinum-base alloys containing 25 to 30 Rh, 6 to 10 W, 0 to 1.0 Hf, and 0 to 0.5 Ti (wt %) can be fabricated by hot rolling in air between 1000 and 1250°C followed by cold working at room temperature with intermediate anneals. The formability is quite good: a 1¼-in.-diam hemisphere of the Pt–30% Rh–8% W–0.25% Hf–0.10% Ti alloy was made from a 0.030-in.-thick blank by cold forming over a mandrel, with two intermediate anneals at 1200°C.

The tensile properties of the new alloys were determined at temperatures to 1316°C. The tensile strengths increase with the tungsten content. Hafnium and titanium additions further improve the strength of the ternary alloy base, especially at the higher temperatures. Also, the hafnium and titanium additions inhibit grain growth and increase the 1-hr recrystallization temperature from 1050 to 1200°C. The new alloys are much stronger than Pt–30% Rh, iridium, and TZM at temperatures to 1093°C and are comparable to iridium and TZM at 1316°C. In terms of the impact resistance [defined as fracture strain × (UTS + YS)/2] at 1316°C, the Pt–30% Rh–8% W–1.0% Hf–0.2% Ti is the best among all the candidate alloys (see Fig. 21.1).

To further qualify the use of Pt-Rh-W alloys as the capsulating material, sheet specimens were held at 1100°C in 1×10^{-5} torr oxygen. After 253 hr the alloy showed only a small reduction of the room-temperature ductility and no change in the 825°C ductility.

The oxidation behavior for these alloys was determined at 760, 1000, and 1200°C in air. Alloying with up to 10% W, 1% Hf, and 0.5% Ti did not impair the excellent oxidation resistance of the Pt–30% Rh base. The oxidation rates for the alloys are only 5 times those for unalloyed platinum but lower than those of

1. Summary of talk presented at ANS meeting in Las Vegas, Nevada, June 1972; ORNL-4813 (in press).

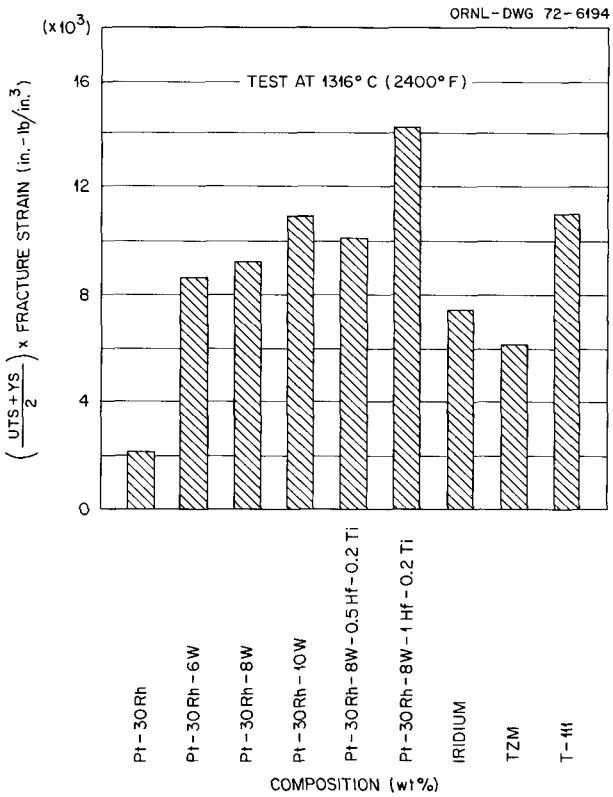

Fig. 21.1. Impact capabilities of cladding materials for isotopic heat sources.

molybdenum- and tantalum-base alloys by four orders of magnitude.

CHARACTERIZATION OF Pt-Rh-W ALLOYS

J. H. Erwin H. Inouye

A family of improved platinum alloys containing 26 to 30% Rh and 6 to 10% W as the principal alloying elements was recently developed for possible use in thermoelectric generators for space power. In a typical application, alloy sheet would be used to encapsulate the isotopic fuel in the heat source. The objective of this study is to fully characterize one or two alloys to qualify them for this application.

Four-pound ingots of Pt-2608 (nominal composition Pt–26% Rh–8% W) have been routinely hot rolled between 1000 and 1200°C in air to sheet 0.040 to 0.050 in. thick, then cold rolled to 0.030 in. at room temperature. The formability of sheet thus produced and as determined by a modified Olsen cup test depends on the annealing temperature of the test blanks. Optimum formability as evidenced by the maximum in the cup height occurs in blanks annealed at approximately 1000°C. This temperature is at or just below the recrystallization temperature of this alloy.

Eddy-current inspection of sheet produced from several heats sometimes revealed isolated areas of inhomogeneity. Metallographic examination of these areas showed narrow stringers of a hard second phase, which was identified as unmelted tungsten by x-ray analysis. Segregated tungsten causes laminations in formed parts and low tensile properties. This problem has been overcome through the use of powdered tungsten and a modified melting procedure.

CHARACTERIZATION OF IRIDIUM

C. T. Liu

The isotopic fuel in a heat source of an advanced radioisotope thermoelectric generator (RTG) for space power will be clad with iridium. One of the principal requirements of the cladding is to contain the fuel under accident conditions, such as a launch abort or unplanned reentry from earth orbit and subsequent earth impact. Tensile properties of iridium were determined at possible launch abort temperatures. No well-defined ductile-to-brittle transition temperature (DBTT) was observed in terms of the elongation. Reduction in area did increase significantly above 500°C, which is in agreement with the DBTT as reported in the literature.[2] The fracture surfaces showed a brittle-to-ductile transition between 500 and 760°C.

Iridium annealed at 1500°C and then subjected to a heat pulse of 2000°C for 5 min, which simulates reentry heating, has significantly lower yield strength than as-annealed specimens at room temperature and 1093°C. Most significant is the serious loss of ductility at 1093°C caused by the heat pulse. The tensile properties of iridium at 1316°C were unaffected by the heat pulse.

2. R. W. Douglas et al., *High Temperature Properties and Alloying Behavior of Refractory Platinum Group Metals,* NP-10939, Battelle Memorial Institute (August 1961).

22. Development of Uranium Nitride Fuels for NASA

J. L. Scott

A technology program for a compact fast reactor for space power is in progress at the NASA Lewis Research Center. The 2-MW reactor uses UN fuel clad in T-111 and is cooled with lithium.[1] Its lifetime is 50,000 hr with a coolant outlet temperature of 1220°K. In support of the program, we are conducting both irradiation tests of prototypic pins and basic fabrication studies on UN. These activities are a follow-on to a basic UN development program previously funded at ORNL by the AEC. One irradiation capsule, UN-6, contains UO_2, which is a backup to UN for the compact fast reactor.

IRRADIATION TESTING OF URANIUM NITRIDE

T. N. Washburn B. Fleischer K. R. Thoms[2]

The irradiation of capsules UN-4 and UN-5 in the ORR was continued during the last year, and a third capsule experiment, UN-6, containing UO_2 pellets was inserted August 3, 1971. Detailed descriptions of our capsule design[3] and previous test results[4–6] have been reported. After 1550 hr of operation at a cladding temperature of about 850°C, the heat rating of capsule UN-6 was increased to raise the middle pin cladding temperature to 925 to 960°C while limiting the maximum pin center line to 1600°C. The status of the three capsules as of May 1972 is given in Table 22.1.

Cladding thermocouple failure due to shorting, which forms a new junction, was the principal operational difficulty. Sufficient operating experience was obtained before failure of the thermocouples, however, to permit continued irradiation of the capsules. Capsule temperatures were inferred from calorimetric measurements.

In the NaK blanket gas ^{133}Xe was detected after about 6000 hr of irradiation of UN-4 and 8500 hr of irradiation of UN-5. The activity found was quite small, amounting to about 10^{-5} of the fission-product gas present in the capsules. The source of the activity will be determined by postirradiation examination.

1. M. H. Krasner, H. W. Davison, and A. J. Diaguila, *Conceptual Design of a Compact Fast Reactor for Space Power*, NASA-TMX-67859 (June 13, 1971).
2. Reactor Division.
3. V. A. DeCarlo, F. R. McQuilkin, R. L. Senn, K. R. Thoms, and S. C. Weaver, *Design of a Capsule for Irradiation Testing of Uranium Nitride Fuel*, ORNL-TM-2363 (February 1969).
4. T. N. Washburn, D. R. Cuneo, and E. L. Long, Jr., "Irradiation Performance of Uranium Nitride at 1500°C," *Amer. Ceram. Soc. Bull.* **50**, 427 (1971).
5. T. N. Washburn, K. R. Thoms, S. C. Weaver, D. R. Cuneo, and E. L. Long, Jr., "Examination of UN-Fueled Pins Irradiated at 1400°C Cladding Temperature," *Trans. Amer. Nucl. Soc.* **13**, 101 (1970).
6. S. C. Weaver, K. R. Thoms, and V. A. DeCarlo, "Irradiation Testing of UN in ORR," *Trans. Amer. Nucl. Soc.* **12**, 547 (1969).

Table 22.1. Status of capsules UN-4, UN-5, and UN-6

Capsule	Irradiation time (hr)	Current cladding temperature[a] (°C)	Average heat generation rate (kW/ft)	Estimated burnup (% FIMA)
UN-4	9310	976	9.9	2.52
UN-5	9000	991	9.6	2.37
UN-6	1550	845[b]	4.6	
	6050	942	4.9	1.17

[a]Temperature of cladding on middle of three pins in capsule.
[b]Temperature of cladding for first 1550 hr of irradiation. The heat rating was then increased.

We made neutron radiographs to obtain data on the dimensional behavior of both fuel pins and pellets within each capsule. Very little change was found for any of the pins, but some pellets developed cracks and changed dimensions.

UN FABRICATION STUDIES

R. A. Potter V. J. Tennery

The basic objective of this study was to fabricate 85% dense UN pellets that are thermally stable to about 2300°C. We thermally conditioned powders of uranium nitride at several different temperatures in the range 1100 to 1500°C. The powders were characterized by particle size distribution measurements, specific surface area measurements, and chemical analysis.

Specimens prepared from the conditioned powders were sintered at four different temperatures in the range 1700 to 2300°C and characterized by density measurements, metallography, porosimetry, and chemical analysis. Specimens prepared from powders conditioned at 1400°C for 3 hr and sintered at 2100°C resulted in microstructures of interest to NASA. They contained interlocking porosity and were about 85% of theoretical density. Specimens of 75% or greater density when thermally tested for 100 hr at 1365°C in vacuum were dimensionally and chemically stable. No change in crystal size was observed; however, some change in pore configuration was detected.

We also developed a process for synthesizing nitrogen-rich uranium sesquinitride powder. Uranium mononitride pellets made from $UN_{1.74}$ densified to approximately 85% of theoretical when sintered at 2300°C. Microstructures were comparable to those of specimens prepared from the 1400°C thermally conditioned powder.

23. Physical Metallurgy of Refractory Alloys

R. G. Donnelly

The program provides a base technology evaluation of materials for use in isotopic heat sources for space power applications. During this period these activities were aimed specifically at solving materials problems encountered in SNAP-19 radioisotope thermoelectric generators for use aboard the Pioneer space probe. These results have further impact because the SNAP-19 generator is also planned for use on the Viking mission to Mars.

EMBRITTLEMENT OF T-111 PIONEER FUEL CAPSULES

C. T. Liu H. Inouye

The failure of the T-111 strength member in several test Pioneer heat sources in the summer of 1971 was traced to the embrittlement of the alloy by oxygen contamination. The source of the oxygen was the PuO_2 fuel, the graphite, and the MIN-K insulation. Although the degree of contamination could be reduced by the use of barriers, degassing of the components, and gettering of the noxious gases, oxygen contamination could not be entirely eliminated. Thus, the establishment of the relationship between the oxygen content and the ductility of T-111 was crucial to qualify the Pioneer heat source for flight by March 1972. The data obtained are shown in Fig. 23.1.

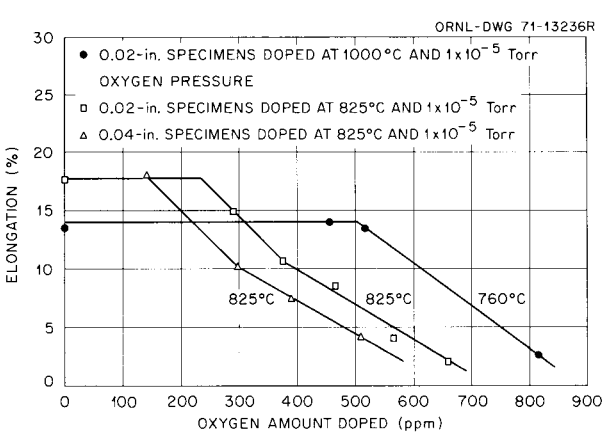

Fig. 23.1. High-temperature ductility of oxygen-doped T-111.

In addition to these vital data, ORNL established (1) that reentry heating can ductilize otherwise brittle T-111 containing up to 4000 ppm O, (2) that the ductility of oxygen-contaminated T-111 is fortuitously a maximum at the design temperature of 825°C, and (3) the reaction kinetic data necessary to estimate the extent of oxygen contamination between the time of fueling the launch.

Molybdenum-base alloys and molybdenum-coated T-111 were found to be suitable alternate "fixes" if the prime fix (method of reducing contamination) mentioned above failed.[1-4]

EVALUATION OF PIONEER TEST CAPSULES

H. Inouye H. E. McCoy, Jr.
E. L. Long, Jr. R. W. Knight

Assistance to the Pioneer project in the fall–winter of 1971 consisted of measuring the mechanical properties of sections of the T-111 strength member cut from test capsules PF-3, PF-7, and PF-9. Tensile and bend tests were coupled with detailed scanning electron microscopic studies of the fracture surfaces to help evaluate the Pioneer "fix."

Consulting services were provided to the Space Nuclear Systems (SNS) Division of the AEC on a

1. C. T. Liu, *Fuels and Materials Development Program Quart. Progr. Rep. Mar. 31, 1971,* ORNL-TM-3416, pp. 194–98.
2. R. G. Donnelly and P. Patriarca, *Fuels and Materials Development Program Quart. Progr. Rep. Sept. 30, 1971,* ORNL-TM-3550, pp. 224–34.
3. R. G. Donnelly and P. Patriarca, *Fuels and Materials Development Program Quart. Progr. Rep. Dec. 31, 1971,* ORNL-TM-3707, pp. 259–74.
4. C. T. Liu, H. Inouye, and R. W. Carpenter, "Mechanical Properties and Structure of Internally Oxidized Ta–8 W–2 Hf (T-111) Alloy," paper presented at AIME Spring Meeting, Boston, May 1972.

variety of problems related to the feasibility of using T-111 as the strength member. Consulting services to Teledyne Isotopes, and SNS subcontractor, were instrumental in salvaging one heat source that was accidentally exposed to air during assembly.

The Metals and Ceramics Division, in cooperation with the Plant and Equipment Division, fabricated palladium housings for the zirconium getters that were incorporated into the Pioneer generators as part of the "fix."

MECHANICAL PROPERTIES AND STRUCTURE OF INTERNALLY OXIDIZED Ta–8% W–2% Hf (T-111) ALLOY[5]

C. T. Liu H. Inouye
R. W. Carpenter

Effects of internal oxidation on the mechanical properties and structure of Ta–8% W–2% Hf (T-111) alloy have been studied. Internal oxidation treatments were performed on 0.02-in.-thick sheet material in a furnace at 1000°C and 1×10^{-5} torr dynamic oxygen pressure. After being doped, the specimens were heat treated at various temperatures. Calculations based on the lattice-parameter measurement indicate that the oxygen solubility in T-111 is around 100 ppm at 1700°C. The tensile properties of oxygen-contaminated specimens were determined in vacuum at temperatures to 1316°C (2400°F). The results for specimens with oxygen contents up to 3000 ppm heat treated at 1700°C show a slight increase in strength and a decrease in ductility. Beyond this level, the strength increases and ductility decreases sharply with oxygen contamination. Heat-treated T-111 loses its ductility completely when the oxygen content reaches 4000 ppm; in contrast, the as-doped T-111 is brittle at an oxygen level of only 800 ppm. Extremely fine, coherent precipitates were observed in electron micrographs of as-doped specimens. These coarsen upon annealing and eventually form discrete HfO_2 particles. With an increase of oxygen content, precipitate particles gradually appear on the grain boundaries and finally connect into a network at an oxygen level of 4000 ppm.

5. Summary of paper presented at AIME Spring Meeting, Boston, May 1972.

24. Tungsten Metallurgy

A. C. Schaffhauser

The objective of this program is to provide the base technology on tungsten alloys for advanced space-power and general reactor technology applications. We are developing fabrication processes for tungsten alloys based on modification of conventional extrusion, chemical vapor deposition, and welding techniques. Since the primary criterion for the use of tungsten alloys for these applications is based on the creep properties, we are conducting extensive long-time tests at the temperatures of interest. We are also determining the mechanisms that control the creep behavior and the effect of interactions with the vapor species from an isotope or reactor fuel. The behavior of tungsten alloys under fast-neutron irradiation is also being evaluated.

FABRICATION OF EXPERIMENTAL TUNGSTEN MATERIALS

J. I. Federer R. E. McDonald
A. C. Schaffhauser

We are developing fabrication techniques for experimental tungsten materials needed for the thermionic reactor project. The reference fuel cladding material for this application is chemically vapor deposited (CVD) tungsten. Previously we showed that the creep properties of CVD tungsten depend on the fluorine impurity content of the deposit, which can be controlled by adjusting the deposition parameters.[1] We fabricated a number of large sheet deposits of CVD tungsten having either low (5 to 10 ppm) or high (15 to 25 ppm) fluorine contents. The machining techniques and standard operating procedures have been established for consistently fabricating 12 to 16 creep specimens per deposit. Specimens have been supplied for our creep testing program (see the following section) and a cooperative creep testing program with NASA-Lewis Research Center.

1. R. L. Stephenson and J. I. Federer, "Creep Rupture Properties of CVD-Tungsten," pp. 90–94 in *IEEE Conference Record of 1970 Thermionic Convention Specialist Conference, October 26–29, 1970,* The Institute of Electrical and Electronics Engineers, New York, 1970.

We also developed fabrication techniques for alternate fuel cladding materials. Nominal 1-in.-diam × 0.040-in.-wall thickness tubes of arc cast tungsten and W–2% ThO_2 machined from extruded tubing were supplied to Gulf General Atomic for thermionic fuel element irradiation testing.

THE HIGH-TEMPERATURE CREEP PROPERTIES OF CHEMICALLY VAPOR DEPOSITED TUNGSTEN[2]

H. E. McCoy, Jr. J. O. Stiegler
A. C. Schaffhauser

The creep-rupture properties of several deposits of chemically vapor deposited (CVD) tungsten were determined at 1650°C and stresses between 2000 and 10,000 psi. Above 3000 psi the creep-rupture properties could be correlated directly with the fluorine impurity content. Material containing 13 to 25 ppm F had 2 to 10 times longer rupture lives, $^1/_{10}$ to $^1/_{100}$ the minimum

2. Abstract of paper presented at Third International Conference on Chemical Vapor Deposition, Salt Lake City, Utah, April 24–27, 1972.

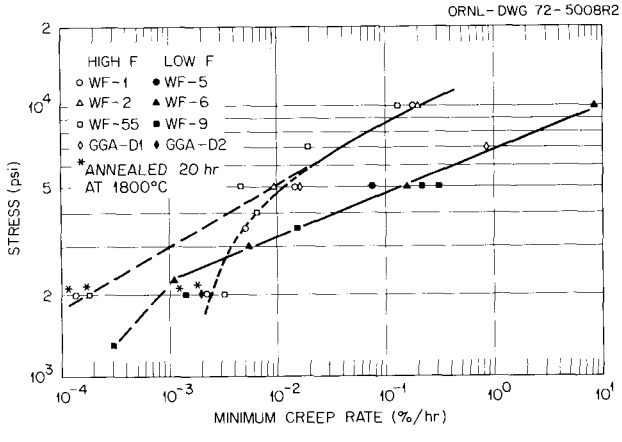

Fig. 24.1. Comparative creep rates of several lots of CVD tungsten at 1650°C. (Low F is 2–7 ppm, high F is 13–25 ppm.)

creep rate, and $\frac{1}{2}$ to $\frac{1}{10}$ the rupture ductility of material containing 2 to 7 ppm F. At stresses between 2000 and 3000 psi the minimum creep rate trend appears to reverse, and the purer material has a lower minimum creep rate (Fig. 24.1). However, annealing 20 hr at 1800°C before testing lowered the minimum creep rate of the high-fluorine material by a factor of 100 but had little effect on the low-fluorine material. This annealing treatment is typical of the thermal history of a thermionic diode during fabrication; therefore, the higher fluorine material appears to have a significant strength advantage for that application.

Electron microscopy of tested creep specimens has shown that the creep properties of CVD tungsten are controlled by fluorine impurities in the form of very small gas bubbles and the stress-induced growth of gas bubbles into grain boundary voids.

LOW-STRESS CREEP TESTING OF TUNGSTEN

A. C. Schaffhauser W. L. McCollough[3]

We are obtaining design-type creep data on CVD tungsten at stresses to produce 1% creep in 1000 to 50,000 hr. The strain measuring techniques used previously for obtaining creep-rupture data (see preceding section) are not sufficiently accurate at low stresses for design. Five ultrahigh-vacuum, high-temperature creep machines with optical extensometers are collecting the design data required for the thermionic reactor program. The optical strain measurement instrumentation and specimen targets are currently measuring strain to $\pm 3 \times 10^{-4}$ in. accuracy at 1650°C. Design changes in the instrumentation and specimen targets are in progress to obtain even greater accuracy.

A test matrix and cooperative creep testing program with NASA-Lewis Research Center has been established. The primary emphasis is on obtaining data at 1500, 1650, and 1800°C on low-fluorine duplex CVD tungsten,[4] the reference material for thermionic fuel elements, and high-fluorine material that has greater creep strength.

Creep tests of CVD tungsten at 1650°C and 1000 and 2000 psi are in progress on a duplex deposit (GGA-D2) containing 5 ppm F and a fluoride deposit (WF-55) containing 20 ppm F. All specimens were annealed 20 hr at 1800°C before testing. The 2000-psi data for both deposits are plotted in Fig. 24.1 and confirm the previous results. The high-fluorine material has about $\frac{1}{10}$ the creep rate of the low-fluorine duplex material. Tests in progress at 1000 psi have produced 0.1% strain in 2400 hr for deposit WF-55 and 0.05% strain in 750 hr for deposit GGA-D2.

3. Consultant.
4. Supplied by Gulf General Atomic, San Diego, Calif.

CREEP PROPERTIES OF W–3.8% ThO_2

H. E. McCoy, Jr.

The creep-rupture properties of W–3.8% ThO_2 have been determined under several conditions. The $\frac{1}{4}$-in.-diam material was prepared by the Westinghouse Electric Corporation[5] and had been cold worked 91%. Creep specimens having a gage section 1 in. long × $\frac{1}{8}$ in. diam were prepared and tested in vacuum in the as-received condition.

The stress-rupture properties are compared in Fig. 24.2 with two previously reported[6] curves for W–2% ThO_2. The limited number of data points at a given temperature makes it impossible to draw complete stress-rupture curves. The time to rupture at a given stress is not appreciably different for the two materials at 1650°C for rupture times up 100 hr. For longer rupture times the W–2% ThO_2 deviates from linearity, but the W–3.8% ThO_2 does not appear to have this break. At 2200°C the rupture life of the W–3.8% ThO_2 is about 100 times that of W–2% ThO_2. However, the heat of W–3.8% ThO_2 that we are studying has shorter rupture lives than those reported by Westinghouse for a similar heat, which had 1-hr and 10-hr rupture stresses of 12,500 and 9500 psi respectively.[7]

The minimum creep rates were also measured in these tests. At 1650°C the strengths of the two materials are quite similar. At 2200°C the allowable stress for the W–2% ThO_2 is significantly lower than that for the W–3.8% ThO_2. The fracture strains at all temperatures were good, with the minimum being 7.5% at 2000°C.

EFFECT OF CARBURIZATION ON THE CREEP PROPERTIES OF TUNGSTEN ALLOYS

H. Inouye

The creep properties of 0.040-in.diam tungsten wire are being measured while it is being carburized with low-pressure CH_4 at thermionic temperatures. In tests

5. Westinghouse Electric Corporation, Lamp Division, Bloomfield, N.J.
6. H. E. McCoy, *Creep-Rupture Properties of Tungsten and Tungsten-Base Alloys*, ORNL-3992 (August 1966).
7. H. G. Sell, W. R. Morcom, and G. W. King, *Development of Dispersion Strengthened Tungsten Base Alloys*, AFML-TR-65-407, Part II (1966).

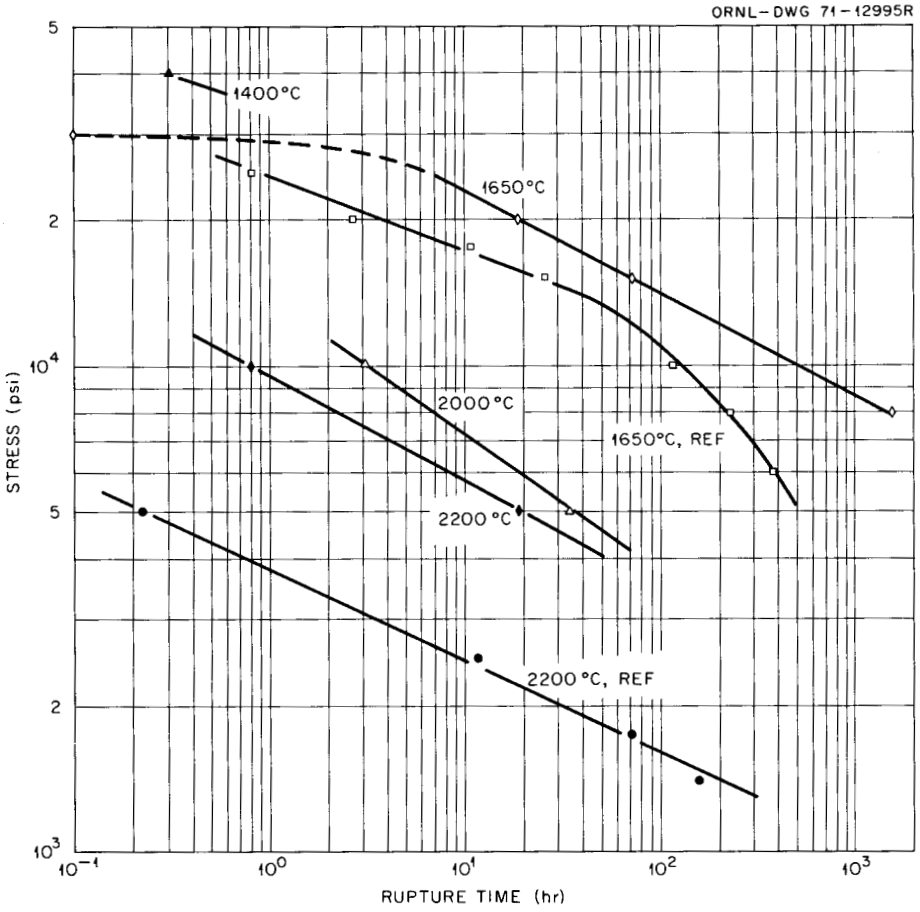

Fig. 24.2. Comparison of stress-rupture properties of W–3.8% ThO_2 with referenced W–2% ThO_2 properties. Ref: H. E. McCoy, *Creen-Rupture Properties of Tungsten and Tungsten-Base Alloys,* ORNL-3992 (1966).

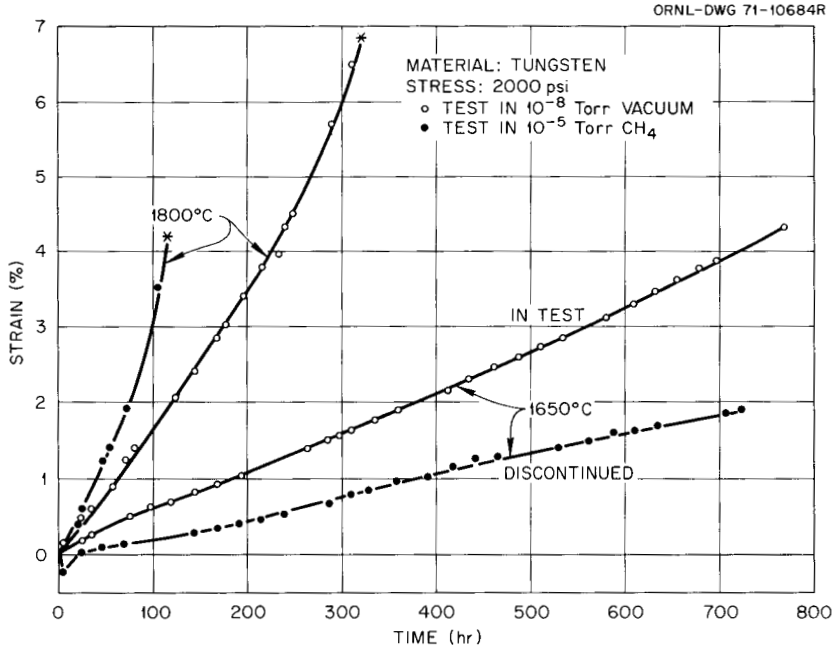

Fig. 24.3. Creep properties of tungsten in vacuum and low-pressure CH_4.

at 1800°C and a stress of 2000 psi, both the rupture ductility and rupture life progressively decreased with the CH_4 pressures; in contrast, tests at 1650° C show the opposite effect. Typical creep curves for tungsten tested in vacuum and in 10^{-5} torr CH_4 are shown in Fig. 24.3. X-ray analyses show W_2C on the surfaces of specimens exposed to CH_4 at 1650°C but not on specimens tested 1800°C. Chemical analyses show carbon contents ranging from 1100 to 1800 ppm independent of the CH_4 pressure.

RADIATION DAMAGE TO REFRACTORY METALS AS RELATED TO THERMIONIC APPLICATIONS[8]

F. W. Wiffen

The effects of fast neutron irradiation on the bcc refractory metals are reviewed with emphasis on materials and conditions typical of thermionic applications in space power systems. Changes produced in the microstructure are characterized as a function of irradiation temperature. The effects of fluence, alloying, and purity are examined where data are available. Swelling and changes in the mechanical and electrical properties produced by neutron irradiation are briefly reviewed. The major effects expected are in the collector and cooler portions of the emitter in a thermionic diode where swelling, increases in electrical resistivity, and losses of ductility are anticipated during reactor operation.

HIGH-TEMPERATURE FAST-NEUTRON IRRADIATION OF TUNGSTEN ALLOYS

F. W. Wiffen R. K. Williams

A single-capsule, high-temperature experiment[9] was irradiated in the EBR-II to a total exposure of 6331 MWd. The calculated peak fluence was $7.8 \pm 2.0 \times 10^{21}$ neutrons/cm^2 (>0.1 MeV). The capsule contained five specimen holders designed to operate at irradiation temperatures ranging from 600 to 1500°C. The specimen holders contained rod specimens 0.10 in. in diameter, with 2-in.-long specimens for postirradiation resistivity measurements and 1-in.-long specimens for sectioning to provide electron microscopy samples. Sample materials include tungsten and tungsten-rhenium alloys prepared by powder metallurgy, arc melting, and CVD. Postirradiation examination of this experiment will include determination of swelling by measurements of geometry and immersion density, void classification by transmission electron microscopy, and measurements of electrical properties including low- and high-temperature resistivity.

Room temperature electrical resistivity (ρ) data were obtained on three tungsten and three W–25% Re samples that had been irradiated in EBR-II to a fluence of approximately 3.7×10^{22} neutrons/cm^2 (>0.1 MeV). The tungsten samples were irradiated at nominal temperatures of 800, 900, and 1000°C and the maximum increase in the ρ of those specimens was 17%. This result indicates that irradiation-induced damage at these temperatures does not have a large effect on the ρ of tungsten. The W–25% Re samples were irradiated at 700, 800, and 900°C and the respective changes were +6, −10, and −11%. These results indicate that irradiation induces a phase change or ordering in the alloy, and this possibility is being investigated.

8. Abstracted from ORNL-TM-3629 (February 1972).
9. F. W. Wiffen, *Fuels and Materials Development Program Quart. Progr. Rep. Mar. 31, 1972,* ORNL-TM-3797, pp. 263–66.

Part IV. Reactor Development Support

25. Gas-Cooled Reactor Program

J. H. Coobs

Our materials effort in support of the Gas-Cooled Reactor Program is directed primarily toward the development of unclad ceramic fuel elements for high-temperature gas-cooled converter reactors (HTGRs), such as the Fort St. Vrain Reactor and the larger reactors recently sold by Gulf General Atomic. The reference fuel elements consist of hexagonal graphite blocks containing coated $(Th,U)O_2$ or $(Th,U)C_2$ microspheres and are designed to retain most of the fission-product activity within the fuel element to simplify maintenance.

Our program has consisted principally of developing techniques for bonding coated particles into fuel elements and preparing, characterizing, and irradiation testing pyrolytic carbon coatings, coated particles, and simulated bonded fuel elements. After demonstrating the successful performance of intrusion-bonded fuel sticks in several experiments, the emphasis has shifted to the preparation and testing of coated fuel particles derived from ion exchange resin beads and investigations of the chemical equilibria in particles and the reactions producing failure. Irradiation testing is now done principally in HFIR target and reflector positions. Bonded-bed specimens and resin-derived particles have survived irradiation to fast-neutron exposures exceeding the peak HTGR fluence of 8×10^{21} neutrons/cm^2 (>0.18 MeV) and to burnups of about 30 at. % heavy metal. Temperatures have spanned the range experienced in an HTGR, 600 to 1300°C.

We are also participating with Gulf General Atomic in a cooperative effort to develop fuel elements for a Gas-Cooled Fast Breeder Reactor (GCFBR). We completed an experiment in the ORR to test a vented fuel pin, which was adopted as the reference GCFBR design, and prepared the fuel pin for another similar test. Five fuel pins that simulate the vented design were also constructed and will be tested in EBR-II along with the eight pins previously prepared.

COATED PARTICLES FROM ION EXCHANGE RESINS

C. B. Pollock M. D. Silverman[1]

An alternate way to fabricate HTGR "fissile" fuel particles using ion exchange resins is being developed.[2] Spherical cation exchange resin beads are contacted with uranyl salt solution under favorable chemical loading conditions until they are saturated with the heavy metal ion. The loaded beads are then dried, carbonized, and heat treated to form the fuel kernel. These particles consist of a fuel phase dispersed very uniformly in a low-density carbon kernel. These kernels are then coated with successive layers of carbon and silicon carbide to form the fuel particles.

Resin Selection

Visual and microscopic examination of various strong-acid resins indicated that those sulfonated at lower temperatures (e.g., Dowex 50W, Duolite C-25) contained fewer cracked spheres, both before and after heat treatment. Commercial resins contain up to 4% ash by weight (mainly metallic impurities such as Al, Fe, Cu, Pb, and Ni), whereas analytical grades can run as little as 0.05%; however, sufficient water washes during wet screening and resin preparation (before fuel loading) can reduce the ash content of commercial resins to 0.1% or less.

1. On loan from Reactor Division.
2. C. B. Pollock, J. L. Scott, and W. P. Eatherly, *Metals and Ceramics Div. Annu. Progr. Rep. June 30, 1971*, ORNL-4770, pp. 140–43.

Fuel Loading

The fuel kernels are made by contacting fuel solutions under conditions favorable to the exchange reaction. Previously we[3] demonstrated the feasibility and reproducibility of loading strong-acid resins with uranium from uranyl nitrate solution. This process has been optimized and demonstrated in an automatic semicontinuous contactor by the Chemical Technology Division.[4]

To avoid the complications of using sulfur-containing strong-acid resin particles and to obtain higher fuel loadings, we have concentrated on weak-acid resins. Loading studies conducted by K. J. Notz and P. A. Haas of the Chemical Technology Division indicated that, of the various weak-acid resins tested, IRC-72 manufactured by Rohm and Haas was the best on the basis of fewer cracked spheres as well as easier and more efficient loading. Therefore, we have used IRC-72 for all subsequent carbonization and heat-treatment studies on weak-acid resins.

Carbonization and Heat Treatment

Weak-acid resins. Differential thermal analysis and thermogravimetric analysis curves made on weak-acid resin IRC-72, along with qualitative gas chromatography, indicated that the following processes probably occur during carbonization in an inert atmosphere: (1) water is largely removed between 100 and 200°C, although small amounts persist to about 400°C; (2) the polymer breaks up between 300 and 350°C; (3) carbonization and decarboxylation take place in the 350 to 450°C range; and (4) carbonization appears to be complete by approximately 600°C, but a minor loss in weight occurs on further heating to 1000°C.

Carbonization and heat-treatment times as well as temperatures have been studied and determined; further study is needed on rates of heating. We have aimed at producing a mixed UO_2-UC_2 kernel that contains about 10% carbide. The resulting fuel kernel should be covered with a buffer and sealing layer before SiC coating. Data presented by Lindemer[5] and Leitnaker and Godfrey[6] have been used as a basis for these conversion studies.

Strong-acid resins. The metal-loaded resins are carbonized in a fluidized-bed furnace and then heat treated to a higher temperature to control the fuel form. A preliminary x-ray diffraction study of fuel particles made from strong-acid resins has revealed several compounds. For kernels heated at low temperatures (below 1200°C), conventional Debye-Scherrer powder diffraction patterns show only broad diffuse lines typical of poorly crystallized material containing very small crystals. Diffraction patterns of thin samples of the same material, taken by the electron microscope at very high energies, reveal an oxysulfide phase similar to UO_2.

Samples heated to 1400°C and higher yield patterns when conventional powder techniques are employed. The dominant fuel phase is again an fcc phase similar to UO_2, but it now has a lattice constant of 10.8 Å, approximately twice that of UO_2. Weaker UC_2 and carbon diffraction lines are also observed.

Particle Design and Modeling

Fuel particles from resins differ in many respects from conventional fully dense fuel particles. Therefore, to optimize the performance and maximize the service life of these particles, different coating designs were required. As reported previously,[2] computer codes developed here and at Gulf General Atomic have been used to predict fuel particle behavior under various conditions of temperature, fluence, and burnup, and particles for irradiation proof-testing were designed on this basis. A number of experimental particles are now available for postirradiation examination, and certain particle designs are being modified. For example, we find it necessary to retain a thin low-density buffer layer to provide a debonding layer between the kernel and the inner carbon and SiC layers.

ANALYSIS OF CHEMICAL FAILURE OF URANIA FUEL PARTICLES IN THE HTGR[7]

T. B. Lindemer H. J. deNordwall[8]

Analysis of existing data for the so-called "amoeba effect" in HTGR particles containing urania has led to a model for coating failure. This model extends the

3. J. L. Scott, J. M. Leitnaker, and C. B. Pollock, *Metals and Ceramics Div. Annu. Progr. Rep. June 30, 1970,* ORNL-4570, pp. 61–62.
4. K. J. Notz and P. A. Haas, *Chem. Tech. Div. Annu. Progr. Rep. Mar. 31, 1972,* ORNL-4794, pp. 7–15.
5. T. B. Lindemer, "Rate Controlling Factors in the Carbothermic Synthesis of Advanced Fuels," *Nucl. Appl. Technol.* **9**, 711–15 (1970).
6. J. M. Leitnaker and T. G. Godfrey, "Thermodynamic Properties of Uranium Carbides via the U-C-O System," *J. Chem. Eng. Data* **11**, 392–94 (1966).
7. Revised abstract from *Amer. Ceram. Soc. Bull.* **57**, 390 (April 1972).
8. Reactor Chemistry Division.

analysis originally developed by Flowers and Horsley[9] and is based on the transport of carbon via CO and CO_2 in a temperature gradient. Application of the model to specific data permitted the calculation of the total pressure of CO and CO_2 in the particle; these calculated pressures agreed in the low pressure range with measurements made by other investigators. Moreover, these pressures are in the range of CO pressures over the SiC-SiO_2-C equilibrium, indicating that this system may be chemically buffering the pressure of CO in the particle. Eventual failure of the final pyrocarbon coating as a result of access of the fuel system to this coating may depend on localized oxidation of silicon carbide, radial cracks across the silicon carbide layer, or possible interaction of silicon carbide with fission products.

FUEL ELEMENT FABRICATION STUDIES FOR HTGR FUELS

R. L. Hamner J M Robbins
W. P. Eatherly

Our program for the development of fuel elements for high-temperature gas-cooled converter reactors consists principally of carbonization studies and the investigation of warm molding and extrusion as techniques to fabricate continuous-matrix-type elements.

Carbonization

The present concept for processing intrusion-bonded fuel sticks involves embedding the fuel sticks in graphite or alumina powder for support during carbonization, removing the sticks from the powders before subsequent heat treatment at 1800°C, and insertion into the fuel holes of the graphite fuel block. This operation is not only cumbersome but presents a serious problem in materials handling, particularly in a remote fabrication facility. To simplify this step in processing, we determined the feasibility of carbonizing and heat treating the fuel sticks in the fuel block. The intrusion-bonded specimens were prepared with two types of matrices: (1) 15V pitch containing 28.5 wt % NF 6353 graphite filler and (2) Varcum, a thermosetting prepolymerized furfuryl alcohol, containing 40 wt % GLC 1074 graphite filler. The specimens were carbonized in the bores of sections cut from a graphite fuel block. The modes of carbonization consisted of carbonizing the specimens in horizontal and vertical positions, restrained and unrestrained in the block, on fast and slow heating cycles, and in uncoated bores or bores coated with natural flake graphite powder.

The Varcum-bonded specimens showed no indication of sticking to the block. Pitch-bonded specimens showed a variable degree of sticking but no tendency to stick in the coated blocks. The specimens bonded end to end, as expected. They deformed very little during in-block carbonization; the maximum out-of-roundness was generally about 0.001 in. for a nominal 0.490-in.-diam fuel stick. No broken particles were observed by metallographic examination after carbonization and heat treatment.

These results indicate that in-block carbonization is feasible and should be investigated in full-scale fuel blocks.

Warm Molding

We continued studies on continuous-matrix-type fuel elements aimed at improved thermal conductivity.[10] The major variables involved were particle volume loading and matrix composition. Ashland grade 240 pitch, GLC 1074 graphite powder, Thermax, and 600-μm-diam pyrolytic-carbon-coated particles were used in the study.

With uniform particle volume loadings of 30%, a bonding matrix with 25 wt % pitch resulted in a higher matrix density than one with 30 wt % pitch (1.5 vs 1.46 g/cm^3), but the surfaces were not consistently as good. Pitch contents of 35 wt % or greater resulted in gross distortion of specimens during carbonization. Also, for the same particle volume loading, matrix densities decreased as Thermax content was increased from 15 to 35 wt %. Particle volume loadings in the range of 20 to 41% did not affect the matrix density, but at a volume loading of 45% the matrix density dropped significantly, 5%. Warm-molded specimens with matrix densities of 1.46 to 1.49 g/cm^3 and with particle volume loadings of 33 and 42% are now in the HFIR for irradiation testing.

Extrusion

The obvious technique for fabricating continuous-matrix-type fuel elements is extrusion, which is not only relatively simple but is amenable to fabricating long lengths at high production rates. After all components are blended, the mixture is extruded into graphite

9. R. H. Flowers and G. W. Horsley, *The Influence of Oxide Kernels on the Manufacture and Performance of Coated Particle Fuels,* AERE-R-5949 (1968).

10. J M Robbins, R. L. Hamner, and W. P. Eatherly, *Metals and Ceramics Div. Annu. Progr. Rep. June 30, 1971,* ORNL-4770, pp. 143–44.

PHOTO 0110-72

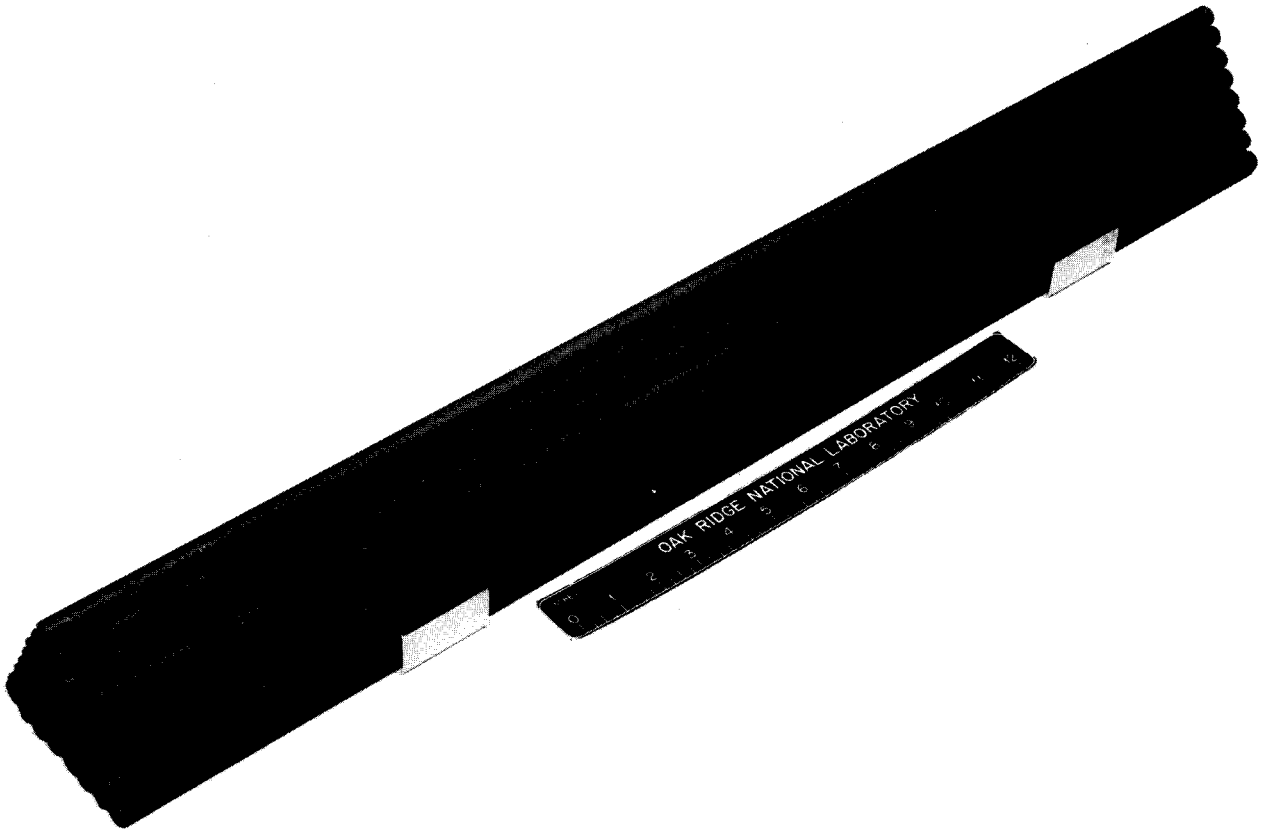

Fig. 25.1. Fuel rods with a matrix density of 1.75 g/cm^3 and a particle volume loading of 31% prepared by extrusion. The neat stacking of randomly selected rods demonstrates their straightness and uniformity.

trays and remains in them during subsequent processing. The matrix materials used in our development work were a graphitized needle coke powder containing 13 wt % Thermax as a filler and Varcum as a binder. Pyrolytic-carbon-coated ThC_2, ThO_2, or inert (carbon) particles were used as fuel. Extrusions were made on a semiproduction scale (≈600 ft) at a rate of 10 ft/min, and although the reduction ratio in the press was 45, no pressure registered on the pressure gage. A stack of 30-in.-long extrusions after carbonizing and heat treating at 1800°C is shown in Fig. 25.1. Diametral control was good – 0.491 ± 0.002 in., the matrix density was 1.75 g/cm^3, and the particle volume loading was 31%. Extrusions selected at random were fitted into the fuel holes of a reference graphite fuel block without difficulty. By radiographic examination the fuel distribution appeared to be good. Approximately one-third (80) of the extrusions were weighed, and the weights of 95% of these were within 2% of the mean value, indicating relatively uniform fuel content from rod to rod. Very little work has been done on analysis for broken particles; however, qualitative analyses of some extrusions containing high-quality coated particles indicated that, at a volume loading of 30% , coatings were not damaged during the extrusion process.

THERMAL CONDUCTIVITY OF BONDED HTGR FUEL MATERIALS

R. S. Graves W. M. Ewing
D. L. McElroy

Our previous measurements[11] suggested that an increased thermal conductivity, λ, would result if the electrical resistivity, ρ, of bonded fuel sticks could be reduced below a nominal value of 8000 $\mu\Omega$-cm at room temperature. Measurements of λ (±3%) and ρ (±0.4%) from 80 to 400°K were completed on two samples that contained inert particle volume loadings of 30.4 and 43.9% and had room-temperature ρ values of 4590 and

11. R. S. Graves and W. M. Ewing, *Metals and Ceramics Div. Annu. Progr. Rep. June 30, 1971*, ORNL-4770, p. 144.

Table 25.1. Thermal conductivity and electrical resistivity of two bonded fuel sticks

Temperature (°K)	Sample JH 105-1 (30.4%)		Sample JH 112-1 (43.9%)	
	ρ^a	λ^b	ρ^a	λ^b
100	5537	0.060	6919	0.047
200	4953	0.125	6303	0.098
300	4779	0.150	5838	0.123
400		0.160	5475	0.127

[a]Electrical resistivity in $\mu\Omega$-cm.
[b]Thermal conductivity in W cm^{-1} $(°K)^{-1}$.

5875 $\mu\Omega$-cm respectively. These slurry-blended, warm-molded specimens had a 1.44-g/cm^3 matrix fabricated from 30 wt % type 240 pitch, 55 wt % GLC 1074 graphite filler, and 15 wt % Thermax. The specimens were heat treated at 1800°C for 30 min in argon before we obtained the smoothed λ and ρ results listed in Table 25.1. These λ values are 3 to 4 times those observed[11] for specimens containing 65 vol % inert particles.

An in situ calibration of new Chromel-P vs constantan thermocouples was completed, using a miniature platinum resistance thermometer, to prepare the guarded longitudinal heat flow apparatus for λ and ρ measurements on extruded samples. An extruded specimen containing 28.5 vol % inert particles in a 1.74-g/cm^3 matrix had a room-temperature ρ value of 1915 $\mu\Omega$-cm, whereas an extruded specimen without particles had a ρ value of 1611 $\mu\Omega$-cm and a density of 1.8 g/cm^3.

HFIR IRRADIATION TESTING OF HTGR FUELS AND FUEL ELEMENTS

J. H. Coobs — J. A. Conlin[12]
R. B. Fitts — D. M. Hewette II
J. L. Scott — B. H. Montgomery[12]
J M Robbins — C. B. Pollock

Irradiation testing of fuels and fuel element materials involved two types of experimental facilities. Small, uninstrumented HT capsules that occupy a target position in HFIR, where the maximum fast-neutron fluence is 1.2×10^{15} neutrons cm^{-2} sec^{-1} (>0.48 MeV), permit rapid attainment of the design HTGR exposure. Two of these capsules were irradiated to complete a series planned for very high exposure. A second type consists of the relatively large instrumented and swept HRB capsules, which are located in the removable reflector region of HFIR, where the fast flux is about 35% of that in the target region. Irradiation and examination of one HRB capsule were completed and another, HRB-3, was built and commenced irradiation.

12. Reactor Division.

Irradiation Performance of HTGR Fuel Sticks Bonded with Reference and Advanced Matrix Materials

The second experiment in the HFIR reflector facilities, capsule HRB-2, contained fuel sticks prepared by intrusion bonding with the reference Fort St. Vrain matrix and with various other matrix filler materials. This instrumented and swept experiment was irradiated for 257 days (11 cycles) at 1100 to 1300°C to test the integrity and behavior of the coated particles and fuel sticks at high burnup (12% FIMA in fertile ThC_2 and ThO_2 particles and 24% FIMA in mixed carbide particles) and the design maximum HTGR fast-neutron fluence of about 8×10^{21} neutrons/cm^2 (>0.18 MeV). The fission-gas release rates were steady at acceptable levels ($R/B \approx 10^{-5}$). After irradiation the 14 short (0.7-in.-long) fuel sticks were intact, although six of them showed slight debonding at the edges. Both 2-in.-long fuel sticks broke into three segments but were otherwise in good condition. Polished sections confirmed the good performance of the matrix structure and of the TRISO- and BISO-coated particles. Only two failed particles were detected, and these were BISO-coated resin-derived fissile particles observed in a specimen that received maximum exposure. These failures were attributable to interactions with the shrinking matrix. The six fuel sticks that contained TRISO-coated particles shrank 1.0 to 1.6% in length, while specimens that contained BISO-coated particles shrank 3.0 to 4.5%, as expected. Thus HTGR fuel sticks bonded with reference and alternative matrix materials will survive the maximum design exposure.

Irradiation-Induced Dimensional Changes in Intrusion-Bonded Fuel Sticks

All available ORNL data on fuel stick dimensional changes during irradiation are summarized in Figs. 25.2 and 25.3. The dimensional changes are obtained from pre- and postirradiation diameter and length measurements. The bulk of the data was obtained on single fuel sticks of 0.5 to 2 in. in length and 0.2 to 0.5 in. in diameter tested in the HFIR. The data given at 1×10^{21} neutrons/cm^2 fast fluence are from RTE-7, a large-scale test in the Peach Bottom Reactor. Each average diametral change plotted for that test is derived from a sample composed of six or seven 2-in.-long × 0.5-in.-diam fuel sticks.

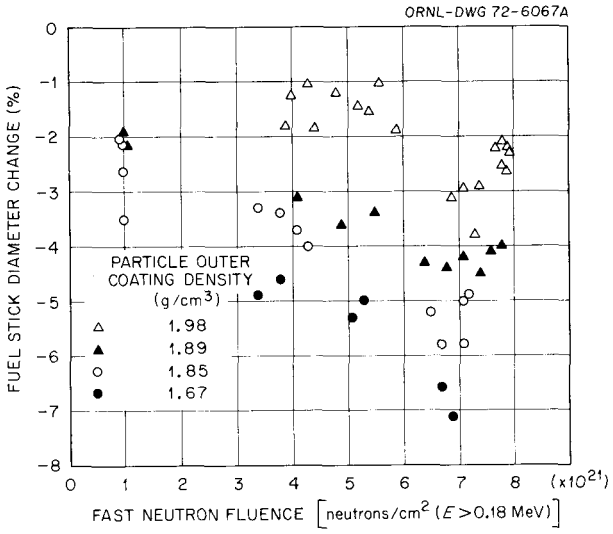

Fig. 25.2. Irradiation-induced dimensional changes in fuel sticks containing BISO-coated particles (HT-4, HT-6, RTE-7, HRB-2).

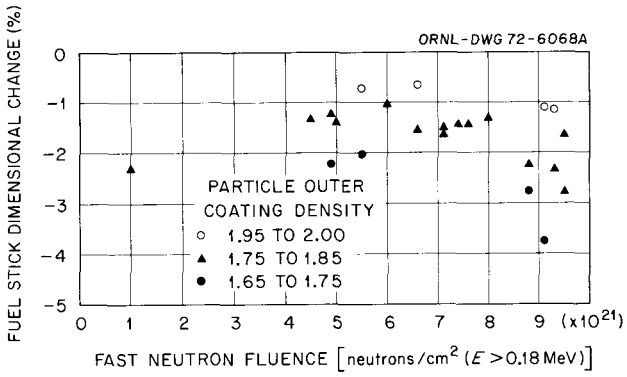

Fig. 25.3. Irradiation-induced dimensional changes in fuel sticks containing TRISO-coated particles (HT-8, RTE-7, HRB-2).

The dimensional changes in an intrusion-bonded fuel stick, where the particles are in a close-packed configuration (≈62% volume loading), are thought to be controlled by the dimensional changes of the particle coatings.[13] This appears to be consistent with our observations in that the sticks containing TRISO-coated particles, with their more stable SiC layers, exhibit less dimensional change than do the sticks containing BISO-coated particles. In addition, the dimensional changes in both types of sticks are related inversely to the density of the outer pyrolytic carbon coating. No effect of irradiation temperature, which ranged between 750 and 1350°C, has been apparent in these tests.

These summary plots point out a shortage of data on dimensional changes at low fast fluences. This situation prevents determination of the initial rate of diameter change for HFIR-irradiated fuel sticks and precludes analysis of dose rate, time, and temperature effects on dimensional changes.

Performance of Coated Particles in HFIR Experiments

Testing of loose and bonded coated particles showed that reference TRISO-coated ThC_2 and experimental BISO-coated ThO_2 fertile particles would perform well at design temperatures and fast-neutron exposures to burnup levels about 50% greater than design maximum. A series of samples with experimental TRISO designs on inert kernels that were irradiated to fast-neutron exposures ranging from one-third to twice the design values in accelerated HFIR target experiments demonstrated that survival of the isotropic outer coating layers of TRISO particles is relatively insensitive to the coating density, provided the density is 1.75 g/cm^3 or greater. Shrinkage of fuel sticks made with particles having low-density outer coatings would be a problem, however.

The first two samples of fueled weak-acid resin particles with monolayer carbon coatings performed well when irradiated to 10 at. % burnup at 1000°C in HFIR. Testing of several samples of fueled strong-acid resins was completed. BISO-coated fueled strong-acid resins performed well at full exposure and burnup of 30 at. % at 1300°C, and one sample performed without failure at lower exposure (4×10^{21} neutrons/cm^2) and approximately 60 at. % burnup at about 1100°C. Other samples with BISO and monolayer coatings performed well at lower exposures and temperatures. A phase separation or migration of materials that was observed in fueled strong-acid resins irradiated at high temperatures (>1300°C) and caused some attack on the coatings is being investigated.

GAS-COOLED FAST BREEDER REACTOR FUEL ELEMENT DEVELOPMENT

R. B. Fitts A. W. Longest[12]
R. A. Bradley E. J. Manthos

Most of the effort to develop a fast breeder reactor is being applied to the sodium-cooled LMFBR. There is,

13. J. L. Scott, D. M. Hewette II, J. H. Coobs, J. A. Conlin, and B. H. Montgomery, *Metals and Ceramics Div. Annu. Progr. Rep. June 30, 1971*, ORNL-4770, pp. 144–46.

however, much interest on the part of many utilities[14] in the development of the gas-cooled fast breeder reactor (GCFBR) as an alternate. It has the potential of lower cost power production and would avoid the sodium void coefficient problem and maintenance difficulties, which are peculiar to the liquid-metal-cooled systems.[15,16]

An irradiation testing program is being conducted in cooperation with Gulf General Atomic to evaluate the performance of various fuel pin designs for use at GCFBR operating conditions. These tests are being conducted in a thermal flux environment in the Oak Ridge Research Reactor and in a fast flux in the EBR-II. The first test of a vented GCFBR-type fuel pin (GB-9) completed irradiation in the ORR, and its postirradiation examination began. The second pin of this type (GB-10) was prepared for thermal flux testing. In addition, the first seven EBR-II test pins were irradiated to 30,000 MWd/ton burnup; one was removed and sent to Argonne National Laboratory for examination, and five new pins were fabricated and encapsulated in preparation for fast flux irradiation.

Thermal Reactor Experiments

The first irradiation test (GB-9) or a vented GCBFR fuel pin[17] containing an integral charcoal trap was completed. It operated for 471 full-power days at the design operating conditions of 15 kW/ft peak heat generation rate, 685°C peak cladding outer surface temperature, and 300°C charcoal trap temperature. A burnup of 53,500 MWd/ton was accumulated in the $(U,Pu)O_2$ fuel, and all of the original test objectives were accomplished. Additional exposure up to 75,000 MWd/ton had been scheduled, but the failure of a tube outside the capsule prevented further operation. The fuel pin received initial postirradiation examination at ORNL and was sent to Argonne National Laboratory (ANL) for detailed examination. This experiment showed that a vented fuel pin of the reference GCFBR design will operate very satisfactorily to 50,000 MWd/ton in a thermal flux environment. In addition, important new information was obtained on the release of fission gas[18,19] from a vented fast reactor fuel pin and on the distribution of volatile fission products[19,20] such as iodine and cesium within the fuel pin.

The test capsule and fuel pin for the second test of the vented concept (GB-10) are similar to GB-9. The fuel pins differ in that GB-10 contains solid rather than annular fuel pellets,[21] and both capsule and fuel pin have been modified to provide increased capability for sampling the fission gases in various regions of the fuel pin. The release of gases from the whole fuel pin and from the region below the charcoal trap can be monitored as in GB-9. In addition, the gases in the UO_2 blanket or in the $(U,Pu)O_2$ fuel region can be separately monitored in GB-10. The assembly of this capsule is complete, and irradiation is expected to begin in July 1972.

Fast Reactor Experiments

Eight fuel pins and capsules were fabricated last year[17] for irradiation in the EBR-II to test GCFBR-type fuel pins with integral charcoal traps under fast reactor operating conditions. The first seven were fabricated into an EBR-II subassembly and have been irradiated to a fuel burnup of 30,000 MWd/ton. One of these was discharged and sent to ANL for postirradiation examination and analysis. This pin was replaced with the eighth pin from the original set, and the subassembly was reinserted in the EBR-II for further irradiation. During the past year we have also fabricated five more fuel pins (see Chap. 15) and capsules for incorporation into this EBR-II subassembly as original pins are removed for examination.

---

14. J. R. Lindgren, P. W. Flynn, N. L. Baldwin, R. B. Fitts, and A. W. Longest, "Irradiation Testing and Development of Fast Breeder Reactor $(U,Pu)O_2$ Fuel Rods," pp. 736–37 in *Proceedings of the Conference on Fast Reactor Fuel Element Technology,* ed. by B. Farmakes, American Nuclear Society, Hinsdale, Ill., 1971.

15. *An Evaluation of Alternate Coolant Fast Breeder Reactors,* WASH-1090 (April 1969).

16. Peter Fortescue, "A Reactor Strategy: FBR's and HTGR's," *Nucl. News* **15**(4), 36–39 (April 1972).

17. R. B. Fitts, A. W. Longest, T. N. Washburn, and J. A. Conlin, *Metals and Ceramics Div. Annu. Progr. Rep. June 30, 1971,* ORNL-4770, pp. 146–48.

18. A. W. Longest, N. L. Baldwin, J. A. Conlin, R. B. Fitts, and J. R. Lindgren, "Fission Gas Release Measurements from Fast Breeder $(U,Pu)O_2$ Fuel," *Trans. Amer. Nucl. Soc.* **13**, 604 (1970).

19. A. W. Longest, R. B. Fitts, and J. A. Conlin, "Fission Gas Release Behavior in a Vented $(U,Pu)O_2$ GCFBR Fuel Pin," *Trans. Amer. Nucl. Soc.* **15**, 197 (1972).

20. Personal communication, L. A. Neimark, Argonne National Laboratory.

21. R. A. Bradley, "GB-10 Fuel Pin," *Fuels and Materials Development Program Quart. Progr. Rep. Mar. 31, 1972,* ORNL-TM-3797, p. 4. See also R. A. Bradley et al., "Development of Fabrication Processes," Chap. 15, this report.

26. Heavy Section Steel Technology

D. A. Canonico

The Heavy Section Steel Technology Program is an engineering effort to determine the structural behavior of the thick plates and pressure vessels needed for large light water nuclear reactors. The overall program emphasizes the effects of flaws, discontinuities, and inhomogeneities on the integrity of the reactor vessel during both shutdown and operation. Extensive testing programs are being conducted on weldments and plates. These include the determination of strength and classical fracture toughness properties as well as the development and application of fracture mechanics for those steels currently being used in the fabrication of light-water nuclear pressure vessels.

We participate as both consultants and experimentalists. First, we serve on the staff of the Program Office as metallurgical consultants and are expected to contribute to decisions that require metallurgical knowledge. In addition, we are involved experimentally in those tasks that require the facilities and expertise available within the Division.

CHARACTERIZATION OF HEAVY SECTION STEEL PLATES

W. J. Stelzman R. G. Berggren

Studies aimed at determining the variability of mechanical properties of state-of-the-art pressure vessel steels are continuing. Our studies have recently concentrated upon HSST plates 02 and 03, both of which are ASTM A533 grade B Class 1 steel.

Tensile results[1] from miniature 0.178-in.-diam specimens taken from various depths, orientations, and plate locations in HSST plates 02 and 03 indicate that yield stress within a plate shows some variability depending on location and depth; however, these variations within a plate are not abnormal. For instance, plate 03 exhibits a variation at the surface, whereas plate 02 exhibits a variation at the quarter-thickness depth. Plate 02 does show a general trend towards higher tensile strength values than either plate 01 or 03, which appear to exhibit similar tensile properties.

Tensile tests on HSST plates 01, 02, and 03 indicate somewhat lower elongations for plate 02. However, these lower values have been attributed to geometric differences between specimens rather than material differences. The strength and elongation data from all three plates show little sensitivity to specimen orientation parallel to the plate surface, but the reduction-in-area data indicate that the longitudinal orientation provides higher values than the transverse direction.

Charpy V-notch impact data were also obtained at the aforementioned plate locations. Plate 02 generally provided lower transition temperatures at the surface and quarter-thickness levels than plates 01 and 03 when compared at the 30 ft-lb correlation energy level. Comparison of the upper shelf energies is difficult because of the inherent scatter in these values. However, data from the longitudinal specimens indicate lower transition temperatures and higher shelf energies than from the transverse specimens from all three plates.

HYDROGEN TECHNIQUE FOR GENERATING SHARP CRACKS IN LOW-ALLOY HIGH-STRENGTH STEELS

D. A. Canonico J. D. Hudson

The newly developed hydrogen technique for generating sharp cracks in low-alloy high-strength steels was previously[2] described. During this past year we have employed the technique to provide cracks in scaled-down intermediate test vessels that are approximately 6 in. in diameter. We have also cracked tensile specimens that are being tested at Southwest Research Institute in conjunction with the large flawed tensile specimens that simulate the intermediate test vessel.

1. R. G. Berggren and W. J. Stelzman, "Characterization of Heavy Section Steel Plate," *HSST Program Semiannu. Progr. Rep. Feb. 28, 1972*, ORNL report in preparation.

2. D. A. Canonico and J. D. Hudson, *Metals and Ceramics Div. Annu. Progr. Rep. June 30, 1971*, ORNL-4770, pp. 150–51.

The most significant use of this technique was in providing a "pop-in" condition in a study to establish the K_{Ia} (a measure of arrest fracture toughness) of the ASTM A533 Grade B Class 1 steel used in nuclear pressure vessels. The technique employed consisted of producing the electron-beam weld in the fracture toughness specimen, setting the specimen in the test equipment, loading the specimen to the desired stress, and then charging it with hydrogen to produce the cracks. The technique was satisfactorily employed at the Materials Research Laboratory, Glenwood, Illinois, and arrest toughness as a function of temperature was determined.

STATIC AND DYNAMIC FRACTURE TOUGHNESS TESTS ON PRECRACKED CHARPY SPECIMENS

W. J. Stelzman

A study[3] to measure the potential of the Charpy-type specimen for determining both the static and dynamic fracture toughness parameters was started using HSST program A533 Grade B Class 1 carbon steel. The purpose is to compare the fracture toughness characteristics of a small, simple specimen with those of the large compact tension specimen customarily used.

The specimens used were the standard Charpy bar (0.394 × 0.394 × 2.165 in.) broached with the 45° V-notch and 0.010-in. root radius to two depths, 0.040 and 0.080 in. Fatigue cracking to a desired depth, usually midspecimen depth (0.197 in.), is then performed. An alternate method of precracking was used. Hydrogen is introduced electrolytically into the weld zone of an electron beam weld to generate cracks[2] (the hydrogen is then baked out at 400°F for 2 hr). The specimens for this method of precracking were either unnotched or notched to a depth of 0.040 in. and then precracked to a total depth of 0.080 in. After being notched and precracked, the specimens were tested in either slow bend (static) or impact (dynamic). The fracture toughness parameters, K_{Icd} and K_{Idd}, were determined by the equivalent energy method proposed by Witt[4] and the ASTM standard[5] E-399-70T.

The dependence of the fracture toughness parameter on the stress applied to the specimen at the onset of the fatigue cycle was investigated to determine the highest stress level that could be applied consistent with a reasonable cycle time without affecting the fracture toughness parameter. This portion of the study considered a temperature range from −50° to 150°F, a stress range from 20,000 to 50,000 psi (29 to 73% of σ_y), and a total precrack depth range from 0.150 in. (38%) to 0.270 in. (69%) in a specimen thickness of 0.394 in. Within the scatter of the data, the fracture toughness value from slow bend data, K_{Icd}, was not significantly affected by the temperature, the outer fiber stress, or the precrack depth ranges of the study.

From the partial results obtained over a temperature range of −50° to 200°F, the fracture toughness values from impact or dynamic testing, K_{Idd}, are not significantly affected by the precrack depth between 0.080 and 0.200 in., the 0.040 or 0.080 in. depth of notch when precracked to the 0.200 in. depth, or the method of precracking to the 0.080 in. depth. Also, the "notched only" specimens provide higher fracture toughness values, signifying that the fracture toughness transition for the "notched only" specimens occurs at a lower temperature than for the precracked specimens. These data agree quite well with data obtained by Shabbits[6] from large compact tension specimens.

The partial results from the slow bend or static testing over the −50 to 200°F temperature range show that the fracture toughness values, K_{Icd}, are not sensitive to the 0.040 or 0.080 in. depth of notch before precracking and that the "notched only" specimens also provide higher fracture toughness values than the precracked specimens. Also, there are indications that the slow bend test will provide fracture toughness transitions at lower temperatures than comparable dynamic test results. The electron beam weld precracking may provide lower fracture toughness values than the fatigue precracking when followed by slow bend testing. For the present, the K_{Icd} values appear to be somewhat higher than the values obtained by Shabbits[7] from larger compact tension specimens from HSST plate 02 material. However, fracture toughness values from

3. W. J. Stelzman, "Static and Dynamic Fracture Toughness Tests on Precracked Charpy Specimens," *HSST Program Semiannu. Progr. Rep. Feb. 28, 1972,* ORNL report in preparation.

4. F. J. Witt, "The Equivalent Energy Method for Calculating Elastic-Plastic Fracture," paper 12 presented at HSST Program Fifth Annual Information Meeting, Oak Ridge National Laboratory, March 25–26, 1971.

5. Part 31, "Metals – Physical, Mechanical Nondestructive, and Corrosion Tests, Metallography, Fatigue, Effect of Temperature;" *1970 Annual Book of ASTM Standards,* American Society for Testing and Materials, E 399-70T, pp. 917–27, July 1970.

6. W. O. Shabbits, *Dynamic Fracture Toughness Properties of Heavy Section A533 Grade B Class 1 Steel Plate,* WCAP-7623 (December 1970).

7. W. O. Shabbits, W. H. Pryle, and E. T. Wessel, *Heavy Section Fracture Toughness Properties of A533 Grade B Class 1 Steel Plate and Submerged Arc Weldment,* WCAP-7414 (December 1969).

Charpy thickness compact tension specimens tested by Mager[8] of Westinghouse from HSST plate 01 material agree quite well with the data obtained from the precracked Charpy specimens. This raises the additional question of whether there is a difference in fracture toughness between plates 01 and 02. Steps are being taken to resolve this question.

8. T. R. Mager, Westinghouse Electric Corporation, personal communication to F. J. Witt.

27. Military Reactor Fuel Element Procurement Assistance

R. J. Beaver

This task provides technical assistance to the AEC and military services in procurement of reactor components. Included are such items as standardization of specifications, review of technical requirements for procurement packages, and participation in fuel procurement as well as quality control audits of fuel fabricators.

The majority of 34 Type II Fuel Element Assemblies ordered by the U.S. Army's Power Branch through the AEC Division of Reactor Development and Technology, Washington, for the MH-1A power reactor on the U.S.S. Sturgis, Gatun Lake, Panama Canal Zone, have been manufactured by the Kerr-McGee Corporation. Sixteen of these assemblies were delivered to the reactor late in May and accepted at that site under surveillance of an ORNL representative. During the course of this procurement, careful attention was given to these activities, including resident inspection at Kerr-McGee, assessment of qualifications at subcontractors, and a detailed audit of Kerr-McGee. Approximately 400 documents associated with processing, inspection, and certification were reviewed and recommended to the AEC (Chicago Operations Office) for appropriate action.

28. Molten-Salt Reactor Program

J. R. Weir, Jr. H. E. McCoy, Jr.

The Molten-Salt Reactor Program has successfully operated and terminated an experimental reactor (Molten-Salt Reactor Experiment, MSRE) and is engaged in the development work needed before constructing a molten-salt breeder reactor (MSBR).

Hastelloy N from the MSRE had shallow intergranular cracks, and considerable attention has been given to the cause and cure for the cracking. The Hastelloy N used in the MSRE vessel was embrittled by exposure to thermal neutrons, and considerable progress has been made in developing an alloy with improved resistance to embrittlement by irradiation. Graphite, the moderator for an MSBR, continues to be studied from the standpoints of increasing the dimensional stability under neutron irradiation and developing sealing methods for reducing the permeability to ^{135}Xe, a nuclear poison. To make a thermal molten-salt reactor breed, most of the fission products and protactinium must be removed. Methods for accomplishing this have been developed by the Reactor Chemistry and Chemical Technology Divisions. These methods use bismuth and bismuth-lithium alloys, and only some of the refractory metals and graphite are likely to be compatible with these metals. Compatibility must be demonstrated, and methods must be developed for fabricating these materials.

INTERGRANULAR CRACKING OF STRUCTURAL MATERIALS EXPOSED TO FUEL SALT

H. E. McCoy, Jr.

Although the Hastelloy N removed from the MSRE appeared sound, shallow cracks a few mils deep were found in some of the samples.[1] This phenomenon is of considerable importance and is being studied further. Our work involves (1) further examination of the materials from the MSRE, (2) experiments to determine whether intergranular attack will occur under certain conditions, (3) studies of alloys containing or exposed to numerous fission products, (4) numerous experiments with tellurium to determine its effects on Hastelloy N, and (5) limited experiments with other alloys, such as type 304L stainless steel and Ni-200, to determine their susceptibility to cracking. Our objectives are to determine the cause of the cracking; the dependence of the rate on temperature, time, and fission product concentration; and a reasonable solution to the problem.

Examination of Hastelloy N from the MSRE

B. McNabb, Jr. H. E. McCoy, Jr.

Surveillance samples were removed periodically during operation of the MSRE,[2–5] and several components were removed at the end of operation. These components had been at 500 to 650°C for about 31,000 hr. They included the control rod thimble, sections of the primary heat exchanger, several parts from the pump bowl, and a freeze valve (105) that failed as operation was being discontinued.

Numerous tests and examinations have been made on these samples, and the following conclusions seem warranted.

1. All metal surfaces that were exposed to fuel salt show intergranular cracking when strained at 25°C.

1. B. McNabb, Jr., and H. E. McCoy, *Metals and Ceramics Div. Annu. Progr. Rep. June 30, 1971*, ORNL-4770, p. 157.

2. H. E. McCoy, *An Evaluation of the Molten-Salt Reactor Experiment Hastelloy N Surveillance Specimens – First Group*, ORNL-TM-1997 (November 1967).

3. H. E. McCoy, *An Evaluation of the Molten-Salt Reactor Experiment Hastelloy N Surveillance Specimens – Second Group*, ORNL-TM-2359 (February 1969).

4. H. E. McCoy, *An Evaluation of the Molten-Salt Reactor Experiment Hastelloy N Surveillance Specimens – Third Group*, ORNL-TM-2647 (January 1970).

5. H. E. McCoy, *An Evaluation of the Molten-Salt Reactor Experiment Hastelloy N Surveillance Specimens – Fourth Group*, ORNL-TM-3063 (March 1971).

2. Irradiation of the metal does not seem to be a factor, since the heat exchanger (very low neutron fluence) and the control rod thimble (very high neutron fluence) showed similar amounts of cracking.

3. The degree of cracking seems to vary around the circuit. The deepest cracks were formed in parts from the pump bowl and the shallowest in freeze valve 105. The cracks in the other parts were of intermediate severity, but about equivalent to each other.

4. The severity of cracking decreased sharply in going from a liquid to a gas space.

5. The surveillance series showed that the maximum depth of cracking was not a detectable function of time, but the number of cracks increased with time.

6. Most samples had microscopically visible grain boundary cracks when they were removed from the MSRE. The number visible was greatest in the heat exchanger tubing. Many of the samples had only occasional visible cracks.

7. Several metallographic observations show that very small strains can open the cracks. The cracks also seem to propagate quickly to a certain depth and then no further with further straining.

8. Fission products have penetrated a few mils into the metal. Some of these, such as Te, Sb, Sr, Cs, and Ce, were concentrated on the crack surfaces along with sulfur.

9. Several heats of material with modified compositions were included as surveillance samples and cracked as severely as the heats of standard composition.

Intergranular Corrosion of Hastelloy N

J. W. Koger

One possible cause of the integranular cracking is some as-yet-undetected form of corrosion.

We are using loop NCL-16 [Hastelloy N circulating $LiF\text{-}BeF_2\text{-}UF_4$ (65.5-34.0-0.5 mole %)] to study this possibility. Before its use in the cracking studies, loop NCL-16 had operated for 29,500 hr with a fuel salt circulating in the system. The maximum weight loss after this period was 2.9 mg/cm^2, and the largest weight gain was 1.7 mg/cm^2. Assuming uniform loss, the maximum corrosion rate was 0.05 mil/year. The chromium content of the salt had increased 500 ppm, and the iron had decreased about 100 ppm in 29,500 hr.

For our study of cracking, we initially added 500 ppm FeF_2 to the loop. Specimens were removed and weighed, and portions were examined metallographically 450 and 1100 hr after the first addition. Then an additional 500 ppm FeF_2 was added. Specimens were then analyzed 800 and 1800 hr after this second addition, with the total exposure to the highly oxidizing salt being 2900 hr. Metallographic examination after the initial FeF_2 additions disclosed grain boundary attack, which altered the polishing characteristics of the specimen, but no cracks were visible. Examination of the hottest specimen 800 hr after the second addition revealed more grain boundary attack but no cracks. The surface of the specimen was "lacy" because of severe corrosion by the salt and chromium removal from the alloy. This specimen was bent, inducing some cracking in the depleted area, but no cracks penetrated the matrix. Specimen examination after the total 2900 hr exposure disclosed that the weight losses were 6 times greater than in the previous 29,500 hr operation of the loop, and cracks were visible to a depth of 0.5 mil. The cracks are similar to those seen in the MSRE samples but much shallower.

Intergranular Cracking of Materials Exposed to Several Fission Products and Sulfur

H. E. McCoy, Jr. J. H. Shaffer[6] B. McNabb, Jr.

Techniques were developed for exposing small metal tensile specimens to vapors of S, Se, I_2, Te, and a mixture of As, Cd, and Sb. These elements have sufficient vapor pressure to transfer at 650°C, so that the tensile samples and a small amount of these elements can be sealed together in quartz and placed in a furnace for annealing. The amount of each element has been enough to result in a concentration of 100 ppm in the outer 5 mils of the sample (≈0.01 mg/cm^2). Hastelloy N specimens have been exposed to these environments for 2000 hr at 650°C, deformed at 25°C, and sectioned for metallographic examination. Only the tellurium caused detectable cracking.

Experiments were also run in which samples of Ni-200 and type 304L stainless steel were exposed to 0.01 mg/cm^2 each of iodine, tellurium, and combinations of the two for 1000 hr at 650°C. Hastelloy N was exposed to tellurium for 1000 hr in the same experiments. Only the Hastelloy N sample showed significant intergranular cracking. The samples of nickel and type 304L stainless steel did not crack after exposure to any of the environments.

A method was also developed for plating tellurium on Hastelloy N, and this procedure produced cracking. Several alloys were plated with 0.05 mg/cm^2 Te and annealed at 650°C for 1000 hr. All iron-base alloys (including pure iron and several stainless steels) except Incoloy 800 (Fe–32% Ni–20% Cr) completely resisted

6. Reactor Chemistry Division.

cracking under these conditions. The nickel-base alloys generally obeyed the trend that alloys containing 15% Cr or more resisted cracking. Copper and Monel resisted cracking under these conditions. About 20 heats of Hastelloy N with different alloying modifications were included. These varied in the severity of cracking, but the presence of 2% Nb was the only common addition to those alloys showing improved resistance.

Effect of Tellurium on the Mechanical Properties of Several Alloys

H. E. McCoy, Jr. B. McNabb, Jr.

Samples of Hastelloy N, type 304 stainless steel, and Ni-200 were exposed to tellurium vapor under stress at 650°C. The Hastelloy N had deep intergranular cracks after only 2.5% strain, but the number of cracks in the stainless steel and nickel was not noticeably above that obtained in an inert environment. The Hastelloy N and nickel samples formed nickel-tellurium compounds, and the only reaction product that could be detected on the stainless steel was an oxide.

Hastelloy N tube burst specimens were electroplated with tellurium and tested in salt at 650°C. Tellurium decreased the rupture life and increased the incidence of intergranular fracture.

Mechanical Properties of Hastelloy N Modified with Several Elements

H. E. McCoy, Jr.

Several elements are formed as fission products and may diffuse into the structural metal and alter its mechanical properties. Alloys have been made with nominal additions of 0.01% of several of these elements. Sulfur is of interest because it is a residual impurity in the salt and may have been introduced through oil that leaked into the pump bowl. The alloys have the composition of standard Hastelloy N, with additions of Se, Tc, Ru, Sn, Sb, Te, S, and As.

The test program for these alloys is to obtain tensile data at 25 and 650°C in the solution-annealed condition. The alloys will then be aged for various times at 650°C and some of the testing sequence repeated. Limited tests have been run to date, but several trends already seem obvious.

1. The yield stresses of the solution-annealed alloys varied at both 25 and 650°C. These variations were small and were likely related to differences in carbon content rather than the small alloy addition.

2. The fracture strains at 25°C were quite high for all alloys. The fracture strains in tensile tests at 650°C were generally above 25%. Alloys containing Se, Te, and S had fracture strains slightly below 25%.

3. Several of the alloys had lower stress-rupture properties than the undoped alloy, but reductions of a factor of 2 or less were likely due to the lower carbon concentrations of some alloys. However, alloys containing tellurium and sulfur had reductions in stress-rupture properties and fracture strain outside the range attributable to carbon content.

4. Aging for 1000 hr at 650°C slightly increased the yield stress at 25°C of most alloys but had no detectable influence on the fracture strain. The stress-rupture properties and fracture strains were generally improved by aging.

5. Tellurium and sulfur were more deleterious when chromium was not present in the alloy.

6. Metallographic examination showed that profuse integranular cracks are formed in alloys containing tellurium and sulfur when they are strained at elevated temperatures but not at 25°C.

Identification of Interaction Products of Tellurium with Structural Materials

R. E. Gehlbach

The purpose of our program is to identify which fission products are responsible for cracking, the form in which the elements are present, the rate-controlling factors, and ways of overcoming the problem. Several microanalytical tools are being utilized to identify the cause of cracking. Initial studies are involving primarily unirradiated materials exposed to elements that were present in the MSRE fuel salt as fission products, particularly tellurium.

Unirradiated specimens were exposed to tellurium by electroplating, vapor deposition, elevated-temperature creep testing in tellurium vapor, mass spectrometer–Knudsen effusion cell experiments, and preparation of doped alloys. Although we are concentrating primarily on Hastelloy N, specimens of Ni-200 and type 304L stainless steel are also being studied.

We observed very strong interactions between tellurium and Hastelloy N, which result in the formation of various telluride phases. Most of the work to date has involved identification of reaction products by x-ray diffraction techniques discussed in Chap. 4 of this report.

Creep tests in tellurium. Several specimens have been exposed to tellurium vapor during creep tests at 650°C. A sample of Hastelloy N that had been stressed at 30,000 psi at 650°C and failed after 556 hr with 4% strain had a large amount of fuzzy reaction product,

consisting of particles and needles, on the surface. Both morphologies of the reaction product are the $NiTe_{0.69}$ intermetallic compound. Metallographic examination of a polished cross section revealed an oxide-like reaction about 0.5 mil deep along the edge and extending into many intergranular cracks. The particles and needles adhered to this reaction layer. Electron probe microanalysis indicated that the particles were nearly pure nickel telluride, containing about 1% Fe as the only other detectable element. The oxide-like reaction layer contained approximately 15% Te, 27% Mo, 12% Cr, 5% Fe, and 2 to 3% Ni. We have not yet identified the phase(s) in this layer.

Samples of Ni-200 and type 304L stainless steel exposed to tellurium vapor while being stressed were slightly darkened but did not form large amounts of reaction products. X-ray diffraction analyses of the surfaces indicate that a small amount of Ni_3Te_2 is present on the Ni-200 but only $(Fe,Cr)_3O_4$ is detectable on the stainless steel. The thin surface layer on the Ni-200, electrolytically stripped and examined in the electron microscope, is made up of large particles of the telluride on a thin film covered with numerous small thin platelets.

A subsequent set of specimens similarly exposed revealed a thick layer of powdery reaction products on Hastelloy N samples stressed at 650°C and 593°C and Ni-200 stressed at 650°C. Both Hastelloy N specimens formed $NiTe_{0.69}$ plus an additional phase, whereas the Ni-200 reaction product is Ni_3Te_2 with an additional phase(s). The stainless steel was slightly darkened and speckled but had no other visible reaction product. This set of specimens has been reloaded for additional exposure with replenishment of tellurium.

Knudsen effusion cell experiments. We are working with J. D. Redman, Reactor Chemistry Division, who is exposing Hastelloy N foils to tellurium vapor in a Hastelloy N Knudsen effusion cell coupled to a time-of-flight mass spectrometer. Specimens were electropolished and degassed before tellurium vaporization. The first specimen, reacted at 412°C, produced $NiTe_2$ as the major telluride. Other phases are present but have not been identified. Neither Ni_3Te_2 nor $NiTe_{0.69}$ is detectable. A second specimen was reacted at 412°C and then heated to 650°C. Tellurium vapor was emitted during the 650°C exposure. The resulting reaction products are $NiTe_{0.69}$ and other phase(s) as yet unidentified. A third foil with initial reaction at 412°C and further exposure at 750°C is currently at 750°C, with large quantities of tellurium vapor being emitted. At least one additional experiment is planned, using a preoxidized Hastelloy N foil for the reaction.

The exposed foils contained a sheet of reaction product that could be removed with tweezers. The 650°C foil also had a powdery layer on the outer surface of the reaction layer. The foils are quite brittle and are being prepared for metallographic examination, electron probe microanalysis, scanning electron microscopy, and Auger spectroscopy.

Intergranular Cracking Studies

H. E. McCoy, Jr.

All Hastelloy N surfaces exposed to fuel salt exhibited intergranular cracking, particularly after deformation at 25°C. We have not been able to produce these cracks under various corrosion conditions and have developed considerable evidence that they result from the diffusion of tellurium along the grain boundaries. The laboratory experiments show that cracking can be produced by tellurium. Several materials show better resistance to cracking by tellurium than Hastelloy N and offer encouragement that a resistant alloy can be found. In-reactor experiments will be required to confirm that the alloy is indeed resistant.

FURTHER STUDIES OF HASTELLOY N

H. E. McCoy, Jr.

The material used in the MSRE was embrittled by exposure to thermal neutrons. We have found that small additions of Ti, Zr, Hf, and Nb reduce the embrittlement. However, practical considerations involving effects on fabricability and ease of commercial scale-up have led us to concentrate on an alloy with about 2% Ti.

A MSBR will use different fuel and coolant salts than the MSRE. The changes in composition of the fuel salt involve adding thorium and deleting zirconium, and we expect minor chemical effects so that only proof tests need be conducted. The coolant salt will likely be sodium fluoroborate, and its characteristics are much different than those of the $LiF\text{-}BeF_2$-base salts. Considerable corrosion work is in progress to study the compatibility of the coolant salt with Hastelloy N. A power reactor will also have a steam generator instead of an air radiator such as was used with the MSRE. This requires that the material be compatible with steam, and studies are in progress to determine whether Hastelloy N will be suitable.

Development of a Titanium-Modified Hastelloy N

H. E. McCoy, Jr. B. McNabb, Jr.

Our initial work to improve the resistance of Hastelloy N to embrittlement by neutron irradiation[7,8] involved alloys with titanium additions up to 0.5%. These alloys had good postirradiation properties when irradiated at 650°C, but the properties deteriorated rapidly as the irradiation temperature was increased.[9] The good properties were associated with the formation of fine MC-type carbide and the poor properties with the formation of coarse M_2C-type carbide. Studies[10] of a series of laboratory melts containing up to 3% Ti showed that the titanium concentration for optimum properties was about 2%. Above this level the brittle intermetallic Ni_3Ti formed and the ductility decreased.[11]

Studies of small commercial melts confirmed our work with small laboratory melts. Unirradiated alloys containing from 0.45 to 2.1% Ti increase in strength with increasing titanium content. The allowable stress for a given creep rate increases almost 50% over this range.

These same alloys have been irradiated from 650 to 760°C to thermal fluences of about 3×10^{21} neutrons/cm^2. The property of major concern is the fracture strain. Samples of all four alloys that were irradiated at 650°C had fracture strains in excess of 4%. As the irradiation temperature was increased, the strain decreased to less than 0.5% for the alloy with 0.45% Ti. The alloys with about 1% Ti had fracture strains as low as 1% after irradiation at 760°C. The alloy with 2.1% Ti had fracture strains above 3% after irradiation at 760°C.

Alloys with 2% Ti have excellent weldability and corrosion resistance to the fuel and coolant salts. We see no reason why this alloy cannot be produced commercially in the quantities required for a MSBR.

Electron Microscope Studies

R. E. Gehlbach S. W. Cook

Our microstructural studies to characterize precipitation in Hastelloy N alloys have primarily involved observations made on Ni_3Ti and strain-induced precipitation in several laboratory and small commercial heats.

As previously reported,[12] the lenticular Ni_3Ti precipitates in small laboratory heats of Hastelloy N when the titanium concentration is approximately 2% and above. We have observed this precipitation in a 1% Ti heat. Although Ni_3Ti precipitation is very profuse and homogeneous in the 2.9% Ti alloy, it nucleates at MC carbides present in the stacking fault morphology for lower titanium concentrations. (This carbide morphology is obtained during aging after annealing at 1260°C, rather than the usual 1177°C, and forms around primary MC particles that are partially dissolved during the anneal.)

A different morphology of intermetallic precipitation was observed in the heat with 2.9% Ti. The specimen was aged 10,000 hr at 700°C following a 1 hr anneal at 1260°C. Rather extensive sheets occurred in the vicinity of primary carbide particles and appeared to extend in the same direction (although not necessarily on (111) planes) as the MC carbide that precipitated in the stacking fault morphology. We have not positively identified these intermetallic phases but have indications that the fine lenticular phase is the metastable γ'-Ni_3Ti and the second type is the stable η-Ni_3Ti phase.

Examination of a commercial heat of 2.1% Ti-modified Hastelloy N revealed precipitation of a noncarbide phase in a sheetlike morphology. This precipitate appeared to nucleate at grain boundaries in the gage section of creep samples that were stressed at elevated temperatures. It was not present in unstressed material. Electron diffraction patterns indicated that it may be η-Ni_3Ti; its morphology is similar to that observed in both the laboratory heat containing 2.9% Ti and the stressed titanium-niobium commercial alloys discussed previously. Other studies[13] indicate that nucleation of eta phase is enhanced by deformation.

---

7. H. E. McCoy, R. L. Beatty, W. H. Cook, R. E. Gehlbach, C. R. Kennedy, J. W. Koger, A. P. Litman, C. E. Sessions, and J. R. Weir, "New Developments in Materials for Molten-Salt Reactors," *Nucl. Appl. Technol.* 8, 156–69 (1970).

8. H. E. McCoy and J. R. Weir, "Development of a Titanium-Modified Hastelloy N with Improved Resistance to Radiation Damage," pp. 290–311 in *Irradiation Effects in Structural Alloys for Thermal and Fast Reactors*, Amer. Soc. Test. Mater. Spec. Tech. Publ. 457, American Society for Testing and Materials, Philadelphia, 1969.

9. M. W. Rosenthal et al., "Recent Progress in Molten-Salt Reactor Development," *At. Energy Rev.* 9(3), 601–50 (August 1971).

10. H. E. McCoy and C. E. Sessions, *MSR Program Semiannu. Progr. Rep. Feb. 28, 1971*, ORNL-4676, p. 192.

11. R. E. Gehlbach and S. W. Cook, *MSR Program Semiannu. Progr. Rep. Aug. 31, 1971*, ORNL-4728, p. 129.

12. R. E. Gehlbach and S. W. Cook, *MSR Program Semiannu. Progr. Rep. Feb. 29, 1972*, ORNL-4782, chap. 11, in press.

13. J. M. Oblak et al., "Heterogeneous Precipitation of Metastable γ' Ni_3Ti in a Nickel-Base Alloy," *Acta Met.* **19**, 355–63 (1971).

We have examined material from several new titanium- and hafnium-modified commercial alloys. The titanium-modified heats were prepared by both electroslag remelting and vacuum arc remelting and contained 1.5 to 2.0% Ti. Primary MC carbide (a = 4.30 Å) was present in the alloys after solution annealing at 1180°C. Grain boundary carbide precipitation after aging 200 hr at 704°C was quite similar to that which occurred in the Alvac series of alloys,[14,15] with carbides in irregular grain boundaries and extending 0.5 to 1.0 μm into the matrix. Fine MC carbide precipitated around the primary particles in the matrix. Although most of the primary precipitate particles were MC carbide, some appeared to be Ni_3Ti. This compound did not precipitate in the specimens aged 200 hr. We will be examining material aged for longer times in the range 650 to 760°C.

The hafnium-modified heats contained large quantities of primary carbide. We expect this carbide to be extremely rich in hafnium because of its high lattice parameter (4.62 Å, compared with 4.64 Å for HfC).

Fluoride Salt Corrosion

J. W. Koger

The success of a molten salt reactor system depends strongly on the compatibility of the piping materials with the molten salts used in the primary and secondary circuits of the reactor. We undertook to determine what salt-alloy systems are compatible and to determine quantitatively the amount of corrosion that will occur. We also investigated the effects of such variables as alloy constituents, temperature, salt impurities, salt velocity, and exposure times. Nickel-base alloys, more specifically Hastelloy N and its modifications, are considered the most promising for use in molten salts and are being evaluated in most of the experiments. Stainless steels are also being studied. The experiments are operated under design parameters based on the Molten Salt Breeder Reactor, and most tests are conducted in nonisothermal dynamic systems such as thermal convection and pumped loops. The salts of interest either are $LiF\text{-}BeF_2$ based with UF_4 (fuel), ThF_4 (blanket), or ThF_4 and UF_4 (fertile-fissile) or an $NaBF_4\text{-}NaF$ mixture (coolant salt). The following significant observations were made this year.

Fuel, blanket, and fertile-fissile salts. 1. A thermal-convection loop of Hastelloy N with standard and niobium-modified Hastelloy N insert specimens, which circulated a simulated MSRE fuel salt with 1 mole % ThF_4, was terminated after 9.2 years of operation when a failure occurred in the piping underneath a ceramic bushing. Attack in the hot section (700°C) was manifested by formation of subsurface voids having a maximum depth of 4 mils. Deposits less than 1 mil thick were noted in the cold regions.[16–18]

2. A type 304L stainless steel thermal-convection loop with the same salt has operated for 8.8 years at a maximum temperature of 688°C. On the basis of weight changes and the assumption of uniform material removal, the corrosion rate of the removable specimen at the highest temperature was 1.1 mils/year.[16,17]

3. A Hastelloy N thermal-convection loop equipped with electrochemical probes to measure the U^{3+}/U^{4+} ratio (oxidation potential of the salt) operated with the MSRE fuel salt for 7000 hr at a maximum temperature of 650°C. We are correlating specimen weight change data and salt analyses with the electrochemical measurements. The maximum corrosion rate is 0.02 mil/year, assuming uniform material removal.[16,17]

4. The corrosion rate of removable specimens in Hastelloy N thermal-convection loops containing blanket and fertile-fissile salts operating at a maximum temperature of 700°C was 0.04 mil/year, assuming uniform corrosion. Modified Hastelloy N alloys which contain 0.2 to 2.5% Ti and no iron have generally shown better corrosion resistance than the unmodified Hastelloy N. The corrosion reactions in the fertile-fissile systems involve primarily the oxidation of chromium by both FeF_2 and UF_4. The overall corrosion process is controlled by solid-state diffusion of chromium in the alloy. No differences in mass transfer were seen in a Hastelloy N system in which the salt contacted liquid bismuth and in a system that contained no bismuth.[16,17]

5. A mathematical description was developed to explain selective removal of certain alloy constituents in molten salt systems. The treatment was for cases in which both diffusion through the liquid film and

14. R. E. Gehlbach and S. W. Cook, *MSR Program Semiannu. Progr. Rep. Aug. 31, 1970,* ORNL-4622, pp. 164–65.

15. R. E. Gehlbach and S. W. Cook, *MSR Program Semiannu. Progr. Rep. Feb. 28, 1970,* ORNL-4548, pp. 131–38.

16. J. W. Koger, *MSR Program Semiannu. Progr. Rep. Aug. 31, 1971,* ORNL-4728, pp. 138–53 and 177.

17. J. W. Koger, *MSR Program Semiannu. Progr. Rep. Feb. 29, 1972,* ORNL-4782, in press.

18. J. W. Koger, "Hastelloy N Alloys after Nine Years Exposure to a Molten Fluoride Salt," oral presentation given at American Nuclear Society 1972 Annual Meeting, Las Vegas, Nev. Summary published in *Trans. Amer. Nucl. Soc.* **15**, 227 (1972).

solid-state diffusion in the alloy, as influenced by coolant characteristics and composition, dominated the corrosion mechanism. Effects in both the hot and cold zone were included, and equations were derived for both transient and steady-state cases. Applicability of the derived equations was demonstrated by comparison of predicted values with experimental results in molten salt systems.[19,20]

Coolant salt. 1. Corrosion of Hastelloy N in the $NaBF_4$–8 mole % NaF coolant salt depends largely on the amount of hydrogen-containing impurities in the salt. The inadvertent leakage of moist air into a Hastelloy N thermal-convection loop containing the sodium fluoroborate abruptly increased the corrosion rate. The rate returned to relatively low values once the leaks were corrected. At the maximum temperature position (605°C), the corrosion rate over 30,000 hr (including the time of air inleakage) averaged[16,17] 0.7 mil/year. By comparison, a Hastelloy N loop with purer fluoroborate salt (<500 ppm oxide) experienced[16,17] a weight loss equivalent to 0.19 mil/year over a 12,000-hr period at a maximum temperature of 687°C.

2. Steam was injected into a Hastelloy N thermal-convection loop system containing sodium fluoroborate. This resulted in a 0.5-mil attack during the first 200 hr at 607°C. However, the overall corrosion rate was just over 1 mil/year in 23,000 hr. Over 2 mils of deposited material was found on specimens in the cold leg, but the loop has continued to operate without a significant change in flow rate.[16,17]

3. A Hastelloy N pumped loop containing $NaBF_4$–8 mole % NaF completed 4000 hr operation at a maximum salt temperature of 620°C. The average weight loss at 620°C for 4000 hr was 10.8 mg/cm^2 (equivalent to over 2.0 mils/year uniform loss). The corrosion rate for this loop was higher than that in a thermal-convection loop with salt of a similar impurity content at comparable temperatures. This suggests that the impurity-controlled corrosion reactions are controlled by rate of solution and depend on velocity.[16,17]

4. A second Hastelloy N pumped loop, from which the corrosion specimens can be removed without dumping the salt or cutting open the loop, has operated for over 5000 hr at a maximum temperature of 620°C. Measurable temperature-gradient mass transfer occurred. Higher weight losses and gains occurred initially for the specimens exposed to higher velocity salt. A definite "downstream effect" was obvious early in the life of the loop. The first specimen of three exposed to the salt (same temperature, same velocity for each specimen) showed the largest gain or loss. The corrosion rate of all specimens has decreased during testing. After 5000 hr exposure, the corrosion rates of the hottest specimens (two different velocities) are now about the same, indicating that the controlling mechanism of corrosion has changed from a solution rate control to a velocity-independent solid-state chromium diffusion control. A compound containing hydrogen, $NaBF_3OH$ (which is important for trapping tritium), has remained in the salt during the 5000-hr operation.[16,17]

5. Haynes alloy No. 25, inadvertently placed in a Hastelloy N thermal-convection loop that circulated $NaBr_4$–8 mole % NaF, suffered damage by selective leaching of cobalt and chromium. The mechanism of attack was activity-gradient and temperature-gradient mass transfer. Haynes alloy No. 25 was more susceptible than Hastelloy N to attack by the fluoroborate mixture.[21]

6. We tested the corrosion properties of eight braze alloy–Hastelloy N combinations in $NaBF_4$–8 mole % NaF at 607°C for 4776 hr. The brazes included Au-Ni, Ag-Cu, Cu, and several types of Ni-Cr-Fe alloys. On the basis of weight changes, metallographic observations, and microprobe analysis, the Cu and Ag-Cu brazes appeared to be most corrosion resistant under the conditions of our test.[16,17]

Corrosion of Hastelloy N in Steam

B. McNabb, Jr. H. E. McCoy, Jr.

Unstressed specimens of standard Hastelloy N have been exposed to steam for 11,000 hr at 538°C in TVA's Bull Run Steam Plant. The metal loss rate continues to be less than 0.25 mil/year. Several modified alloys have also been exposed to steam under similar conditions, and their metal loss rates were slightly higher. Some of the specimens have been removed and examined metallographically. The corrosion on the standard air-melted alloy occurred as blisters that penetrated about 0.4 mil.

19. R. B. Evans III, J. W. Koger, and J. H. DeVan, *Corrosion in Polythermal Loop Systems II. A Solid-State Diffusion Mechanism with and without Liquid Film Effects,* ORNL-4575 (vol. 2) (June 1971).

20. J. W. Koger, R. B. Evans III, and J. H. DeVan, "Corrosion in Polythermal Liquid Metal and Fused Salt Loop System," oral presentation given at American Nuclear Society 1971 Winter Meeting, Miami Beach, Fla. Summary published in *Trans. Amer. Nucl. Soc.* **14**, 627 (1971).

21. J. W. Koger and A. P. Litman, *Mass Transfer between Hastelloy N and Haynes Alloy No. 25 in a Molten Sodium Fluoroborate Mixture,* ORNL-TM-3488 (October 1971).

The blisters were most frequent in the vacuum-melted alloy and extended 0.8 mil. One modified alloy with no titanium had intergranular penetrations about 10 mils deep. An alloy with 2.1% Ti had a thin uniform oxide.

Several stressed samples are also being exposed to steam in this facility. Three have failed thus far, but the data scatter makes it impossible to conclude whether the rupture lives are the same in argon and steam.

GRAPHITE STUDIES

W. P. Eatherly

The immediate objectives of the graphite program are the development of improved radiation-resistant experimental graphites and the development of techniques to seal the graphite against gaseous high-cross-section fission products, notably ^{135}Xe. The emphasis has been shifted from the bulk graphite to the sealing problem, but some work on graphite fabrication is continuing.

Reduction of Helium Permeability of Graphite by Pyrolytic Carbon Sealing

C. B. Pollock

The breeding performance of a molten-salt reactor is significantly affected by the extent to which ^{135}Xe can be stripped from the fuel salt and prevented from entering the graphite moderator. Effective sealing of graphite surfaces is therefore highly desirable. Pyrolytic carbon is the desired sealing material because of its low neutron cross section and its compatibility with the fuel salts. We have developed two techniques for sealing with pyrolytic carbon. The first plugs surface pores with pyrolytic carbon using a vacuum-pulse impregnation process. The second deposits a continuous layer of pyrolytic carbon on the surface of the graphite.

Currently, graphite samples are being satisfactorily sealed by coating with dense layers of isotropic carbon derived from propene (C_3H_6). The coatings are being deposited on fixed samples in the range 1100 to 1300°C in a carbon resistance furnace.

Typical coating thicknesses of 2 to 6 mils are achieved in 3 to 15 min with a hydrocarbon supply rate of 2 to 4 liters/min. A diluent gas (helium) is used during the coating process, and all samples are stress relieved after coating. Helium leak rates are less than 10^{-8} cm^2/sec at STP for all samples.

Scanning electron and light microscopy show that coatings are very uniform and free of defects. The coatings have densities near 2.0 g/cm^3 and appear to be nearly isotropic. The bond between the coating and the graphite is good, and some surface impregnation has occurred.

Characterization of Pyrolytic Carbon Sealants for Graphite

W. H. Cook

Advances made in the scanning electron microscope (SEM) designs and examination techniques have recently made the SEM a powerful tool complementary with reflected light microscopy in the examination of graphite specimens. We are utilizing these on unirradiated and fast-neutron-irradiated graphite specimens. This involves the examinations of original machined surfaces, fractured surfaces, and ceramographically polished surfaces. The major effort has been to make detailed microstructural examinations of pyrolytic carbon sealants that are being evaluated as a means for decreasing the gas permeabilities of polycrystalline grades of graphite to $<10^{-8}$ cm^2/sec for helium at STP.[22] Past work involved primarily 1,3-butadiene, C_4H_6, as a pyrolytic carbon source, and recent work uses propene, C_3H_6. These are used to seal 0.128-in.-ID × 0.400-in.-OD × 0.500-in.-long specimens of grade AXF graphite.[23] The irradiated samples examined to date have accumulated fluences to 2.0×10^{22} neutrons/cm^2 (>50 keV) at 715°C.

Some of the major observations associated with the pyrolytic carbon sealant derived from C_4H_6 for unirradiated and irradiated specimens are given below, together with the resulting changes in experimental procedure.

1. A serious lack of control of uniformity in the pyrolytic carbon sealants obtained in old furnaces was eliminated in new furnaces designed specifically for sealing the hollow cylindrical specimens.
2. In some of the old furnaces and techniques, some of the coatings developed V-shaped cracks during deposition.
3. Existing or newly formed surface cracks in the coatings enlarged during irradiation and developed square cross sections.
4. Sharp edges on the hollow cylinders of grade AXF graphite caused flaws in the pyrolytic carbon sealing. These flaws acted as crack and spalling propagation centers during irradiation. Rounded corners appear to have eliminated this during the deposition; however, we lack irradiation evaluation at this time of the design change. These and other examinations have correlated well with the measured helium permeability on the unirradiated and irradiated specimens.

---

22. W. H. Cook, *MSR Program Semiannu. Progr. Rep. Feb. 29, 1972,* ORNL-4782, in press.

23. This is the standard shape of graphite used for the MSRP graphite irradiations in the High Flux Isotope Reactor.

The pyrolytic carbon sealants as deposited and as irradiated can be nondestructively examined. The current SEM equipment and capability of resolution were not available to us previously. The quality of the current technology has enabled us to monitor selected specimens from the as-coated state through successive accumulations of fluence. This should provide more accurate information about the pyrolytic carbon coatings and the neutron damage effects.

Helium Permeability Measurements on Various Grades of Graphite

W. H. Cook J. L. Griffith

Gas permeability is a critical parameter for the Molten Salt Breeder Reactor (MSBR) graphite moderator and in some special applications to fuel processing equipment designs that use graphite or amorphous carbon. Therefore, we measure the helium permeability coefficient, viscous permeability, and slip coefficient for the grades that are under more detailed evaluation. These values enable us to calculate the permeability of a grade for any ideal gas. Currently, the helium permeabilities are determined at room temperature.

The nominal helium permeabilities for 19 grades of graphite have been reported[24,25] since the last annual report. Their values ranged from 2×10^{-4} to 1.54 cm^2/sec at STP. However, all but three grades had values less than 0.2 cm^2/sec. Based on their highest values and in order of increasing permeabilities the grades were Graph-i-tite "A", Graph-i-tite "G", AXF-5QBC, ATJS, HS-82, 1226, AXM-5Q, 9948, P-03, H-395, HL-18, 2044, 2020, ATJS-G, AXZ-5Q, A-681, A-680, and SA-45. None of these were optimized for MSBR applications, so it is not surprising that their permeabilities are relatively high.

Procurement of New Grades of Graphite

W. H. Cook W. P. Eatherly

We have continued our procurement of new grades of graphite directed toward the objectives of (1) identifying grades that have superior resistance to fast neutron damage and (2) attaining a better understanding of the details of the mechanisms of neutron damage.

The nature of our objectives plus the results[26] from the irradiation of more than 40 different common and special grades of graphite to fluence levels of 4×10^{22} neutrons/cm^2 (>50 keV) has allowed us to be more selective in our current procurement program. Basically, we are concentrating on special and experimental grades of graphite. Some are being supplied from our own experimental fabrication facilities. Others are acquired from commercial vendors.

Carbon materials received from Poco Graphite Inc.[27] will provide us with specimens for precursors of grade AXF fired at 1400, 1800, 2000, 2200, 2500, and 3000°C. We plan to use these to expand an irradiation study that began on a carbon-black-base series.[28] In that series, neutron irradiation caused initially sharp contractions that depended on the final heat treatment temperature and then a linear expansion with fluence that was independent of the final heat treatment temperature.[29] The objective is to determine if similar effects occur in the low-fired precursors of grade AXF.

Also, we have acquired other special grades that are primarily isotropic. These are based on materials using carbon black, air-blown (Robinson) coke, and proprietary fillers. Their grade designations and bulk densities have been reported.[30] More recent acquisitions are isotropic grades A800,[31] H395,[32] and H395X,[32] with bulk densities ranging from 1.64 to 1.85 g/cm^3.

X-Ray Studies

O. B. Cavin

We have continued using the sphere technique[33] for determining the crystalline anisotropy of experimental graphites of interest to the Molten Salt Reactor Program. Graphites supplied by vendors as well as those

24. W. H. Cook and J. L. Griffith, *MSR Program Semiannu. Progr. Rep. Aug. 31, 1971,* ORNL-4728, pp. 118–19.
25. W. H. Cook and J. L. Griffith, *MSR Program Semiannu. Progr. Rep. Feb. 29, 1972,* ORNL-4782, in press.
26. C. R. Kennedy and W. P. Eatherly, *MSR Program Semiannu. Progr. Rep. Aug. 31, 1971,* ORNL-4728, pp. 112–14.
27. W. H. Cook and W. P. Eatherly, *MSR Program Semiannu. Progr. Rep. Feb. 29, 1972,* ORNL-4782, in press.
28. O. B. Cavin and W. P. Eatherly, *MSR Program Semiannu. Progr. Rep. Feb. 28, 1971,* ORNL-4676, pp. 171–73.
29. C. R. Kennedy and W. P. Eatherly, *MSR Program Semiannu. Progr. Rep. Aug. 31, 1971,* ORNL-4728, pp. 113–14.
30. W. H. Cook and W. P. Eatherly, ibid., pp. 114–16.
31. Manufactured by Stackpole Carbon Company, St. Marys, Pa.
32. Manufactured by Great Lakes Carbon Corporation, New York.
33. O. B. Cavin, *MSR Program Semiannu. Progr. Rep. Feb. 28, 1969,* ORNL-4369, pp. 219–21.

fabricated at ORNL and Y-12[34] are under consideration. The Bacon anisotropy factors of a number of these materials[35] ranged from 1.006 to 1.289. We also demonstrated that the dimensional anisotropy can be determined independently by using spherical samples whose stem axes are mutually perpendicular. The values obtained by this technique from samples with perpendicular orientations agreed within experimental error with theoretical expectations. Three mesophase graphites were slightly anisotropic. This was not anticipated because of the apparently random texture in the filler particles.

The graphite used in the core of an MSBR must have a helium permeability below 10^{-8} cm^2/sec to exclude the fission gases (^{135}Xe) from the porosity.[36] To accomplish this, the Carbon Development Group has been surface sealing irradiation samples with a layer of pyrolytic carbon. For maximum irradiation stability, isotropy of this surface coating is necessary. The Gas-Cooled Reactor Program uses an optical technique first reported by Gruebmeier and Scheidler[37] for determining the anisotropy of thin surface coatings. This technique is being adapted to study the pyrolytic carbon coatings on graphite of interest to the Molten Salt program. The x-ray-determined anisotropy parameters and those obtained optically will be correlated. This will extend the range of our capabilities from bulk anisotropy values obtained by x-ray techniques to values from thin films obtained by optical methods. We are also determining the lattice parameters and crystallite sizes of the coatings placed on irradiation samples.

These studies, applied not only to the substrate graphite but also to the surface coatings, will help in the understanding of the irradiation behavior and help to guide the development of better pyrolytic carbon surface sealants.

Thermal Conductivity of Graphite

J. P. Moore T. G. Kollie

The electrical resistivity, ρ, and thermal conductivity, λ, of samples of H-337 and AXF-5Q graphites were reported previously.[38] Three samples of each were irradiated in HFIR to various fluences at 550, 650, and 750°C. Measurements of λ and ρ on two AXF-5Q samples irradiated at 550 and 650°C to fluences of 2.6 $\times$ 10^{21} and 4.2 $\times$ 10^{21} neutrons/cm^2 have been completed. Neutron irradiation reduced λ at room temperature from 1.3 to 0.31 W cm^{-1} $°C^{-1}$ and at 600°C from 0.73 to 0.33.

A vitreous-silica dilatometer for coefficient of thermal expansion measurement (α) in the range −195 to 900°C was tested (Chap. 7 of this report). Measurements on the above graphites will begin when current tests on National Bureau of Standards certified α standards of fused silica and copper are completed.

Irradiation of Graphite

C. R. Kennedy W. P. Eatherly

We have a program to fabricate advanced types of graphite for extended reactor life. The graphite desired has a monolithic structure with very strong grain boundaries to resist shearing deformation caused by irradiation growth. This type of structure is obtained by the use of green cokes to reduce or eliminate the binder shrinkage cracks during fabrication. We have preliminary results from an irradiation to 1.5 $\times$ 10^{22} neutrons/cm^2 and have returned these samples to the reactor for further exposure.

The experimental grades are all molded, and the experiment is designed so that we will be able to compare the two green fillers, Robinson and Santa Maria, and these fillers with Thermax additions. We will also be able to compare the effects of the coke modification process on both fillers. We will also examine the effect of bulk density variations of 1.65, 1.76, and 1.89 g/cm^3 in the Robinson coke series, and 1.66 and 1.74 g/cm^3 in the Santa Maria series. This will afford invaluable base-line data for evaluating impregnation effects in the future. We will also have a direct comparison of the effect of different binder systems using coal tar pitch 15V, petroleum pitch 240, furan–petroleum-pitch mixtures, and a plasticizer.

The irradiation results to date on the Robinson-base graphite are given in Fig. 28.1. Similar results apply to the Santa Maria material. Both the Robinson and Santa Maria graphites are farily stable and isotropic to this fluence, and density variations, different binders, and Thermax additions appear not to have measurably

34. Chemical Engineering Department, Development Division, Y-12 Plant.

35. O. B. Cavin, *MSR Program Semiannu. Progr. Rep. Aug. 31, 1971,* ORNL-4728, pp. 116–17.

36. W. H. Cook, *Metals and Ceramics Div. Annu. Progr. Rep. June 30, 1969,* ORNL-4470, pp. 191–92.

37. H. B. Gruebmeier and G. P. Scheidler, *An Optical Method for the Determination of the Local Anisotropy of Pyrolytic Carbon Layers and Graphite,* ORNL-tr-2127 (May 28, 1969).

38. J. P. Moore and T. G. Kollie, *Metals and Ceramics Div. Annu. Progr. Rep. June 30, 1971,* ORNL-4770, pp. 169–70.

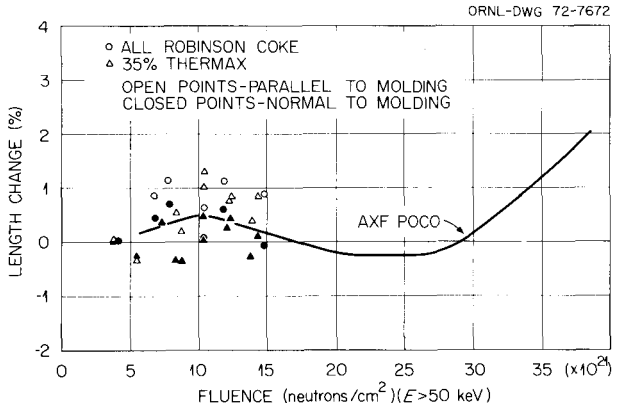

Fig. 28.1. HFIR irradiation results for Robinson grades at 715°C.

affected the results. This stability is very encouraging; however, results to much higher fluences must be obtained before conclusions can be reached about extended life.

CHEMICAL PROCESSING MATERIALS

J. R. DiStefano

Chemical processes are being developed for the isolation of protactinium and the removal of fission products from molten-salt breeder reactors. Techniques such as fluorination to remove uranium, reductive extraction to isolate protactinium, and a metal-transfer process to remove rare earths are being studied. The reductive-extraction and metal-transfer processes are based on the extraction of protactinium and rare earths from the fuel salt into molten bismuth-lithium solutions, and our program is aimed at selecting materials for these applications. The choice of materials is limited because of the relatively high solubility of many conventional materials in bismuth. Refractory metals such as Mo, W, Rh, and Ta appear promising along with several grades of graphite.

During the past year, our efforts have concentrated on the fabrication of a molybdenum reductive-extraction test stand for metallurgical and chemical engineering evaluation. This has required the development of complex fabrication and joining techniques not previously applied to molybdenum. We have also continued to test the compatibility of molybdenum, TZM, tantalum, T-111, iron-base brazing alloys, and various grades of graphite with bismuth-lithium solutions under several processing conditions.

Construction of a Molybdenum Reductive-Extraction Test Stand

J. R. DiStefano A. J. Moorhead

Work was continued on the construction of a molybdenum reductive-extraction test stand.[39,40] Both bismuth and molten salt will countercurrently circulate through a 1 ⅛-in.-OD × 5-ft-long packed column. The flow rate of each fluid is controlled by removable orifices in the bottom of two 3 ⅞-in.-OD × 8-in.-long feed pots. The bismuth and salt mixture will be separated in 3 ⅞-in.-OD × 16-in.- and 18-in.-long end sections immediately above and below the column. Four different sizes of molybdenum tubing will interconnect the various components.

Development of a liquid-level probe for this system is reported in Chap. 20 of this report.

A full-size mockup was constructed to aid in design of the loop and to establish the step-by-step fabrication sequence. Primary fabrication of the container half sections and machining of all components have been completed.

Tubing for the various connecting lines was obtained, inspected, and certified for use. Commercial molybdenum tubing varied in ductility. Although fabrication history is an important factor, we traced the brittle behavior of ¼-in.-OD × 0.020-in.-wall and ⅜-in.-OD × 0.025-in.-wall material to the presence of a brittle inner layer. We suspect that the tubing became contaminated during fabrication, and cleaning procedures were inadequate.[41] Etching off this layer left the tubing ductile at room temperature. The following sections describe other fabrication and joining studies relating to the construction of this test stand.

Fabrication Development of Molybdenum Components

R. E. McDonald A. C. Schaffhauser

We have completed fabrication and procurement of the molybdenum components for the chemical processing test loop. This task included fabrication development of 4-in.-OD × 3 ¼-in.-ID back-extruded molyb-

39. J. R. DiStefano, *Metals and Ceramics Div. Annu. Progr. Rep. June 30, 1971,* ORNL-4770, p. 162.

40. J. R. DiStefano and A. J. Moorhead, *MSR Program Semiannu. Progr. Rep. Feb. 29, 1972,* ORNL-4782, in press.

41. J. R. DiStefano, *MSR Program Semiannu. Progr. Rep. Aug. 31, 1971,* ORNL-4728, pp. 164–65.

denum vessels, production of the required back extrusions, and coordination of machining and procurement of components from a subcontractor.[42]

The back-extrusion process and tooling developed to fabricate components having an internal length up to 11 in. have been described previously.[43] The feed pots, lower disengaging vessel, and upper disengaging vessel each required two back extrusions having internal lengths of 3.5, 7.75, and 9 in. respectively. The halves were welded and brazed. All the required back extrusions plus three spares were successfully fabricated and machined to final dimensions. Extrusion at 1600 to 1700°C was required to produce the required back-extruded lengths.[44]

Molybdenum Welding Development

A. J. Moorhead

Procedures were developed for welding the three basic types of joint required in construction of the test stand: tube-to-header, header-to-header, and tube-to-tube. We have successfully made all of the necessary welds on mockup parts of the same material, having the same fabrication history and configuration as actual test stand components.

Tube-to-header welds were made joining $\frac{1}{2}$-, $\frac{7}{8}$-, and 1-$\frac{1}{8}$-in.-OD tubes to five pot half sections. All of these electron-beam welds, which have a trepanned joint configuration, were helium leak-tight after welding. A special weld of this type in which a $\frac{1}{4}$-in.-diam vent tube is welded to the inside of the feed pot bottoms was also successfully made. The latter component requires two welds for attachment: (1) a $\frac{5}{8}$-in.-diam washer is welded to the tube, and (2) the washer is welded to the molybdenum half section. Although two repair welds were required, we were able to make this weld helium leak-tight and dimensionally acceptable without melting the protruding tube with the electron beam.

Six back-extruded half sections were joined by the electron beam process to form three pots. All three of these header-to-header welds were defect free when inspected with fluorescent penetrant. For two of these welds, molybdenum pins passing radially through the step joint were used to hold the half sections in close proximity, as required for electron beam welding. The pins were necessary because the bent configuration of the tubes and the many internal components in actual test stand parts prohibit the use of a spring-loaded bar passing axially through the pot, as had been used on earlier welds to provide end loading.

Tube-to-tube field welding procedures[45] have been optimized on actual $\frac{1}{4}$-, $\frac{3}{8}$-, and $\frac{1}{2}$-in.-diam loop tubing with a new welding programmer, which allows the speed of the commercial orbiting-arc head to be increased during the weld cycle. This improves the uniformity of the welds by eliminating the heat buildup that occurs whenever automatic circumferential welds are made on small-diameter tubing. A yoke fixture was designed and built to hold the tubes in alignment for welding, thus minimizing stresses on the welds. In construction of the test stand this yoke will be left around a weld until a reinforcing band is attached by brazing. In addition, $\frac{7}{8}$- and 1 $\frac{1}{8}$-in.-diam tube-to-tube welds were made automatically in an argon-filled chamber using an extensively modified commercial orbiting-arc head of another design. The successful development of this device will make it unnecessary to rotate large sections of the test stand, as would be required if manual gas tungsten-arc welding were used to join the 5-ft-long column to the disengaging sections.

Development of Techniques for Brazing Molybdenum

N. C. Cole

Joining of molybdenum test stand components has required both the development of filler metals and several unique brazing techniques. Filler metals were developed to satisfy the requirements of (1) brazing temperature below 1200°C to minimize recrystallization and grain growth of the molybdenum and (2) corrosion resistance to bismuth-lithium solutions at 650°C. Evaluation of several potential filler metals for this application has been completed and reported.[46] We have selected the iron-base alloy Fe–15% Mo–5% Ge–4% C–1% B as the filler metal that best meets our requirements.

Tube-to-header welded and roll-bonded joints will be back brazed, and sleeves will be brazed around tube-to-tube and header-to-header welded joints. These will provide reinforcement of the welds as well as a seal in case a leak should develop in the weld area.

---

42. Thermo Electron Corporation, Metals Division, Woburn, Mass.

43. A. C. Schaffhauser and R. E. McDonald, *MSR Program Semiannu. Progr. Rep. Aug. 31, 1971,* ORNL-4728, pp. 166–69.

44. R. E. McDonald and A. C. Schaffhauser, *MSR Program Semiannu. Progr. Rep. Feb. 29, 1972,* ORNL-4782, in press.

45. A. J. Moorhead, *Metals and Ceramics Div. Annu. Progr. Rep. June 30, 1971,* ORNL-4770, pp. 162–63.

46. N. C. Cole and J. W. Koger, ibid, pp. 163–64.

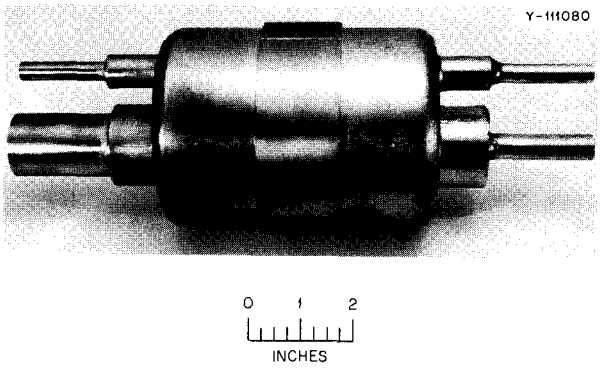

Fig. 28.2. Mockup of a feed pot of the molybdenum chemical processing test stand.

Back brazing and header-to-header sleeve brazing will be accomplished in a vacuum furnace. However, after the subassemblies are joined, they will be too large for existing furnaces. Therefore, portable furnaces that use either induction or resistance heating sources have been developed to fit around the component to be brazed.[47] Only a local area will be heated, but atmospheric protection (inert-gas environment) must be provided to avoid contamination.

Several mockups of large components have been brazed. Figure 28.2 shows a 3 $^7/_8$-in.-diam pot into which short lengths of tubing were roll bonded or welded and then back brazed. A split ring was also brazed around the header-to-header girth weld.

Corrosion of Structural Materials in Bismuth

O. B. Cavin J. L. Griffith B. W. McCollum
L. R. Trotter

We are studying the compatibility of bismuth and bismuth-lithium solutions with construction materials for a continuous fuel salt processing plant. These studies are performed at 600 to 700°C using three experimental techniques: (1) static capsule tests, (2) quartz thermal convection loops containing the samples in up to 0.01 wt % (0.3 at. %) Li in bismuth, and (3) all-metal thermal convection loops containing up to 3 wt % (48 at. %) Li in bismuth.

In graphite crucible tests at 700°C, pure bismuth did not penetrate the porosity of the three grades ATJ, AXF, and Graphitite A. However, when 3 wt % (48 at. %) Li was added to the bismuth, the liquid metal penetrated the open porosity, as shown by radiographs of the crucibles.[48] The amount of penetration appears to be a function of the available open porosity in the polycrystalline graphite. We have not observed any chemical reactions between the liquid metal and the graphite.

We reported previously[49] that T-111 (Ta–8 wt % W–2 wt % Hf) alloy was unattacked but lost its room-temperature ductility after testing in a quartz thermal-convection loop containing pure bismuth or Bi–100 ppm Li at 700°C for 3000 hr. In this test the tensile samples were 0.020-in.-thick sheet specimens. We recently tested an all-metal T-111 alloy loop that contained 0.125-in.-diam cylinderical samples in 2.5 wt % (43 at. %) Li in bismuth and operated for 3000 hr at 695°C. Again, no dissolution or mass transfer was detected, but the samples retained their room-temperature ductility.

A protective inner coating of tungsten was placed on a Hastelloy N thermal convection loop.[50] When bismuth was circulated in this loop at 700°C, the tungsten coating cracked and within 24 hr the liquid metal came through the loop wall.[48]

An all-metal molybdenum loop containing 0.125-in.-diam cylindrical specimens in Bi–2.5 wt % (43 at. %) Li is operating and will soon complete the scheduled 3000-hr test. We are also conducting a 10,000-hr test of molybdenum samples in a quartz thermal convection loop containing Bi–0.01 wt % (0.3 at. %) Li.

We will conduct more extensive investigation of graphite permeation by liquid metals considering such variables as alteration of surface tension of the melt and the effect of lithium additions on wetting characteristics.

47. N. C. Cole, "Development of Brazing Techniques for Fabricating the Molybdenum Test Loop," *MSR Program Semiannu. Progr. Rep. Feb. 29, 1972,* ORNL-4782, in press.

48. O. B. Cavin et al., *MSR Program Semiannu. Progr. Rep. Feb. 29, 1972,* ORNL-4782, in press.

49. O. B. Cavin and L. R. Trotter, *MSR Program Semiannu. Progr. Rep. Aug. 31, 1971,* ORNL-4728, p. 173.

50. J. I. Federer, *MSR Program Semiannu. Progr. Rep. Feb. 28, 1971,* ORNL-4676, pp. 231–32.

29. Thorium Utilization

A. L. Lotts

The Thorium Utilization Program is being conducted within the context of the National HTGR Fuel Recycle Program Plan, which was issued last year;[1] our activities are being carried out in cooperation with the Chemical Technology Division of ORNL, the Idaho Chemical Processing Plant, and Gulf General Atomic. All of these are involved in the development of the head-end processes and chemical processes for HTGR fuel. Our task is to provide the necessary development for refabrication of HTGR fuel that is obtained in the use of the Th-^{233}U fuel cycle. The ultimate aim of our program is to demonstrate economic fuel recycle techniques for this reactor in a pilot-scale facility, the Thorium-Uranium Recycle Facility at ORNL. Our program consists of refabrication process development on an engineering scale, development of remote pilot-scale equipment that can be used in TURF, and irradiation of fuels produced in engineering-scale equipment. In addition, we conceptually design large commercial-scale refabrication plants, using such designs as a guide to our development and pilot-scale work, and evaluate process alternatives on an economic basis. The program utilizes extensively technology developed in the Gas-Cooled Reactor Program, the progress of which is reported in Chap. 25.

Processes and equipment are being developed to fabricate 25 kg/day of oxide fuel into the HTGR graphite fuel blocks. The demonstration with ^{233}U is now scheduled to start in TURF in 1977. Additional attention and emphasis arose from the sale by Gulf General Atomic of six large reactors to utilities in the United States. All of these reactors will utilize the Th-^{233}U fuel cycle, thus confirming the need for full development of techniques for carrying out processes involved in this fuel cycle.

1. Oak Ridge National Laboratory and Gulf General Atomic, *National HTGR Fuel Recycle Development Program Plan*, ORNL-4702 (August 1971).

THORIUM-URANIUM RECYCLE FACILITY

J. M. Chandler[2]

The Thorium-Uranium Recycle Facility (TURF) and its equipment were operated and maintained in operational readiness in support of the heavily shielded process cell bank and the in-cell process equipment. To do this, for example, we overhauled and did preventive maintenance to both air compressors, removed several manipulator slave ends from cell B, decontaminated and repaired them and returned them to service, rebuilt a damaged electromechanical manipulator, repaired cell B TV system, and replaced some faulty electrical motors and bearings in addition to doing programmed routine preventive maintenance to all TURF equipment. In addition, other programs of limited scope were carried out in the facility.

Neutron counting equipment and associated peripheral equipment were installed remotely in cell G after it had been mocked up outside the cell to test its parts for proper fit and to test installation procedures. The neutron counting equipment comprised a 3 X 4 X 5 ft stainless steel tank containing an assortment of cavities and cutouts to accommodate instrumentation and provide storage bins. A table-top work bench was installed on top of the water tank. An inclined runway was installed from cubicle 2 to the work bench, a horizontal distance of 15 ft. This item also had attached to it a spur that serves as a chute between cubicles 2 and 3. A 55-gal stainless steel barrel was positioned on the cell G floor, and a 14-ft-long, 3-in.-diam aluminum tube was inserted into the center of the barrel. The barrel was filled with water and is used to store sources as large as 100 mg of ^{252}Cf. Experience gained in the design and remote installation of equipment in a highly contaminated and crowded cell will be useful in future TURF work.

2. On loan from Chemical Technology Division.

A 250-gal surge tank was installed in the cooling water supply line originating at the HFIR cooling tower area. The surge tank was attached perpendicular to the 10-in.-diam water line and is maintained two-thirds full of air. This is to protect the TURF piping from water hammer, which occurs in the lines when the large HFIR cooling water recirculation pumps are started and stopped.

The television camera was placed in service in cell B for use with the LMFBR thermocouple test program. Several modifications to the TV system were necessary before satisfactory remote viewing was possible. This is our first use of the in-cell viewing equipment, and valuable operating experience is being gained in the use of this TV system for working remotely in one of the hot cells.

The air filter on cell F inlet was replaced after a year of service. Its pressure drop had increased to 3.5 in. H_2O pressure, and this was limiting the ventilation air supply to cell F to a value below the desired 500 scfm. No other cell inlet filters have been changed from the original ones installed in 1967.

Shipping arrangements were made and RTE-7 was delivered from Peach Bottom, Pennsylvania, to ORNL using the Peach Bottom Single Element Shipping Cask DOT-SP-5938. The loaded cask was involved in a highway accident while en route to ORNL. A report[3] describes the actions taken to safely retrieve the cask, deliver its contents to ORNL, inspect it, repair it, and return it to service as soon as practical.

Work continued on the conceptual design of materials handling equipment for use at TURF during the HTGR fuel recycle demonstration program scheduled initially for TURF beginning FY 1973. Equipment for removing off-specification fissile and fertile particles and waste was conceived. This equipment would feature removal through a specially designed roof plug. A design was also conceived for unloading ^{233}U nitrate solution from the ORNL solution carrier to a storage tank located in cell D.

The HTGR program plan was revised to locate the Head-End Pilot Plant demonstration work at the Idaho Chemical Processing Plant (ICPP). Therefore, our conceptual design for particle handling may be modified for use at Idaho. Our design was used as a basis for estimating equipment cost for budget preparation and for a commercial plant. The uranium solution unloading and storage operations will be necessary for the TURF demonstration program.

3. J. M. Chandler, *The Peach Bottom Spent Fuel Element Shipping Cask Accident*, ORNL-TM-3844 (Dec. 8, 1971).

REFABRICATION DEVELOPMENT

J. D. Sease

The objective of the HTGR refabrication development program is to develop the technology necessary for the design and operation of a pilot-scale remote fueled graphite line in the Thorium Uranium Recycle Facility (TURF). This pilot line, scheduled for operation in 1976–1977, will be $^1/_{20}$ the scale of a commercial recycle facility and will produce two fuel blocks per day containing approximately 25 kg of heavy metal. The major development areas in the Metals and Ceramics Division are associated with coating of fuel particles, stick fabrication, and element assembly, only the first two having been active this year.

Coating

W. J. Lackey W. H. Pechin

Particle coating equipment, processes, and inspection techniques are being developed to allow preparation of the proposed HTGR recycle fuel particles described in Table 29.1. This year we coated more than 200 kg of particles of this type in 1- to 2-kg batches on a semiproduction scale in our two 5-in.-diam development coating furnaces. The particles were coated while being fluidized by gas that entered the heated bed of particles through either a single inlet cone or a flat porous plate. A number of modifications were made to the prototype remote coater, and although additional modifications will be required for fully remote operation, this coater is currently a highly automated, versatile, and reliable system.

Equipment modifications included alteration of the furnace electrodes to permit tighter clamping of the heating element assembly to minimize thermal and electrical resistance, fabrication of more rigid molybdenum heat shields, installation of a particle transfer system, and installation of a critically safe soot filter.

Table 29.1. High-temperature gas-cooled reactor recycle fuel particles

	Fissile Particle	Fertile Particle
Kernel composition	$(Th-20\%\ U)O_2$	ThO_2
Kernel diameter, μm	350	400
Buffer carbon thickness, μm	80	50
Outer pyrolytic carbon thickness, μm	120	70
Total particle diameter, μm	750	640

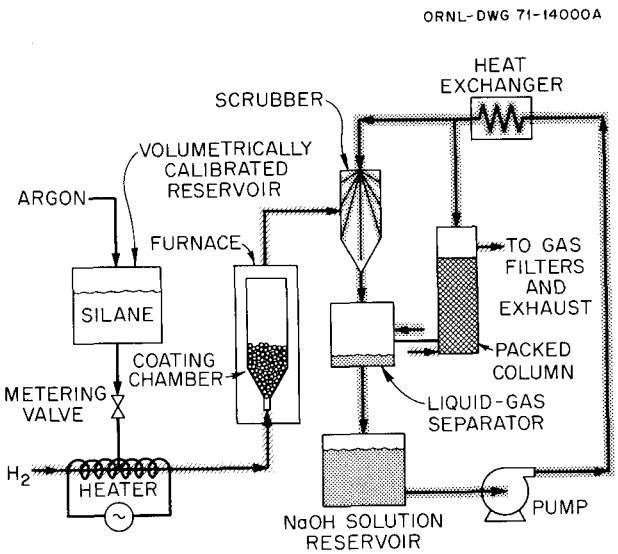

Fig. 29.1. Schematic of equipment for depositing SiC in the 5-in.-diam prototype remote coater.

Particles that had been separated from the soot and soot balls that form during deposition of carbon coatings could be pneumatically transferred in a 160-ft-long, $^3/_8$-in.-diam stainless steel tube that at points was elevated as much as 17 ft above the tube inlet and exit. Transfer of uncleaned particles occasionally blocked the transfer line, so a separator has been designed for installation to the unloading port of the coating furnace.

Several equipment modifications were made to prepare SiC coatings should this additional coating be required. Equipment for deposition of SiC coatings is shown schematically in Fig. 29.1. To introduce silane into the gas we force it out of a volumetrically calibrated glass reservoir with argon pressure through a metering valve. Two scrubbers in series removed all the HCl from the furnace effluent. With this system we deposited SiC coatings with a density of 3.21 g/cm^3. These coatings were fine grained with smooth surfaces, indicating that the silicon carbide should have high tensile strength.

Significant progress was made toward understanding and learning how to reduce the particle-to-particle variation in buffer coating thickness. Detailed analysis of statistically designed buffer coating experiments showed the variation for a given coating run to decrease for smaller charges, longer run times, higher diluent gas flow rates, and smaller included angles of the conical gas distributor. The relative standard deviation of coating thickness correlated with the product diluent flux times time. The degree of mixing occurring in the fluidized bed was of major importance. To improve the mixing, coating runs were made with considerably higher flow rates of diluent gas and acetylene. The resulting particle-to-particle relative standard deviation of coating thickness was about 14%, compared to 20 to 25% typically observed in the past for our system. An equation was developed to predict the standard deviation of the coating thickness as a function of the hydrocarbon flow rate, the helium flow rate, the furnace load, the mean particle diameter, the coating time, and the standard deviation of particle diameter.

We found both positive and negative correlations of buffer coating thickness with particle diameter. The nature of the correlation depends strongly on both load and run time.

We are setting up a series of computer files to store the coating inspection data and perform the necessary calculations. A program was written to utilize these files in maintaining a control chart for the carbon weight determination. This program indicated an average relative standard deviation for the carbon weight determination of 0.42% for buffer coated material. A similar treatment of particle density data from buffer runs indicated a standard deviation of 0.02 g/cm^3.

We greatly speeded measurement of particle diameters and coating thicknesses by equipping the split-image eyepiece with a digital output that is read directly into a PDP-8/E computer.[4] The time required to measure 50 particles from a typical radiograph was reduced from 90 to 15 min or less, and the formerly time-consuming statistical processing of the data is done simultaneously. We are now extending the use of this computer to other applications in refabrication inspection as shown in Fig. 29.2.

We are developing an electronic particle size analyzer based on the light blockage principle similar to a machine we have already evaluated.[5] The principal improvements will be the inclusion of 1000 channels instead of the ten available on the old machine and digital output of data to allow direct interfacing with automatic data processing equipment. The increased number of channels will provide greater precision and allow us to measure particle samples throughout the expected size range without range changing or recalibration.

4. Manufactured by Digital Equipment Corporation, Maynard, Mass.

5. J. D. Sease, F. J. Furman, W. H. Pechin, J. G. Stradley, and C. F. Sanders, *Metals and Ceramics Div. Annu. Progr. Rep. June 30, 1971*, p. 172.

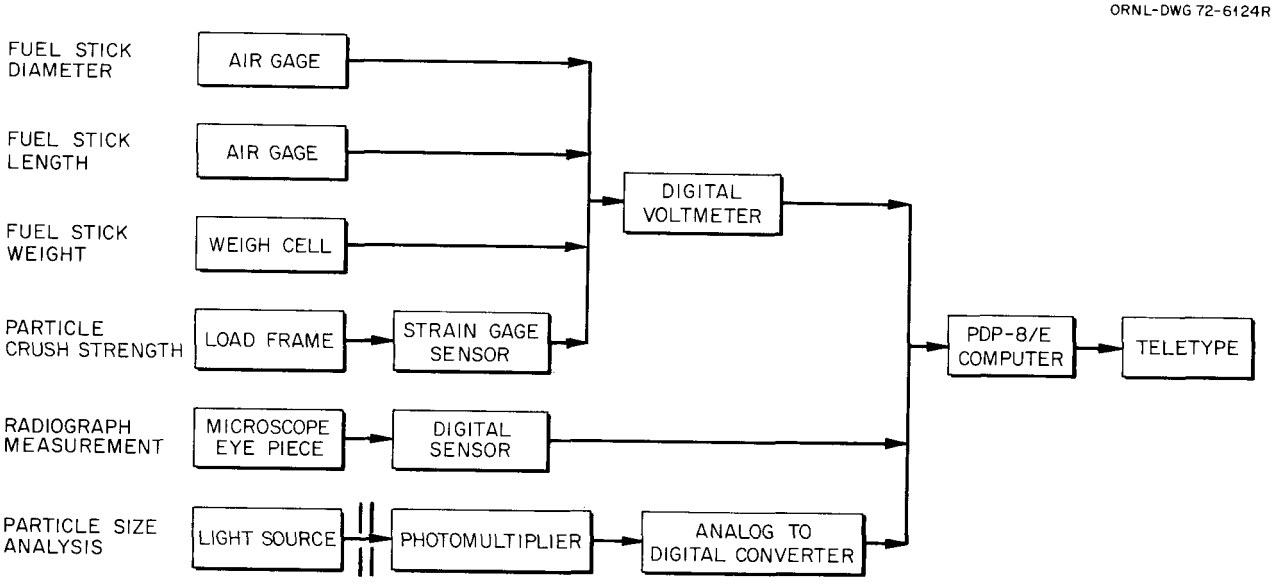

Fig. 29.2. HTGR fuel characterization data system.

A tentative sampling scheme we prepared for the TURF plant is shown in Table 29.2. The sampling levels shown in this table are only estimates; the actual sampling frequency will depend upon the uniformity of the product and the precision of the analyses. We will be relying heavily on the electronic particle size analyzer for the routine process control. The radioassay equipment will be the same as that mentioned below for fuel stick inspection.

Stick Fabrication

R. A. Bradley C. F. Sanders

The purpose of our fuel stick fabrication work is to develop processes and design equipment suitable for fabricating about 9000 HTGR fuel sticks per day at TURF. The fuel sticks are about 0.5 in. in diameter X 2 in. long and contain mixtures of fissile and fertile coated particles bonded by a matrix of coal tar pitch and graphite filler. The principal activities in fuel stick fabrication are blending and loading particles into molds, injecting the matrix into a bed of particles to form a stick, and carbonizing and annealing the stick. The fuel stick characterization will consist of inspection to determine the filler distribution, the amount of broken particles, the fuel distribution, the variation in fuel content from stick to stick, and the amount of fuel in a given stick or a batch of sticks.

We are investigating two approaches to particle blending and mold loading. In one approach, fissile and fertile particles sufficient for several hundred fuel sticks are batch blended, and then the quantity required for a single stick is volumetrically measured and dispensed into the mold. A pneumatic blender using short-duration pulses of high-velocity gas to lift and spin the particle bed was tested. The blending of fissile and fertile particles was good for about 95 vol % of the bed; however, near the top and bottom of the bed the blend contained excessive amounts of the smaller fissile particles. This blender is being modified to provide a continuous flow of gas through a porous bottom plate to fluidize and mix the particles.

The other approach to particle blending and mold loading is to weigh or measure the amount of each kind of particles required for a single stick and blend them by simultaneously feeding them at controlled rates into a stick mold. The difficulty in this approach is in simultaneously feeding the two types of particles into the mold, since the volume ratio of fertile to fissile particles may be as high as 10. A controlled orifice feeder-blender is being tested for this purpose.

We have continued the development of the slug injection technique for fabricating fuel sticks.[6,7] In this process a preformed slug of matrix material is warm

6. J. D. Sease, W. H. Pechin, F. J. Furman, J. G. Stradley, and C. F. Sanders, *Metals and Ceramics Div. Annu. Progr. Rep. June 30, 1971*, ORNL-4770, pp. 172–74.

7. R. A. Bradley, C. F. Sanders, and D. D. Cannon, *Gas-Cooled Reactor and Thorium Utilization Programs Annu. Progr. Rep. Sept. 30, 1971*, ORNL-4760, in preparation.

Table 29.2. Tentative scheme for analysis of particles in TURF

Sampling levels:
I = 1 to 10% of batches sampled
II = 10 to 50% of batches sampled
III = 100% of batches sampled

Material type	Radioassay	Particle size analysis	Carbon burnoff	Mercury pycnometer	Radiography	Gradient density analysis	Shape analysis	Metallography	Coating contamination analysis	Chemical assay	Impurity analysis
Bare kernels	III	III		III						I	III
Buffer coated		III	II	II	II						
ILTI coated		III	II	II	II	I					
SiC coated		III	II	II	II	II					
OLTI coated		III	II	II	II	I	III	III	III		
Batch blended	III	III	III	III	III			III		I	III
All rejects	III										

ORNL-DWG 71-9836R

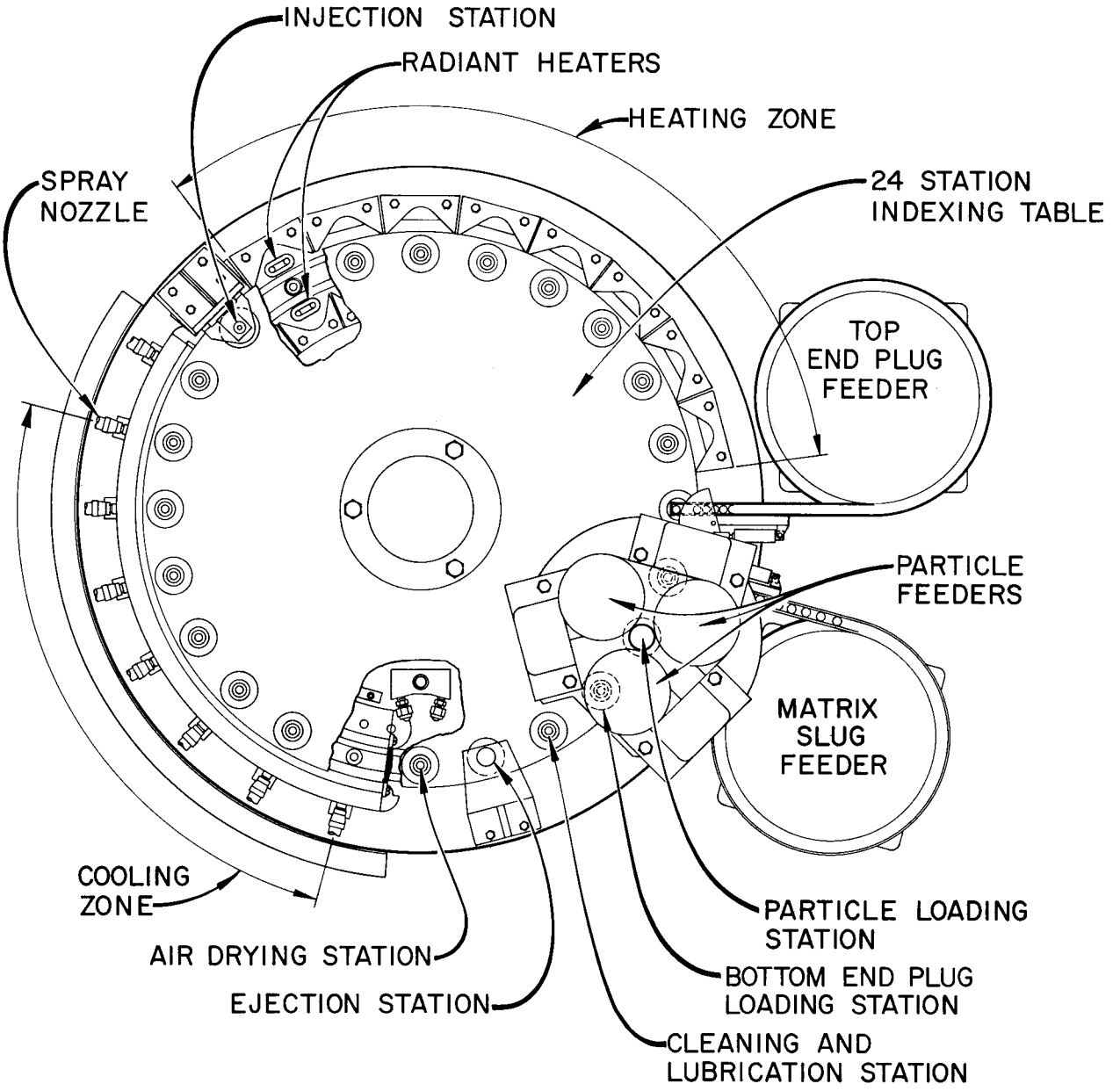

Fig. 29.3. Prototype fuel stick machine.

pressed through the bed of particles. The feasibility of this process was demonstrated during the fabrication of approximately 200 plutonium-bearing fuel rods for the irradiation experiment described in Chap. 34 and during the fabrication of several thousand fuel sticks for head-end reprocessing studies by the Chemical Technology Division.

An automatic fuel stick machine was designed and fabricated. This machine, which is shown schematically in Fig. 29.3, is basically a rotary index table with the fuel stick mold attached to the table. As the table indexes, the mold moves through a series of stations where the bottom end plug, the coated particles, the matrix slug, and the top end plug are fed into the mold automatically. The mold then passes through several stations where infrared radiant heaters preheat the mold and particle bed to 160 to 180°C. The matrix is then injected into the bed of coated particles, the dies are cooled by a water spray, and the stick is ejected from the mold. Although this machine was designed to

produce only 500 fuel sticks per day, the intrusion rate studies described below indicate that it will have a capacity several times that when fully operational.

We studied the effect of intrusion pressure and temperature on the rate of intrusion of matrix into a bed of particles. This study is important in finding the rate at which fuel sticks can be made by the process. The effects of temperature and pressure on the intrusion rate are shown in Figs. 29.4 and 29.5, respectively. The intrusion rate is a function not only of temperature and pressure, but also of the length of bed intruded. At constant temperature and pressure the intrusion rate varies inversely with the length of bed. A 2-in. bed of particles can be intruded with reference Fort St. Vrain Reactor matrix in about 10 sec with an injection pressure of 1000 psi at 170°C.

Fuel sticks are heated to 800°C to convert the coal tar pitch to carbon. During carbonization the sticks are packed in Al_2O_3 powder to maintain their dimensional stability. They are subsequently annealed at 1800°C to remove residual volatiles and stabilize their dimensions. Using these carbonizing and annealing techniques we have controlled the diameter of the fuel sticks to within ±0.002 in. of nominal.

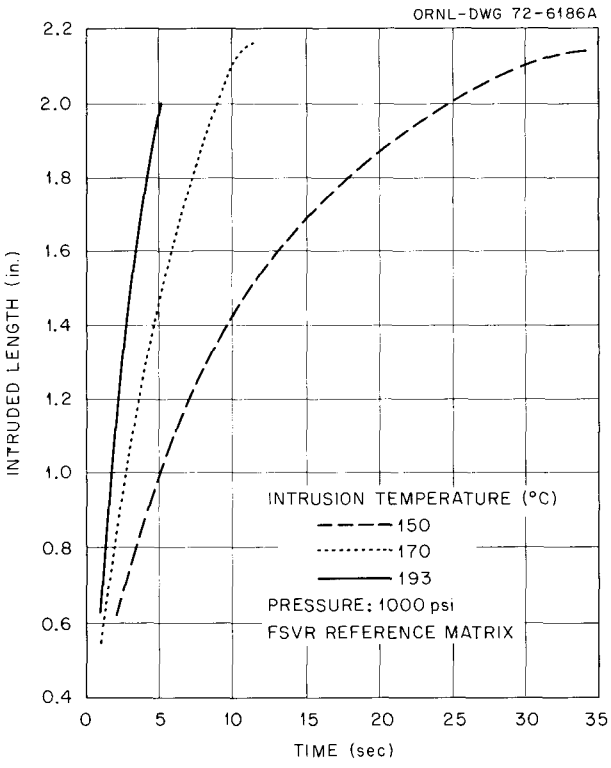

Fig. 29.4. Effect of temperature on intrusion rate.

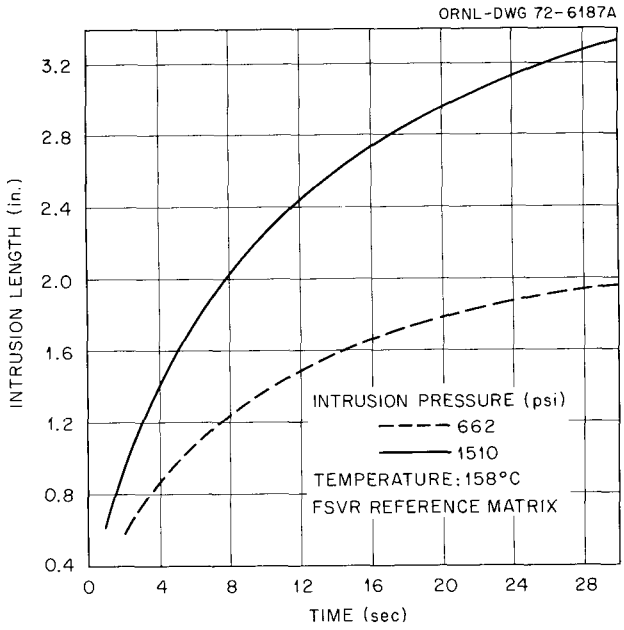

Fig. 29.5. Effect of pressure on intrusion rate.

For the characterization of fuel sticks we have techniques for determining the filler distribution and the particle distribution. We have determined the combined stick contamination and fuel particle breakage by fission gas released on several samples.[8] The major problem in characterizing the fuel stick is determining the amount of fissionable material in each stick to the precision needed for this program. We are investigating a multispectra neutron irradiation technique. With this technique we will induce fission in the material using different energy neutrons and count the delayed neutrons.

REFABRICATION EQUIPMENT DESIGN

J. D. Sease F. C. Davis[9]

The reference process for the Refabrication Pilot Plant is to prepare BISO-coated fuel particles, fabricate fuel sticks by the slug injection process, and carbonize and anneal fuel sticks before insertion into the fuel blocks. Flowsheets for the reference process, which depict the individual steps, were updated. The flowsheet, which is similar to that presented last year,[7] is subdivided into three areas: the Microsphere Coating,

8. J. D. Sease, C. F. Sanders, W. P. Eatherly, D. P. Harmon, and W. J. Scheffel, "Fabrication of Plutonium Fuels for HTGR," paper presented at ANS meeting in Las Vegas, Nev., June 19–22, 1972.

9. General Engineering Division.

Head-end reprocessing

Primary and secondary crushing for burner feed preparation

Exo followed by endo fluidized bed burning process – all graphite

Size separation for ash handling

Alumina recycle for ash handling

Crushing and burning of TRISO particles – classified ash treatment

Leaching, centrifuging, washing and drying, solvent extraction feed preparation

Solvent extraction reprocessing

Acid Thorex solvent extraction processes

Microsphere preparation processes

Steam denitration process for ThO_2 microsphere preparation

CUSP process for UO_2 microsphere preparation, $^{235}UO_2$ makeup

CUSP process for UO_2 microsphere preparation, $^{235}UO_2$ recycle

Resin loading process for UO_2 microsphere preparation, $^{233}UO_2$ recycle

Solex process for $(Th,U)O_2$ microsphere preparation

$(Th,^{233}U)O_2$ (Th/U = 4.25) recycle

Fuel fabrication

BISO microsphere coating process, $(Th,U)O_2$

Th/U = 4.25 recycle particles 425 μm

Preliminary results of these estimates are now under review and not available for reporting.

Commercial Recycle Plant Conceptual Design

A brief study was made to evaluate plant design concepts prepared by others and to determine general information such as plant and equipment general arrangement and space requirements that might be related to the processes being considered. This information was used to develop unit cost factors for use in the process evaluation studies, such that total plant cost could be calculated for and related to each given process.

During this study, a set of general criteria for the commercial recycle plant was prepared, and a concept layout for the recycle plant was developed.

HTGR RECYCLE FUELS IRRADIATION

F. J. Homan R. B. Fitts
A. R. Olsen

The irradiation tests on the HTGR recycle program have two main objectives: (1) to provide irradiated fuel for head-end process studies and (2) to provide irradiation proof tests of the products of coated-particle process development. The test conditions of interest include fuel temperatures between 600 and 1300°C, burnup to 20% fissions per initial actinide metal atom (FIMA) in the $(Th,U)O_2$ particles, and fast fluence exposures up to 8×10^{21} neutrons/cm^2.

The first two stages in this program are: (1) accelerated-burnup capsule irradiations and (2) irradiation of seven test fuel elements in the Peach Bottom Reactor.

Large-Scale Irradiations

R. B. Fitts

This cooperative irradiation program with Gulf General Atomic has three main objectives: (1) to provide gram quantities of unirradiated HTGR fuel for head-end reprocessing studies, (2) to provide irradiated fuel blocks for testing engineering-scale reprocessing equipment, and (3) to proof test recycle fuel particles prepared in prototype equipment using the processes to be used in the Thorium-Uranium Recycle Facility. To achieve these objectives a set of Recycle Test Elements (RTE's) is being operated in the Peach Bottom Reactor.[10] The design of the RTE's and the particle types to be tested have been reported.[11] The first six RTE's were irradiated without incident from July 14, 1970, to April 24, 1971. The elements had accumulated about 265 full-power days of operation and a peak fast fluence of about 1.4×10^{21} neutrons/cm^2. One element, RTE-7, was removed and shipped to ORNL for reprocessing studies and fuel examination.

Two of the six fuel bodies in RTE-7 have been examined in detail, and selected fuel samples from two of the remaining bodies were examined for visual appearance and dimensional changes. These samples encompassed all of the fuel types and most of the range of operating conditions in this test element. The fuel sticks were easily removed from the holes in which they operated in the graphite bodies. Their overall performance was excellent, as would be expected for these operating conditions ($<2 \times 10^{21}$ neutrons/cm^2 fast exposure and <1250°C). The dimensional changes exhibited (see Chap. 25) by the fuel sticks were somewhat greater than had been expected but were not excessive. One set of fuel sticks containing TRISO-coated UC_2 and ThC_2 particles was used in head-end reprocessing studies,[12] and more of the fuel will be

10. R. B. Fitts, *Metals and Ceramics Div. Annu. Progr. Rep. June 30, 1971*, ORNL-4770, pp. 174–75.

11. R. B. Fitts, *Metals and Ceramics Div. Annu. Progr. Rep. June 30, 1970*, ORNL-4570, pp. 199–200.

12. D. E. Ferguson et al., *Chemical Technology Div. Annu. Progr. Rep. Mar. 31, 1972*, ORNL-4794, in press.

the Fuel Stick Fabrication, and the Fuel Element Assembly.

Equipment and systems diagrams have been prepared for each of the three process areas. These diagrams break down each area into systems and outline individual pieces of equipment required in each system.

Conceptual designs of several of the components that will be a part of the pilot-plant fuel stick fabrication machine have been prepared. The design is based on the laboratory stick machine (see Fig. 29.3), but a conveyor is used to move the molds from one operation to the next instead of a rotary index table. In each process step, the machine will remove molds from the conveyor to perform the particular operation involved and return the molds to the conveyor. With this concept, each process machine operates at its own cyclic rate, and the conveyor serves as temporary storage in addition to its primary function of transferring molds. This machine will make about one stick per second.

The heating station consists of a slot or channel induction coil mounted over the conveyor. Molds moving along the conveyor will pass through this coil. Exposure time within the coil will be controlled by two mold escapement mechanisms – one at the entrance to the coil and the other at the exit. Controlling this exposure time will control the heating and thus the final temperature. Once heated, the mold is ready for insertion into the press. It does not appear feasible to operate the heating coil and press in precise synchronization. Therefore, a holding oven heated by forced hot air is located between the heating coil and the press. The oven as designed has a 0.5-min holdup capacity.

The press will accept the heated mold, press the molten slug into the interstices between fuel particles, and return the mold to the conveyor. Since the cycle time to press one fuel stick is longer than the desired production rate of one per second, a rotary press will treat several fuel sticks simultaneously.

The cooling station consists of a chamber equipped with water spray nozzles and is mounted over the conveyor. Hot molds traveling on the conveyor will pass through this chamber and be sprayed to remove the heat. The cooling water will be in a closed loop system that is cooled by a coil.

The cooled mold will proceed along the conveyor to an ejection station, where the mold will be aligned over a hole, and a ram will force the fuel stick and associated plugs out of the mold into a unit that will ultimately separate the fuel sticks and the plugs. The empty mold will be returned onto the conveyor and recycled.

COMMERCIAL RECYCLE PLANT STUDIES

J. W. Anderson[9] A. L. Lotts
J. D. Sease

In October of 1971, we recognized a need for evaluating systematically the numerous options for fuel recycle processes that show promise for commercial application. This project was initiated to perform these evaluations to guide development work and provide the basis in some cases for assigning priority for development effort.

To achieve this objective, a series of steps was established to include the identification and listing of the various processes for performing fuel recycle operations having promise of commercial application, a technical assessment of the feasibility of each process, and an economic evaluation of the relative merits of competing processes.

To make a meaningful evaluation of various processes, it is very important to consider the process in its commercial environment. For this reason, work is divided into evaluations of processes and commercial recycle plant design, the latter area considering the commercial environment in which processes would be applied.

Process Evaluation

Early in the study, processes of interest were identified in the areas of head-end reprocessing, solvent extraction reprocessing, fuel preparation, and fuel fabrication. Technical data for the evaluation of some 13 processes were prepared. This included process flow diagrams, equipment and systems diagrams, material and heat balance calculations, space requirement estimates, scale factors, and processing equipment cost estimates. From these data, a capital cost was estimated for a total plant increment associated with each process. These data were prepared for a recycle plant with rated capacities of 0.5, 1.5, and 3 metric tons/day of heavy metal product. To make these assessments, fuel specifications of the alternative fuels of interest were established. These included fuel particles, fuel sticks, and fuel elements, all based upon fuel composition, particle size, and coating design. Included in the evaluations are some 8 types of fuel elements, 16 types of particles, and 68 types of fuel sticks. A computer code was also developed for handling the various pieces of data and to calculate overall cost considering processing options.

Capital cost estimates were prepared for reference processes in the following areas.

used for this purpose as these studies continue. In addition, one of the graphite fuel bodies was examined to determine the concentration and distribution of fission products around the fuel holes after the fuel was removed. The data obtained were consistent with the particle coating types and their operating conditions; the fuel sticks containing TRISO-coated particles released the lowest amount of fission product activity.[13]

Five of the six recycle test elements are continuing their irradiation in the Peach Bottom Reactor. The other element, RTE-4, has been removed after 384 days of full-power operation to a peak fast flux exposure of about 2×10^{21} neutrons/cm^2. It will be returned to ORNL and examined.

13. W. B. Cottrell, *ORNL Nuclear Safety Research and Development Program Bimonthly Report for March and April 1972,* ORNL-TM-3831, in press.

Capsule Irradiation Tests

A. R. Olsen

The irradiation of the two capsules H-1 and H-2 with thermal neutron filter shrouds described previously[14,15] was completed on May 9, 1972. Based on the calculated exposure conditions, both capsules exceeded their planned exposure of 8×10^{21} neutrons/cm^2 (>0.1 MeV) by 8 to 16%. Postirradiation examination has just started.

14. A. R. Olsen, *Metals and Ceramics Div. Annu. Progr. Rep. June 30, 1970,* ORNL-4570, pp. 198–99.

15. A. R. Olsen, *Metals and Ceramics Div. Annu. Progr. Rep. June 30, 1971,* ORNL-4770, p. 174.

Part V. Thermonuclear and Transuranium Research

30. Controlled Thermonuclear Reactor Program

C. J. McHargue

Among the materials problems connected with a controlled thermonuclear reactor are radiation damage and compatibility.

Neutron irradiation in HFIR and EBR-II will be used to study swelling ductility loss, and strengthening of the refractory metals, Nb, V, Mo, and their alloys. The temperature range of 400 to 1000°C will be covered, and a wide range of materials variables will be studied.

Since there are no currently available sources of 14-MeV neutrons with sufficient fluxes to study high fluence effects in metals, an alternate approach will be taken. A quantitative relationship between self-ion and fission neutron damage will be developed. Then the technique will be used in connection with the neutron damage studies to extrapolate to conditions expected in a CTR.

NEUTRON RADIATION DAMAGE

F. W. Wiffen

The Effect of Alloying and Purity on the Formation and Ordering of Voids in BCC Metals[1]

The void populations in Mo, Nb, V, and one alloy of each of these were compared by electron microscopy. All three of the systems responded differently to the alloying. The void concentrations and sizes in the molybdenum and Mo–0.5% Ti irradiated at 790°C were identical within the measurement limits. After irradiation at 585°C the Mo–0.5% Ti contained more voids than the molybdenum, but the sizes were nearly identical. Alloying niobium with 1% Zr reduced the void concentration after irradiation at 790°C by more than an order of magnitude, but this was compensated by an increase in void size. High void concentrations were observed in vanadium irradiated at 385 to 600°C, but samples of V–20% Ti irradiated in the range 475 to 600°C had no detectable voids. The V–20% Ti contained high densities of irradiation-produced dislocations in networks and tangles. Voids in Mo, Mo–0.5% Ti, Nb, and Ta were ordered on a bcc superlattice parallel to the metal bcc lattice. Void ordering was not observable in the Nb–1% Zr or vanadium.

Radiation Damage in Thermonuclear Reactor Primary Structures[2]

Neutron fluxes at the first wall of a controlled thermonuclear reactor (CTR) will be approximately of the same magnitude as the flux in advanced fission reactors being developed today but will be more damaging because of the large fraction of 14-MeV neutrons in the spectrum. Not only will the CTR flux produce more displacement damage than an equivalent flux of fission neutrons (equal fluxes produce about 2.5 times as many displacements in a CTR), but the CTR damage will also be influenced by the production of several hundred parts per million per year of hydrogen and helium and larger amounts of solid elements by transmutation reactions of the high-energy neutrons. The CTR requirements dictate that the first wall be a refractory metal alloy, with niobium-, molybdenum-, and vanadium-base alloys being suggested. The two

1. ORNL-TM-3496 (September 1971).

2. Abstract of talk given at the AIME Spring Meeting, Boston, May 8–9, 1972.

general effects of irradiation on this wall material are expected to be loss of ductility and dimensional instability (swelling) due to both helium and displacement damage. Data from fission reactor neutron damage to bcc refractory metals will be reviewed and used to predict the property changes during CTR service.

HEAVY-ION SIMULATION OF RADIATION DAMAGE

J. O. Stiegler K. Farrell
A. Wolfenden

Preparations for Heavy-Ion Bombardments

Alteration of the ORNL 6-MeV Van de Graaff was started by members of the Physics Division to deliver the beams needed and to accept a suitable specimen chamber. The chamber is being designed by members of the General Engineering Division. Ranges of heavy ions and the distribution of damage are being theoretically studied by O. S. Oen of the Solid State Division.

The Temperature Dependence of Swelling in Pure Metals

This experiment is the first stage in our program of radiation damage studies relative to the CTR. In an actual CTR, damage will be produced at elevated temperatures by a high flux of 14-MeV neutrons, which are expected to cause internal voids and extensive swelling. The damage rates in an accelerator are much higher than those from the energetic neutrons now available in reactors. One consequence of this is that the temperatures at which voids are formed in the accelerator are expected to be higher than those for neutron irradiation. The extent of these temperature shifts has not been determined experimentally, but the information is necessary in order to relate ion bombardment damage to neutron damage. Consequently, the purpose of this first experiment is to determine the temperature dependence of void formation (swelling) in a number of metals during neutron irradiation. These same metals will be used later in the ion bombardment studies, and the temperature shifts will be measured. We will then know the equivalent "neutron irradiation temperature" during ion bombardment.

We chose three high-purity metals (Al, Ni, V) for the experiment because voids are known to form most easily in pure metals and also because we wished to study the simplest possible systems. The experiment was inserted into the B8 position in ORR on May 23, 1972. The intended ranges of temperature were 50 to 250°C for the aluminum, 200 to 650°C for the nickel, and 250 to 850°C for the vanadium. Apparently we underestimated the gamma heating, and the temperatures actually achieved are running a little high, but not high enough for concern. The aluminum is operating at 55 to 250°C, the nickel at 300 to 850°C, and the vanadium at 350 to 900°C. Irradiation will be for one cycle (42 days) in ORR. This gives a fast (>0.1 MeV) fluence of approximately 8×10^{20} neutrons/cm^2. If, at the end of this period, the heaters and thermocouples are still satisfactory we may continue the irradiation for a second cycle. This would enable the damage in the specimens to be observed and measured more easily.

CHEMICAL COMPATIBILITY OF POTENTIAL BLANKET AND FIRST WALL MATERIALS

J. H. DeVan

We are assisting the USAEC and its contractors in delineating compatibility problems associated with proposed CTR design concepts.[3,4] One major problem area concerns the environmental effect of the tritium breeding blanket on the plasma containment vessel. Other compatibility problems are associated with convective heat transfer systems used to derive energy from the reactor.

Because of its high tritium breeding ratio and excellent heat transfer properties, metallic lithium affords an attractive dual-purpose blanket-coolant material for CTR applications. We are conducting corrosion studies with lithium to elucidate problems that are peculiar to the CTR concept. For example, we procured several Nb–1% Zr tubes whose internal surfaces were coated with yttrium oxide to evaluate the electrical insulating properties of this oxide in lithium. Thermal convection loops of a vanadium alloy and a stabilized low-alloy steel were constructed for compatibility testing with lithium. As discussed in Chap. 38, we are also examining a forced-convection loop that circulated lithium for 3000 hr at a maximum temperature of 1370°C. Results of this loop test have been applied to predictions of thermal-gradient mass transfer under CTR conditions.

---

3. L. C. Ianniello, *Fusion Reactor First Wall Materials*, WASH-1206 (April 1972), pp. 25–31.
4. J. H. DeVan, "Corrosion and Compatibility Problems of Thermonuclear Reactors," paper presented at the AIME Spring Meeting, Boston, May 8–9, 1972.

31. Transuranium Program

A. L. Lotts

The Transuranium Program is producing quantities of the heavier transuranium elements for research by successive neutron captures in ^{239}Pu. The program at ORNL started with primarily ^{242}Pu but at present most of the starting material is ^{244}Cm. Target elements containing these isotopes are fabricated in the transuranium processing facility (TRU) and irradiated in the High Flux Isotope Reactor. The target elements are removed periodically from HFIR and chemically processed in TRU to remove the actinides of interest to researchers. The remaining material is then reconstituted and returned as target elements to HFIR. In addition, special targets for irradiation in the HFIR Hydraulic Rabbit Facility and special capsules for researchers are prepared in this program.

The program at TRU is carried out jointly by the Chemical Technology, Metals and Ceramics, and Analytical Chemistry Divisions. Our present task in the program includes the fabrication of targets in TRU for HFIR, the fabrication of HFIR rabbits, the fabrication of special encapsulations for neutron and gamma sources, the evaluation of the performance of the target elements, and the improvement of the processing equipment in TRU as required.

TARGET FABRICATION

J. E. Van Cleve, Jr. L. C. Williams

The production line used to fabricate target rods containing $(Am,Cm)O_2$ as the starting material has operated with minimum trouble as feed was available. During this reporting period, 883 pellets were produced from curium prepared by the resin bead technique. Figure 31.1 shows the structure of a typical HFIR target pellet. A total of 24 targets were fabricated from pellets produced during FY 1972. To date, 19 of these targets, containing from 6.20 to 7.63 g ^{244}Cm each in the form of oxide microspheres, have been inserted within the HFIR core for irradiation. The remote target fabrication equipment has operated satisfactorily with only normal maintenance.

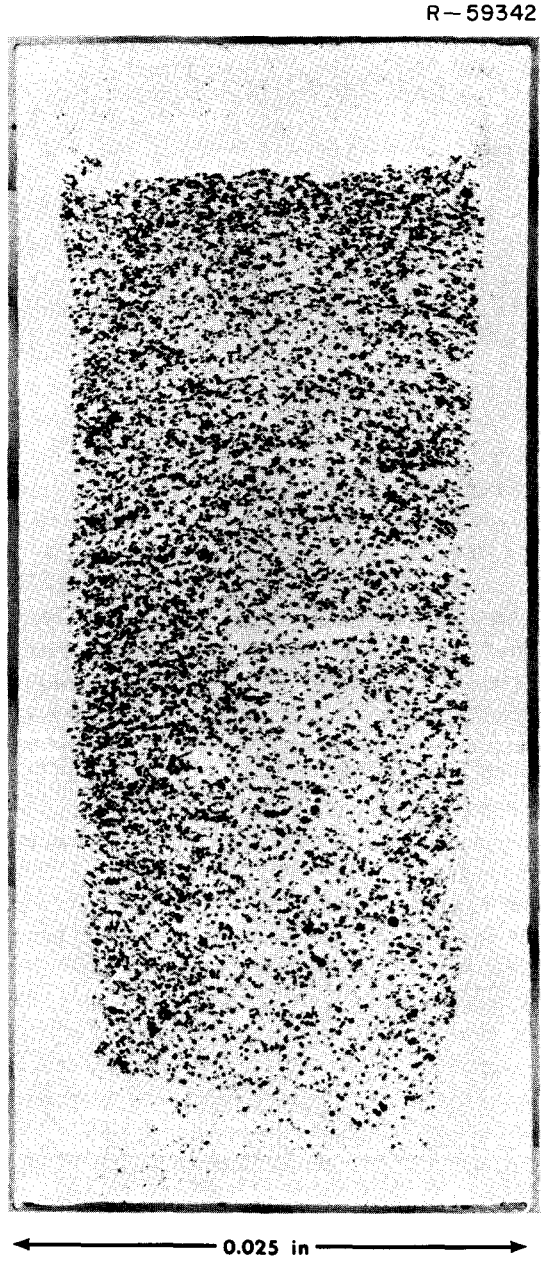

Fig. 31.1. HFIR curium-aluminum target pellet.

HFIR TARGET PERFORMANCE

J. E. Van Cleve, Jr. L. C. Williams

During FY 1972, 19 target rods that had been loaded with oxide shards were removed from the HFIR. Burnups ranged from 62.4 to 85.0% FIMA and fluences from 8.95 to 16.09 $\times 10^{22}$ neutrons/cm^2 (<0.41 eV) and 2.36 to 5.04 $\times 10^{22}$ neutrons/cm^2 (>0.82 MeV). After removal, each target was inspected before processing to recover the contained transuranium elements. No evidence of cracks in the target cladding was found. The pellets for these targets had been pressed to contain 20% void volume. The successful exposure of these targets once again confirms the validity of the target performance model.[1]

NEUTRON SOURCE FABRICATION

J. E. Van Cleve, Jr. L. C. Williams

Much of the ^{252}Cf recovered at TRU during the processing of irradiated HFIR targets is incorporated into neutron sources, which are subsequently loaned to researchers throughout the United States. The 28 sources fabricated during this report period ranged in ^{252}Cf content from 0.20 to 11.2 mg, with a total of 80.79 mg. Neutron sources as prepared at the TRU-TURF complex are supplied to the researcher sometimes singly but usually doubly encapsulated in type 304L stainless steel or Zircaloy-2, as shown in Fig. 31.2. Since the source is a very high neutron emitter, all containment closure welds, weld radiography, and containment leak detection must be performed in-cell.

SPECIAL PROJECTS

J. E. Van Cleve, Jr. L. C. Williams

The primary functions of the Transuranium Processing Facility group are to fabricate targets for irradiation in the HFIR and to encapsulate ^{252}Cf neutron sources

1. R. E. Adams, *Metals and Ceramics Div. Annu. Progr. Rep. June 30, 1971*, ORNL-4770, pp. 179–81.

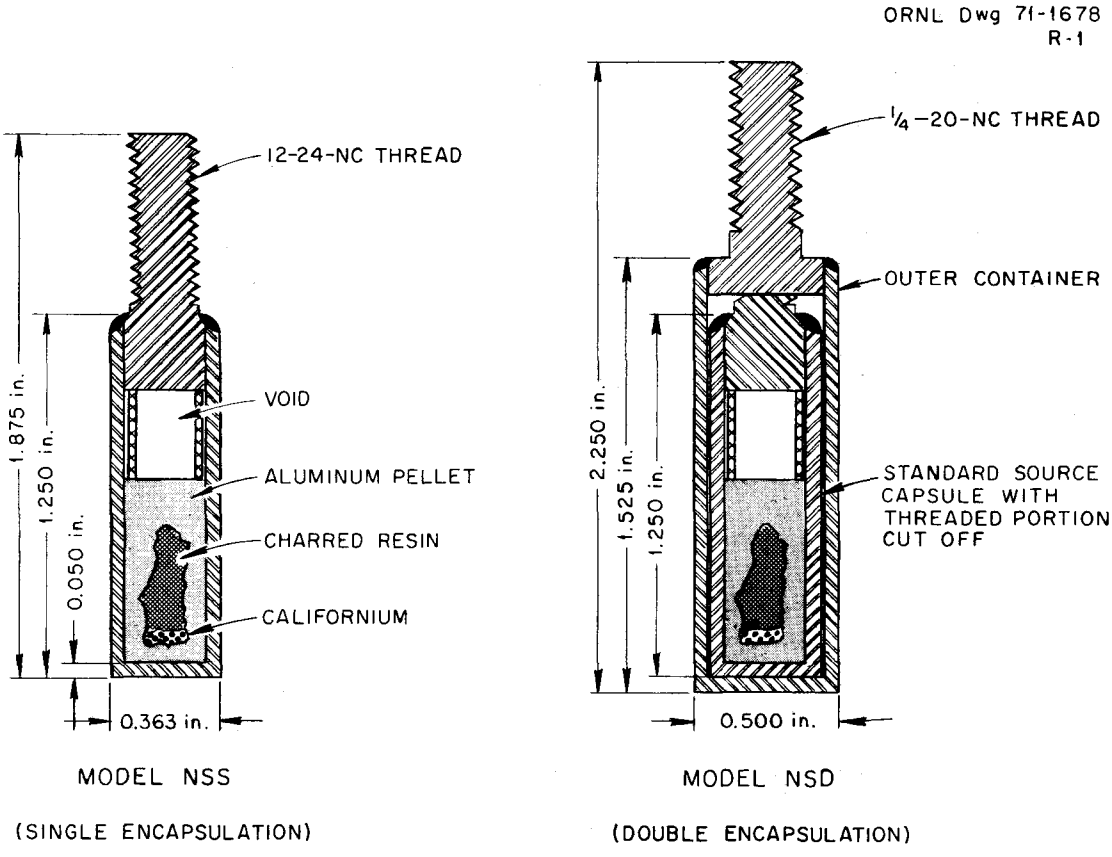

Fig. 31.2. Californium neutron sources.

for research. However, the facilities at TRU are also used for a variety of other purposes such as nonroutine productions, special preparations, and special irradiations in HFIR; in each case a unique service is provided to assist a research program at ORNL or another site.

Special Target

One special target was discharged from HFIR after 14,115 MWd and cut up at TRU for distribution to various experimenters. It had been fabricated from standard target rod hardware but contained a loading as shown in Table 31.1. The postirradiation examination of this target showed no evidence of cladding failure or deterioration.

HFIR Rabbit

A sample containing 250 μg of ^{240}Pu was encapsulated in a standard HFIR rabbit[2] for a five-day exposure in the HFIR Hydraulic Rabbit Facility.

In the general procedure for fabricating HFIR rabbits the minute quantities of the starting isotope are loaded into the rabbit by techniques developed jointly with Chemical Technology personnel. End closure welds are made and radiographed and the entire unit is helium leak tested before insertion into the reactor.

Special Source Fabrication

Two Mössbauer sources, GS-5 and GS-6, were made for experimenters working at the Transuranium Research Laboratory. Source GS-5 was loaded with 0.50 g of ^{240}Pu as the oxide, and GS-6 was loaded with 0.50 g of ^{238}Pu as the oxide. Both sources were doubly contained capsules fabricated from 6061 aluminum alloy. Both inner source containers were loaded and welded in-cell, and the outer container of GS-5 was completed out-of-cell. The outer container of GS-6 was completed in-cell because of the extreme hazard of the ^{238}Pu. Three $1\frac{3}{8}$-in.-diam $\times$ $\frac{1}{16}$-in.-thick absorbers – of ^{238}Pu, ^{236}U, and ^{234}U – were prepared for use in the same Mössbauer studies. Each of the absorbers was potted in epoxy. Figure 31.3 shows the completed source and the ^{236}U absorber in a holding fixture.

2. E. J. Manthos and J. E. Van Cleve, *Metals and Ceramics Div. Annu. Progr. Rep. June 30, 1969*, ORNL-4470, p. 163.

Table 31.1. Loading of special HFIR target

Target substance	Quantity (mg)	Number of units	Type of unit
^{252}Cf	0.010	1	Pellet
^{242}Pu	286	1	Pellet
^{244}Cm	286	1	Pellet
^{248}Cm	0.150	2	Capsules
Silicon		2	High-purity pellets
		2	Spacer–flux monitor pellets
^{244}Cm		16	Standard pellets to fill space

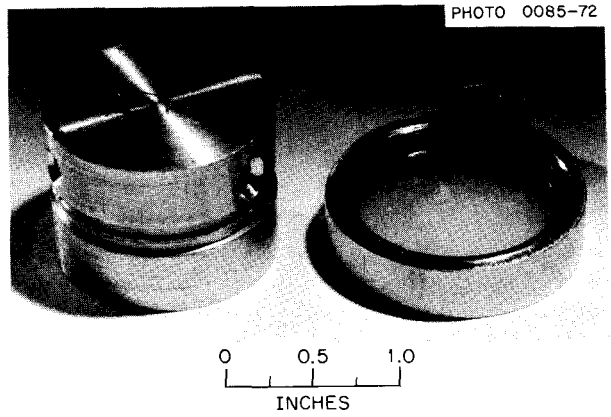

Fig. 31.3. Completed Mössbauer source (left) and uranium absorber (right).

SRL SHIPMENTS

J. E. Van Cleve, Jr. L. C. Williams

Ten shipments of ^{252}Cf containing from 7 to 37 mg each and one shipment of 90 g ^{244}Cm were made to the Savannah River Plant during this report period. The isotopes are prepared for shipment by encapsulation within a stainless steel container using in-cell welding equipment. Each container is inspected and decontaminated before loading into the Savannah River Plant shipping carrier.

DEVELOPMENT OF TECHNIQUES FOR NONDESTRUCTIVE DETERMINATION OF THERMAL CONDUCTIVITY OF TARGET PELLETS

J. E. Van Cleve, Jr. L. C. Williams

Determination of the thermal conductivity, λ, of individual HFIR target pellets would identify the defective pellets, which operate at unacceptably high temperatures. The purpose of this program is to develop a nondestructive, remotely operated test that can be used to determine the λ of every pellet. The approach is to develop an eddy-current technique for measuring

electrical resistivity, ρ, on the cermet cores of the pellets and use dc resistivity and λ measurements on simulated HFIR pellets to calibrate the test.

Thermal Conductivity and DC Electrical Resistivity Calibration Experiment

R. K. Williams R. S. Graves

The speed and accuracy of our comparative heat flow λ apparatus was improved by automatically controlling the temperature of the heater and cooling water. The accuracy improvement was possible because our apparatus modification allows for an isothermal intercomparison of the measuring thermocouples, and these comparisons have shown that the data analysis must account for some small heat losses.

Table 31.2 shows results of measurements on cold-pressed 90%-dense aluminum-Nd_2O_3 pellets. These data indicate that the small oxide particles are very effective in reducing the λ of the as-pressed pellets, but since the HFIR targets are also annealed before insertion in the reactor, measurements on partially sintered pellets are more representative.

Table 31.3 shows dc resistivity and λ data on pressed-and-sintered aluminum pellets. Although sintering has little effect on the density, large changes in ρ and λ were observed, especially for sintering temperatures above 550°C.

Four-probe dc measurements on over 200 samples were also obtained for use as eddy-current standards. These data were obtained with a quartz block knife edge apparatus using our Computer Operated Data Acquisition System for reading and calculating the data.

Table 31.2. Thermal conductivity at 30°C for as-pressed 90%-dense aluminum-Nd_2O_3 pellets

Oxide content (vol %)	λ, thermal conductivity (W cm^{-1} °C^{-1})
0	0.93
8.5	0.14
13.0	0.10
13.8	0.08

Table 31.3. Effect of sintering temperature on the bulk density, electrical resistivity, and thermal conductivity of cold-pressed aluminum pellets

Condition	Density (% of theoretical)	Electrical resistivity at 25°C ($\mu\Omega$-cm)	Thermal conductivity at 30°C (W cm^{-1} °C^{-1})
As pressed	Nominally 90	2000	0.93
	Nominally 90	875	1.03
2 hr, 400°C	89.8	279	
	90.6	467	1.16
2 hr, 450°C	90.2	267	
	90.6	377	
2 hr, 500°C	90.4	19.3	1.24
		29.5	
2 hr, 550°C	92.5	3.65	
	91.4	4.05	
2 hr, 600°C	91.1	4.16	
		4.12	1.75

Nondestructive Testing for Thermal Conductivity

C. V. Dodd W. A. Simpson

The development of an eddy-current test to measure the electrical conductivity (which determines the thermal conductivity as described above) of the aluminum–transuranium oxide core in the HFIR target pellet is proceeding on an analytical and experimental basis. Eddy-current conductivity measurements were performed on uncased pressed aluminum pellets. These measurements indicate that the pellets must be annealed for 2 hr at 550°C to produce pellets with good electrical and therefore thermal conductivity. Measurements have been completed on a new set of ac and dc conductivity standards. When the data reduction is completed this will allow more accurate ac conductivity measurement. The eddy-current technique measures the ac conductivity.

A set of standards has been machined with various diameters. These standards are being measured with various size coils to determine the effect of curvature that will be encountered on the pellets.

Another set of 18 standard pellets was constructed. These pellets had various case thicknesses, case conductivities, and core conductivities. Measurements were performed at two different frequencies to determine the effect of variations in thickness and conductivity of the case on the measurement of core conductivity. Variations in the case conductivity and thickness had a greater effect on the measurements than the same percentage variation in the core conductivity. Two-frequency techniques are being used to reduce these effects.

A computer program has been written to calculate the effect of all variations including drifts due, e.g., to temperature variations. Although this program performs calculations for flat plates, we believe that these results will be approximately correct for cylindrical shapes.

Part VI. Other Program Activities

32. Aluminum Fuel Element Development

R. G. Donnelly G. M. Adamson, Jr.

The objective of these activities is to advance the knowledge concerning those factors that limit irradiation performance of HFIR in particular and research and test reactors in general. These efforts have included evaluation of an irradiation experiment[1] conducted last year in addition to activities in support of the HFIR.

IRRADIATION DAMAGE OF UAl_x AND U_3O_8 FUEL DISPERSIONS[2]

M. M. Martin A. E. Richt
W. R. Martin

Miniature fuel plates were irradiated to determine factors that may influence the performance of aluminum-clad UAl_x and U_3O_8 dispersions in the Advanced Test Reactor (ATR) and the High Flux Isotope Reactor (HFIR). Our primary goal was to establish whether UAl_x- and U_3O_8-bearing fuel plates could be irradiated to fission densities greater than 1.8×10^{21} fissions/cm^3 without failure. The experiment, designated PM capsule 1, consisted of 18 uninstrumented single-core test plates and 3 instrumented double-core plates. It was irradiated in the permanent beryllium reflector region of HFIR for 11,613 MWd. The principal experimental variables were initial void content of the fuel dispersions (i.e., type of fuel dispersoid, dispersoid concentration, and fabrication procedure) and fuel dispersoid particle size. Two grades of U_3O_8, burned and high fired, and arc-cast UAl_x were used at dispersoid concentrations that corresponded to current HFIR and ATR loadings and 25% increases in these loadings.

Postirradiation examination of the test fuel plates showed all to be in excellent condition, without evidence of either actual or incipient failure. Maximum fuel core swelling of 8.8 vol % occurred in a UAl_x-bearing plate irradiated to a ^{235}U burnup of 1.8×10^{21} fissions/cm^3 at 63 to 80°C. The swelling behavior of the aluminum-clad U_3O_8-Al and UAl_x-Al dispersions, however, depended primarily upon the fission density and the effective void content of their cores during irradiation; it was independent of the fuel dispersoid size distribution of less than 44-μm particles. Variations in fuel dispersoid concentration and fuel plate fabrication procedures can alter the void content of these dispersions and, consequently, affect significantly their irradiation-induced swelling behavior.

HFIR FUEL ELEMENT PRODUCTION ASSISTANCE

R. W. Knight

Assistance to Texas Instruments, Inc., has continued throughout the past year. To date, 122 fuel assemblies have been fabricated. The incidence of fuel plate rejections is shown in Table 32.1. The overall yield for 78,262 fuel plates is 92.5%, which is an increase of 0.79% over FY 1971.

A total of 34 approval requests were processed this year. A breakdown of these requests is: 7 for fuel plate waivers; 12 for drawing-route card and standard operating procedure revisions, 7 for purchase of equipment and materials; 4 for disposal or transfer of equipment and materials; 3 for transmission of data on experiments; 1 for revision of fuel element numbering system in accordance with the new AEC directive.

A limited manufacturing run using unclad 6061 alloy for cover plates and frames is continuing. No change in fuel plate yield has been noted, and only slight changes in production parameters are required.

1. M. M. Martin, *Metals and Ceramics Div. Annu. Progr. Rep. June 30, 1971*, ORNL-4770, p. 124.
2. Abstract of report in preparation.

Table 32.1. HFIR fuel plates rejected during manufacture[a]

Reason for rejections	FY 1972		FY 1971		All production to date	
	Number rejected	Percent	Number rejected	Percent	Number rejected	Percent
Compacts	3	0.03	6	0.06	290	0.37
Surface	30	0.31	21	0.23	2039	2.60
Bond defects	100	1.04	134	1.45	3681	4.70
Core location	17	0.18	31	0.33	645	0.82
Homogeneity	137	1.42	122	1.32	1536	1.96
Dimensions	0	0	0	0	142	0.18
Form	1	0.01	0	0	37	0.04
Miscellaneous	3	0.03	0	0	239	0.30
Total	291	3.02	314	3.39	8609	11.00
Accepted on waiver	109	1.13	110	1.19	2735	3.49
Net rejected	182	1.89	204	2.20	5874	7.50

[a]Number manufactured 9624 in FY 1972, 9264 in FY 1971; 78,262 total.

Welding parameters were changed to compensate for a shift in the characteristics of the welding machine. The manufacturer's technicians were called in to check out the machine, and it is still operative within the original design parameters. Work is still continuing on this problem.

Route cards, drawings, and standard operating procedures have been completed to incorporate Al_2O_3 addition to the filler section to increase void volume when approved for production. Similar work has been done for unclad alloy 6061 for frame and cover plates to be used when the present supply of alclad 6061 runs out.

POSTIRRADIATION EXAMINATION OF HFIR FUEL ELEMENTS 100-I AND 100-O

A. E. Richt R. W. Knight

Postirradiation examination of spent HFIR fuel elements 100-I and 100-O is currently under way. Six of the fuel plates in each of these two special fuel elements contain the so-called "burned" grade of U_3O_8, which is considerably less expensive than the "high-fired" type of U_3O_8 currently used in manufacturing fuel plates for the standard HFIR fuel elements. The primary objective of this program is to determine if fuel plates containing burned U_3O_8 perform satisfactorily under actual HFIR operating conditions.

Although the postirradiation examination program is not entirely complete, results obtained to date indicate that the plates containing burned U_3O_8 performed at least as well as and, in some respects, even better than fuel plates containing the high-fired oxide. Both elements operated for a total of 2340 MWd in HFIR (the normal reactivity lifetime of the HFIR fuel elements) with no indications of a fuel plate failure. No evidence of structural damage or significant dimensional changes was apparent during inspection of fuel plates of either type. Sections of the irradiated fuel plates were heat treated to determine the breakaway swelling or blistering temperature of both types of fuel plates. As shown in Fig. 32.1, the blistering temperature of the burned U_3O_8 plates was about 150°C higher than that of the corresponding high-fired U_3O_8 plates.

Should metallographic examination of sections of the irradiated fuel plates reveal no unexpected problems, we would conclude that the cheaper burned U_3O_8 fuel plates will perform quite satisfactorily in HFIR service. Furthermore, the postirradiation blistering tests indicate that the burned U_3O_8 fuel plates would be superior to the standard high-fired U_3O_8 fuel plates during any type of reactor excursion.

MATERIALS PERFORMANCE IN HFIR CONTROL CYLINDERS[3]

R. W. Knight A. E. Richt

The irradiation behavior of the High Flux Isotope Reactor (HFIR) control cylinders has been assessed. After 48,000 MWd of irradiation, the nuclear worth of the control cylinder has not changed significantly. The maximum surface oxide buildup was 0.003 to 0.005 in. thick and occurred over the tantalum-aluminum dispersion. The hardness of the 6061 alloy cladding had

3. Abstract of paper to be published in *Nuclear Technology*.

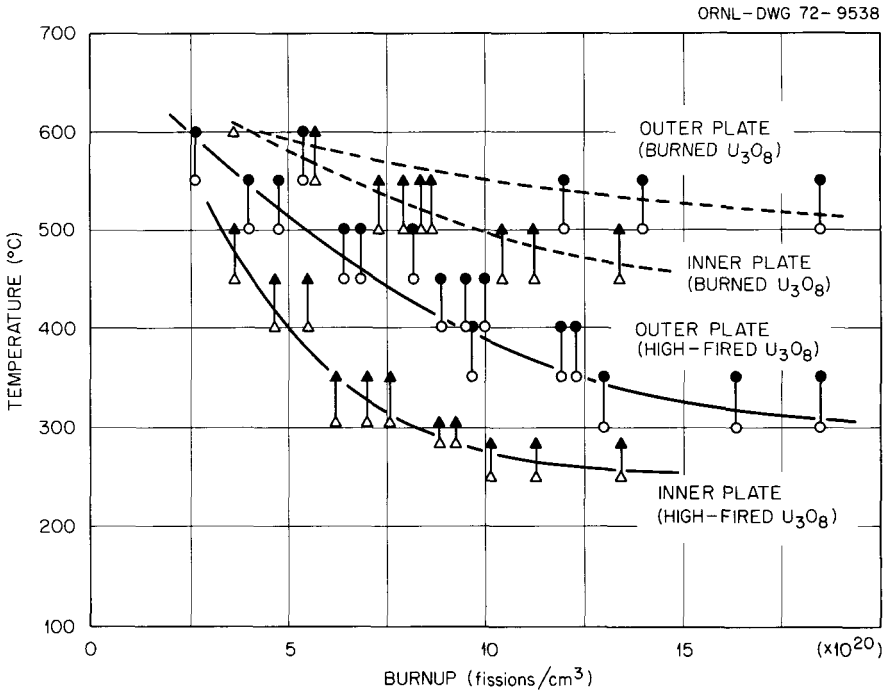

Fig. 32.1. Blistering temperature of HFIR fuel plates with burned and high-fired U_3O_8 as a function of burnup.

increased from 45 DPH at the low-burnup end of the cylinder to 110 DPH over the tantalum-aluminum region, which is located about 5 in. below the area of maximum fast-neutron fluence. Extensive metallographic examination revealed no degradation or reaction in either the tantalum-aluminum or Eu_2O_3-Al portions of the cylinder.

EFFECT OF IRRADIATION ON CREEP-RUPTURE OF 5052 ALUMINUM ALLOY AT 50°C

R. T. King D. R. Cuneo
A. Jostsons[4]

Irradiation damage in the 5052 aluminum alloy (nominally Al–2.5% Mg) was studied. This alloy is of interest because it is used as a reactor structural material. The magnesium in solid solution combines with silicon produced by transmutation of the aluminum to form Mg_2Si precipitate particles during irradiation.[5] The precipitate is finely dispersed throughout the matrix, without any denuded region adjacent to grain boundaries.

Unirradiated 5052 alloy fails at 50°C in creep-rupture tests at stresses between 25,000 and 30,000 psi in times ranging from about 1000 to 0.1 hr respectively. Fractures in the solid-solution alloy are transgranular and characterized by shear dimples, and fracture strains exceed 25%. However, after irradiation at about 50°C to neutron fluences from 0.5 to 1.33 X 10^{22} neutrons/cm^2 (>0.1 MeV), the stresses required to cause failure after about 1000 hr in postirradiation tests were between 52,000 and 56,000 psi. Little, if any, third-stage creep occurred. Fractures originated as intergranular cracks near the surfaces of the specimens and propagated by primarily intragranular shear tearing to link up intergranular cracks that had formed earlier within the specimens. The total elongations of the failed specimens were about 1%. This is the first reported observation of intergranular failure in an as-irradiated aluminum alloy at 50°C.

The strength increase due to irradiation is primarily related to the formation of the Mg_2Si precipitate phase. Intergranular cracking, which led to failure of the irradiated specimens, may be related to the relative ease of deformation in the strengthened matrix and at grain boundaries.

4. On attachment from Australian Atomic Energy Commission Research Establishment.

5. A. Jostsons and R. T. King, "Transmutation-Produced Mg_2Si Precipitation in As-Irradiated Al–2.5% Mg Alloy," *Scripta Met.* 6, 447–51 (1972).

33. Flaws in Welds Studied by Autoradiography[1]

J. P. Hammond G. M. Slaughter

Weld-associated flaws such as cracks, imcomplete alloying, segregates, and dross formation were investigated in welds in types 347 and 304 stainless steel and between Incoloy 800 and Inconel 625 with autoradiography and conventional metallography.[2] By introducing the radioisotope ^{63}Ni homogeneously within filler metal wires (1 mCi/cm^3 of metal) and preparing welds in untraced base metals, many of these features were readily delineated and their character and origin studied. The isotope ^{14}C distributes selectively, and its introduction in type 347 stainless steel revealed the character of carbon segregation (both chemically combined and in solid solution) in this alloy. Isotopes ^{35}S and ^{33}P also distribute selectively, and these tracers are being used to investigate the roles of sulfide and phosphide segregates in weld cracking.

In multipass welds joining the base metals Incoloy 800 and Inconel 625 with ^{63}Ni-traced Inconel 82 filler metal wire, a distinct pattern of heterogeneous alloying between filler metal and base metal was disclosed. The root pass showed the greatest inhomogeneity as well as greatest base metal dilution. Progressively decreased base metal alloying occurred in the second and third layers of weld passes, and subsequent layers were very high in filler metal content. In weld passes adjoining fusion lines, modest overall base metal dilution was noted, but at isolated locations along the fusion line, substantial amounts of base metal concentrate were found contained within the weld desposit. This, together with the disclosure of severe impoverishment with respect to filler metal in the vicinity of the root face of the weld, is most significant, since weld cracking frequently initiates in these regions, and special effort is made to evenly distribute the filler metal to discourage cracking.

Surface encrustations found principally on the root pass of dissimilar-metal welds between Incoloy 800 and Inconel 625 (usually adjoining the Inconel 625 side) were related to contaminants associated with the shielding gas and the base metals together with the elements titanium and aluminum appearing in minor amounts in filler and base metals. These crusts were characterized by autoradiographic means and appropriately labeled dross. Figure 33.1 illustrates flaws disclosed autoradiographically in a weld between Incoloy 800 and Inconel 625.

---

1. Sponsored by Edgewood Arsenal of the U.S. Army.

2. J. P. Hammond, G. M. Slaughter, and F. B. Gurtner, "Heterogeneity of Fusion Welds Determined by Use of ^{63}Ni-Tagged Filler Metal," paper IAEA/SM-159/22 presented at the Symposium on the Use of Nuclear Techniques in the Basic Metal Industries, Helsinki, Finland, July 31 – August 4, 1972.

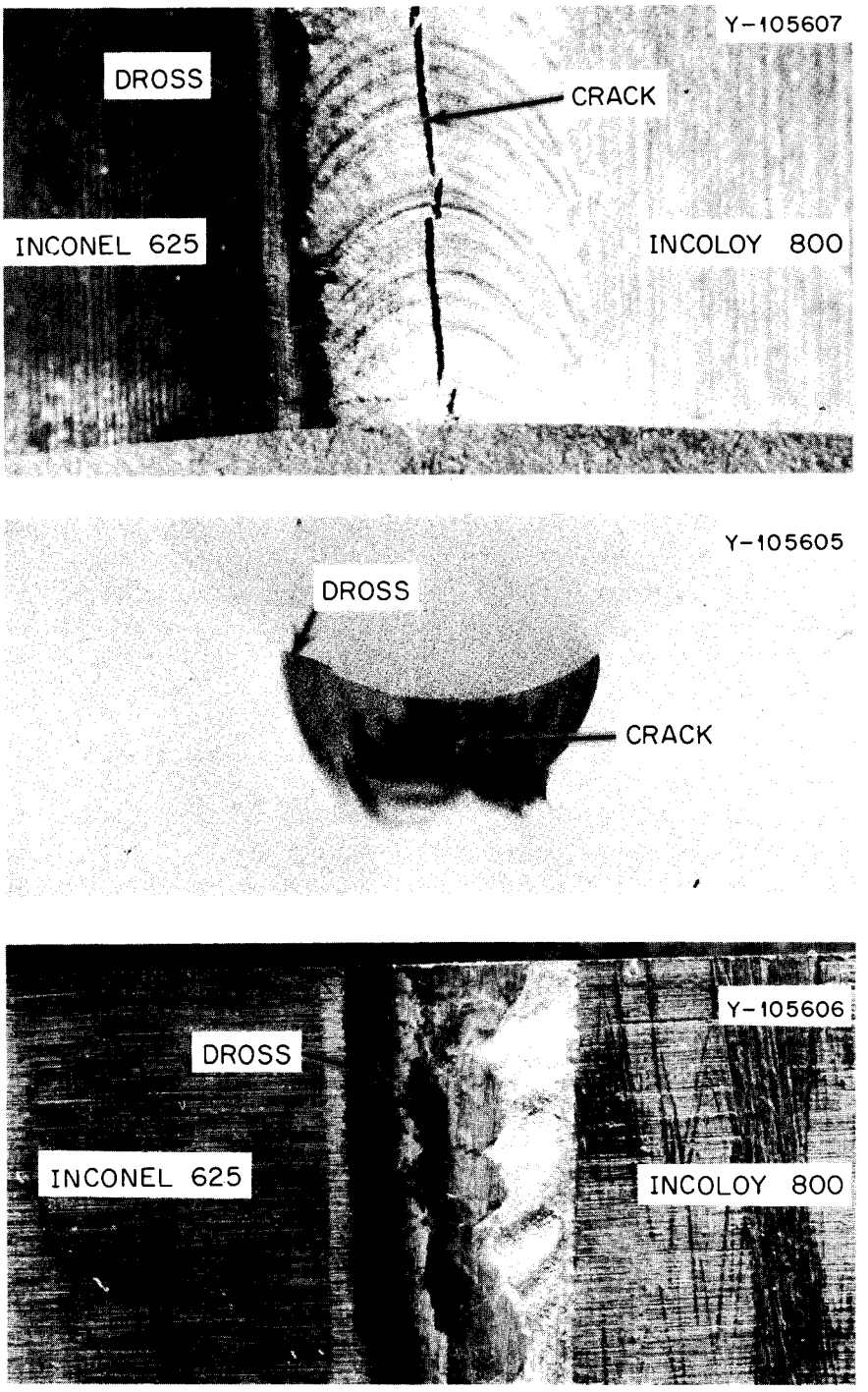

Fig. 33.1. Root pass made between Incoloy 800 and Inconel 625 with ^{63}Ni-containing Inconel 82 filler metal. 5×. Top: surface of face side. Middle: contact autoradiograph of weld cross section. Bottom: surface of root side. Arrows at side of photographs locate section of autoradiograph. Evidence of weld cracking is seen in the autoradiograph along with inhomogeneity of mixing between filler metal and base metal. Dross is seen in the photographs on the face and root sides.

34. Fabrication of Plutonium Test Element

A. L. Lotts C. F. Sanders J. D. Sease

Plutonium is very attractive for high-temperature gas-cooled reactors to replace makeup ^{235}U. Plutonium has a value of \$9 to \$10 per gram for this use.[1] The use of plutonium requires additional containment for fuel element fabrication, but this is offset by eliminating the need for mechanical separation of spent ^{235}U from the bred ^{233}U. Shielding and containment safeguards and remotely operable equipment required for ^{233}U will meet the similar needs for fabricating plutonium. As part of a joint program with the Edison Electric Institute, Gulf General Atomic designed the Plutonium Test Element for irradiation in the Peach Bottom Reactor. We developed processes and materials for this fuel element and later fabricated the plutonium-bearing fuel components for the test element. This is the first plutonium fuel fabricated in this country for irradiation testing in an HTGR. The PTE was placed in the Peach Bottom Reactor during May 1972 and will complete its irradiation in summer 1974.

The fissile kernels for the test element are nominally 100- and 200-μm-diam PuO_2 and 350-μm-diam ThO_2–25% PuO_2. Oxygen-to-plutonium ratios of 1.70 and 1.84 were used for both the large-diameter PuO_2 and the $(Th,Pu)O_2$ kernels. The small PuO_2 kernels were adjusted to the high oxygen-to-plutonium ratio. We used the TRISO coating, which is similar to that on particles for the Fort St. Vrain Reactor[2] and consists of successive layers of low-density pyrolytic carbon, high-density pyrolytic carbon, and silicon carbide, with an outer layer of high-density pyrolytic coating. A summary of the plutonium test element fabrication was presented at the 1972 American Nuclear Society Annual Meeting.[3]

KERNEL PREPARATION

C. F. Sanders R. G. Wymer[4]

The plutonium-containing fuel kernels were prepared by ORNL sol-gel processes.[5,6] The ThO_2-PuO_2 microspheres were made by mixing sols of the two constituents. The fissile microspheres were sintered in argon to 1200°C and then heat treated at 1450°C in Ar–8% H_2 to obtain the oxygen-to-plutonium ratio of 1.84. The 1.70 ratio was obtained by an additional heat treatment in pure hydrogen at 1750°C. The ThO_2 particles were prepared by the conventional sol-gel process.[7] The properties of the kernels prepared for the PTE are summarized in Table 34.1.

COATING

C. B. Pollock D. M. Hewette II E. S. Bomar

The TRISO II coating of this fuel includes a layer of silicon carbide. We previously had coated fuel particles with carbon and partially evaluated the coatings. However, the silicon carbide had not previously been deposited on plutonium-containing fuel particles, and none of the coatings had been subjected to a rigorous

1. H. B. Stewart, R. C. Dahlberg, W. V. Goeddel, D. B. Trauger, P. R. Kasten, and A. L. Lotts, "Utilization of the Thorium Cycle in the HTGR," pp. 2.6-18-2.6-35 in *U.S. Papers for the Fourth United Nations International Conference on the Peaceful Uses of Atomic Energy, Geneva, Switzerland, Sept. 6–16, 1971*, vol. 1.

2. Oak Ridge National Laboratory and Gulf General Atomic, *National HTGR Fuel Recycle Development Program Plan*, ORNL-4702 (August 1971). See also Chap. 29 of this report.

3. J. D. Sease, C. F. Sanders, W. P. Eatherly, D. P. Harmon, and W. J. Scheffel, "Fabrication of Plutonium Fuel Elements," *Trans. Amer. Nucl. Soc.* **15**, 190 (1972).

4. Chemical Technology Division.

5. J. P. McBride, *Laboratory Studies of Sol-Gel Processes at Oak Ridge National Laboratory*, ORNL-TM-1980 (September 1967).

6. P. A. Haas, C. C. Harris, Jr., F. G. Kitts, and A. D. Ryon, *Engineering Development of Sol-Gel Processes at Oak Ridge National Laboratory*, ORNL-TM-1978 (January 1968).

7. R. G. Wymer, *Laboratory and Engineering Studies of Sol-Gel Processes at Oak Ridge National Laboratory*, ORNL-TM-2205 (May 1968).

Table 34.1. Summary of properties of kernels for plutonium test element

Item	Composition	Diameter (μm)			Density		Iron content[c] (ppm)	O/Pu	EBC[d]
		Range[a]	Average	σ	Grams per cubic centimeter	Percent of theoretical[b]			
1	PuO_{2-x}	63–125	110.0	14	10.70	97.2	85	1.81	<2
2	$Th_{0.75}Pu_{0.25}O_{2-x}$	295–420	349	31	9.90	97.2	291	1.69	<2
3	ThO_2	350–450	396	17	10.0	99+	30		50
4	PuO_{2-x}	150–250	202	19	10.36	96.9	<50	1.68	<2
5	$Th_{0.75}Pu_{0.25}O_{2-x}$	295–420	357	28	10.09	98.4	291	1.84	<2
6	PuO_{2-x}	150–250	181	23	10.8	95.7	85	1.84	<2

[a]Screen cut.

[b]Theoretical density calculated for plutonium oxide by $\rho = 10.952 + 0.506y - 2.4Z$, where y = atom fraction of Pu in heavy metal and $Z = 2.00 - O/M$ ratio. For $(Th,Pu)O_2$, density of ThO_2 assumed to be 10.00 g/cm^3; influence of Pu content calculated with previous formula.

[c]Iron content determined by quantitative wet chemical analysis; the approximate precision is ±50 ppm.

[d]Equivalent boron content determined using 2200 m/sec cross sections, *Radiological Health Handbook,* U.S. Department of Health, Education, and Welfare, 1970.

quality control program such as the one to be used in this contract.

The coating program was divided into three parts: equipment design and assembly, fabrication, and inspection. A coating furnace suitable for this application was available in a glove box approved for plutonium operations. To accommodate SiC coatings an off-gas scrubbing system containing solid $CaCO_3$ in NaOH was developed for the HCl vapors produced. The off-gas from carbon coatings consists primarily of hydrogen, which we diluted by air. Important safety features included several absolute filters, hydrogen gas alarms, and numerous pressure sensing devices. The carbon coatings were conventional low-temprature coatings derived from propylene and acetylene, and the silicon carbide was derived from methyltrichlorosilane.

Major achievements in this phase of operation were the successful coating of very small (100 μm) particles of PuO_2 with layers of SiC and carbon and the absence of alpha contamination on the surface of the coatings.

The particles were inspected after each operation by microradiography, metallography, and various chemical analytical techniques. The densities of coatings were determined by a density gradient column technique and checked by mercury density measurements. Coating thicknesses were measured from microradiographs, and polished cross sections of the coated particles were used to inspect the microstructure of the coatings. The degree of isotropy of the carbon coatings was estimated visually under polarized light. A composite of the micrographs of the coated plutonium particles in bright field and polarized light is shown in Fig. 34.1. The surface alpha contamination was less than 10^{-8} of the contained plutonium, which was extremely good. The data from the inspection program were statistically treated, and the particles satisfied the design criteria.

FUEL STICK FABRICATION

R. A. Bradley W. H. Pechin C. F. Sanders

The coated plutonium-bearing particles were blended with BISO-coated ThO_2 and formed into sticks by injection of a binder of coal tar pitch and 28.5 wt % graphite flour at 150°C and 750 psi by the slug injection process described in Chap. 29 of this report. The sticks were then carbonized at 800°C and annealed at 1800°C. The processes and equipment necessary to fabricate and inspect the sticks had to be developed, and special plutonium glove box equipment for both fabrication and inspection had to be designed, fabricated, installed, and checked out. The equipment operated satisfactorily with no difficulty.

We made approximately 200 0.5-in.-diam × 2-in.-long sticks with essentially 100% acceptance, and 120 were incorporated into the test element. The dimensional control was extremely good within a stick, and the stick-to-stick maximum diameter variation was ±0.001 in. The fuel distribution as determined by gamma spectrometry was satisfactory, and the transferrable alpha contamination was less than 300 dis/min. Fission gas release analysis, which measures combined stick contamination and fuel particle breakage, gave a release-to-birth ratio for Kr^{85m} from 2×10^{-6} to 1×10^{-4}. After incorporation in the graphite element the surfaces were free of all contamination.

ORNL-DWG 71-14339

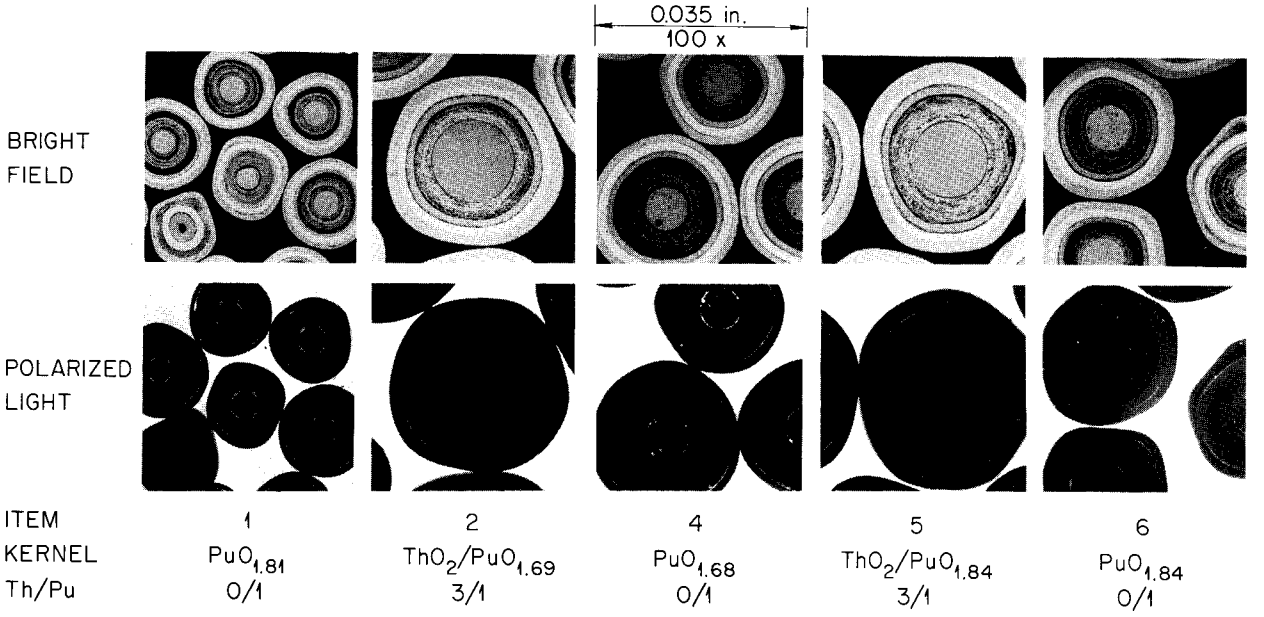

Fig. 34.1. Fissile particles for plutonium test element.

35. Development for the Light Water Breeder Reactor

A. L. Lotts J. L. Scott

The Light Water Breeder Reactor (LWBR) is being developed to demonstrate the feasibility of breeding with a thermal neutron spectrum in an existing light water reactor. The Bettis Atomic Power Laboratory (BAPL) has primary responsibility for this program. Our participation has been the development of a process to be used by the Chemical Technology Division to purify ^{233}U and prepare UO_2 powder for the program, using the process to prepare experimental batches of the powder, and fabrication of $(Th,^{233}U)O_2$ and $^{233}UO_2$ pellets for special experiments.

The powder process development described previously[1] has been completed, and the final report on it is abstracted below. We used the process to prepare 30 kg $^{235}UO_2$ powder for testing by BAPL. The Chemical Technology Division is now successfully using it in a 20-kg/week semiremote pilot plant.

CONVERSION OF URANIUM NITRATE TO CERAMIC-GRADE OXIDE FOR THE LIGHT WATER BREEDER REACTOR: PROCESS DEVELOPMENT[2]

J. M. Leitnaker M. L. Smith[3]
C. M. Fitzpatrick

A limited study was made of an "ADU" process to make UO_2 for use as fissile material dissolved in ThO_2. A factorial study of precipitation included measuring the effects of initial nitric acid content of uranyl nitrate, the temperature of precipitation, the final pH of the solution, and time of digestion on the composition of the uranate cake and the surface area and tap density of the final powder. Studies of drying measured the effect of time, temperature, and grinding of the yellow cake on the surface area and tap density of the final powder. Effects of temperature and time were studied on the composition and surface area of "UO_3" made by heating ammonium uranate in argon. Effects on surface area of the temperature of reduction of uranate in H_2 were studied. Factors affecting stabilization of UO_2 powder were also studied, and the mechanism causing ignition of UO_2 was elucidated.

FABRICATION OF ThO_2-$^{233}UO_2$ PELLETS

E. S. Bomar

A series of ThO_2-$^{233}UO_2$ pellets was needed by Bettis Atomic Power Laboratory for neutron attenuation experiments as part of their program on the Light-Water Breeder Reactor (LWBR). We fabricated about 300 pellets to meet their requirements, using ThO_2 supplied by BAPL and a special lot of $^{233}U_3O_8$ containing 99.54% ^{233}U and <1 ppm ^{232}U, which came from Savannah River. Three pellet sizes and six compositions representing nine combinations were required; the $^{233}UO_2$ content ranged from 0.95 to 5.57%.

We obtained preliminary shrinkage and homogeneity data using ThO_2-$^{235}UO_2$ mixtures as stand-in material. Wet blending in hexane and sintering at 1850°C for 3 hr gave the required minimum density of 9.0 g/cm^3. Examination with the electron-beam microprobe and the scanning electron microscope showed that during sintering the UO_2 dissolved in the ThO_2 matrix, leaving a porous structure and localized high concentrations of uranium. The experimentalist at BAPL confirmed, however, that the degree of homogeneity obtained was satisfactory for their requirements.

The ^{233}U was supplied as $^{233}U_3O_8$. We reduced this to $^{233}UO_2$ with Ar–4% H_2. The first pellets made from the $^{233}UO_2$-ThO_2 mixtures had lamination defects due to loss of moisture from the surface of the powders during handling in the dry argon atmosphere of the glove box. This difficulty was corrected by making a controlled addition of 1% by weight of water.

1. J. D. Sease and J. M. Leitnaker, *Metals and Ceramics Div. Annu. Progr. Rep. June 30, 1971*, ORNL-4770, pp. 199–200.
2. Abstracted from ORNL-4755 (April 1972).
3. Co-op student from Virginia Polytechnic Institute and State University.

During the subsequent sintering runs a substantial majority of the pellets were held, without grinding, to the specified dimensional tolerances: ±3 mils or 1.2% for the smaller pellets and ±5 mils or 1% for the larger pellets. Representative samples were characterized by microscopic examination, autoradiography, dimensional measurements, density, uranium and impurity determinations, and measurement of isotopic content.

FABRICATION OF HIGH-PURITY $^{233}UO_2$ PELLETS

T. G. Godfrey

Two groups of $^{233}UO_2$ pellets were fabricated for physics experiments at Knolls Atomic Power Laboratory. The first group of 44 pellets, 0.240 ± 0.001 in. diam by 0.140 in. long, was made from ultrahigh-purity ^{233}U specially calutron-separated and converted to U_3O_8 by the ORNL Isotopes Division. We reduced the oxides, developed the fabrication scheme, and cold pressed and sintered the pellets in a specially outfitted new alpha glove box in the Interim Plutonium Laboratory. The second group of 102 pellets, 0.240 in. diam by 0.245 in. long, was similarly made from a larger batch of high-purity $^{233}U_3O_8$ to a specified diametral tolerance of ±0.001 in.

36. Graphite Fabrication Studies for Naval Ordnance Laboratory

C. R. Kennedy W. P. Eatherly

New generations of submarine-launched missiles require improved materials for the nose tip, the two properties of interest being ablation and thermal-shock resistance. An outgrowth of the program to produce radiation-resistant reactor graphites has been fabrication techniques that potentially offer graphites with significantly improved nose-tip performance.

Ordinarily graphites are fabricated from a calcined or graphitized coke filler powder and an aromatic binder, commonly pitch. The filler material is relatively stable in volume during subsequent heat treatment, whereas the binder material shrinks some 60 to 70% during graphitization. The resultant structure therefore contains voids and microcracks, which obviously weaken the material.

Our approach to overcome this problem is to employ green cokes as filler materials (i.e., cokes formed at temperatures as low as 400°C). Such materials are still chemically active and shrink some 35% in volume during heat treatment, thus more nearly matching the binder behavior. By employing complex heat-treatment processes, the filler and binder shrinkage characteristics can be closely matched, and the final graphite takes on a crack-free monolithic structure.

The thermal-shock resistance of graphite is a complex function of both the thermal and mechanical properties, but one sensitive key is the ratio of strength to Young's modulus. Figure 36.1 contrasts this ratio for various experimental graphites formulated at ORNL against conventional commercially available graphites. The improvement is obvious.

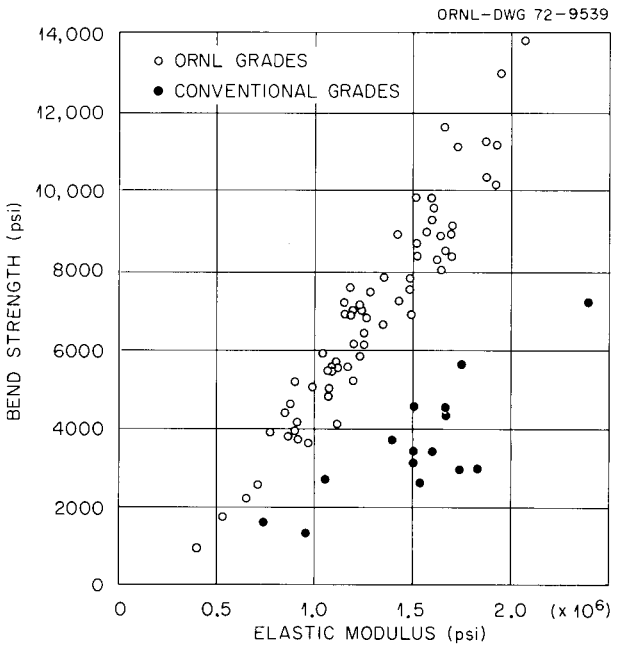

Fig. 36.1. Strength-to-modulus ratio comparison of ORNL graphites to conventional grades.

37. Metallography

R. J. Gray

Three metallography groups continue to carry the service load. The General Metallography Group studies nonradioactive and alpha radioactive samples, the Electron Metallography Group is responsible for scanning electron microscopy and microprobe analysis, and the Radiation Metallography Group studies radioactive materials requiring hot cell shielding and remote handling. In addition to service functions, technique developments and research and development activities are conducted to allow us to keep abreast of the art and science of metallography performed by other metallographers and allow us to make contributions in our particular areas of expertise.

SCANNING ELECTRON MICROSCOPY

D. R. Cuneo

In October 1971 we installed a Japan Electron Optics Laboratory model U3 scanning electron microscope at the hot cell area (High Radiation Level Examination Laboratory). This valuable supplement to data analysis has operated with less than 5% downtime due to failure of any of its components. We have utilized it to examine fracture surfaces of metal and ceramic materials, primarily for experimenters within the Division; however, examinations have been performed for at least four other ORNL divisions.

Our scanning electron microscope has a magnification range of about 50 to over 100,000X. Generally little is learned from surveying specimens of interest to the Division of magnifications greater than 30,000X. The microscope is usually operated to detect secondary electrons emitted from the specimen surface, because in this mode of operation the topography displayed is independent of variations in surface composition. If the microscope is operated as a backscattered electron detector, the display will reflect variations in the atomic number of elements in the surface being scanned. The microscope has the capability of being operated as a transmission electron detector for thin or replicated specimens. Attempts were made to utilize this capability in conjunction with the nondispersive x-ray attachment to determine metallic elements in animal tissue. Such usage led to contamination of the electron optics system of the microscope, necessitating frequent cleaning of the components. Attempts to use the x-ray attachment to analyze areas of interest on specimens with significant beta-gamma activities revealed that such activities jam the x-ray detection system. We hope to circumvent this limitation.

Although most of our examinations have been carried out for nonradioactive specimens, by use of simply constructed lead holders we have been able to examine and photograph the topography of specimens with beta-gamma activities as great as 10 to 15 R/hr with no exposure to the operator. We expect to construct a small holder from depleted uranium to allow examination of specimens of somewhat greater activities. A partial listing of materials examined includes: various stainless steels, aluminum, special alloys such as T-111, graphite with and without coatings, neutron absorber materials such as B_4C and Eu_2O_3, fuel microspheres with and without coatings, particles from a gas filter system of the Peach Bottom Reactor, and broken resin bead screening from the HFIR.

Although the photographs shown in Fig. 37.1 are at quite low magnification, we believe they demonstrate rather dramatically the value of pre- and postirradiation scanning microscopy for materials of interest in reactor development programs. The *a* view shows an unirradiated anistropic pyrocarbon strip that was of approximately the same thickness (*c* axis) as the irradiated strip seen in the *b* view. The length and width of the irradiated specimen decreased to about one-half of the preirradiation dimensions, while the thickness increased 6 to 7 times.[1]

A fracture surface of B_4C irradiated for 9700 MWd and described in Chap. 14 is displayed in Fig. 37.2. By

1. Experiment by D. M. Hewette II, C. R. Kennedy, W. H. Cook, and W. P. Eatherly.

R-59590

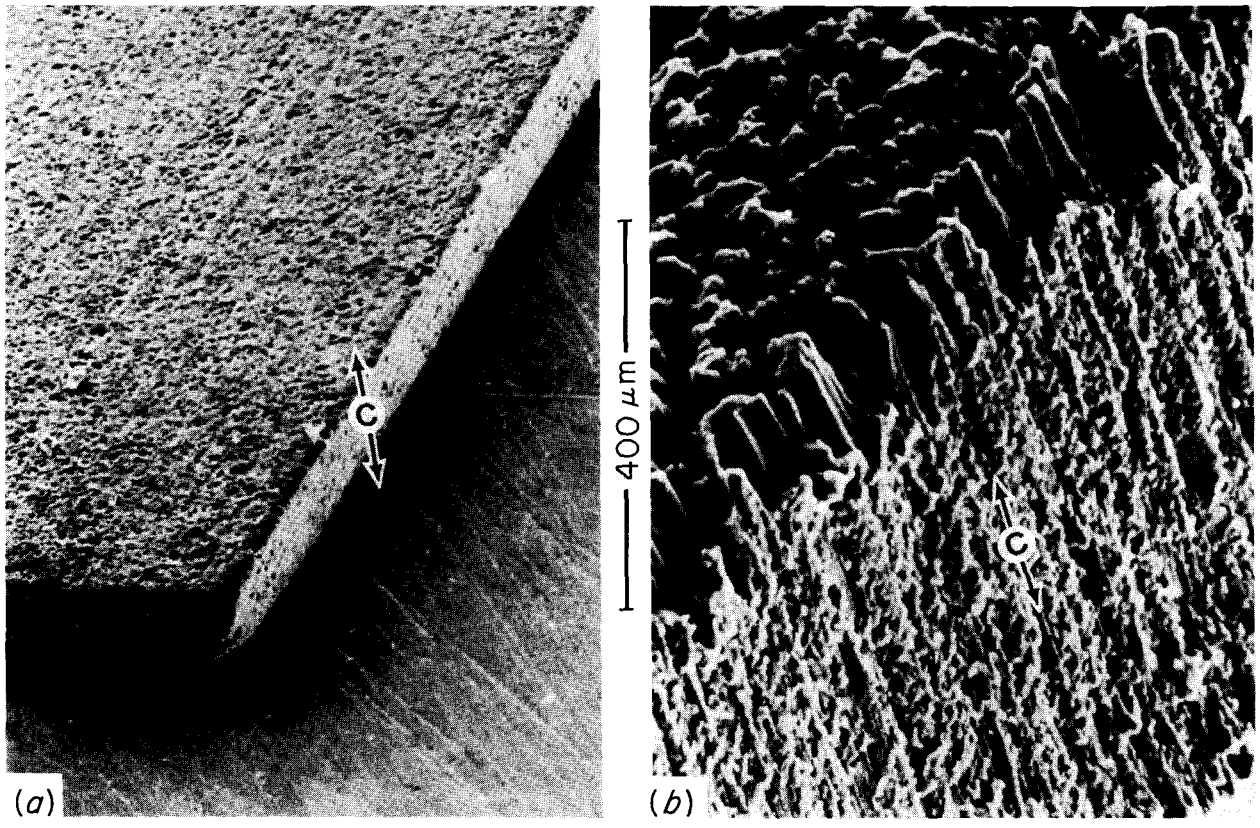

Fig. 37.1. Pyrolytic carbon strips deposited from methane at 2000°C. (*a*) Unirradiated control, (*b*) specimen irradiated at 715°C to a fluence of 3.2×10^{22} neutrons/cm^2 (>50 keV).

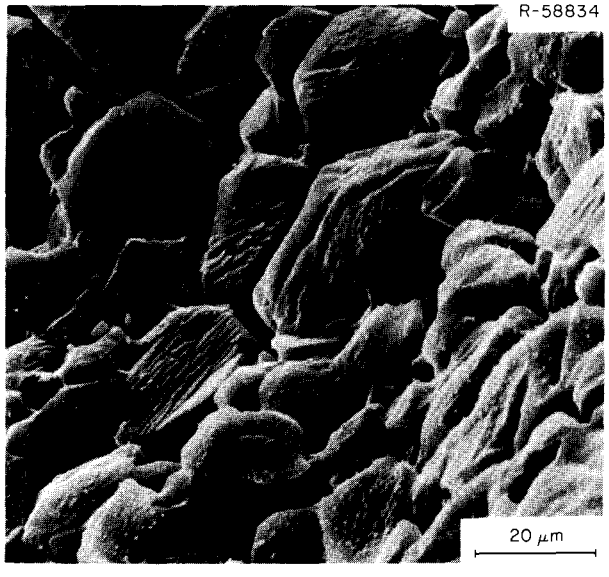

Fig. 37.2. Irradiated B_4C fracture surface after annealing at 1600°C for 1 hr at 10^{-5} torr.

ESCA analysis[2] a surface concentration of 1 to 2 wt % lithium was determined. Presumably, the lithium is in the small white decorations seen on the surface, as the oxide or nitride. The irradiated 20%-cold-worked type 316 stainless steel fracture surface of a tensile specimen[3] seen in Fig. 37.3 illustrates the considerable depth of focus capability of the scanning microscope. In Fig. 37.4 we see an irradiated pyrolytic-carbon-coated resin-core fuel microsphere. A portion of its coating popped off during either irradiation or postirradiation handling. A stereo pair of pictures taken of this particle at higher magnification allows a very interesting view of a portion of the interior of the coating and resin-core surface. The view seen in Fig. 37.5 includes carbide precipitate particles seen[4] in a

2. ESCA–photoelectron spectroscopy by L. D. Hulett, Analytical Chemistry Division.

3. Work of E. E. Bloom.

4. D. Fahr, *Fuels and Materials Development Program Quart. Progr. Rep. Mar. 31, 1972*, ORNL-TM-3787, pp. 98–105.

grain boundary separation after room-temperature fracture of type 304 stainless steel irradiated at 420°C to a fluence of 1.4×10^{23} neutrons/cm^2.

We believe that because of its excellent depth of focus and minimal sample preparation requirements, the scanning electron microscope has become an important tool in the Division's research and development programs.

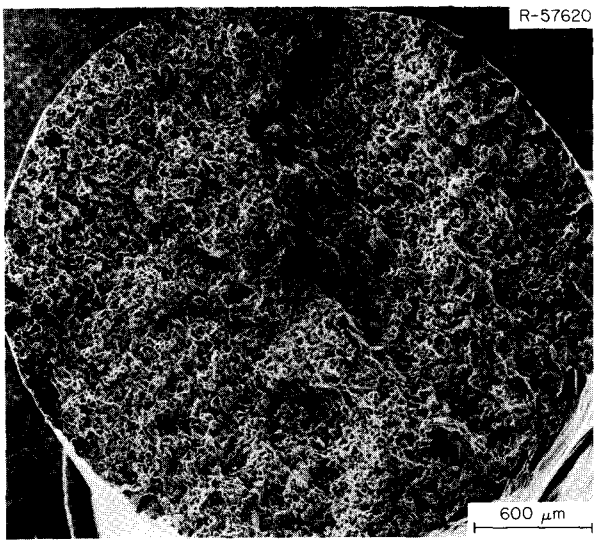

Fig. 37.3. Fracture surface of type 316 stainless steel irradiated at 680 to 725°C to a fluence of 2.3×10^{22} neutrons/cm^2 (>100 keV).

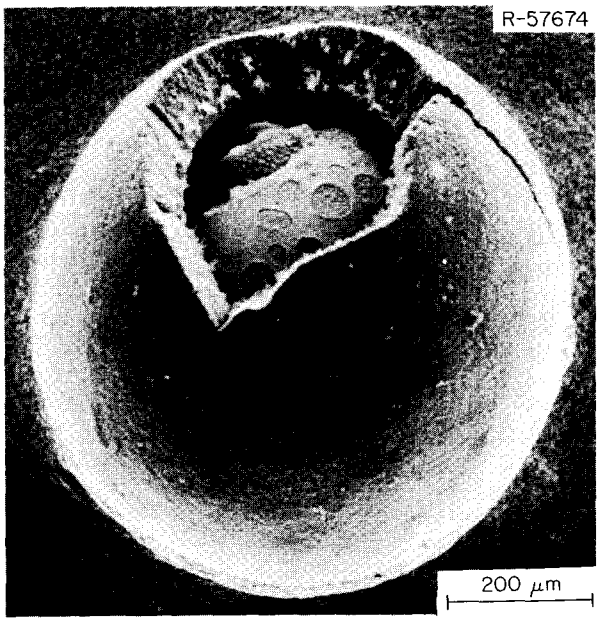

Fig. 37.4. Fuel microsphere irradiated for four cycles in a HFIR target experiment.

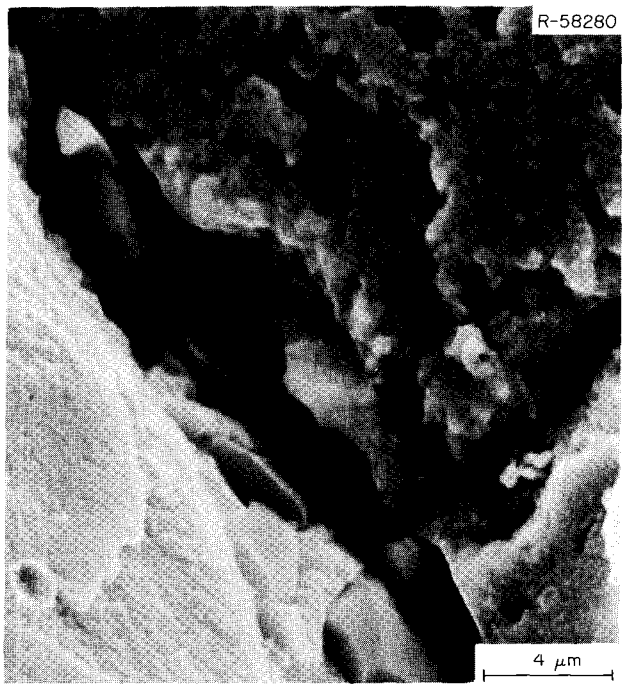

Fig. 37.5. Irradiated type 304 stainless steel showing carbide precipitate particles at a grain boundary separation.

MICROPROBE ANALYSIS

H. V. Mateer T. J. Henson
R. S. Crouse

A piece of 4340 steel that fractured during fabrication had unusual features on the fracture surface that appeared to be collections of microspheres. Examination in the scanning electron microscope using the energy-dispersive x-ray spectrometer proved the spheroids to be almost pure iron. During the x-ray analysis of the surface, strong indications of lead appeared in areas not covered by the microspheres. Since this element was totally unexpected, the lead spectrum was confirmed by comparison with a lead standard. To further verify this fact, the sample was sectioned, polished, and examined in the electron-beam microprobe, which has greater selectivity in element separation than does the scanning microscope. Lead was confirmed as being present, but only on the surface and not in the bulk sample, It seems, therefore, that lead did not contribute to the fracture, but somehow got on the surface after fracture. Figure 37.6 shows the surface and the x-ray spectra. The copper peak was thought to have come from the brass sample stub.

Y-114257

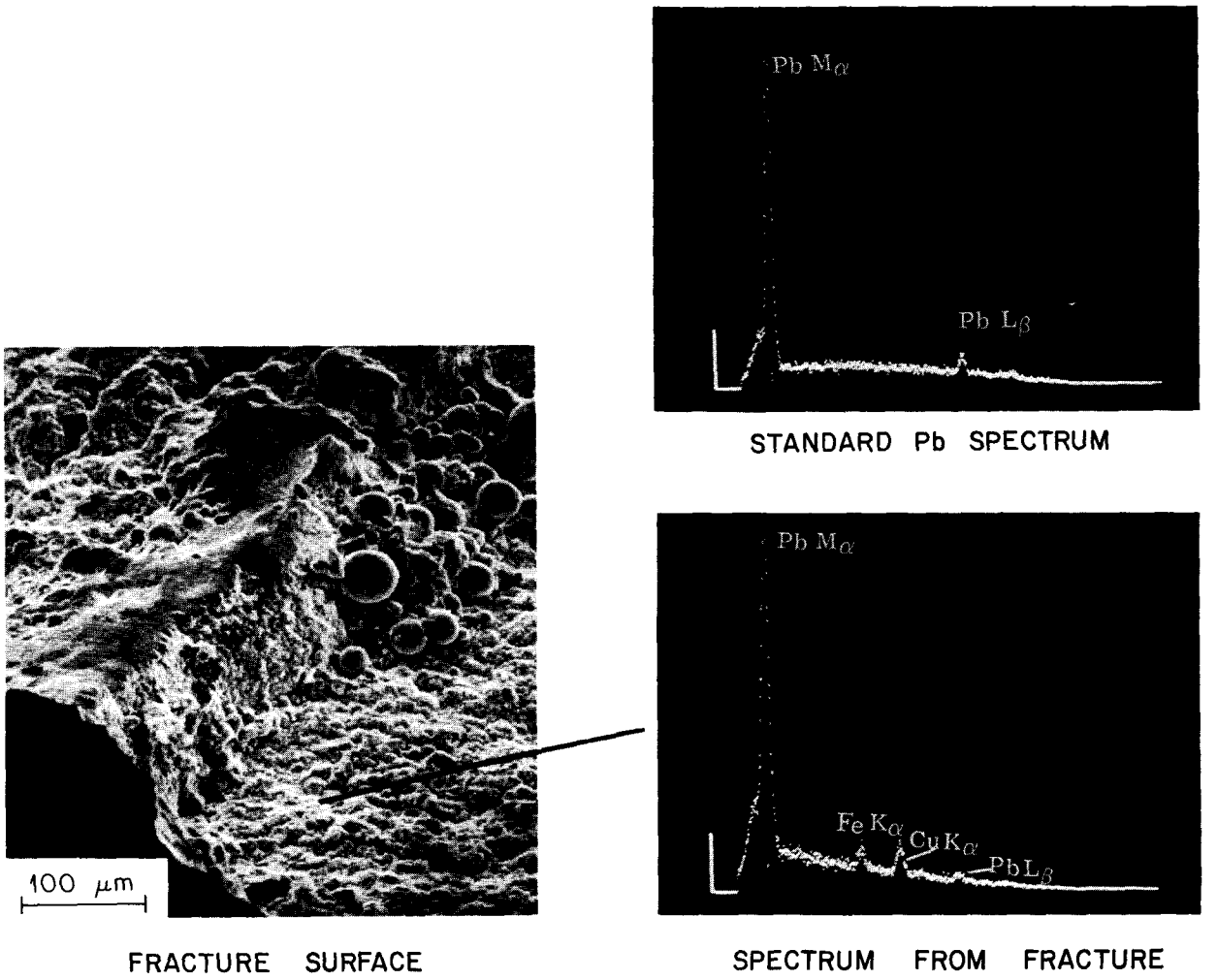

Fig. 37.6. Nondispersive x-ray analysis of 4340 steel fracture.

Work continued in service for the Surface Phenomena Group in their study of the oxidation of uranium alloys.[5] Step scan traverses were made across the metal-oxide interface of a U–7% Zr alloy oxidized at 800°C in 5×10^{-2} torr O_2 to determine the behavior of the zirconium. Figure 37.7 is a plot of the uranium and zirconium concentration against traverse distance. The values for the points are fully corrected by the Zeibold and Oglivie procedure[6] and show a depletion of zirconium in the metal at the interface and an enriched zone in the oxide. Figure 37.8 qualitatively demonstrates a display of Zr *La* x rays taken from the

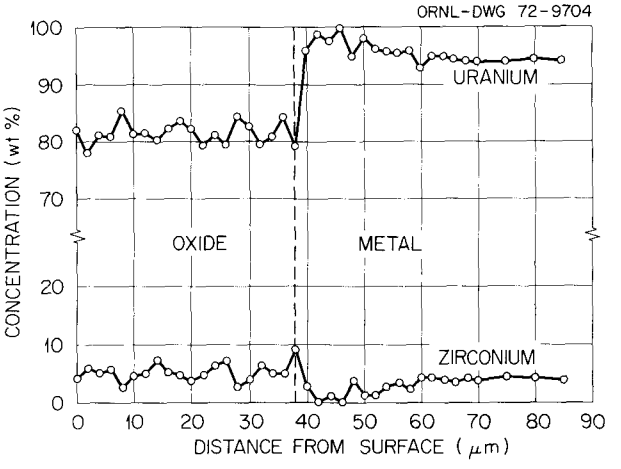

Fig. 37.7. Step scan traverse across the metal-oxide interface of U–7% Zr oxidized at 800°C in 5×10^{-2} torr O_2.

5. R. S. Crouse, H. V. Mateer, T. J. Henson, and J. L. Miller, Jr., *Metals and Ceramics Div. Annu. Progr. Rep. June 30, 1971*, ORNL-4770, pp. 186–90.

6. T. O. Zeibold and R. E. Oglivie, *Anal. Chem.* **36**, 322–27 (1964).

Y-110718

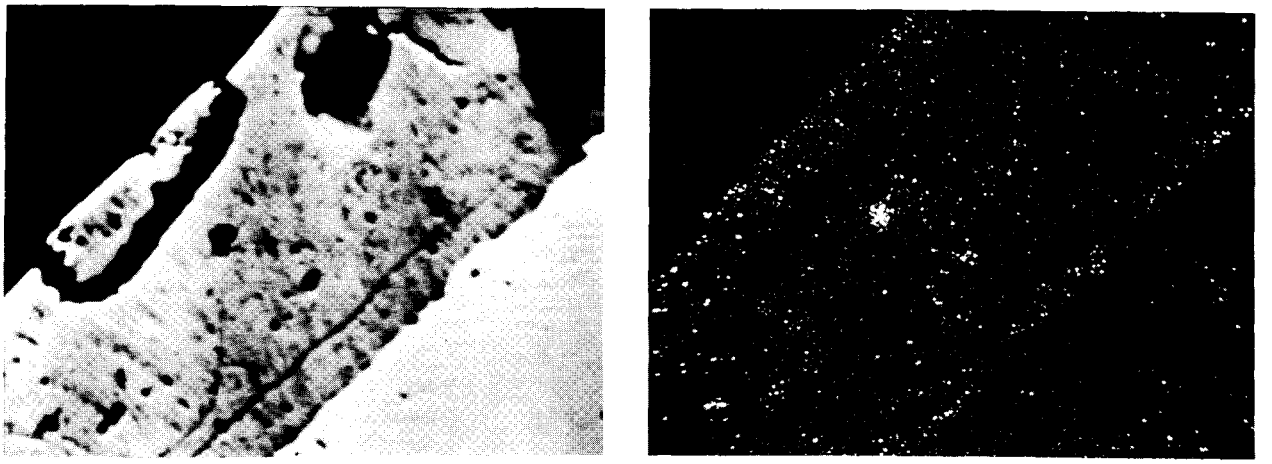

Fig. 37.8. Electron-beam scanning images of oxide-metal interface. Left: backscattered electrons. Right: Zr $L\alpha$ x rays.

microprobe rate meter signal. This technique is somewhat time consuming, but the background signal can be reduced electronically, permitting display of smaller compositional differences than is possible with the signal direct from the pulse-height analyzer.

To average intensity readings in an inhomogeneous oxide layer we used an elongated beam, $3 \times 150\ \mu m$. We caused the electron beam to sweep very rapidly in a static line oriented parallel to the oxide-metal interface and moved the sample in steps under the beam. This is effective when the sample contains many inhomogeneities. Figure 37.9 shows how the sample was scanned by the beam.

A microprobe examination of a ThO_2–4.5% UO_2 sample revealed an interesting distribution phenomenon. Although the nominal composition was 4.5% UO_2, the UO_2 was distributed primarily at the edge of the voids in the sample. A traverse across a large void shown in Fig. 37.10 indicated a concentration of uranium of at least 67 wt %. This may be low since there was probably loss of x-ray intensity into the void area as the beam approached the edge. The x-ray displays indicate a rim rich in uranium. Subsequent examination in the scanning microscope showed the voids to be typical of naturally occurring voids in this type of ceramic material.

An improved beam scanning system has been installed on the shielded microprobe and greatly improves our ability to exactly select a point for analysis. Using a backscattered electron or sample current image on the cathode ray tube we examine a sample very much as in a scanning electron microscope. When a spot of interest is located, the scan is stopped and the beam is

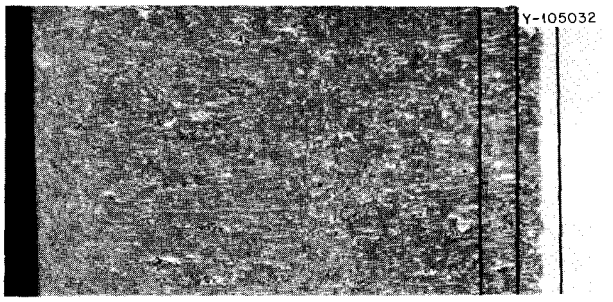

Fig. 37.9. Inhomogeneous oxide on a uranium-molybdenum alloy. The lines indicate typical areas over which the elongated beam swept.

electronically displaced to rest in the spot. Then x-ray diffraction analysis can be performed.

This capacity enabled us to determine a molybdenum-to-ruthenium ratio on an irradiated $(U,Pu)O_2$ fuel pin; the determination had previously been impossible. Figure 37.11 is a composite photomicrograph of the fuel pin from the central void to the cladding, showing some of the metallic fission products. These are dispersed throughout the sample in decreasing size and number from the central void to the cladding. The specimen was divided into four zones, 200, 600, 1000, and 1300 μm from the void. In each zone, six to ten particles and adjacent oxide were analyzed for molybdenum and ruthenium. The average molybdenum-to-ruthenium ratios were: zone 1, 0.07; zone 2, 0.40; zone 3, 0.61; and zone 4, 9.9. Because of the extremely high radioactive background a high sample current was used, and the results are to be interpreted with caution.

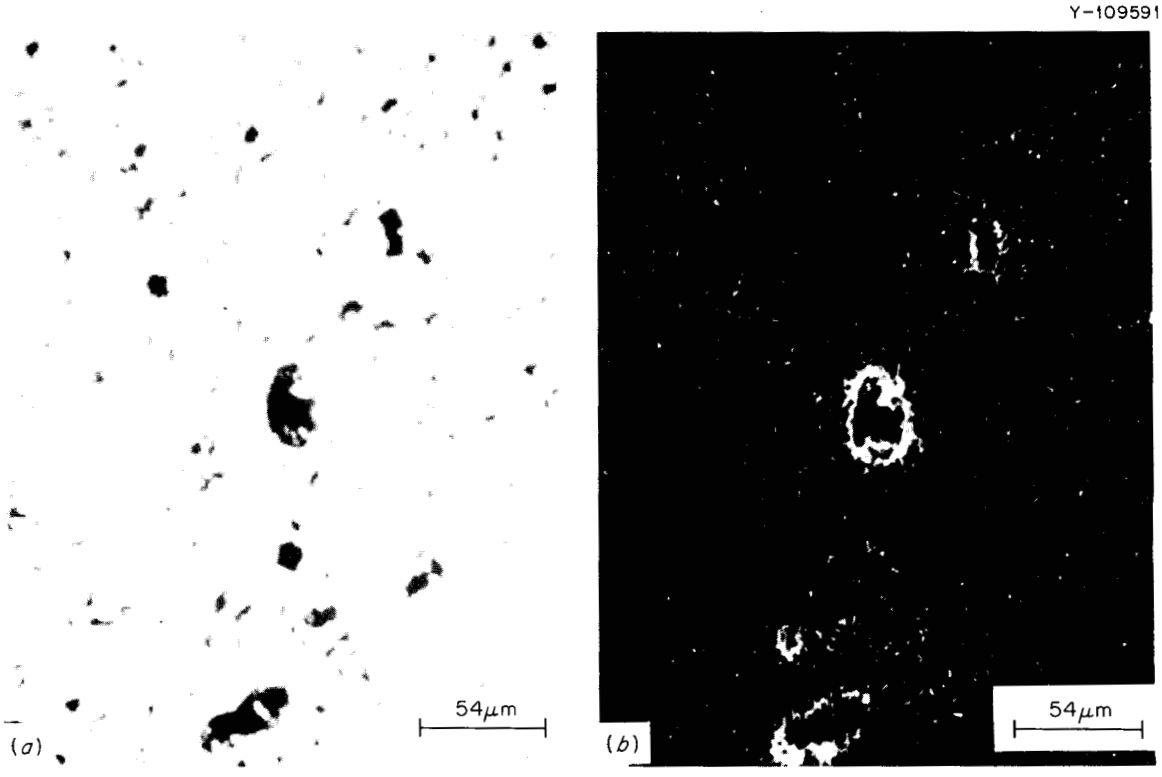

Fig. 37.10. Electron-beam scanning images of large void area in a ThO_2-UO_2 specimen. (*a*) Secondary electron image. (*b*) Display of U $M\beta$ x rays.

Fig. 37.11. Composite photomicrograph of a fuel pin from central void to cladding. Note the fission product visible in the oxide as white spots.

EPITAXIAL FERROMAGNETIC ETCHING

R. J. Gray

The progress in the use of a commercial product, Ferrofluid,[7] in "magnetic etching" was introduced last year.[8] Added development for extending the applications of this technique has continued;[9,10] and the Francis F. Lucas Award for Excellence in Metallography was received at the Annual American Society for Metals Metallographic Exhibit at Detroit, Michigan, in October 1971. The entry is shown in Fig. 37.12.

Ferromagnetic etching was applied to detect strain-induced martensite in type 304 stainless steel. A tensile specimen of austenitic type 304 stainless steel that had been annealed 1 hr at 2000°F before testing was polished on a median longitudinal plane. Examining the entire median plane by magnetic etching revealed the microstructural characteristics from the highly cold worked martensitic (ferromagnetic) fracture area to the unchanged threaded austenitic (nonmagnetic) area (Fig. 37.13). Microstructure near the shoulder of the tensile specimen (photo 1 in Fig. 37.13) shows isolated diagonal crystal slip lines of magnetic martensite.

7. Ferrofluid (water base), Ferrofluids Corp., Burlington, Mass.

8. R. J. Gray, *Metals and Ceramics Div. Annu. Progr. Rep. June 30, 1971*, ORNL-4770, pp. 191–92.

9. R. J. Gray, *Revealing Ferromagnetic Microstructure with Ferrofluid*, ORNL-TM-3681 (March 1971).

10. R. J. Gray, "Revealing Ferromagnetic Microstructure with Ferrofluid," presented at the Fourth International Metallographic Society Meeting, to be published by International Microstructural Analysis Society, 562 Melody Dr., Northglenn, Colo. 80221.

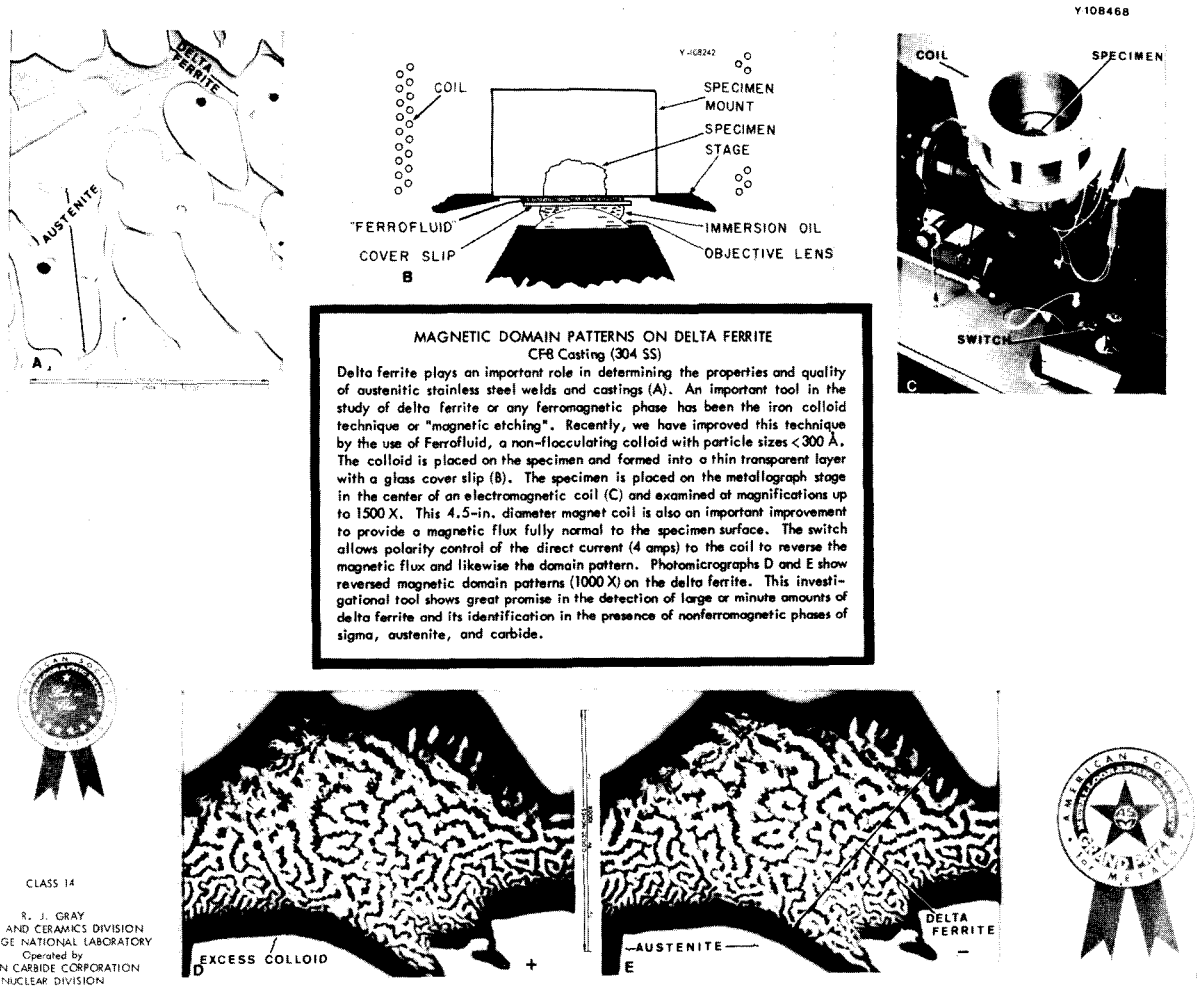

Fig. 37.12. Display that won Francis F. Lucas award, best in show, for excellence in metallography, at the annual American Society for Metals Metallographic Exhibit at Detroit, Michigan, in October 1971.

Y-114259

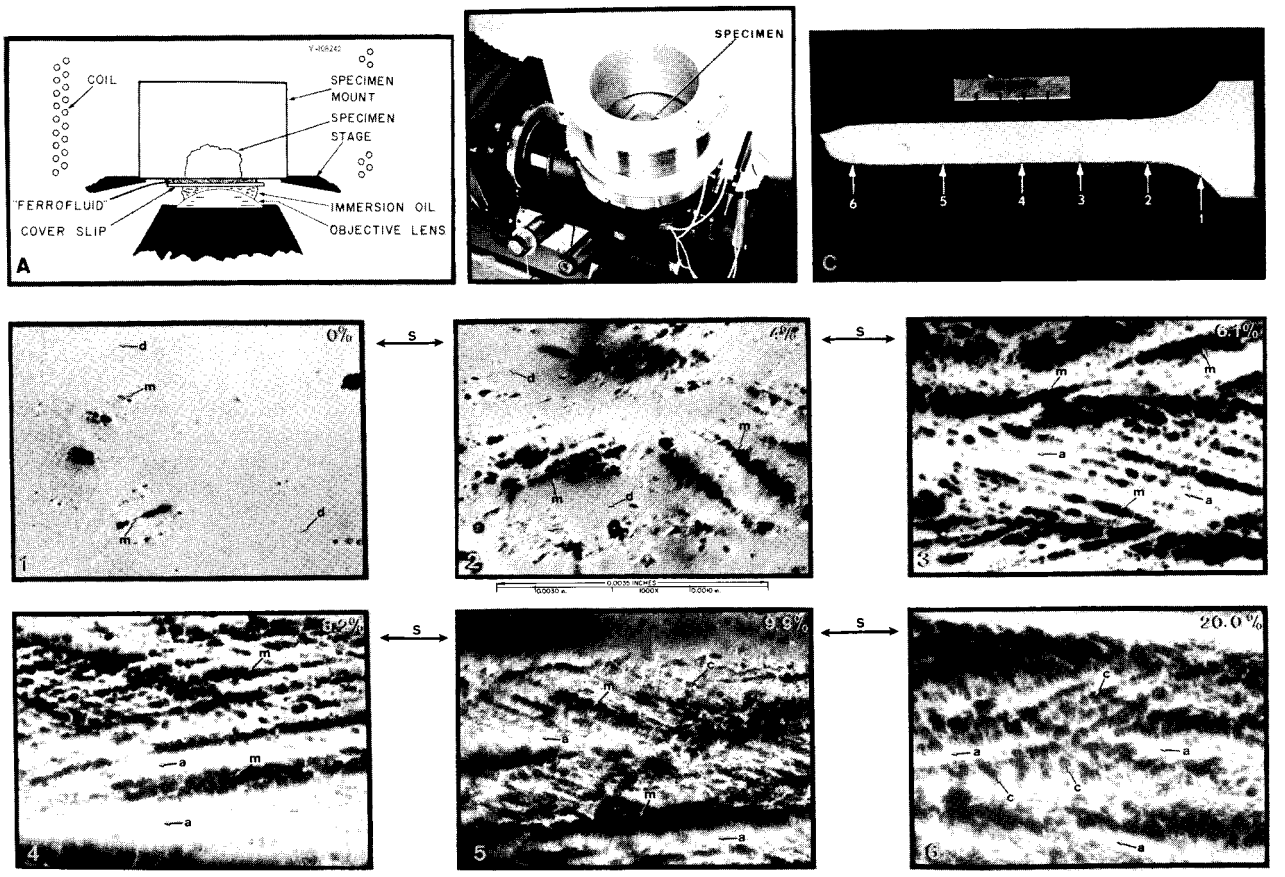

Fig. 37.13. The detection of strain-induced martensite in type 304 stainless steel by "ferromagnetic etching." The fabrication of some wrought stainless steels may require strengthening by cold working, which can result in martensite transformation. This transformed product may have a deleterious effect on the performance of the components, so the presence, distribution, and morphology of the strain-induced martensite must be known. Ferromagnetic martensite in amounts exceeding 0.1% in a nonmagnetic austenitic matrix can be shown by iron colloid "magnetic etching." The slip-formed martensite motivates the colloid particles (<300 Å) to form epitaxial patterns in a magnetic field. Sketch *A* shows the specimen in position after $\frac{1}{8}$ drop of ferromagnetic colloid was applied and formed into a thin transparent layer with a 0.006-in.-thick cover glass. Photo *B* shows the 4.5-in.-diam magnetic coil, which is energized by 1.0 to 4.0 A dc. Areas of examination on the median plane of a failed tensile specimen (photo *C*) are indicated with correspondingly numbered photomicrographs at 1000×. Magnegage measurements of bulk percentages of ferromagnetic martensite are indicated. Dark dots (arrows *d*) in photos 1 and 2 are metastable colloid colonies on the nonmagnetic austenite due to the magnetic flux overpowering the normal vibratory (Brownian) movement of the suspended particles. Minimal diagonal martensite bands (arrows *m*) relative to the stress axis ($\overset{S}{\longleftrightarrow}$) can be seen in the shoulder area (1). Diagonal slip densities increase nearer the fracture (2–6). Close to the fracture, high-density cross slip causes the diagonal slip bands to segment (arrows *c*). Heterogeneity of the slip mechanism is apparent from the presence of banded untransformed austenite (arrows *a*).

Diagonal strain bands of martensite continue to increase in the microstructures in positions 2 through 6. The long diagonal martensitic bands display a definite breakup in continuity near the fracture. Heterogeneous bands of austenite devoid of strain-induced martensite are also very apparent near the fracture.

Fatigue test results of type 301 stainless steel annealed at 2000 and 1750°F are shown in Fig. 37.14. The microstructures of the threaded regions of the two fatigue test specimens are shown in Fig. 37.14*a* and *b*. Incomplete homogenization to form austenite is evident in Fig. 37.14*b*. Some grain boundary ferrite can be seen. Microstructures near the fractures of the two fatigue specimens are shown in Fig. 37.14*c* and *d*. Figure 37.14*c* shows clearly that the strain-induced martensite in the fatigue specimen annealed at 2000°F occurred principally within the grains, whereas the principal location for strain-induced martensite in the 1750°F-annealed specimen occurred at the grain boundaries (Fig. 37.14*d*).

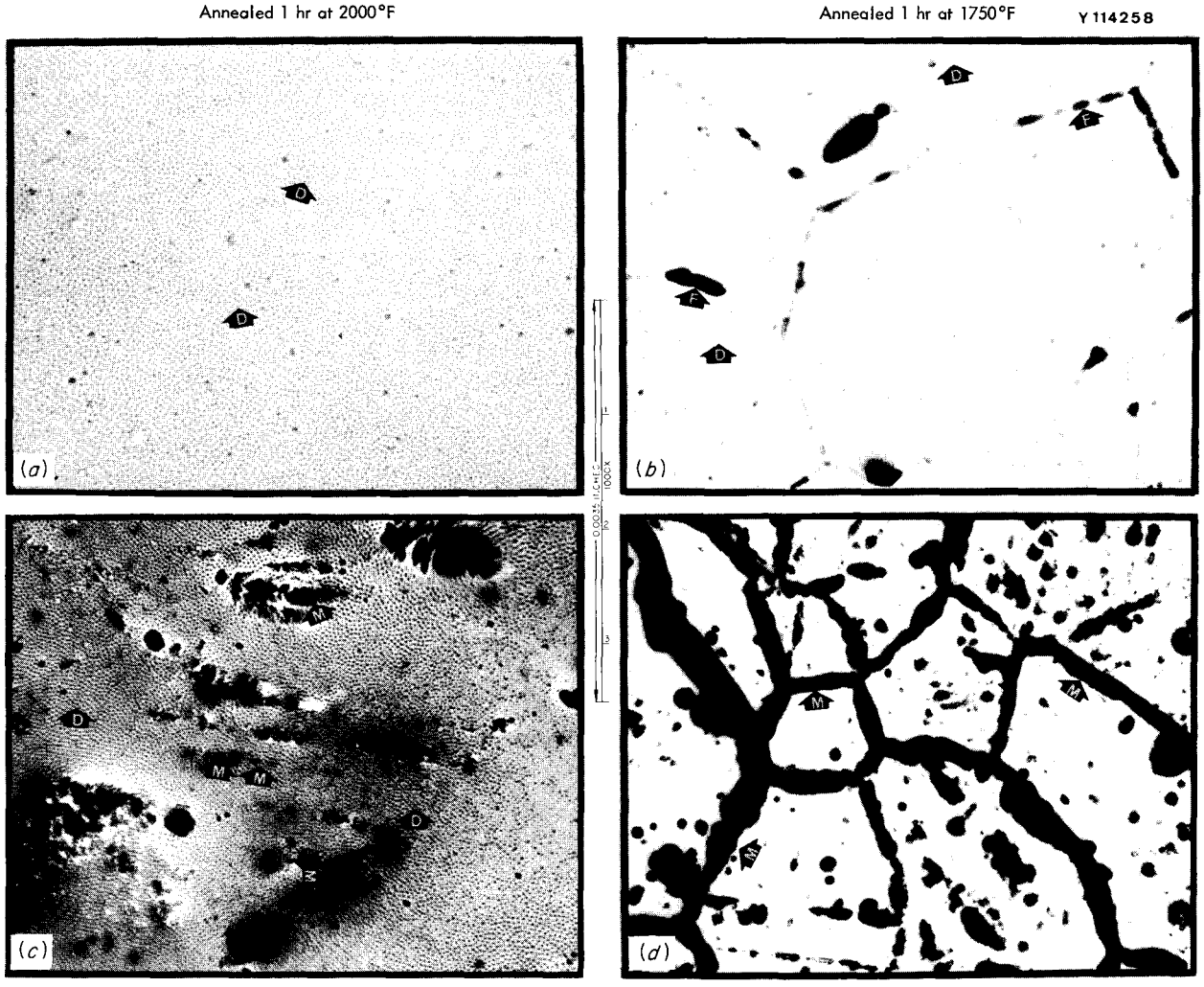

Fig. 37.14. Magnetic etching of type 301 stainless steel fatigue specimens. Threaded region: (*a*) Dots (arrows *D*) on the nonmagnetic austenite are metastable colonies of colloid particles due to the magnetic flux overpowering the normal Brownian movement. (*b*) Some residual ferrite (arrows *F*) is present at grain boundaries because of the lower annealing temperature. Test region: (*c*) Some strain-induced martensite (arrows *M*) is present at slip bands with no indication of martensite at grain boundaries. (*D*) A heavy concentration of strain-induced martensite (arrows *M*) is present at grain boundaries.

Cinematographic pictures have been made of the applications of ferromagnetic etching, and further uses of this interesting technique are continuing.

EXAMINATION OF FAILED PROSTHETIC APPLIANCES

R. J. Gray

A neglected area of materials science and technology is the development of suitable materials for internal prosthetic devices. Such devices operate in a hostile environment (body fluids resembling sea water in composition) but are often designed without regard for compatibility. Failed devices are normally replaced by identical pieces with no attempt to find and correct the cause of failure. We have entered this field by doing some failure analysis on devices obtained from an orthopedic surgeon.

The examination included type 316 stainless steel pins (Fig. 37.15) that had been inserted into the central (medullary) cavity of the thigh bone (femur) to bridge a fracture of the bone shaft (diaphysis) region. One pair of pins displayed cavitation corrosion and another had fractured. The fractured pins had been centerless ground, and circumferential gouges from the grinding wheel nucleated fissures probably caused by low-cycle fatigue at the location of repeated flexure. The fissures

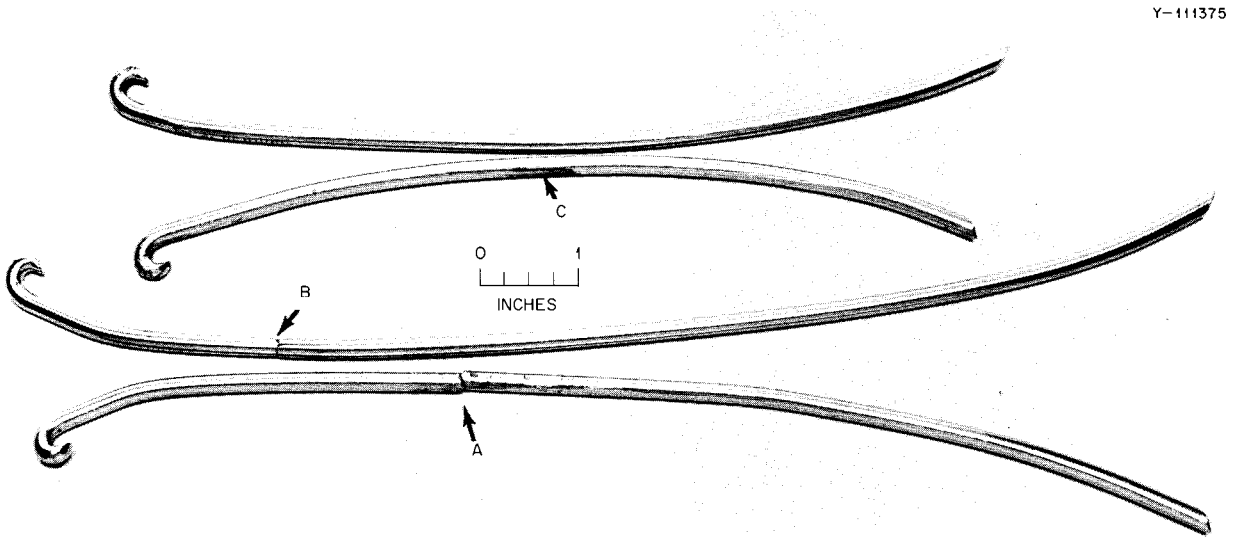

Fig. 37.15. Retrieved type 316 stainless steel pins. The upper pair of pins was crossed in the central (medullary) cavity, and cavitation corrosion occurred. The lower pair of pins failed in service.

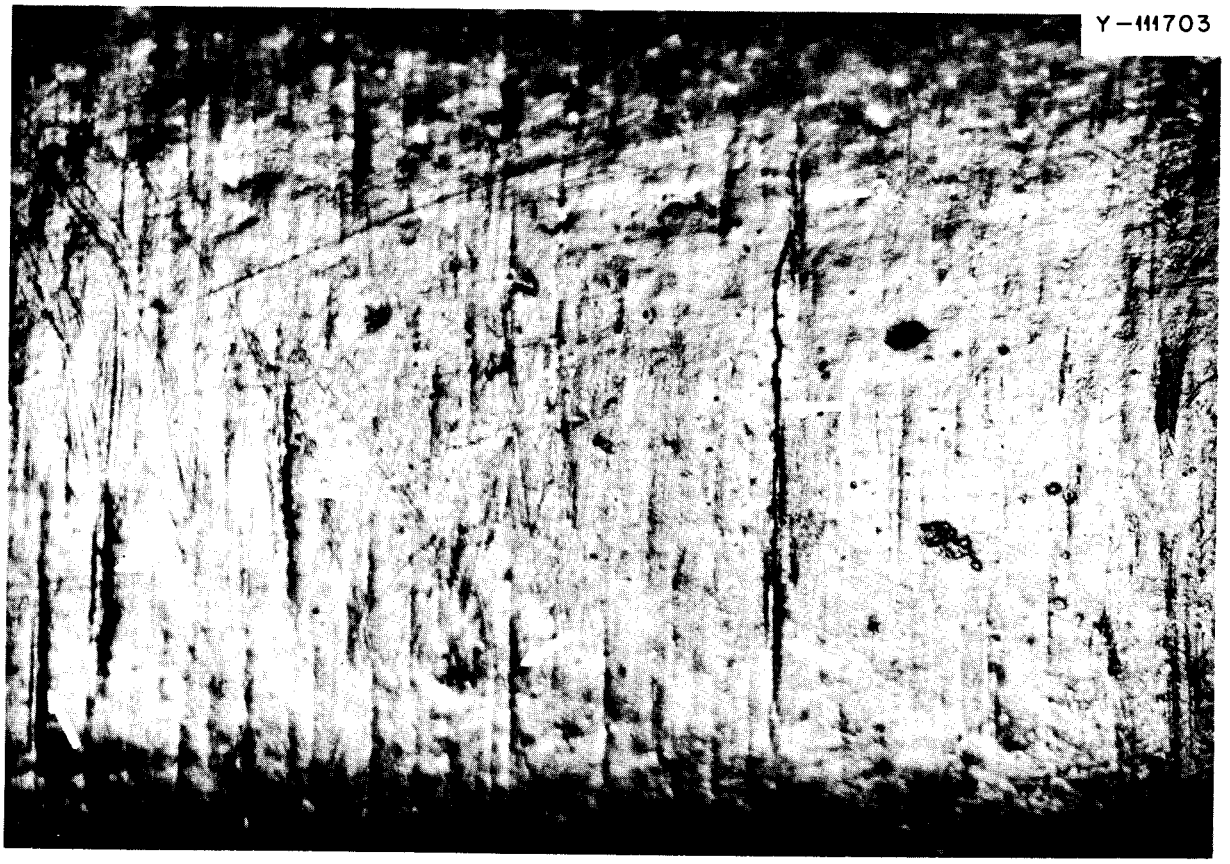

Fig. 37.16. Surface near the fracture of prosthetic pin. Arrows point out numerous fissures nucleating in centerless grinding wheel gouges. Arrow 1 shows a continuing fracture that originated in two surface gouges (arrows 2). 100×.

combined and progressed until the pins failed. An area near the major fracture is shown in Fig. 37.16. Finishing the pins by fine grinding and electrolytic polishing would have extended their life.

Self-tapping type 316 stainless steel screws secured a nail plate that bridged a fracture of the proximal end of the femur. These screws fractured and had to be removed (Fig. 37.17). Examination showed fissures at all thread roots in the upper third of each screw. Tensile forces and the hostile environment caused stress-corrosion cracking (Fig. 37.18). Apparently an alloy less sensitive to this cracking is needed.

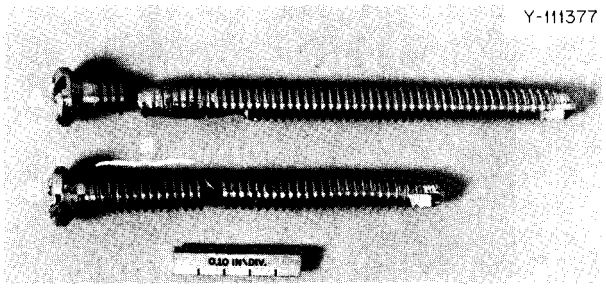

Fig. 37.17. Self-tapping type 316 stainless steel screws that secured a nail plate for bridging a fracture of the proximal end of the femur. The fractured ends of screw A were damaged during retrieval. Area *a* of screw B contained fissures in all thread roots.

Lack of engineering materials knowledge prevents the orthopedic surgeon from providing his supplier with meaningful information on failures. With this absence of feedback, materials progress of prosthetic appliances can be exceedingly slow. Although the amount of effort that we have expended is minimal, it appears to provide a basis for improved specification of components.

METALLOGRAPHIC EXAMINATION OF THE ALCO/BLH STEAM GENERATOR

B. C. Leslie

We have prepared, examined, and photographed 206 metallographic specimens taken in areas of interest from the dissected steam generator. Of these specimens, 45 were tube-to-tube-sheet welds from both the top and bottom tube sheets of the steam generator. Several of these weld joints exhibited cracks in both the weld metal and base metal. Figure 37.19 is a tube-to-tube-sheet weld from the bottom tube sheet, showing cracks progressing through most of the weld.

ALPHA AUTORADIOGRAPHY

T. M. Kegley, Jr. H. R. Gaddis

In the metallography of nuclear materials, alpha autoradiography using cellulose nitrate has proven to be very useful in the determination and detection of

Fig. 37.18. Longitudinal median view of the 11th thread root from the screw head (see area *a*, screw B, of Fig. 37.17). Note typical stress corrosion pattern of the fissure. 500×.

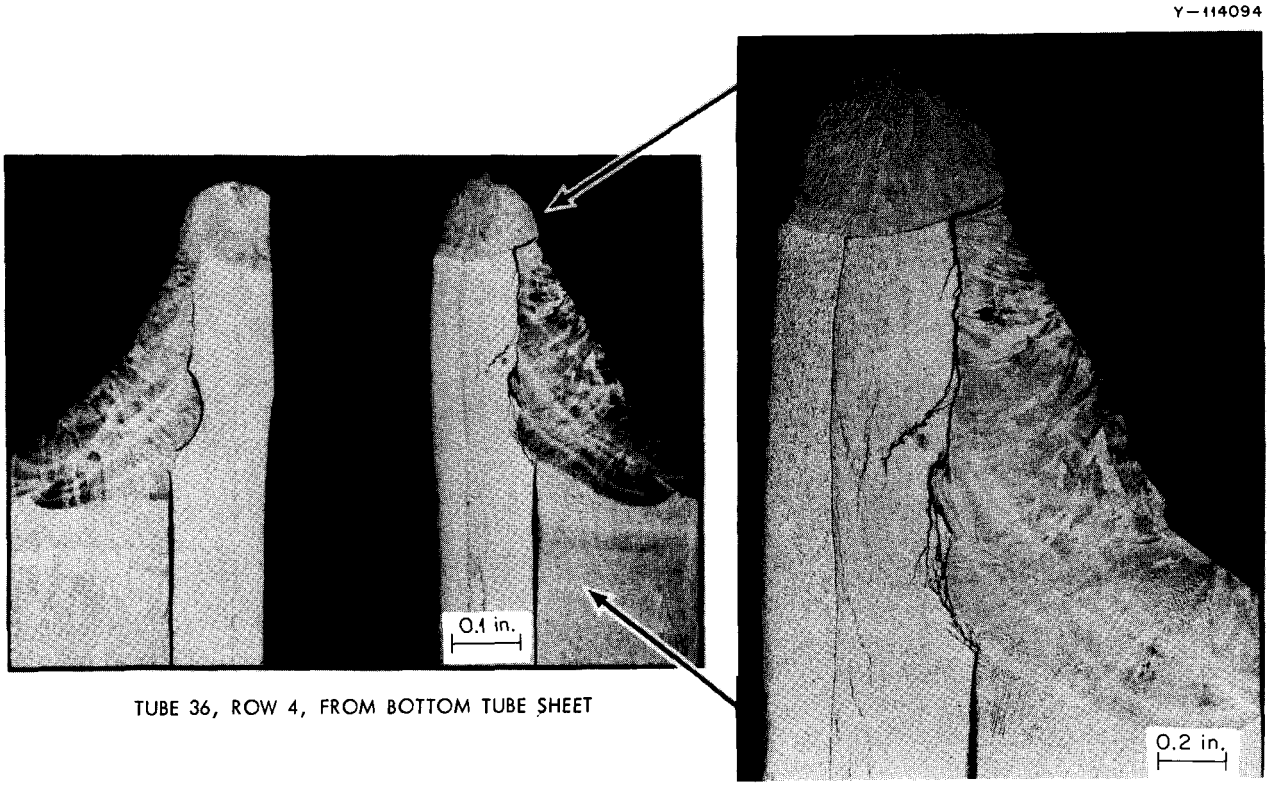

Fig. 37.19. Tube-to-tube-sheet weld from the bottom tube sheet from the Alco/BLH steam generator, showing crack propagation.

inhomogeneities in materials containing alpha emitters of Pu, Th, and U. The particular techniques developed and employed have been described earlier[11] and in a recent publication.[12]

Cellulose nitrate autoradiographs can be interpreted incorrectly if (1) exposures to alpha radiation are too long, (2) development time in NaOH is too long, or (3) temperature of development is too high. An excess in any of these factors causes the autoradiograph to reverse itself so that a constituent of very strong activity will appear very weak in the radiograph. Figure 37.20 shows the same autoradiograph of UO_2-ThO_2 fuel compact after 4 and 8 min development in 6.5 *N* NaOH. The UO_2 is fully enriched in ^{235}U, so that particles of UO_2 should be very active as compared to ThO_2. At 4 min development, the UO_2 particle appears strongly active as it should, while at 8 min development, the particle appears to show almost no activity.

11. T. M. Kegley, Jr., *Metals and Ceramics Div. Annu. Progr. Rep. June 30, 1970*, ORNL-4570, p. 221.

12. T. M. Kegley, Jr., *Metallography* **5**, 113–23 (1972).

BETA AUTORADIOGRAPHY

T. M. Kegley, Jr. M. D. Allen

We have used both the liquid emulsion technique[13] and the stripped film technique[14] in the microautoradiography of welds containing ^{63}Ni. Although the liquid emulsion technique is perhaps the easiest to use, the stripped film technique using Kodak AR.10 film produces autoradiographs of similar or equal quality. Figure 37.21 shows a microautoradiograph of the root pass of a weld joining Incoloy 800 to Inconel 625 using Inconel 82 filler metal containing ^{63}Ni. The autoradiograph shows a rather sharp delineation be-

13. R. E. Gehlbach, M. D. Allen, and J. D. Braun, "Autoradiography Study of Carbon-14 in Hastelloy N," pp. 113–18 in *Proceedings, First Annual Technical Meeting, International Metallographic Society, Inc., November 11, 12, and 13, 1968 – Colorado, U.S.A.*, ed. by K. A. Johnson and J. H. Bender, International Metallographic Society, Inc., Los Alamos, N.M., 1969.

14. H. J. Gomberg et al., *High Resolution Autoradiography for Study of Grain Boundaries in Metals*, PB-111558, 1954.

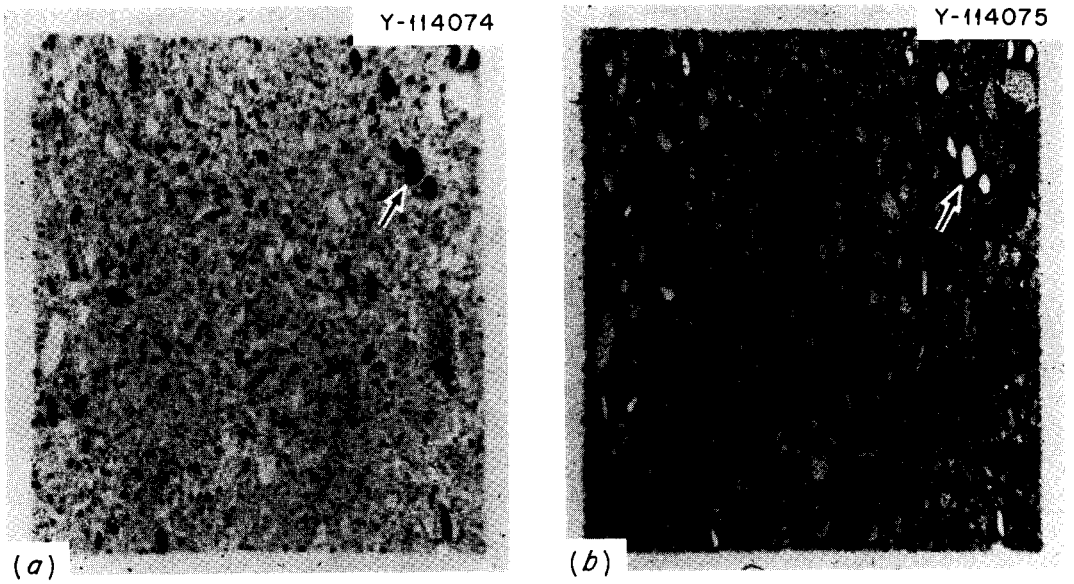

Fig. 37.20. Alpha autoradiograph of fuel compact of UO_2 and ThO_2. Enriched UO_2 particle shown by arrow. Cellulose nitrate film exposed 15.5 hr to fuel compact before development in 6.5 *N* NaOH at 57°C. Developed (*a*) 4 min and (*b*) 8 min.

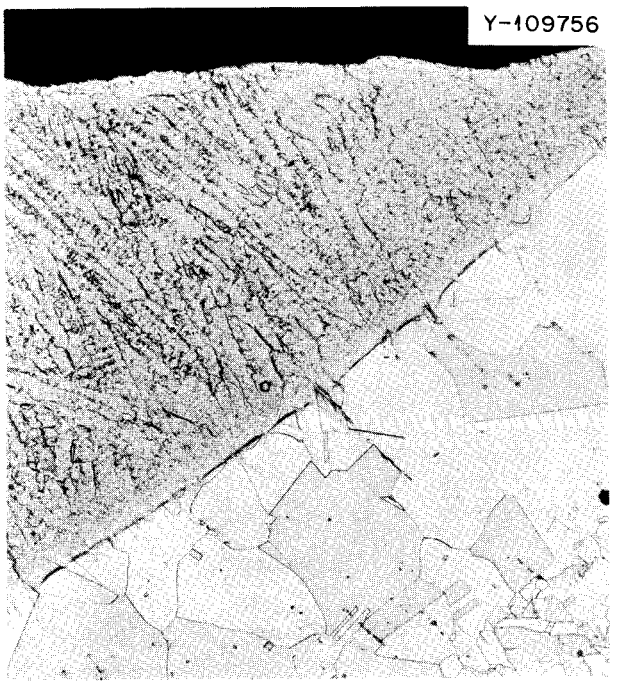

Fig. 37.21. Microautoradiograph of root pass of weld at fusion line between weld and Incoloy 800 base metal. Inconel 82 filler metal contained ^{63}Ni; Kodak Ar.10 stripping film emulsion exposed 64 hr before development.

Fig. 37.22. Microautoradiograph of nickel specimen. Protective film of collodion applied by dipping in solution of 1 part collodion to 3 parts amyl acetate. Kodak nuclear track emulsion NTB-2 exposed 65 hr to ^{127}Te before development.

tween the distribution of ^{63}Ni between the weld and the Incoloy 800 base metal.

Normally when using the liquid emulsion technique, we have avoided use of a protective film between the emulsion and the specimen because of the adherence difficulty and the decrease in resolution. With specimens of nickel we found it necessary to use a film of collodion to obtain suitable autoradiographs. Figure 37.22 shows an autoradiograph of a nickel specimen whose surface had been plated with the beta emitter ^{127}Te and then annealed 3000 hr at 760°C. The NTB-2 emulsion has reacted with the surface at places where the protective collodion film was inadvertently scraped from the surface. The extent of diffusion of the tellurium isotope into the nickel is clearly evident in the region where the collodion film remained intact.

ALPHA METALLOGRAPHY FACILITY

R. J. Gray B. C. Leslie
H. R. Gaddis

In addition to the preparation and examination of the routine samples containing plutonium, much work was done on the fuel particles and fuel rods for the Plutonium Test Element described in Chap. 34. These rods contain fuel particles coated with pyrolytic carbon and silicon carbide and bonded by a carbonaceous matrix. Silicon carbide coatings are very hard and are easily cracked during metallographic preparation. Since SiC coatings had not been prepared previously in the glove box suite, some additional techniques had to be developed for processing these samples.

The alpha facility equipment was designed to accommodate the standard metallographic mount ($1\frac{1}{4}$ in. diam × 1 in. high). The fuel rods are nominally 0.5 in. in diameter × 2 in. long, and the examination required that we look at a longitudinal section of the entire rod. Therefore, we designed a precast mount $2\frac{7}{8}$ in. diam × $\frac{3}{4}$ in. high to accommodate these large specimens. We had to modify the remote saw to facilitate cutting these longer lengths and the grinding and polishing equipment to handle the $2\frac{7}{8}$-in. mounts. These changes were made, and the fuel rods were examined with negligible loss in quality of work or preparation time. Figure 37.23 shows the fuel particles embedded in the fuel rod matrix.

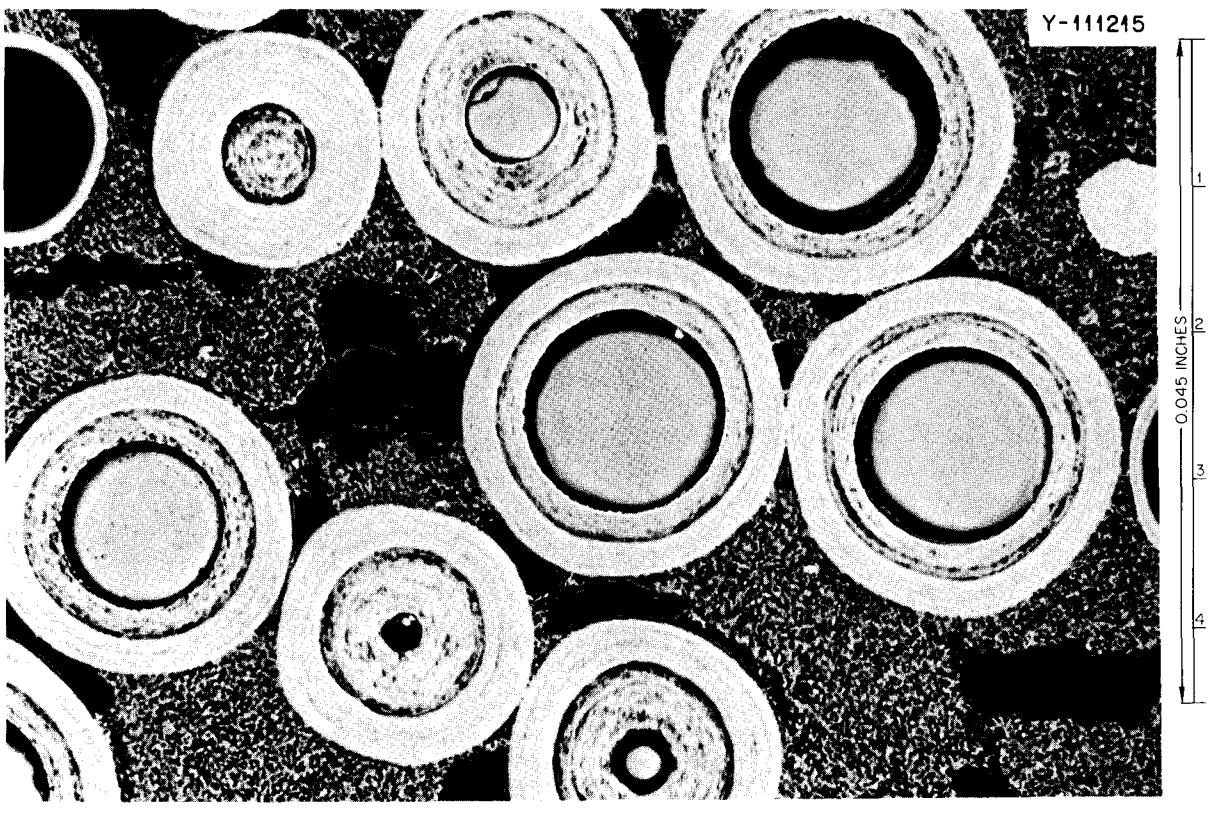

Fig. 37.23. Fuel particles embedded in the matrix of a fuel rod.

COLOR TELEVISION PROGRAM

R. J. Gray D. A. Canonico

On May 21, 1972, a color television program carrying the title "Metallurgy the Beautiful Science" was presented on WATE, Channel 6, Knoxville, Tennessee, sponsored by the University of Tennessee Department of Communications. A concerted effort was made to present a technical subject for the lay audience. The important position of metallurgy in the nuclear power field was shown. The audience was shown laboratory activities in specimen preparation and numerous photomicrographs, and the importance of microstructural examinations was explained. This 30-min taped program has been transferred to 16-mm color film and is now available from the ORNL film library for public showing.

38. NASA T-111 Loop Studies

E. L. Long, Jr. J. H. DeVan

We completed a metallographic and chemical examination of an engineering-scale, forced-circulation loop[1] that circulated lithium for 3000 hr at a maximum temperature of 1370°C. The loop was constructed of the tantalum-base alloy T-111 (Ta–8% W–2% Hf) and operated with a temperature difference of 170°C at a maximum velocity of 20 fps. Small sheet and annular specimens of T-111 were incorporated in the loop to enable us to measure the effects of mass transfer as well as any changes in the mechanical properties of this alloy.

The visual appearance and weight changes of the T-111 specimens have been reported.[2] A maximum weight gain of 0.7 mg/cm^2 occurred at the minimum temperature of the loop (1200°C), and a maximum weight loss of about 0.9 mg/cm^2 was found at 1360°C. The surfaces of the specimens that gained weight were covered with a crystalline deposit, and specimens that lost weight exhibited superficial grain-boundary grooving. These contrasting surface features, as revealed by scanning electron microscopy, are shown in Fig. 38.1. Although we have not yet identified the crystalline compound, electron microprobe analysis revealed that it contains up to 88% Hf. At the point of maximum weight loss, the exposed T-111 surfaces were depleted in hafnium from the before-test level of 2% down to 0.8%.

Miniature sheet tensile samples were machined from a select number of the T-111 sheet specimens to provide the effect of the temperature profile of the loop on any change in mechanical properties. To determine if there were any gross indications of degradation of the mechanical properties of the T-111 tubing, sections of the loop were crush-tested. All the tests were performed at room temperature. The results of the tensile testing are shown in Fig. 38.2. There was a decrease in both the ultimate strength and the 0.2% offset yield strength, as compared to archive material, although the percent elongation remained essentially unchanged. None of the tubing sections cracked during the crush test.

1. B. Fleisher, *Metals and Ceramics Div. Annu. Progr. Rep. June 30, 1970*, ORNL-4570, pp. 103–4.
2. R. L. Klueh, *Metals and Ceramics Div. Annu. Progr. Rep. June 30, 1971*, ORNL-4770, pp. 113–14.

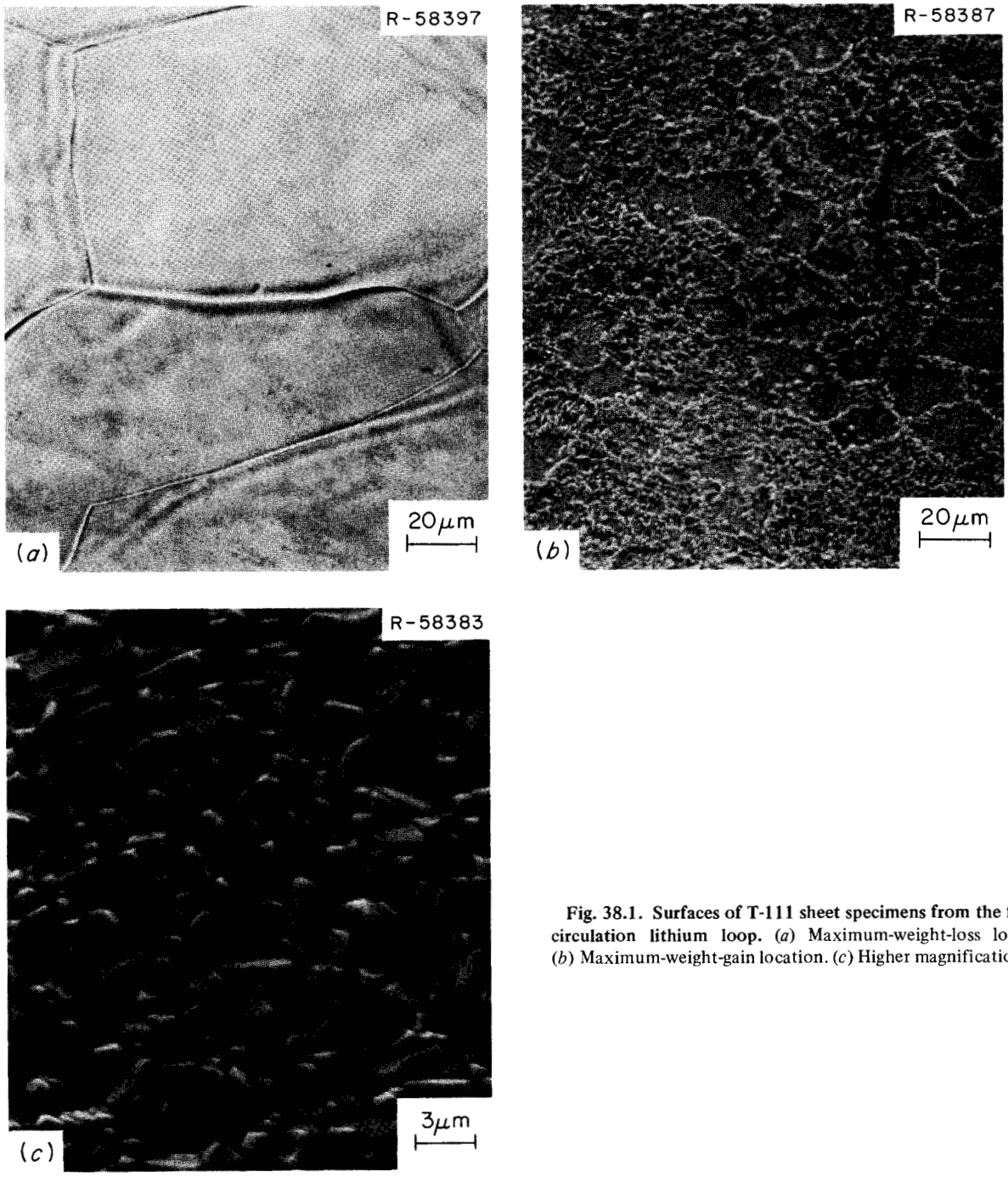

Fig. 38.1. Surfaces of T-111 sheet specimens from the forced-circulation lithium loop. (*a*) Maximum-weight-loss location. (*b*) Maximum-weight-gain location. (*c*) Higher magnification of *b*.

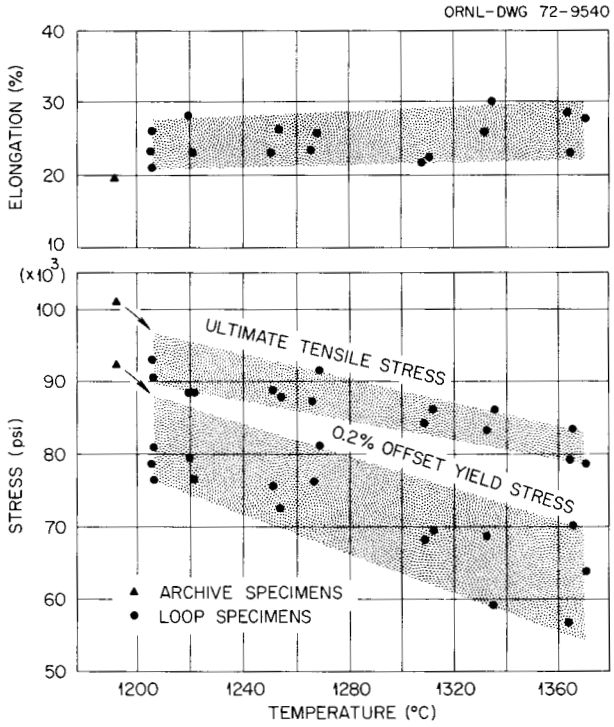

Fig. 38.2. Effect of operating temperature on the elongation, ultimate strength, and 0.2% offset yield strength of the T-111 miniature tensile specimens from the forced-circulation lithium loop.

39. NERVA Program Metallurgical Support

R. E. Clausing

We have provided support for the Materials and Structures Branch of the AEC-NASA Space Nuclear Systems Office on the NERVA Program.[1–4] This includes technical consultation for NASA and its contractors and also experimental research on (1) outgassing characteristics of NERVA fuel elements and (2) adhesion and friction of NERVA materials and components in simulated space environments. Final reports are being prepared on these two subjects, and brief summaries are given below.

THE GASEOUS ENVIRONMENT INSIDE A NERVA REACTOR IN SPACE

R. E. Clausing D. S. Easton

The gaseous environment inside a NERVA reactor during the coasting phases of space operations was predicted as a function of time and core temperature. The predictions are based on experimental outgassing data from NERVA XEII fuel elements[5] and the assumptions that (1) the fuel elements constitute the major source of gas influx; (2) the vacuum conductance between the core and space is essentially that of the open rocket nozzle; (3) the partial pressure of each gas in the system is described by the relation $P_n = q_n/C_n$, where $P_n \equiv$ the partial pressure of the nth gas (torr), $q_n \equiv$ the outgassing rate of the nth gas (torr-liter/sec), $C_n \equiv$ the conductance to space (liters/sec); and (4) the outgassing rates for each gas are of the form $q_n = A(t/t_0)^B$, where t_0 is a constant, t is time in hours, and A and B are empirical constants, are different for each gaseous species and fuel element type, and vary according to the handling or prior operational history of the fuel element.

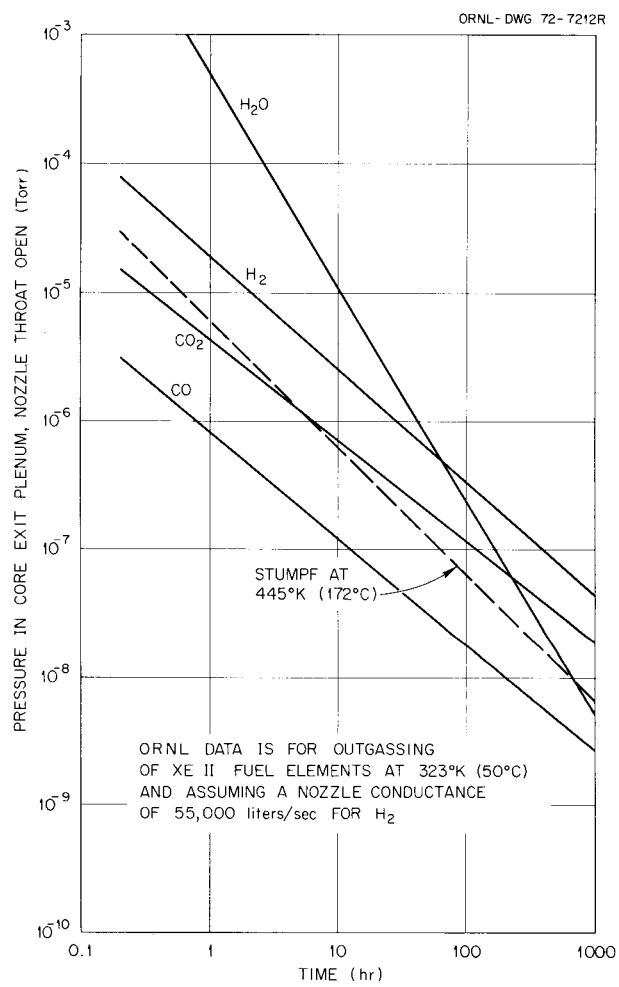

Fig. 39.1. Comparison of pressure predicted for NERVA manned Mars mission by Stumpf in WANL-TME-1706 with partial pressures predicted from ORNL data for the outgassing of XEII fuel elements.

1. R. E. Clausing et al., *Metals and Ceramics Div. Annu. Progr. Rep. June 30, 1968,* ORNL-4370, pp. 235–37.
2. R. E. Clausing et al., *Metals and Ceramics Div. Annu. Progr. Rep. June 30, 1969,* ORNL-4470, pp. 218–21.
3. R. E. Clausing et al., *Metals and Ceramics Div. Annu. Progr. Rep. June 30, 1970,* ORNL-4570, pp. 224–27.
4. R. E. Clausing et al., *Metals and Ceramics Div. Annu. Progr. Rep. June 30, 1971, ORNL-4770,* pp. 195–98.
5. D. S. Easton and R. E. Clausing, "Outgassing of Nuclear Rocket Fuel Elements," *J. Vacuum Sci. Technol.* 7, S116–23 (1970).

A mathematical expression was developed and experimental data were used to predict the partial pressures of various gases in the internal engine environment under two conditions: (1) after initial insertion into space but before the first engine operation and (2) after engine operation. For example, as shown in Fig. 39.1, water vapor is the major constituent for the first 50 hr in space for the unfired engine at 50°C, but hydrogen dominates thereafter. We predicted partial pressures for 12 gases at a variety of temperatures and times and obtained similar information for conditions after the engine has been fired. The data presented are for the core exit plenum chamber, which has the lowest pressure in the system. Multiplication factors are given to aid in estimating the pressures elsewhere in the reactor.

FRICTION OF GRAPHITE IN VACUUM AND HYDROGEN

R. E. Clausing D. S. Easton

The development of a nuclear engine for reliable use in space requires that the effects of the space environment on materials and components be taken into account. The tendency of atomically clean surfaces to adhere or to exhibit high coefficients of friction is one of the most important space-related phenomena. The design of the core lateral support system of NERVA requires a knowledge of the frictional properties of the materials involved. We have tried to simulate the internal engine environment and examine the effect of this environment on the behavior of proposed NERVA materials.[4,5] This study has revealed a wide variety of results on the frictional behavior for two types of graphite (P-03 and ZTA) sliding on itself in ultrahigh vacuum and hydrogen. In experiments using a cantilever-beam apparatus with loadings up to 100 psi, coefficients of sliding friction ranged from 0.04 to 1.3. The effects of temperature, gas pressure, wear velocity, normal force loading, and previous outgassing were studied, and all substantially influenced the coefficients of static and sliding friction. Velocity effects include a memory in which the sample, subjected first to high-velocity motion and then to low-velocity motion, has a coefficient that returns slowly to the lower coefficient associated with low velocities. A peak for the static coefficient of friction occurs only when the direction of rubbing is reversed. This suggests that motion produces on the sample surface an oriented structure that is altered by motion in a new direction. Surfaces and wear particles were examined with a scanning electron microscope.

The results of this study have important implications for the design of nuclear rocket engines or gas-cooled reactors that require graphite to slide over graphite or metal surfaces in inert environments or hydrogen. In many cases the high coefficients are intolerable; however, the possibility exists that conditions can be controlled within reactors to obtain the coefficient of friction desired for particular purposes. For example, low values may be desired for control rods and other sliding parts, while high values are wanted for some parts of the support systems and for vibration damping. The ability to control the coefficient of friction may be useful in the fabrication of graphite or graphite nuclear fuel elements and in nonnuclear applications in which either high or low coefficients of friction are desired.

Table 39.1 lists values for the sliding coefficient obtained in ultrahigh vacuum and in hydrogen at 1 torr as functions of normal force loading, velocity, and temperature. Note the dramatic changes that occur in hydrogen near 650°F (400°C). For example, the coefficient of friction in hydrogen at 550°C, 60 psi, and 1 in./min is 0.35; when the temperature is raised to 650°C, the coefficient is 0.05 to 0.08.

Table 39.1. Effect of velocity, loading, temperature, and environment on the dynamic coefficient of friction.

Material: ZTA graphite vs itself

Loading		Velocity (in./min)	Coefficient of friction for each temperature (°F) and environment[a]																		
Pounds	Pounds per square inch		75	75	75*	400*	450*	500		550*	600*	600	650*	650	700		800	850	900	1000		1050*
			H_2	Vac.	H_2	H_2	H_2	H_2	Vac.	H_2	H_2	H_2	H_2	H_2	H_2	Vac.	H_2	H_2	H_2	H_2	Vac.	H_2
2.5	8.1	0.5	0.68	0.22				0.18	0.32						0.18	0.90				0.08	0.62	
		1.0	0.74	0.22				0.48	0.32						0.18	0.98				0.14	0.72	
		5.0	0.80	0.22				0.80	0.32						0.40	1.16				0.30	0.78	
		10.0	0.86	0.22				0.82	0.32						0.70	1.24				0.40	0.80	
		20.0	0.86	0.22				0.84	0.32						0.88	1.26				0.50	0.80	
		50.0	0.78	0.22				0.86	0.32						0.94	1.32				0.52	0.94	
		100.0	0.74	0.22				0.88	0.32						1.00	1.34				0.60	1.02	
5.0	16.3	0.5	0.64	0.21				0.16	0.30						0.09	0.67				0.05	0.47	
		1.0	0.64	0.21				0.33	0.30						0.09	0.73				0.07	0.56	
		5.0	0.61	0.21				0.61	0.30						0.20	0.82				0.09	0.59	
		10.0	0.50	0.21				0.65	0.30						0.52	0.89				0.17	0.59	
		20.0	0.28	0.21				0.65	0.32						0.66	0.94				0.32	0.62	
		50.0	0.24	0.21				0.65	0.32						0.71	0.97				0.48	0.63	
		100.0	0.20	0.21				0.65	0.32						0.71	1.00				0.56	0.67	
10	33	0.5	0.43	0.23				0.15	0.32						0.06	0.56				0.035	0.43	
		1.0	0.43	0.23				0.40	0.33						0.10	0.64				0.04	0.50	
		5.0	0.40	0.23				0.60	0.33						0.27	0.77				0.05	0.51	
		10.0	0.36	0.24				0.65	0.38						0.47	0.82				0.10	0.52	
		20.0	0.29	0.24				0.65	0.39						0.65	0.85				0.20	0.55	
		50.0	0.30	0.25				0.60	0.39						0.67	0.88				0.35	0.57	
		100.0	0.31	0.26				0.50	0.33						0.67	0.88				0.56	0.60	
18.4	60.0	0.5	0.51	0.17				0.12	0.38				0.07		0.06	0.56				0.04	0.42	
		1.0	0.49	0.19		0.61	0.58	0.42	0.39	0.35	0.18		0.08	0.05	0.08	0.62				0.04	0.42	0.05
		3.0			0.56	0.60	0.58	0.43		0.56	0.22	0.41	0.20				0.07	0.06	0.04	0.04	0.42	0.06
		5.0	0.47	0.19		0.59	0.57	0.64	0.40	0.56	0.40			0.29	0.24	0.74				0.05	0.42	0.07
		10.0	0.34	0.21	0.51	0.55	0.56	0.64	0.39	0.57	0.60		0.48	0.49	0.49	0.83				0.07	0.43	
		20.0	0.21	0.22	0.32	0.46	0.48	0.58	0.35					0.56	0.64	0.85				0.18	0.44	0.20
		50.0	0.23	0.24	0.25	0.37		0.54	0.34			0.57		0.61	0.67	0.86	0.67	0.50	0.43	0.26	0.45	0.24
		100.0	0.25	0.17				0.54	0.32						0.76	0.87				0.43	0.48	

[a]Environment: hydrogen, 1 torr; vacuum, $\approx 10^{-9}$ torr. An asterisk on the temperature indicates experiments with a second specimen pair.

Presentations at Technical Meetings

Compiled by Frances A. Scarboro and Brenda S. Jeffers

Proceedings of the International Working Sessions of Fusion Reactor Technology, ORNL, Oak Ridge, Tenn., June 28–July 2, 1971

F. W. Wiffen,* "Radiation Damage in CTR's"

F. W. Wiffen,* "Radiation Damage"

Third International Conference on Crystal Growth, University of Marseille, Marseille, France, July 5–9, 1971

G. W. Clark,* J. C. Wilson, B. F. Oliver, and A. T. Chapman, "Directional Solidification in a Multicomponent Metal-Metal Oxides System"

Second International Conference on Calorimetry and Thermodynamics (26th Annual Calorimetry Conference), University of Maine, Orono, Maine, July 12–14, 1971

T. G. Kollie,* D. L. McElroy, R. K. Adams, and J. M. Jansen, "Measurement Accuracy of a Computer Operated Data Acquisition System"

T. G. Kollie,* D. L. McElroy, and C. R. Brooks, "Magnetic and Configurational Ordering Effects on the Specific Heat Capacity and Electrical Resistivity of Ni_3Fe Between 1.2 and 1200 K"

Alan Wolfenden,* "Calorimetric Determination of the Stored Energy of Cold Work in Metals"

Gordon Conference on Corrosion, New London, N.H., July 26–30, 1971

R. E. Pawel,* "Stress Measurements During the Oxidation of Refractory Metal Alloys"

International Conference on Mechanical Behavior of Materials, Kyoto, Japan, Aug. 15–20, 1971

R. E. Predmore, R. J. Arsenault,* and C. J. Sparks, Jr., "Strengthening and Fracture of Ta-Mo, Nb-W, Mo-W, and Ta-Nb Alloys Induced by Solution Hardening and the Size Effect Associated with Short Range Ordering"

American Nuclear Society Meeting (Conference on Reactor Operating Experience), Denver, Colo., Aug. 9–11, 1971

D. O. Hobson and P. L. Rittenhouse,* "Cladding Embrittlement during a Loss-of-Coolant Accident"

20th Annual Conference on Applications of X-Ray Analysis, Denver, Colo., Aug. 11–13, 1971

Cullie J. Sparks, Jr., and Dale A. Gedcke,* "Rapid Recording of Powder Diffraction Patterns with Si(Li) X-Ray Energy Analysis System: W and Cu Targets and Error Analysis"

The American Crystallographic Association Summer Meeting (Small Angle Scattering Session), Iowa State University, Ames, Iowa, Aug. 15–21, 1971

R. W. Hendricks,* C. J. Sparks, Jr., and L. B. Shaffer, "A Comparison of Three Methods for Absolute Intensity Calibration"

L. B. Shaffer and R. W. Hendricks,* "Optimization of Camera Parameters for the Kratky Small-Angle X-Ray Collimation System"

---

*Speaker.

Fourth United Nations International Conference on the Peaceful Uses of Atomic Energy, Geneva, Switzerland, Sept. 6–16, 1971

E. A. Evans,* E. E. Kintner, E. L. Zebroski, L. A. Neimark, and C. M. Cox, "The Status of Engineering Design and Irradiation Testing of the Stainless-Steel-Clad Mixed Oxide Fuel System for Fast Breeder Reactors"

A. L. Lotts,* T. N. Washburn, L. Geller, H. H. Klepfer, and W. H. Layman, "The Status of Thermal Reactor Fuel Manufacture in the United States"

R. Salmon,* J. T. Roberts, A. L. Lotts, T. N. Washburn, and W. H. McVey, "Price Forecasting and Resource Utilization for the Fuel Cycle Industry of the United States"

P. G. Shewmon,* G. W. Cunningham, C. E. Dickerman, D. P. Hines, F. J. Homan, G. A. Last, and P. Murray, "Analytical Methods to Design and Predict Performance of Fast Reactor Fuel Elements"

H. B. Stewart,* R. C. Dahlberg, W. V. Goeddel, D. B. Trauger, P. R. Kasten, and A. L. Lotts, "Utilization of the Thorium Cycle in the HTGR"

American Chemical Society Meeting, Washington, D.C., Sept. 12–17, 1971

G. L. Powell,* C. E. Holcombe, Jr., and R. E. Clausing, "The Surface Structure of Lithium Hydride"

J. L. Scott,* J. M. Leitnaker, and C. B. Pollock, "HTGR Fuel Particles Derived from Ion-Exchange Resins" (invited paper)

5th International Materials Symposium, University of California, Berkeley, Calif., Sept. 13–17, 1971

K. H. G. Ashbee,* "Water Damage in Glass Fiber/Polyester Resin Composites"

R. W. Carpenter,* "Transmission and Scanning Electron Microscope Observations of Niobium-Hafnium Alloys"

S. M. Ohr, Alan Wolfenden, and T. S. Noggle,* "Electron Displacement Damage in Graphite and Aluminum"

Alan Wolfenden,* "Electron Displacement Damage in Aluminum: Effect of Purity"

A. Wolfenden,* K. Farrell, and J. O. Stiegler, "The Role of Electron Microscopy in the Understanding of Neutron Irradiation-Produced Swelling"

Fourth Annual Technical Meeting of the International Metallographic Society, Inc., Denver, Colo., Sept. 21–23, 1971

K. Farrell* and J. T. Houston, "Annealing of Radiation Damage in Aluminum"

K. Farrell* and J. T. Houston, "Creep Cavitation of Tungsten"

R. J. Gray,* "Revealing Ferromagnetic Microstructures with Ferrofluids"

First International Conference on "Structural Mechanics in Reactor Technology," Berlin, Sept. 20–24, 1971

F. J. Homan, "A Parametric Analysis of Fuel-Cladding Mechanical Interactions" (presented by R. W. Weeks, ANL)

United States-Japan Seminar on Radiation Effects in Metals and Structural Materials, Kyoto, Japan, Sept. 28–30, 1971

E. E. Bloom* and J. O. Stiegler, "Void Damage in Neutron Irradiated Structural Metals"

11th International Thermal Conductivity Conference, Albuquerque, N.M., Sept. 27–Oct. 1, 1971

D. L. McElroy,* "Thermal Conductivity Implications"

J. P. Moore and D. L. McElroy,* "A Guarded-Longitudinal-Heat-Flow Technique for Measurement of Thermal Conductivity, Electrical Resistivity, and Seebeck Coefficient Between 300 and 1000 K"

Fall Meeting of the Electrochemical Society, Cleveland, Ohio, Oct. 3–8, 1971 (Symposium on Anodic Oxide Films)

R. E. Pawel* and J. P. Pemsler, "Impurity Distributions in Anodic Films on Tantalum"

1971 Thermionic Conversion Specialists Conference, San Diego, Calif., Oct. 4–7, 1971

A. C. Schaffhauser,* H. Inouye, and H. E. McCoy, "Materials Development at ORNL for Thermionics Applications"

F. W. Wiffen,* "Radiation Damage to Refractory Metals as Related to Thermionic Applications"

Society of Aerospace Material and Process Engineers (SAMPE) Meeting, Huntsville, Ala., Oct. 5–7, 1971

H. E. McCoy,* R. E. Gehlbach, and B. McNabb, "Development of New Nickel-Base Alloys for High-Temperature Service"

G. M. Slaughter,* D. A. Canonico, and R. G. Donnelly, "Welding and Brazing of Advanced Refractory Alloys"

R. L. Stephenson,* "Application of the Larson-Miller Parameter to Niobium-Base Alloys"

1971 Winter Meeting of the American Nuclear Society, Miami Beach, Fla., Oct. 17–21, 1971

E. E. Bloom* and J. O. Stiegler, "Postirradiation Mechanical Properties of Standard and Titanium-Modified Stainless Steels"

D. A. Canonico,* "Characterization of Heavy Section Steel Weldments"

T. L. Chandler and C. K. H. DuBose, "Electron Microscopy Specimen Preparation in a Hot Cell" (presented by E. M. King)

G. L. Copeland,* R. G. Donnelly, and W. R. Martin, "Irradiation Performance of Boron Carbide Powders Containing Free Boron"

B. Fleischer,* T. N. Washburn, and K. R. Thoms, "Calorimetry as an Aid to Thermal Analysis of Irradiation Capsules"

B. E. Foster, S. D. Snyder,* and V. A. DeCarlo, "High-Intensity, High-Resolution Neutron Radiography of Nuclear Fuels"

G. M. Goodwin and B. F. Early,* "Plasma-Arc Welding of an Isotope Capsule"

D. O. Hobson,* "Analyses of LOCA Transients in Terms of Cladding Embrittlement"

F. J. Homan,* "Use of a Fuel Performance Model to Analyze Materials Data"

J. W. Koger,* R. B. Evans III, and J. H. DeVan, "Corrosion in Polythermal Liquid Metal and Fused Salt Loop Systems"

C. T. Liu,* H. Inouye, and R. G. Donnelly, "New Pt-Rh-W Cladding Alloys for Space Isotopic Heat Sources"

E. L. Long, Jr.,* and J. L. Miller, Jr., "Installation of the Shielded Electron Microprobe Analyzer at Oak Ridge National Laboratory"

M. M. Martin and R. G. Donnelly,* "Fabrication of Helium Permeable Cermets for Application to Curium Fuels"

M. M. Martin, A. E. Richt, and W. R. Martin, "Irradiation Performance of Aluminum-Base Dispersion-Type Fuel Plates" (presented by G. M. Adamson, Jr.)

A. R. Olsen,* "Sol-Gel Sphere-Pac $(U,Pu)O_2$ Fuel Performance in EBR-II Irradiation Tests"

J. L. Scott,* J. H. Coobs, R. L. Hamner, and J M Robbins, "Development of Bonding Materials for HTGR Fuel Elements"

G. M. Slaughter, J. H. DeVan,* and R. H. Jones, "Posttest Examination of the LMEC ALCO/BLH Steam Generator"

F. W. Wiffen,* "The Effect of Temperature on the Microstructure of Neutron-Irradiated Tantalum"

J. M. Williams,* N. E. Hinkle, and W. P. Eatherly, "Effect of Neutron Irradiation at 110 K on Thermal Conductivity of Beryllium"

Fall Meeting of the Metallurgical Society of the American Institute of Mining, Metallurgical, and Petroleum Engineers, Detroit, Michigan, Oct. 18–21, 1971

R. E. Clausing,* G. L. Powell, and C. E. Holcombe, "LEED-AES-EID Studies of Lithium Hydride" (Metal Show and Materials Engineering Congress)

W. A. Coghlan,* "The Use of Computer Simulation to Index Complex Auger Electron Spectra"

N. C. Cole,* G. M. Goodwin, and G. M. Slaughter, "Effect of Heat Treatment on Corrosion Properties of Austenitic Stainless Steel Welds"

K. Farrell* and J. T. Houston, "Crystallography of a Gas Bubble in Tungsten" (1971 Metals Show)

K. Farrell* and J. T. Houston, "Temperature-Dependent Radiation Damage in Aluminum" (1971 Metals Show)

R. J. Gray,* "Magnetic Domain Patterns on Delta Ferrite" (1971 Metals Show)

A. Jostsons* and K. Farrell, "Radiation Voids in Magnesium"

A. Jostsons,* E. L. Long, Jr., J. E. Ferguson, and K. Farrell, "Swelling in Aluminum and Its Alloys"

W. R. Martin,* G. A. Reimann, and R. T. King, "Ultrafine Grain Size Type 316 Stainless Steel" (Session on Ultrafine Grain Size Materials)

R. A. Vandermeer,* "The Behavior of Grain Boundaries During Recrystallization of Dilute Aluminum-Gold Alloys" (Session on Nature and Behavior of Grain Boundaries) (invited paper)

A. Wolfenden,* "Effects of Preinjected Hydrogen on the Electron Displacement Damage in 1100 Aluminum"

M. H. Yoo* and S. M. Ohr, "Elastic Interaction of a Point Defect with a Prismatic Dislocation Loop in Hexagonal Crystals"

Symposium on "High Temperature Materials," BhaBha Atomic Research Centre, Bombay, India, Oct. 29, 1971

Krishna Kuman Sinha* and Joseph P. Hammond, "Dispersion Hardening in Molybdenum and Its Evaluation by Hot-Hardness Test"

Fall Meeting of the Nuclear Division of the American Ceramic Society, Anaheim, Calif., Oct. 30–Nov. 3, 1971

R. A. Bradley* and F. G. Kitts, "Fabrication of $(U,Pu)O_2$ Pellets from Sol-Gel Microspheres"

J. P. De Luca and J. M. Leitnaker, "Review of the Thermodynamic Properties of the Chromium-Nitrogen System" (presented by V. J. Tennery)

W. J. Lackey,* R. A. Bradley, and C. M. Cox, "In-Reactor and Out-of-Reactor $(U,Pu)O_2$ Grain Growth Kinetics"

J. D. Sease,* W. H. Pechin, and C. F. Sanders, "HTGR Refabrication Development"

V. J. Tennery* and T. G. Godfrey, "Oxidation Properties of $(U,Pu)O_2$"

C. S. Yust* and C. J. McHargue, "Further Observations on the Deformation of Hyperstoichiometric UO_2 Single Crystals"

29th Pittsburgh Diffraction Conference, Mellon Institute, Pittsburgh, Pa., Nov. 3–5, 1971

Robert W. Hendricks,* "The Role of Soller Slits in Small-Angle X-Ray Scattering Collimation Systems"

Cullie J. Sparks, Jr.,* "X-Ray Powder Diffraction Patterns with an Energy Analysis System: Errors from Alignment and Energy Measurement"

1971 Fall Meeting of the Nuclear Division Basic Science Division of the American Ceramic Society, Gatlinburg, Tenn., Nov. 3–6, 1971

C. S. Yust* and C. J. McHargue, "Deformation of Hyperstoichiometric UO_2 Single Crystals"

IAEA Panel Meeting on NDT of Reactor Core Components and Pressure Vessels, Vienna, Austria, Nov. 29–Dec. 3, 1971

R. W. McClung, "Nondestructive Testing of Irradiated Fuel Elements in the U.S.A." (rapporteur – C. A. Mann, England)

R. W. McClung,* "On Nondestructive Examination of Nuclear Fuel Pellets in the U.S.A."

R. W. McClung, "On Nondestructive Testing in the U.S.A. of Prestressed Concrete Pressure Vessels for Nuclear Reactors" (rapporteur – R. Roche, Saclay, France)

R. W. McClung,* "Use of Nondestructive Testing in the U.S.A. During Fabrication and Surveillance of Pressure Tubes"

Symposium on Analytical Methods in the Nuclear Fuel Cycle, Vienna, Austria, 29 Nov.–3 Dec., 1971

W. H. Pechin, R. A. Bradley, W. J. Lackey, and J. D. Sease, "Analysis of $(U,Pu)O_2$ Fuels at Oak Ridge National Laboratory" (presented by W. R. Laing, Analytical Chemistry Division)

Ninth Annual Solid State Physics Conference, Manchester, England, Jan. 4–6, 1972

G. M. Stocks,* R. W. Williams, and J. S. Faulkner, "Electronic Densities of States of Ag-Pd Alloys Using the Coherent Potential Approximation"

1972 National Association of Corrosion Engineers Corrosion Research Conference, St. Louis, Mo., Mar. 20–24, 1972

J. W. Koger,* "Effect of Impurities on Corrosion by Molten Fluoride Salts"

The American Physical Society Meeting, Atlantic City, N.J., Mar. 27–30, 1972

J. S. Faulkner,* "Comments on the Coherent Potential Approximation for Dilute Alloys"

G. S. Painter,* "A Combined Green's Function-Discrete Variational Method for Calculating the Electronic Structure of Crystal Compounds"

G. M. Stocks,* R. W. Williams, and J. S. Faulkner, "Electronic Densities of States of Ag-Pd Alloys"

Third International AWS-WRC Brazing Conference, 53rd Annual Meeting of the American Welding Society, Detroit, Mich., Apr. 10–14, 1972

D. A. Canonico* and G. M. Slaughter, "Brazing Stainless Steels to Refractory Metals"

N. C. Cole* and G. M. Tolson, "Corrosion of Nickel-Base Brazing Filler Metals in Boiling Potassium"

Francis B. Gurtner and Joseph P. Hammond,* "The Development of Low-Level Radioactive Welding Wire Using Impounded Tracers for Defect Detection"

Joseph P. Hammond,* N. C. Binkley, and G. M. Slaughter, "Bonding of Tungsten with a Fugitive Alloy Binder"

P. P. Holz,* G. M. Slaughter, and G. M. Goodwin, "Development of an Automated Welder for Nuclear Pipe Construction"

L. C. Williams* and J. E. Van Cleve, "In-Cell Fabrication of HFIR Target Rods and Special Neutron Sources"

83rd Meeting of the Acoustical Society of America, Buffalo, N.Y., Apr. 18–21, 1972

Laszlo Adler* and H. L. Whaley, "Advantages of a Two-Transducer Frequency Analysis Technique to Characterize Discontinuities"

American Nuclear Society Conference on Reactor Materials Performance, Richland, Wash., Apr. 24–26, 1972

R. J. Beaver* and A. E. Richt, "Boron Concentration Gradient for Improved Thermal Reactor Performance of Boron-Stainless Steel Control Rods"

E. E. Bloom* and J. R. Weir, Jr., "Effect of Neutron Irradiation on the Ductility of Austenitic Stainless Steel"

G. L. Copeland,* R. G. Donnelly, and W. R. Martin, "Irradiation Behavior of Boron Carbide"

F. J. Homan,* "Performance Modeling of Neutron Absorbers"

W. J. Lackey,* F. J. Homan, and A. R. Olsen, "Porosity and Actinide Redistribution During Irradiation of $(U,Pu)O_2$"

G. M. Slaughter, J. H. DeVan, and J. P. Hammond, "Materials for LMFBR Steam Generators" (presented by J. R. Weir, Jr.)

Third International Conference on Chemical Vapor Deposition, Salt Lake City, Utah, Apr. 24–27, 1972

J. I. Federer,* W. R. Martin, K. W. Haff, and D. W. Ramey, "Chemical Vapor Deposited Refractory Metal Capsules for Radioisotope Sources"

J. I. Federer* and A. C. Schaffhauser, "Chemical Vapor Deposition and Characterization of Tungsten-Rhenium Alloys"

J. I. Federer* and L. E. Poteat, "A Study of the Adherence of Tungsten and Molybdenum Coatings"

74th Annual Meeting of the American Ceramic Society, Washington, D.C., May 6–11, 1972

A. T. Chapman,* J. Brynestad, J. C. Wilson, and G. W. Clark, "Stoichiometry Changes in Molten Uranium Dioxide"

F. J. Homan* and W. R. Martin, "Modeling of Swelling and Gas Release in Neutron Absorbers"

W. J. Lackey* and F. J. Homan, "Porosity and Actinide Redistribution, Grain Growth, and Desintering in $(U,Pu)O_2$"

J. M. Leitnaker,* T. B. Lindemer, and F. J. Homan, "Analysis of Intergranular Cladding Attack in LMFBR Fuel Pins"

T. B. Lindemer* and H. J. deNordwall, "Analysis of Chemical Failure of Urania Fuel Particles in the HTGR"

T. B. Lindemer,* "Kinetics of the UO_2-C-N_2 Reaction at 1695°C"

T. S. Lundy,* R. A. Padgett, and M. D. Banus, "Cation Self Diffusion in Titanium Monoxide"

C. S. Morgan,* K. H. McCorkle, and G. L. Powell, "Desintering of Thoria, II"

C. B. Pollock,* J. L. Scott, W. P. Eatherly, J. H. Coobs, and R. B. Fitts, "Recent Developments and Irradiation Experience with Resin-Derived Fuels"

Spring Meeting of the Metallurgical Society of the American Institute of Mining, Metallurgical, and Petroleum Engineers, Boston, Mass., May 8–11, 1972

J. V. Cathcart,* "The Mechanical Properties of Scales and Their Influence on High Temperature Gas-Metal Reactions"

R. E. Clausing, D. S. Easton,* and R. A. Strehlow, "The Effect of Low Pressure Hydrogen on the Friction Properties of Graphite"

W. A. Coghlan,* "The Diffusion of Point Defects Near a Prismatic Dislocation Loop"

J. H. DeVan,* "Corrosion and Compatibility Problems of Thermonuclear Reactors"

D. S. Easton* and R. E. Clausing, "Friction of Graphite in a Simulated Space Environment"

C. T. Liu,* H. Inouye, and R. W. Carpenter, "Mechanical Properties and Structure of Internally Oxidized Ta–8W–2Hf (T-111) Alloy"

B. T. M. Loh,* "Vacancies in Solid Solutions"

R. A. Vandermeer* and J. C. Ogle, "The Rolling Texture of Cu_3Au"

F. W. Wiffen,* "Radiation Damage in Thermonuclear Reactor Primary Structures"

M. H. Yoo,* "Elastic Interaction of Prismatic Dislocation Loops with Point Defects under Applied Stress"

Symposium on Defect Interactions in Solids, Bangalore, India, May 9–13, 1972

A. Wolfenden,* "Work Hardening Theories Analyzed in Terms of Stored Energy Data"

Conference on the Local Structural Order and Decomposition of Titanium, Uranium and Zirconium-Base B.C.C. Solid Solutions, Cornell University, Ithaca, N.Y., May 15, 1972

R. W. Carpenter,* "Diffuse Intensity Distribution Associated with Transition Alpha Metastable Precipitate"

R. A. Vandermeer,* "The Body-Centered Cubic (γ) to Tetragonal (γ_0) Phase Transformation in Uranium-Niobium-Zirconium Alloys"

H. L. Yakel,* "The Decomposition of Uranium-Base B.C.C. Alloys"

Fifth International Congress on Metallic Corrosion, Tokyo, Japan, May 21–27, 1972

J. V. Cathcart,* R. E. Pawel, and G. F. Petersen, "High Temperature Oxidation of Uranium Alloys"

Third International Conference on Sintering and Related Phenomena, University of Notre Dame, South Bend, Ind., June 5–7, 1972

C. S. Morgan,* K. H. McCorkle, and G. L. Powell, "Sintering and Desintering of Thoria"

18th Annual Meeting of the American Nuclear Society, Las Vegas, Nev., June 18–22, 1972

E. E. Bloom* and J. O. Stiegler, "Effect of Irradiation on Titanium-Modified Type 316 Stainless Steel"

D. A. Canonico* and G. M. Slaughter, "Weldability of Niobium-Stabilized 2¼ Cr–1 Mo Steel"

R. E. Clausing* and D. S. Easton, "The Gaseous Environment Inside a NERVA Reactor in Space"

N. C. Cole and J. W. Hendricks, "Compatibility of Brazes with Liquid Metals and Molten Salts" (presented by D. A. Canonico)

G. L. Copeland, H. L. Yakel, and C. K. H. DuBose, "Evaluation of Fast-Reactor-Irradiated Boron Carbide Powders" (presented by W. R. Martin)

D. S. Easton and R. E. Clausing,* "Friction of Graphite in Inert and Hydrogen Atmospheres"

K. Farrell* and R. T. King, "Radiation-Induced Strengthening and Intergranular Fracture in Aluminum"

R. B. Fitts* and F. L. Miller, "Analysis and Performance of Instrumented Fuel Pins"

F. J. Homan,* "Influence of Materials Data Uncertainty on Fuel Pin Performance Predictions"

H. Inouye,* C. T. Liu, and R. G. Donnelly, "New Platinum-Rhodium-Tungsten Alloys for Space Isotopic Heat Sources"

A. Jostsons* and C. K. H. DuBose, "Electron Microscopy of Fast-Reactor-Irradiated Boron Carbide"

J. W. Koger,* "Hastelloy N Alloys After Nine Years Exposure to a Molten Fluoride Salt"

A. W. Longest, R. B. Fitts,* and J. A. Conlin, "Fission Gas Release Behavior in a Vented $(U,Pu)O_2$ GCFBR Fuel Pin"

A. L. Lotts, J. D. Sease,* and R. G. Wymer, "HTGR Fuel Refabrication Development"

A. J. Moorhead* and G. M. Slaughter, "Welding of a Molybdenum Test Stand for Chemical Processing"

A. R. Olsen,* "High-Burnup Irradiation Tests of Sphere-Pac Sol-Gel Fuels"

J. D. Sease,* C. F. Sanders, W. P. Eatherly, D. P. Harmon, and W. J. Scheffel, "Fabrication of Plutonium Fuels for HTGR"

R. L. Senn,* J. A. Conlin, and R. B. Fitts, "An Improved Capsule Design for Experimental Measurement of Fuel-Cladding Mechanical Interaction"

Alan Wolfenden,* "Electron Irradiation Damage in Aluminum near the Threshold Energy"

American Society for Testing and Materials Symposium on the Effects of Radiation on Structural Materials, Los Angeles, Calif., June 26–28, 1972

E. E. Bloom* and J. O. Stiegler, "Effect of Irradiation on the Microstructure and Creep-Rupture Properties of Type 316 Stainless Steel"

R. T. King,* A. Jostsons, and K. Farrell, "Neutron Irradiation Damage in a Precipitation Hardened Aluminum Alloy"

International Carbon Conference, Baden-Baden, Germany, June 26–30, 1972

J. L. Scott,* C. B. Pollock, R. L. Hamner, J M Robbins, J. H. Coobs, and W. P. Eatherly, "Fabrication and Irradiation Behavior of Advanced Fuel Sticks for the HTGR"

American Society for Testing and Materials Symposium on Testing for Prediction of Materials Performance in Structures and Components, Los Angeles, Calif., June 27, 1972

R. W. McClung,* "The Role of Nondestructive Evaluation in Predictive Testing"

Publications

Compiled by Meredith R. Hill

Adler, Laszlo, and H. L. Whaley, "Interference Effect in a Multifrequency Ultrasonic Pulse Echo and Its Application to Flaw Characterization," *J. Acoust. Soc. Amer.* 51(3) Pt. 2: 881–87 (March 1972).

Ashbee, K. H. G., "Defects in Boron Carbide before and after Neutron Irradiation," *Acta Met.* 19(10): 1079–85 (October 1971).

Ashbee, K. H. G., and C. K. H. DuBose, "Dislocation Nodes in Boron Carbide, with Special Reference to Non-Stoichiometry," *Acta Met.* 20(2): 241–45 (February 1972).

Ashbee, K. H. G., "Water Damage in Glass Fiber/Polyester Resin Composites," pp. 1205–22 in *Electron Microscopy and Structure of Materials* (Proc. 5th Int. Materials Symp., Berkeley, Sept. 13–17, 1971), ed. by Gareth Thomas, R. M. Fulrath, and R. M. Fisher, University of California Press, Berkeley, 1972.

Askill, J., "Tracer Diffusion in the Chromium-Nickel System," *Phys. Status Solidi (a)* 8: 587–96 (1971).

Avery, R. E., D. A. Canonico, P. Patriarca, G. F. McKittrich, C. S. Shira, W. Yeniscavich, and R. W. Straiton, "Nickel and High-Nickel Alloys," Chap. 67 in *Welding Handbook,* 6th ed., Sect. 4, "Metals and Their Weldability," ed. by Len Griffing, American Welding Society, Miami, Florida, 1972.

Begun, G. M., J. Brynestad, K. W. Fung, and G. Mamantov, "Raman Spectra of the Molten $AlCl_3$-$ZnCl_2$ System and Molten Cs_2ZnCl_4," *Inorg. Nucl. Chem. Lett.* 8(1): 79–88 (January 1972).

Berggren, R. G., and W. J. Stelzman, "Radiation Strengthening and Embrittlement in Heavy Section Plate and Welds," *Nucl. Eng. Des.* 17(1): 103–15 (August 1971).

Binkley, N. C., *State-of-the-Art Review – Weldability of Stabilized 2¼ Cr–1 Mo Steels,* ORNL-TM-3490 (August 1971).

Bloom, E. E., and J. O. Stiegler, "Postirradiation Mechanical Properties of Standard and Titanium-Modified Stainless Steels," (Summary) *Trans. Amer. Nucl. Soc.* 14(2): 557–59 (October 1971).

Bloom, E. E., *Nucleation and Growth of Voids in Stainless Steels During Fast Neutron Irradiation,* ORNL-TM-3492 (October 1971); also pp. 1–30 in *Radiation-Induced Voids in Metals* (Proc. Int. Conf. Albany, N.Y., June 9–11, 1971), ed. by J. W. Corbett and L. C. Ianniello, AEC Symp. Ser. 26, CONF-710601 (April 1972).

Bloom, E. E., and J. O. Stiegler, "Effect of Irradiation on Titanium-Modified Type 316 Stainless Steel," (Summary) *Trans. Amer. Nucl. Soc.* 15(1): 253–54 (June 1972).

Bourgette, D. T., D. V. Keller, and R. L. Stephenson, "Effect of High Vacuum on Some Important Properties of Metals and Alloys," Chap. XI, pp. 858–61 in *Vacuum Metallurgy,* ed. by O. Winkler and R. Bakish, Elsevier Publishing Company, Amsterdam, 1971.

Bradley, R. A., and J. D. Sease, "The Design and Operation of a Plutonium Laboratory," *Nucl. Mater. Manage.* 1(1): 11–14 (April 1972).

Breillatt, J. P., B. W. Harrell, and K. W. Boling, "Fabric Formation in Centrifugal Fields: Fibrin (35975)," *Proc. Soc. Exp. Biol. Med.* 138(2): 719–22 (November 1971).

Buchanan, M. G., and R. W. Hendricks, "A Program for the Evaluation of Weighting Functions Used in Small-Angle X-Ray Scattering," *J. Appl. Cryst.* 4, Pt. 2: 176–77 (April 1971).

Canonico, D. A., and R. G. Berggren, "Tensile and Impact Properties of Thick-Section Plate and Weldments," *Nucl. Eng. Des.* 17(1): 4–15 (August 1971).

Canonico, D. A., "Transition Temperature Considerations for Thick-Wall Steel Nuclear Pressure Vessels," *Nucl. Eng. Des.* 17(1): 149–60 (August 1971).

Canonico, D. A., "Characterization of Heavy Section Steel Weldments," (Summary) *Trans. Amer. Nucl. Soc.* 14(2): 585 (October 1971).

Canonico, D. A., and G. M. Slaughter, "Weldability of Niobium-Stabilized 2¼ Cr–1 Mo Steel," (Summary) *Trans. Amer. Nucl. Soc.* 15(1): 228 (June 1972).

Cardwell, R. G., B. E. Foster, and J. C. Gower, "An Integrated System of Nuclear Materials Control at Oak Ridge National Laboratory," pp. 85–100 in *Inst. Nucl. Mater. Manage. Annu. Meet. 11th,* Institute of Nuclear Materials Management, P.O. Box 10814, Pittsburgh, Pa., 1970.

Cardwell, R. G., "Control of Materials in Research: A Special Management Problem," *Nucl. Mater. Manage.* 1(1): 8–10 (April 1972).

Carpenter, R. W., "Transmission and Scanning Electron Microscope Observations of Niobium-Hafnium Alloys," pp. 667–77 in *Electron Microscopy and Structure of Materials* (Proc. 5th Int. Materials Symp., Berkeley, Sept. 13–17, 1971), ed. by Gareth Thomas, R. M. Fulrath, and R. M. Fisher, University of California Press, Berkeley, 1972.

Cathcart, J. V., R. E. Pawel, and G. F. Petersen, *Oxidation Properties of Two Uranium Alloys (U–16.6 at. % Nb–5.6 at. % Zr and U–21 at. % Nb),* Y-1800 (October 26, 1971).

Cathcart, J. V., R. E. Pawel, and G. F. Petersen, "The Oxidation Properties of U-16.6 at. % Nb–5.6 at. % Zr and U–21 at. % Nb," *Oxid. Metals* 3(6): 497–521 (November 1971).

Cathcart, J. V., and G. F. Petersen, *The Low-Temperature Oxidation of U-Nb and U-Nb-Zr Alloys,* ORNL-TM-3587 (December 1971); also *J. Nucl. Mater.* 43(2): 86–92 (May 1972).

Cathcart, J. V., "The Structure and Properties of Thin Oxide Films," pp. 17–36 in *Oxidation of Metals and Alloys* (papers presented at a Seminar of the American Society for Metals, October 17 and 18, 1970), American Society for Metals, Metals Park, Ohio, 1971.

Chakraborty, A. K., and W. R. Martin, "A Container for Blending Dispersed Powders and Homogeneity Determination," *Int. J. Powder Met.* 7(4): 3–6 (1971).

Chandler, J. M. *Thorium-Uranium Recycle Facility,* ORNL-TM-3422 (July 1971).

Chandler, T. L., and C. K. H. DuBose, "Electron Microscopy Specimen Preparation in a Hot Cell," (Summary) *Trans. Amer. Nucl. Soc.* 14(2): 881–82 (October 1971).

Cheng, C. C., C. V. Dodd, and W. E. Deeds, "General Analysis of Probe Coils Near Stratified Conductors," *Int. J. Nondestruct. Test.* 3(2): 109–30 (September 1971).

Clausing, R. E., and D. S. Easton, "The Gaseous Environment Inside a NERVA Reactor in Space," (Summary) *Trans. Amer. Nucl. Soc.* 15(1): 203 (June 1972).

Coghlan, W. A., *A Computer Program to Calculate Auger Transitions for a Surface Containing Several Kinds of Atoms,* ORNL-TM-3575 (October 1971).

Coghlan, W. A., and R. E. Clausing, *A Catalogue of Calculated Auger Transitions for the Elements,* ORNL-TM-3576 (November 1971).

Coghlan, W. A., "Constant Stress-Continuous Load Compression Creep Machine for Small Single Crystals," *Rev. Sci. Inst.* 43(3): 464–67 (March 1972).

Cole, N. C., R. G. Gilliland, and G. M. Slaughter, "Weldability of Tungsten and Its Alloys," *Weld. J. (Miami)* 50(9): 419-s–426-s (September 1971).

Cole, N. C., and J. W. Hendricks, "Compatibility of Brazes with Liquid Metals and Molten Salts," (Summary) *Trans. Amer. Nucl. Soc.* 15(1): 237–39 (June 1972).

Copeland, G. L., R. G. Donnelly, and W. R. Martin, "Irradiation Performance of Boron Carbide Powders Containing Free Boron," (Summary) *Trans. Amer. Nucl. Soc.* 14(2): 573 (October 1971).

Copeland, G. L., L. Queener, and W. R. Martin, *Experimental Investigations of Fabrication of Th–20 wt % U for the UMBR Fuel Element,* ORNL-TM-3499 (October 1971).

Copeland, G. L., C. K. H. DuBose, R. G. Donnelly, and W. R. Martin, *Transmission Electron Microscopy of Irradiated Boron Carbide,* ORNL-TM-3577 (January 1972); also *J. Nucl. Mater.* 43(2): 126–32 (May 1972).

Copeland, G. L., H. L. Yakel, and C. K. H. DuBose, *Evaluation of Fast-Reactor Irradiated Boron Carbide Powders,* ORNL-TM-3729 (May 1972).

Copeland, G. L., H. L. Yakel, and C. K. H. DuBose, "Evaluation of Fast-Reactor-Irradiated Boron Carbide Powders," (Summary) *Trans. Amer. Nucl. Soc.* 15(1): 246–47 (June 1972).

Cox, C. M., D. R. Cuneo, and E. J. Manthos, *Performance of Sphere-Pac and Pelletized (U,Pu)O_2 During Severe Overpower Transients,* ORNL-TM-3384 (July 1971); also pp. 701–24 in *Proc. Conf. Fast Reactor Fuel Element Technology,* ed. by Ruth Farmakes, American Nuclear Society, Hinsdale, Illinois.

Cox, C. M., and R. E. Adams, *Safety Analysis and Test Specifications for Transient Tests of Sol-Gel (U,Pu)O_2 Fuel Pins (ORNL Series I),* ORNL-TM-3574 (December 1971).

Crouse, R. S., and R. J. Gray, "Evaluation of the Bausch & Lomb Research II Metallograph," pp. 194–217 in *Technical Papers of the 22nd Metallographic Group Meeting, held June 19–21, 1968, Gulf General Atomic, Inc., San Diego, California,* CONF-680614 (December 1971).

De Luca, J. P., and J. M. Leitnaker, *Review of Thermodynamic Properties of the Chromium-Nitrogen System,* ORNL-TM-3618 (December 1971).

De Luca, J. P., and J. M. Leitnaker, "Phase Behavior in the Pu-Cr-N System," *J. Amer. Ceram. Soc.* 55(5): 273–74 (May 1972).

DeVan, J. H., "Compatibility," pp. 25–31 in *Fusion Reactor First Wall Materials* (Summary of a Meeting Held at AEC-Germantown, January 1972), WASH-1206 (April 1972).

DiStefano, J. R., and R. E. McHenry, *Compatibility of Strontium Compounds with Super Alloys at 900 and 1100°C,* ORNL-4625 (November 1971).

DiStefano, J. R., and K. H. Lin, *Compatibility of Curium Oxide with Refractory Metals at 1650°C and 1850°C,* ORNL-4773 (April 1972).

Dodd, C. V., and W. A. Simpson, "Measurement of Small Magnetic Permeability Changes by Eddy-Current Techniques," *Mater. Eval.* 29(10): 217–21 (October 1971).

Dodd, C. V., and W. A. Simpson, Jr., *Thickness Measurements Using Eddy-Current Techniques,* ORNL-TM-3712 (March 1972).

DuBose, C. K. H., and C. Jones, "Techniques for the Preparation of Transmission Electron Microscopy Specimens from Tubing," pp. 269–81 in *Technical Papers of the 22nd Metallographic Group Meeting, held June 19–21, 1968, Gulf General Atomic, Inc., San Diego, California,* CONF-680614 (December 1971).

Easton, D. S., C. A. Giles, S. H. Merriman, and R. E. Clausing, *Program for Computing Partial Pressures from Residual Gas Analyzer Data,* ORNL-TM-3455 (September 1971).

Easton, D. S., and R. E. Clausing, "Friction of Graphite in Inert and Hydrogen Atmospheres," (Summary) *Trans. Amer. Nucl. Soc.* 15(1): 206–7 (June 1972).

Fahr, Dieter, "Stress- and Strain-Induced Formation of Martensite and Its Effects on Strength and Ductility of Metastable Austenitic Stainless," *Met. Trans.* 2(7): 1883–92 (July 1971).

Farrell, K., J. T. Houston, A. Wolfenden, R. T. King, and A. Jostsons, *Effects of Structural Imperfections on Voids in Aluminum,* ORNL-TM-3493 (September 1971).

Farrell, K., and B. T. M. Loh, "Hardness–Flow Stress–Grain-Size Relationships in Iron," *J. Iron Steel Inst.* 209(11): 915–18 (November 1971).

Farrell, K., and J. O. Stiegler, "Application of Electron Fractography to the Study of High Temperature Cavitation in Tungsten," pp. 71–79 in *Application of Electron Fractography to Materials Research, Spec. Tech. Publ. 493,* American Society for Testing and Materials, Philadelphia, 1971.

Farrell, K., J. T. Houston, A. Wolfenden, R. T. King, and A. Jostsons, "Effects of Structural Imperfections on Voids in Aluminum," pp. 376–85 in *Radiation-Induced Voids in Metals* (Proc. Int. Conf., Albany, N.Y., June 9–11, 1971), ed. by J. W. Corbett and L. C. Ianniello, AEC Symp. Ser. 26, CONF-710601 (April 1972).

Farrell, K., and R. T. King, "Radiation-Induced Strengthening and Intergranular Fracture in Aluminum," (Summary) *Trans. Amer. Nucl. Soc.* 15(1): 245 (June 1972).

Faulkner, J. S., and P. W. Milonni, *Adding Group Theory to KKR Band-Theory Programs for FCC and BCC Structures,* ORNL-TM-3589 (November 1971).

Faulkner, J. S., "Electronic States in Disordered Alloys: Comparison of Methods," *Int. J. Quantum Chem.* 5(Symp. 5): 543–53 (December 1971).

Federer, J. I., and L. E. Poteat, *A Study of the Adherence of Tungsten and Molybdenum Coatings,* ORNL-TM-3609 (December 1971); also pp. 591–99 in *Proc. 3d Int. Conf. Chemical Vapor Deposition,* American Nuclear Society, Hinsdale, Illinois, 1972.

Federer, J. I., W. R. Martin, K. W. Haff, and D. W. Ramey, *Chemical Vapor Deposited Refractory Metal Capsules for Radioisotope Sources,* ORNL-TM-3608 (December 1971); also pp. 740–46 in *Proc. 3d Int. Conf. Chemical Vapor Deposition,* American Nuclear Society, Hinsdale, Illinois, 1972.

Federer, J. I., and E. L. Long, Jr., *Failure Analysis of a Type 416 Stainless Steel Bolt in HFIR,* ORNL-TM-3682 (April 1972).

Federer, J. I., and A. C. Schaffhauser, "Chemical Vapor Deposition and Characterization of Tungsten-Rhenium Alloys," pp. 242–52 in *Proc. 3d Int. Conf. Chemical Vapor Deposition,* American Nuclear Society, Hinsdale, Illinois, 1972.

Finch, C. B., and G. W. Clark, "High-Temperature Solution Growth of Single-Crystal Plutonium Dioxide," *J. Cryst. Growth* 12: 181–82 (1972).

Fitts, R. B., E. L. Long, Jr., and J. M. Leitnaker, *Observations of Fuel-Cladding Chemical Interactions as Applied to GCBR Fuel Rods,* ORNL-TM-3385 (July 1971); also pp. 431–58 in *Proc. Conf. Fast Reactor Fuel Element Technology,* ed. by Ruth Farmakes, American Nuclear Society, Hinsdale, Illinois, 1971.

Fitts, R. B., J. L. Miller, Jr., and E. L. Long, Jr., *Observations on Tungsten-Rhenium Thermocouples Used In-Reactor in $(U,Pu)O_2$ Fuel Pins,* ORNL-TM-3617 (February 1972).

Fitts, R. B., and F. L. Miller, "Analysis and Performance of Instrumented Fuel Pins," (Summary) *Trans. Amer. Nucl. Soc.* 15(1): 180 (June 1972).

Fleischer, B., T. N. Washburn, and K. R. Thoms, "Calorimetry as an Aid to Thermal Analysis of Irradiation Capsules," (Summary) *Trans. Amer. Nucl. Soc.* 14(2): 763 (October 1971).

Foster, B. E., S. D. Snyder, and R. W. McClung, *Imperfections in Chemical Munitions as Detected by X-Ray Scanning,* ORNL-TM-3467 (August 1971).

Foster, B. E., S. D. Snyder, and V. A. DeCarlo, "High-Intensity, High-Resolution Neutron Radiography on Nuclear Fuels," (Summary) *Trans. Amer. Nucl. Soc.* 14(2): 536 (October 1971).

Foster B. E., S. D. Snyder, V. A. DeCarlo, and R. W. McClung, *Development and Operation of a High-Intensity High-Resolution Neutron Radiography Facility,* ORNL-4738 (December 1971).

Frye, J. H, J. E. Cunningham, and staff, *Metals and Ceramics Div. Annu. Progr. Rep. June 20, 1971,* ORNL-4770.

Frye, J. H , "Technology Forecast '72, Modified Nuclear Alloys Add Resistance to Embrittlement," *Metal Prog* 101(1): 56 (January 1972).

Gehlbach, R. E., "Electron Microscope-Microprobe Analysis of Precipitation," pp. 289–96 in *Technical Papers of the 22nd Metallographic Group Meeting, held June 19–21, 1968, Gulf General Atomic, Inc., San Diego, California,* CONF-680614 (December 1971).

Goodwin, G. M., and B. F. Early, "Plasma-Arc Welding of an Isotope Capsule," (Summary) *Trans. Amer. Nucl. Soc.* 14(2): 591–92 (October 1971).

Gray, R. J., and B. C. Leslie, "More on the Metallographic Applications of Xenon Lamp Systems," pp. 65–73 in *Proc. 3rd Annu. Tech. Meet. Metallographic Soc., Nov. 16, 17, and 18, 1970,* International Metallographic Society, Santa Fe, New Mexico, 1971.

Gray, R. J., and B. C. Leslie, "An Alpha Metallography Laboratory at Oak Ridge National Laboratory," pp. 226–57 in *Technical Papers of the 22nd Metallographic Group Meeting, held June 19–21, 1968, Gulf General Atomic, Inc., San Diego, California,* CONF-680614 (December 1971).

Gray, R. J., "Technology Forecast '72, Magnetic Etching Reveals Magnetic Domains," *Metal Prog.* 101(1): 82 (January 1972).

Gray, R. J., *Revealing Ferromagnetic Microstructures with Ferrofluid,* ORNL-TM-3681 (March 1972).

Gyorffy, B. L., "Coherent-Potential Approximation for a Nonoverlapping-Muffin-Tin-Potential Model of Random Substitutional Alloys," *Phys. Rev. B* 5(6): 2362–84 (March 1972).

Hendricks, R. W., and L. B. Schaffer, *Some Properties of Octafluorocyclobutane (C_4F_8) of Interest in X-Ray Absolute Intensity Experiments,* ORNL-TM-3407 (July 1971).

Hendricks, R. W., *PROGRAM WEIGHT: A FORTRAN IV Program for Evaluation of Weighting Functions Used in Small-Angle X-Ray Scattering,* ORNL-TM-1950, Rev. 2 (March 1972).

Hewette II, D. M., J. H. Coobs, J. L. Scott, J. A. Conlin, and R. L. Senn, *Irradiation of Pyrolytic-Carbon-Coated Fuel Particles to Fast Fluences Significant for HTGR's,* ORNL-TM-3441 (May 1972).

Hobson, D. O., "Analyses of Deformation and Texture as Functions of Fabrication in Mandrel-Drawn Tubing," pp. 199–213 in *Metal Forming Interrelation Between Theory and Practice* (Proc. Symp. Relation Between Theory and Practice of Metal Forming, Cleveland, Ohio, October, 1970), ed. by A. L. Hoffmanner, Plenum Press, New York, 1971.

Hobson, D. O., and P. L. Rittenhouse, "Cladding Embrittlement During Loss-of-Coolant Accident," (Summary) *Trans. Amer. Nucl. Soc.* 14, Suppl. 2: 141 (August 1971).

Hobson, D. O., M. F. Osborne, and G. W. Parker, "Comparison of Rupture Data from Irradiated Fuel Rods and Unirradiated Cladding," *Nucl. Technol.* 11(4): 479–90 (August 1971).

Hobson, D. O., "Analyses of LOCA Transients in Terms of Cladding Embrittlement," (Summary) *Trans. Amer. Nucl. Soc.* 14(2): 700–701 (October 1971).

Hobson, D. O., and P. L. Rittenhouse, *Deformation and Rupture Behavior of Light-Water Reactor Fuel Cladding,* ORNL-4727 (October 1971).

Hobson, D. O., *Tubing Fabrication Parameters and Their Application to Texture Control in Zircaloy Tubing,* ORNL-TM-3500 (October 1971).

Hobson, D. O., and P. L. Rittenhouse, *Embrittlement of Zircaloy-Clad Fuel Rods by Steam During LOCA Transients,* ORNL-4758 (January 1972).

Homan, F. J., *Oak Ridge National Laboratory Solutions to a Modeling Round-Robin Exercise,* ORNL-TM-3360 (August 1971).

Homan, F. J., *A Parametric Analysis of Fuel–Cladding Mechanical Interactions,* ORNL-TM-3508 (August 1971).

Homan, F. J., "Use of a Fuel Performance Model to Analyze Materials Data," (Summary) *Trans. Amer. Nucl. Soc.* 14(2): 629 (October 1971).

Homan, F. J., C. M. Cox, and W. J. Lackey, "Comparisons Between Predicted and Measured Fuel Pin Performance," pp. 243–58 in *Proc. Conf. Fast Reactor Fuel Element Technology,* ed. by Ruth Farmakes, American Nuclear Society, Hinsdale, Illinois, 1971.

Homan, F. J., "Influence of Materials Data Uncertainty on Fuel Pin Performance Predictions," (Summary) *Trans. Amer. Nucl. Soc.* 15(1): 183–84 (June 1972).

Houston, J. T., and K. Farrell, "Void Coarsening in High Purity Aluminum During Postirradiation Annealing," *J. Nucl. Mater.* 40(2): 225–29 (August 1971).

Inouye, H., C. T. Liu, and R. G. Donnelly, "New Platinum-Rhodium-Tungsten Alloys for Space Isotopic Heat Sources," (Summary) *Trans. Amer. Nucl. Soc.* 15(1): 163–64 (June 1972).

Irvine, A. R., J. H. Evans, L. B. Shappert, and D. A. Canonico, *LMFBR Spent Fuel Transport: Conceptual Design and Partial Safety Analysis of a Sodium-Cooled Cask,* ORNL-TM-3689 (February 1972).

Jostsons, A., E. L. Long, Jr., J. O. Stiegler, K. Farrell, and D. N. Braski, *Annealing of Voids in Aluminum,* ORNL-TM-3494 (October 1971); also pp. 363–75 in *Radiation-Induced Voids in Metals* (Proc. Int. Conf., Albany, N.Y., June 9–11, 1971), ed. by J. W. Corbett and L. C. Ianniello, AEC Symp. Ser. 26, CONF-710601 (April 1972).

Jostsons, A., and C. K. H. DuBose, "Electron Microscopy of Fast-Reactor-Irradiated Boron Carbide," (Summary) *Trans. Amer. Nucl. Soc.* 15(1): 247–48 (June 1972).

Jostsons, A., and R. T. King, "Transmutation-Produced Mg_2Si Precipitation in an Irradiated Al–2.5% Mg Alloy," *Scripta Met.* 6(6): 447–51 (June 1972).

Kegley, T. M., Jr., "The Quantimet Television Microscope – Its Operation and Evaluation," pp. 168–93 in *Technical Papers of the 22nd Metallographic Group Meeting, held June 19–21, 1968, Gulf General Atomic, Inc., San Diego, California,* CONF-680614 (December 1971).

Kegley, T. M., Jr., "Use of Cellulose Nitrate for Alpha Autoradiography," *Metallography* 5(2): 113–23 (April 1972).

Kerr, H. T., M. J. Bell, and E. E. Bloom, "Neutron Cross-Section Data Applied to the Materials Irradiation Studies at ORNL," p. 485 in *Proc. 3d Conf. Neutron Cross Sections and Technology, Mar. 15–17, 1971,* CONF-710301 (Vol. 2).

King, R. T., E. L. Long, Jr., M. R. Skidmore, and J. E. Beaver, *Failure of Aluminum Tubing in the ORNL 86-Inch Cyclotron,* ORNL-TM-3523 (October 1971).

King, R. T., K. V. Cook, and G. A. Reimann, *Biaxial Creep-Rupture Properties of Defective Stainless Steel Tubing,* ORNL-TM-3711 (April 1972).

Klueh, R. L., "A Feasibility Study of the Determination of Oxygen in Liquid Alkali Metals by Zirconium Gettering," *J. Nucl. Energy* 25(6): 253–61 (June 1971).

Klueh, R. L., "Effect of Oxygen on Niobium-Sodium Compatibility," *Corrosion* 27(8): 342–46 (August 1971).

Klueh, R. L., and J. H. DeVan, *The Effect of Oxygen in Static Sodium on Vanadium and Vanadium Alloys,* ORNL-4739 (November 1971).

Klueh, R. L., and J. H. DeVan, "Liquid-Metal Test Procedures," pp. 405–33 in *Handbook on Corrosion Testing and Evaluation,* ed. by W. H. Ailor, Wiley, New York, 1971.

Klueh, R. L., *The Effect of Oxygen on the Compatibility of Tantalum and Potassium,* ORNL-4737 (November 1971).

Klueh, R. L., and J. H. DeVan, "Vanadium Alloy Development for Sodium-Cooled Reactors," *Nucl. Eng. Des.* 17(3): 371–76 (December 1971).

Klueh, R. L., *The Effect of Oxygen on Tantalum-Sodium Compatibility,* ORNL-TM-3590 (December 1971).

Knight, R. W., and F. L. Sherman, *Development of Manufacturing Procedures for HFIR Fuel Plates to ORNL Specifications,* ORNL-4713 (September 1971).

Koch, C. C., and R. W. Carpenter, "Precipitates and Fluxoid Pinning in a Superconducting Nb-Hf Alloy," *Phil. Mag.* 25(2): 303–20 (February 1972).

Koger, J. W., and A. P. Litman, *Mass Transfer Between Hastelloy N and Haynes Alloy No. 25 in a Molten Sodium Fluoroborate Mixture,* ORNL-TM-3488 (October 1971).

Koger, J. W., R. B. Evans III, and J. H. DeVan, "Corrosion in Polythermal Liquid Metal and Fused Salt Loop Systems," (Summary) *Trans. Amer. Nucl. Soc.* 14(2): 627 (October 1971).

Koger, J. W., "Hastelloy N Alloys after Nine Years Exposure to a Molten Fluoride Salt," (Summary) *Trans. Amer. Nucl. Soc.* 15(1): 227 (June 1972).

Kopp, O. C., and G. W. Clark, "Growth and Crystal Morphology of Lead Sulfide in the Hydrothermal System PbS–RbOH–H_2O," *J. Cryst. Growth* 11: 336–40 (December 1971).

Kroeger, D. M., "A Comparison of Diffusion Penetration Plots Obtained from Alpha Energy Degradation and Electrochemical Sectioning," *J. Nucl. Mater.* 41(3): 345–47 (December 1971).

Lackey, W. J., R. A. Bradley, W. H. Pechin, and T. L. Hebble, "Precision and Source of Variation of Oxygen-to-Metal Determinations for $(U,Pu)O_2$," *Nucl. Technol.* 13(4): 105–7 (April 1972).

Lackey, W. J., and R. A. Bradley, *Microstructure of Sol-Gel-Derived $(U,Pu)O_2$ Microspheres and Pellets,* ORNL-TM-3588 (December 1971); also *Nucl. Technol.* 14(6): 257–68 (June 1972).

Lackey, W. J., "Effect of Temperature on Electrical Conductivity and Transport Mechanisms in Sapphire," pp. 489–502 in *Ceramics in Severe Environments, Materials Science Research,* Vol. 5, ed. by W. Wurth Kriegel and Hayne Palmour III, Plenum Press, New York, 1971.

Leitnaker, J. M., M. L. Smith, and C. M. Fitzpatrick, *Conversion of Uranium Nitrate to Ceramic-Grade Oxide for the Light Water Breeder Reactor: Process Development* ORNL-4755 (April 1972).

Leitnaker, J. M., and K. E. Spear, *Elimination of CO_2 and H_2O as Oxygen Transport Species in Mixed Oxide Fuel Pins,* ORNL-TM-3849 (June 1972).

Lindemer, T. B., and R. A. Bradley, "Kinetic Models for the Synthesis of $(U,Pu)O_{2-y}$ by Hydrogen-Reduction and Carbothermic Techniques," *J. Nucl. Mater.* 41(3): 293–302 (December 1971).

Liu, C. T., and B. T. M. Loh, "Solid Solution Theory and Spinodal Decomposition," *Phil. Mag.* 24(188): 367–88 (August 1971).

Liu, C. T., H. Inouye, and R. W. Carpenter, "A Simple Method of Determination of the Distribution and Solubility Limit of Interstitials in Substitutional Solid Solutions," *J. Less-Common Metals* 25(2): 123–29 (October 1971).

Liu, C. T., H. Inouye, and R. G. Donnelly, "New Platinum-Rhodium-Tungsten Cladding Alloys for Space Isotopic Heat Sources," (Summary) *Trans. Amer. Nucl. Soc.* 14(2): 590–91 (October 1971).

Loh, B. T. M., and K. H. G. Ashbee, *A General Program for Constructing Maps of Kikuchi and Kossel Lines,* ORNL-M-3557 (September 1971).

Loh, B. T. M., "Comments on 'Effect of Mobile Interstitials on the Nucleation of Voids,'" *Scripta Met.* 5(10): 841–43 (October 1971).

Loh, B. T. M., "Nucleation of Dislocation Loops in Solids under Irradiation," *Scripta Met.* 5(12): 1049–52 (December 1971).

Loh, B. T. M., and C. T. Liu, "Vacancies in Ternary Alloys," *Acta Met.* 19(7): 617–20 (July 1971).

Long, E. L., Jr., and J. L. Miller, Jr., "Installation of the Shielded Electron Microprobe Analyzer at ORNL," (Summary) *Trans. Amer. Nucl. Soc.* 14(2): 882 (October 1971).

Long, E. L., Jr., and J. L. Miller, Jr., "Installation of the Shielded Electron Microprobe Analyzer at Oak Ridge National Laboratory," pp. 132–41 in *Proc. 19th Conf. Remote Systems Technol.,* American Nuclear Society, Hinsdale, Illinois, 1971.

Longest, A. W., R. B. Fitts, and J. A. Conlin, "Fission-Gas Release Behavior in a Vented $(U,Pu)O_2$ GCFBR Fuel Pin," (Summary) *Trans. Amer. Nucl. Soc.* 15(1): 197–98 (June 1972).

Lorenz, R. A., D. O. Hobson, and G. W. Parker, "Fuel Rod Failure under Loss-of-Coolant Conditions in TREAT," *Nucl. Technol.* 11(4): 502–20 (August 1971).

Lotts, A. L., *National HTGR Fuel Recycle Development Program Plan,* ORNL-4702 (August 1971).

Lotts, A. L., J. D. Sease, and R. G. Wymer, "HTGR Fuel Refabrication Development," (Summary) *Trans. Amer. Nucl. Soc.* 15(1): 187–88 (June 1972).

Lubell, M. S., and D. M. Kroeger, "Evidence to Support the Rigidly Pinned Vortex Model for the Peak Effect," pp. 394–98 in *Superconductivity* (Proc. Intern. Conf. Science of Superconductivity, Stanford University, August 1969), ed. by F. Chilton, North Holland Publishing Company, Amsterdam, Netherlands, 1971; also in special issue of the journal *Physica* 55: 394–98 (October 1971).

Martin, M. M., and R. G. Donnelly, "Fabrication of Helium Permeable Cermets for Application to Curium Fuels," (Summary) *Trans. Amer. Nucl. Soc.* 14(2): 576–77 (October 1971).

Martin, M. M., A. E. Richt, and W. R. Martin, "Irradiation Performance of Aluminum-Base Dispersion-Type Fuel Plates," (Summary) *Trans. Amer. Nucl. Soc.* 14(2): 567–68 (October 1971).

McClung, R. W., *Remote Inspection of Welded Joints,* ORNL-TM-3561 (September 1971).

McClung, R. W., "Nondestructive Monitoring for Optimization of In-Service Performance Tests," *Mater. Res. Stand.* 12(6): 11–16 (June 1972).

McCoy, H. E., and R. E. Gehlbach, "Influence of Zirconium Additions on the Mechanical Properties of a Ni-Mo-Cr Alloy in the Irradiated and Unirradiated Conditions," *J. Nucl. Mater.* 40(2): 151–65 (August 1971).

McCoy, H. E., R. E. Gehlbach, and B. McNabb, "Development of New Nickel-Base Alloys for High-Temperature Service," pp. 245–58 in *Space Shuttle Materials,* Vol. 3 (Nat. SAMPE Tech. Conf. Huntsville, Ala., October 1971) Society of Aerospace Material and Process Engineers, Azusa, California, 1971.

McElroy, D. L., T. G. Kollie, W. M. Ewing, R. S. Graves, and R. M. Steele, *Room Temperature Measurements of Electrical Resistivity and Thermal Conductivity of Various Graphites,* ORNL-TM-3477 (July 1971).

Meyer, A., G. M. Stocks, and W. H. Young, "Knight Shifts of the Alakli Metals," pp. 651–58 in *Electronic Density of States, Nat. Bur. Stand. (U.S.) Spec. Publ. 323,* ed. by L. H. Bennett, U.S. National Bureau of Standards, Special Publications, Washington, D.C., December 1971.

Miller, J. L., Jr., "Replication of Irradiated Materials for Electron Microscopy," pp. 322–35 in *Technical Papers of the 22nd Metallographic Group Meeting, held June 19–21, 1968, Gulf General Atomic, Inc., San Diego, California,* CONF-680614 (December 1971).

Moore, J. P., T. G. Kollie, R. S. Graves, and D. L. McElroy, "Thermal Transport Properties of Ordered and Disordered Ni_3Fe," *J. Appl. Phys.* 42(8): 3114–20 (July 1971).

Moorhead, A. J., and G. M. Slaughter, "Welding of a Molybdenum Test Stand for Chemical Processing," (Summary) *Trans. Amer. Nucl. Soc.* 15(1): 227 (June 1972).

Morgan, C. S., "Observation of Dislocations in High-Temperature Sintering," *High Temp.–High Pressure* 3: 317–24 (December 1971).

Morgan, C. S., "Mechanistic Interpretation of Non-Steady State Sintering," pp. 231–40 in *Modern Developments in Powder Metallurgy,* Vol. 4, ed. by H. H. Hausner, Plenum Press, New York, 1971.

Oetting, F. L., and J. M. Leitnaker, "The Chemical Thermodynamic Properties of Nuclear Materials. I. Uranium Mononitride," *J. Chem. Thermodynamics* 4(2): 199–211 (February 1972).

Ohr, S. M., A. Wolfenden, and T. S. Noggle, "Electron Displacement Damage in Graphite and Aluminum," pp. 964–73 in *Electron Microscopy and Structure of Materials* (Proc. 5th Int. Materials Symp., Berkeley, Sept. 13–17, 1971), ed. by Gareth Thomas, R. M. Fulrath, and R. M. Fisher, University of California Press, Berkeley, 1972.

Olsen, A. R., "High-Burnup Irradiation Tests of Sphere-Pac Sol-Gel Fuels," (Summary) *Trans. Amer. Nucl. Soc.* 15(1): 181–82 (June 1972).

Olsen, A. R., R. B. Fitts, and W. J. Lackey, *In-Reactor Restructuring Temperature and Kinetics for $(U,Pu)O_2$,* ORNL-TM-3387 (July 1971); also pp. 579–602 in *Proc. Conf. Fast Reactor Fuel Element Technology,* ed. by Ruth Farmakes, American Nuclear Society, Hinsdale, Illinois, 1971.

Olsen, A. R., "Sol-Gel Sphere-Pac $(U,Pu)O_2$ Fuel Performance in EBR-II Irradiation Tests," (Summary) *Trans. Amer. Nucl. Soc.* 14(2): 596–98 (October 1971).

Olsen, A. R. et al., *Preirradiation Data for ORNL Series II and B & W Oxide Fuel Tests in EBR-II,* ORNL-TM-3446 (November 1971).

Packan, N. H., "Fluence and Flux Dependence of Void Formation in Pure Aluminum," *J. Nucl. Mater.* 40(1): 1–16 (July 1971).

Packan, N. H., "The Effect of Neutron Dose on Void Formation in High Purity Aluminum," pp. 71–78 in *Voids Formed by Irradiation of Reactor Materials* (Proc. British Nuclear Energy Society European Conf., Reading Univ., 24 and 25 March 1971), ed. by S. F. Pugh, M. H. Loretto, and D. I. R. Norris, The British Nuclear Energy Society, London, 1971.

Painter, G. S., D. E. Ellis, and A. R. Lubinsky, "*Ab Initio* Calculation of the Electronic Structure and Optical Properties of Diamond Using the Discrete Variational Method," *Phys. Rev.* 4(10): 3610–22 (November 1971).

Painter, G. S., "Application of Discrete Variational Method to the Electronic Structure of LiF," *Int. J. Quantum Chem.* 5(Symp. 5): 501–13 (December 1971).

Painter, G. S., and D. E. Ellis, "Discrete Variational Method for the Energy Band Problem with LCAO Basis and Non-Spherical Local Potential," pp. 276–83 in *Computational Methods in Band Theory,* ed. by P. M. Marcus, J. F. Janak, and A. R. Williams, Plenum Press, New York, 1971.

Patriarca, P., *Fuels and Materials Development Program Quart. Progr. Rep. June 30, 1971,* ORNL-TM-3540.

Patriarca, P., *Fuels and Materials Development Program Quart. Progr. Rep. Sept. 30, 1971,* ORNL-TM-3550.

Patriarca, P., *Fuels and Materials Development Program Quart. Progr. Rep. Dec. 31, 1971,* ORNL-TM-3703.

Patriarca, P., *Fuels and Materials Development Program Quart. Progr. Rep. Mar. 31, 1972,* ORNL-TM-3797.

Pawel, R. E., and J. V. Cathcart, "Flexure Measurement on a U-Nb-Zr Alloy during Oxidation and Temperature Cycling," *J. Electrochem. Soc.* 118(11): 1776–81 (November 1971).

Pawel, R. E., J. P. Pemsler, and C. A. Evans, Jr., "Impurity Distributions in Anodic Films on Tantalum," *J. Electrochem. Soc.* 119(1): 24–29 (January 1972).

Reynolds, R. W., L. A. Boatner, C. B. Finch, A. Chatelain, and M. M. Abraham, "EPR Investigations of Er^{3+}, Yb^{3+}, and Gd^{3+} in Zircon-Structure Silicates," *J. Chem. Phys.* 56(11): 5607–25 (June 1972).

Richt, A. E., R. W. Knight, and G. M. Adamson, Jr., *Postirradiation Examination and Evaluation of the Performance of HFIR Fuel Elements,* ORNL-4714 (December 1971).

Richt, A. E., and V. O. Haynes, *Inspection of Europium-Bearing Control Rod Absorber OM-2 from Core II and Core III of the Army SM-1A Stationary Medium Power Reactor,* ORNL-TM-3647 (April 1972).

Rittenhouse, P. L., and R. A. Dean, "Preface: Symposium on Fuel Rod Failure and Its Effects," *Nucl. Technol.* 11(4): 473 (August 1971).

Rittenhouse, P. L., "Fuel Rod Failure and Its Effect in Light-Water Reactor Accidents," *Nucl. Safety* 12(5): 487–95 (September–October 1971).

Rittenhouse, P. L., D. O. Hobson, and R. D. Waddell, Jr., *The Effect of Light-Water Reactor Fuel Rod Failure on the Area Available for Emergency Coolant Flow Following A Loss-of-Coolant Accident,* ORNL-4752 (January 1972).

Rosenthal, M. W., P. N. Haubenreich, H. E. McCoy, and L. E. McNeese, "Recent Progress in Molten-Salt Reactor Development," *At. Energy Rev.* 9(3): 601–50 (September 1971).

Sass, S. L., and Bernard Borie, *The Symmetry of the Structure of the Omega Phase in Zr and Ti Alloys,* The Materials Science Center Report 1729, Cornell University, Ithaca, New York, January 19, 1972.

Scott, J. L., J. H. Coobs, R. L. Hamner, and J M Robbins, "Development of Bonding Materials for HTGR Fuel Elements," (Summary) *Trans. Amer. Nucl. Soc.* 14(2): 566 (October 1971).

Scott, J. L., J. A. Conlin, J. H. Coobs, D. M. Hewette II, J M Robbins, R. L. Senn, and B. H. Montgomery, *An Irradiation Test of Bonded HTGR Coated Particle Fuels in an Instrumented Capsule in HFIR,* ORNL-TM-3640 (March 1972).

Sease, J. D., C. F. Sanders, W. P. Eatherly, D. P. Harmon, and W. J. Scheffel, "Fabrication of Plutonium Fuels for HTGR," (Summary) *Trans. Amer. Nucl. Soc.* 15(1): 190 (June 1972).

Senn, R. L., J. A. Conlin, and R. B. Fitts, "An Improved Capsule Design for Experimental Measurement of Fuel-Cladding Mechanical Interaction," (Summary) *Trans. Amer. Nucl. Soc.* 15(1): 218–19 (June 1972).

Sessions, C. E., and E. E. Stansbury, *Comparison of the Thermal Stability of Titanium-Modified Hastelloy N at 650 and 760°C,* ORNL-TM-3321 (July 1971).

Sessions, C. E., and H. E. McCoy, "Effect of Carbon on Irradiation Damage in Titanium-Modified-Modified Hastelloy N," (Summary) *Trans. Amer. Nucl. Soc.* 14(2): 602–03 (October 1971).

Slaughter, G. M., and D. A. Canonico, "Welding and Brazing Filler Metals," *Nucl. Eng. Des.* 17(2): 181–203 (October 1971).

Slaughter, G. M., J. H. DeVan, and R. H. Jones, "Post-test Examination of the LMEC Alco/BLH Steam Generator," (Summary) *Trans. Amer. Nucl. Soc.* 14(2): 787–88 (October 1971).

Slaughter, G. M., and J. H. DeVan, *Interim Information Report on Posttest Examination of Alco/BLH Sodium-Heated Steam Generator,* ORNL-TM-3636 (May 1972).

Slaughter, G. M., D. A. Canonico, and R. G. Donnelly, "Welding and Brazing of Advanced Refractory Alloys," pp. 317–22 in *Space Shuttle Materials,* Vol. 3, (Nat. SAMPE Tech. Conf., Huntsville, Ala., October 1971) Society of Aerospace Materials and Process Engineers, Azusa, California, 1971.

Slaughter, G. M., "Brazing," pp. 60.88–60.103 in *Welding Handbook,* 6th ed., Sect. 3B, ed. by Len Griffing, American Welding Society, New York, 1971.

Spindler, Peter, *Depth of Transmittance of Radially Emitted Radiation into a Cylindrically Shaped Solid with Application to Lithium Fluoride,* ORNL-TM-3660 (June 1972).

Stephenson, R. L., "Application of the Larson-Miller Parameter to Niobium-Base Alloys," pp. 279–86 in *Space Shuttle Materials,* Vol. 3, (Nat. SAMPE Tech. Conf., Huntsville, Ala., October 1971) Society of Aerospace Material and Process Engineers, Azusa, California, 1971.

Stiegler, J. O., *Void Formation in Neutron Irradiated Metals,* ORNL-TM-3495 (September 1971); also pp. 292–337 in *Radiation-Induced Voids in Metals* (Proc. Int. Conf., Albany, N.Y., June 9–11, 1971), ed. by J. W. Corbett and L. C. Ianniello, AEC Symp. Ser. 26, CONF-710601 (April 1972).

Stiegler, J. O., *A Study of the Formation of Creep Cavities in Powder-Metallurgy Tungsten,* ORNL-TM-3350 (September 1971). Ph.D. Thesis, the University of Tennessee, June 1971.

Stiegler, J. O., and E. E. Bloom, "The Effect of Thermo-Mechanical Treatments on Void Formation in Irradiated Stainless Steel," *J. Nucl. Mater.* 41(3): 341–44 (December 1971)

Stocks, G. M., R. W. Williams, and J. S. Faulkner, "Densities of States of Paramagnetic Cu-Ni Alloys," *Phys. Rev. B* 4(12): 4390–4405 (December 1971).

Stocks, G. M., "Electronic States in Some Disordered Noble Metal-Transition Metal Alloys," *Int. J. Quantum Chem.* 5(Symp. 5): 533–41 (December 1971).

Task Group: S. D. Harkness, J. Chow, G. L. Kulcinski, J. Moteff, and F. W. Wiffen, "Radiation Damage," pp. 85–91 in *Fusion Reactor First Wall Materials* (Summary of a Meeting Held at AEC-Germantown, January 1972), WASH-1206 (April 1972).

Task Group: W. D. Nix, J. H. DeVan, F. W. Wiffen, et al., "Summary of Priorities: Emphasis on Problems for Pulsed-Type," pp. 110–13 in *Fusion Reactor First Wall Materials* (Summary of a Meeting Held at AEC-Germantown, January 1972), WASH-1206 (April 1972).

Tennery, V. J., T. G. Godfrey, and R. A. Potter, "Sintering of UN as a Function of Temperature and N_2 Pressure," *J. Amer. Ceram. Soc.* 54(7): 327–31 (July 1971).

Tennery, V. J., and J. L. Botts, "The Chemical Characterization of Uranium Nitrides," *Nucl. Technol.* 13(3): 264–72 (March 1972).

Tennery, V. J., T. N. Washburn, and J. L. Scott, "Fabrication and Irradiation Behavior of Uranium Mononitride," pp. 587–600 in *Ceramics in Severe Environments, Materials Science Research,* Vol. 5, ed. by W. Wurth Kriegel and Hayne Palmour III, Plenum Press, New York, 1971.

Tolson, G. M., L. C. Williams, E. A. Franco-Ferreira, and E. C. Kirstowsky, "Brazing and Shell Assembly for the BONUS Superheater Fuel Element," *Weld. J. (Miami)* 50(9): 641–46 (September 1971).

Waddell, R. D., Jr., "Measurement of Light-Water Reactor Coolant Channel Reduction Arising from Cladding Deformation During a Loss-of-Coolant Accident," *Nucl. Technol.* 11(4): 491–501 (August 1971).

Ward, A. L., J. E. Irvin, L. D. Blackburn, G. M. Slaughter, G. M. Goodwin, and N. C. Cole, *Preparation, Characterization, and Testing of Austenitic Stainless Steel Weldments,* HEDL-TME 71–118 (August 1971).

Washburn, T. N., and J. L. Scott, "Performance Capability of Advanced Fuels for Fast Breeder Reactors," pp. 741–52 in *Proc. Conf. Fast Reactor Fuel Element Technology,* ed. by Ruth Farmakes, American Nuclear Society, Hinsdale, Illinois, 1971.

Werner, W. J., G. M. Slaughter, and F. B. Gurtner, "Development of Filler Metals and Procedures for Vacuum Brazing of Aluminum," *Weld. J. (Miami)* 51(2): 64-s–70-s (February 1972).

Whaley, H. L., and Laszlo Adler, "Flaw Characterization by Ultrasonic Frequency Analysis," *Mater. Eval.* 29(8): 182–88 (August 1971).

Whaley, H. L., and Laszlo Adler, "Determining the Size of Flaws in Materials," *Instrum. Contr. Syst.* 44(10): 98–102 (October 1971).

Whaley, H. L., and Laszlo Adler, "A New Approach to the Old Problem of Determining Flaw Size," *Int. J. Fract. Mech.* 8(1): 112–13 (March 1972).

Wiffen, F. W., "Radiation Damage in CTR's," pp. 140–74 in *Proc. Int. Working Session on Fusion Reactor Technology* (June 28–July 2, 1971, Oak Ridge National Laboratory), CONF-710624.

Wiffin, F. W., "Radiation Damage," pp. 208–21 in *Proc. Int. Working Session on Fusion Reactor Technology* (June 28–July 2, 1971, Oak Ridge National Laboratory), CONF-710624.

Wiffen, F. W., *The Effect of Alloying and Purity on the Formation and Ordering of Voids in BCC Metals,* ORNL-TM-3496 (September 1971); also pp. 386–96 in *Radiation-Induced Voids in Metals* (Proc. Int. Conf., Albany, N.Y., June 9–11, 1971), ed. by J. W. Corbett and L. C. Ianniello, AEC Symp. Ser. 26, CONF-710601 (April 1972).

Wiffen, F. W., "The Effect of Temperature on the Microstructure of Neutron-Irradiated Tantalum," (Summary) *Trans. Amer. Nucl. Soc.* 14(2): 603 (October 1971).

Wiffen, F. W., "Radiation Damage to Refractory Metals as Related to Thermionic Applications," pp. 156–65 in *IEEE Conference Record of 1971 Thermionic Conversion Specialist Conference, October 4–6, 1971,* The Institute of Electrical and Electronics Engineers, New York, 1971. (71 C 63-ED); also ORNL-TM-3629 (February 1972).

Wiffen, F. W., "Radiation Effects on Swelling and Ductility of Fusion Reactor First Wall Materials," pp. 40–43 in *Fusion Reactor First Wall Materials* (Summary of a Meeting Held at AEC-Germantown, January 1972), WASH-1206 (April 1972).

Williams, J. M., N. E. Hinkle, and W. P. Eatherly, "Effect of Neutron Irradiation at 110°K on Thermal Conductivity of Beryllium," (Summary) *Trans. Amer. Nucl. Soc.* 14(2): 606–7 (October 1971).

Williams, R. K., Manoo Veeraburus, and W. O. Philbrook, "Thermal Conductivities of Some Ni-S, Ag-S, and Ag-Te Melts," *Met. Trans.* 3(1): 255–58 (January 1972).

Williams, R. O., "Discussion to 'Mössbauer Effect Study of the 475°C Decomposition of Fe-Cr' by D. Chandra and L. H. Schwartz," *Met. Trans.* 2(8): 2294 (August 1971).

Williams, R. W., and H. L. Davis, "Adjustment of Calculated Band Structures for Calcium by Use of Low-Temperature Specific Heat Data," pp. 57–62 in *Electronic Density of States, Nat. Bur. Stand. (U.S.) Spec. Publ. 323,* ed. by L. H. Bennett, U.S. National Bureau of Standards, Special Publications, Washington, D.C., December 1971.

Wolfenden, A., "The Effects of Electron Irradiation on Pre-Existing Defects in Aluminum," *Jernkont. Ann.* 155(8): 533–34 (August 1971).

Wolfenden, A., "Effects of Preinjected Hydrogen on the Electron Displacement Damage in 1100 Aluminum," *J. Nucl. Mater.* 40(3): 351–52 (September 1971).

Wolfenden, A., "The Energy Stored in Polycrystalline Copper Deformed at Room Temperature," *Acta Met.* 19(12): 1373–77 (December 1971).

Wolfenden, A., "Electron Irradiation Damage in Aluminum Near the Threshold Energy," (Summary) *Trans. Amer. Nucl. Soc.* 15(1): 246 (June 1972).

Wolfenden, A., and K. Farrell, "On the Question of Void Formation in Neutron Irradiated Zirconium," *Scripta Met.* 6(2): 127–30 (February 1972).

Wolfenden, A., "The Effects of Different Microstructure on the Formation of Dislocation Loops in Aluminum during Electron Irradiation," *Micron* 3(1): 51–61 (1972).

Wolfenden, A., K. Farrell, and J. O. Stiegler, "The Role of Electron Microscopy in the Understanding of Neutron Irradiation-Produced Swelling," pp. 984–95 in *Electron Microscopy and Structure of Materials* (Proc. 5th Int. Materials Symp., Berkeley, Sept. 13–17, 1971), ed. by Gareth Thomas, R. M. Fulrath, and R. M. Fisher, University of California Press, Berkeley, 1972.

Yoo, M. H., and B. T. M. Loh, *Numerical Calculation of Elastic Properties for Straight Dislocations in Anisotropic Crystals,* ORNL-TM-3408 (July 1971).

Yoo, M. H., and B. T. M. Loh, "Displacement Fields of Straight Dislocations in Anisotropic Crystals," *J. Appl. Phys.* 43(4): 1373–79 (April 1972).

Yust, C. S., and C. J. McHargue, "Deformation of Hyperstoichiometric UO_2 Single Crystals," *J. Amer. Ceram. Soc.* 54(12): 628–35 (December 1971).

PATENTS

Beatty, R. L., and D. V. Kiplinger, *Pulsed Method for Impregnation of Graphite* (to U.S. Atomic Energy Commission) U.S. Patent 3,664,859. May 23, 1972.

Canonico, D. A., N. C. Cole, and C. W. Houck, *Method for Brazing Graphite and Other Refractory Materials* (to U.S. Atomic Energy Commission) U.S. Patent 3,673,038. June 27, 1972.

Hammond, J. P., *Dispersion Strengthening of Aluminum Alloys by Reaction of Unstable Oxide Dispersions* (to U.S. Atomic Energy Commission) U.S. Patent 3,607,254. Sept. 21, 1971.

Hammond, J. P., and Ji Young Chang, *Process for Producing Dispersion-Hardened Superalloys by Internal Oxidation* (to U.S. Atomic Energy Commission) U.S. Patent 3,615,381. Oct. 26, 1971.

Whaley, H. L., and Laszlo Adler, *Ultrasonic Flaw Determination by Spectral Analysis* (to U.S. Atomic Energy Commission) U.S. Patent 3,662,589. May 16, 1972.

THESES

Pollock, Charles Bruce, *An Investigation into the Phase Stability in the Systems Iron-Tungsten-Carbon and Cobalt-Tungsten-Carbon,* Ph.D. Thesis, North Carolina State University, May 1972.

Weaver, Samuel Cavin, *An Investigation of the Thermal Conductivity, Electrical Resistivity, and Thermoelectric Power of Thorium Nitride–Uranium Nitride Alloys,* Ph.D. Thesis, the University of Tennessee, March 1972.

Author Index

Abraham, M. M., 2, 3
Adamson, G. M., Jr., 146
Adler, Laszlo, 93
Allen, M. D., 168
Anderson, J. W., 137
Arsenault, R. J., 35
Ashbee, K. H. G., 16, 18

Banus, M. D., 9
Beaver, R. J., 116
Begun, G. M., 21
Berggren, R. G., 73,113
Bloom, E. E., 79, 82
Boatner, L. A., 3
Bomar, E. S., 39, 151, 154
Borie, B. S., 34
Boston, C. R., 20, 21
Bradley, R. A., 55, 111, 133, 152
Braski, D. N., 11
Brooks, C. R., 17
Brunton, G. D., 4
Brynestad, J., 20, 21
Buhl, R. A., 58, 59

Campbell, J. J., 31
Canonico, D. A., 75, 76, 77, 113, 171
Carlson, P. T., 8, 9, 10
Carpenter, R. W., 6, 7, 28, 101
Cathcart, J. V., 30
Cavin, O. B., 125, 129
Chandler, J. M., 130
Chapman, A. T., 20
Chatelain, A., 3
Cheng, C. C., 93
Clark, G. W., 1, 2, 3, 4, 20
Clausing, R. E., 175, 176
Coghlan, W. A., 5, 22, 29
Cole, N. C., 73, 128
Conlin, J. A., 110
Coobs, J. H., 106, 110
Cook, K. V., 70, 71, 91, 92, 93
Cook, S. W., 121
Cook, W. H., 124, 125
Copeland, G. L., 17, 49
Crouse, R. S., 159
Cuneo, D. R., 148, 157
Cunningham, G. W., 67

Davis, F. C., 136
Deeds, W. E., 93
DeVan, J. H., 40, 141, 172
Dippennaar, R. J., 27
DiStefano, J. R., 127
Dodd, C. V., 92, 93, 145
Donnelly, R. G., 47, 96, 100, 146
DuBose, C. K. H., 15, 17, 47, 49
Dyslin, D. A., 53

Easton, D. S., 175, 176
Eatherly, W. P., 108, 124, 125, 126, 156
Edelstein, N., 2
Ellis, D. E., 33
Erwin, J. H., 97
Evans, C. A., Jr., 31
Ewing, W. M., 26, 27, 109

Fahr, D., 82
Farrell, K., 11, 12, 13, 14, 15, 141
Faulkner, J. S., 32
Federer, J. I., 102
Ferguson, J. E., 14
Finch, C. B., 2, 3, 4
Fitts, R. B., 58, 66, 110, 111, 138
Fitzpatrick, C. M., 154
Fleischer, B., 58, 98
Foster, B. E., 91, 95
Fung, K. W., 21

Gaddis, H. R., 167, 170
Gardner, W. E., 28
Gaspari, G. D., 32
Gedcke, Dale A., 35

Gehlbach, R. E., 17, 119, 121
Godfrey, T. G., 25, 27, 155
Goodwin, G. M., 73, 74
Graves, R. S., 26, 27, 109, 145
Gray, R. J., 157, 163, 165, 170, 171
Griffith, J. L., 125, 129
Gyorffy, B. L., 32

Hammond, J. P., 42, 149
Hamner, R. L., 108
Harris, L. A., 3, 4, 36
Hendricks, R. W., 37
Henson, T. J., 159
Hewette, D. M. II, 110, 151
Hill, Meredith R., 186
Homan, F. J., 50, 55, 56, 61, 65, 68, 138
Houston, J. T., 11
Hudson, J. D., 113
Hulett, L. D., 20

Inouye, H., 96, 97, 100, 101, 103

Jeffers, Brenda S., 178
Jenkins, J. D., 67
Jostsons, A., 11, 13, 14, 15, 47, 49, 148

Kegley, T. M., Jr., 167, 168
Kennedy, C. R., 126, 156
King, R. T., 11, 14, 70, 71, 74, 148
Klueh, R. L., 88
Knight, R. W., 100, 146, 147
Koch, C. C., 28, 29
Koger, J. W., 118, 122
Kolbe, W., 3
Kollie, T. G., 26, 27, 126
Kopp, O. C., 4
Kroeger, D. M., 28, 29

Lackey, W. J., 65, 131
Leitnaker, J. M., 17, 56, 68, 69, 154
Leslie, B. C., 167, 170
Lindemer, T. B., 107
Liu, C. T., 96, 97, 100, 101
Loh, B. T. M., 5, 15, 16, 18
Long, E. L., Jr., 11, 13, 14, 100, 172
Longest, A. W., 111
Lotts, A. L., 55, 130, 137, 142, 151, 154
Lubinsky, A. R., 33
Lundy, T. S., 9, 10

Mamantov, G., 21
Manley, L C, Jr., 9
Manthos, E. J., 38, 53, 111
Martin, M. M., 53, 146
Martin, W. R., 47, 70, 79, 86, 146
Mateer, H. V., 159
McClung, R. W., 91
McCollough, W. L., 103
McCollum, B. W., 129
McCoy, H. E., Jr., 79, 86, 100, 102, 103, 117, 118, 119 120, 121, 123
McDonald, R. E., 102, 127
McElroy, D. L., 25, 109
McHargue, C. J., 19, 20, 140
McNabb, B., Jr., 117, 118, 119, 121, 123
Miller, F. L., 66
Montgomery, B. H., 110
Moore, J. P. 25, 26, 27, 126
Moorhead, A. J., 127, 128
Mortimer, W. J., 28

Nestor, C. W., 93
Noggle, T. S., 12
Nordwall, H. J. de, 107

Ogle, J. C., 22
Ohr, S. M., 5, 12
Oliver, B. F., 1
Olsen, A. R., 56, 58, 59, 65, 138, 139

Padgett, R. A., 8, 9
Painter, G. S., 33
Papatheodorou, G. N., 21
Patriarca, P., 40
Pawel, R. E., 30, 31
Pechin, W. H., 131, 152
Pemsler, J. P., 31
Perkins, R. A., 8
Petersen, G. F., 30
Pollock, C. B., 106, 110, 124, 151
Potter, R. A., 20, 99
Predmore, R. E., 35

Reimann, G. A., 70, 71
Reynolds, R. W., 3
Richt, A. E., 146, 147
Robbins, J M, 108

Sanders, C. F., 133, 151, 152
Scarboro, Frances A., 178
Scarbrough, J. O., 29
Schaffhauser, A. C., 70, 102, 103, 127
Scott, J. L., 38, 98, 110, 154
Sease, J. D., 55, 131, 136, 137, 151

Senn, R. L., 58
Shaffer, J. H., 118
Silverman, M. D., 106
Simpson, W. A., Jr., 92, 93, 145
Slaughter, G. M., 40, 42, 73, 149
Smith, G. P., 19, 20, 21
Smith, J. H., 93
Smith, M. L., 154
Snyder, S. D., 95
Sparks, C. J., Jr., 35, 36
Spear, K. E., 69
Spriuell, J. E., 17
Steele, R. M., 34
Stelzman, W. J., 113, 114
Stiegler, J. O., 11, 12, 17, 74, 79, 82, 102, 141
Stocks, G. M., 32
Swindeman, R. W., 86

Tennery, V. J., 99
Thoms, K. R., 98
Trotter, L. R., 129
Tunali, N. K., 8

Van Cleve, J. E., 142, 143, 144
Vandermeer, R. A., 22, 23, 24

Waddell, R. D., Jr., 87
Washburn, T. N., 38, 53, 56, 98
Weir, J. R., Jr., 40, 117
Whaley, H. L., 92, 93
Wiffen, F. W., 52, 105, 140
Williams, L. C., 142, 143, 144
Williams, R. K., 26, 105, 145
Williams, R. O., 5, 6
Williams, R. W., 32
Wilson, J. C., 1, 2, 142, 143, 144
Wolfenden, A., 11, 12, 13, 15, 16, 17, 141
Woods, J. W., 53
Wymer, R. G., 151

Yakel, H. L., 3, 34, 36, 49
Yoo, M. H., 5, 22
Yust, C. S., 19, 20

METALS AND CERAMICS DIVISION

August 15, 1972

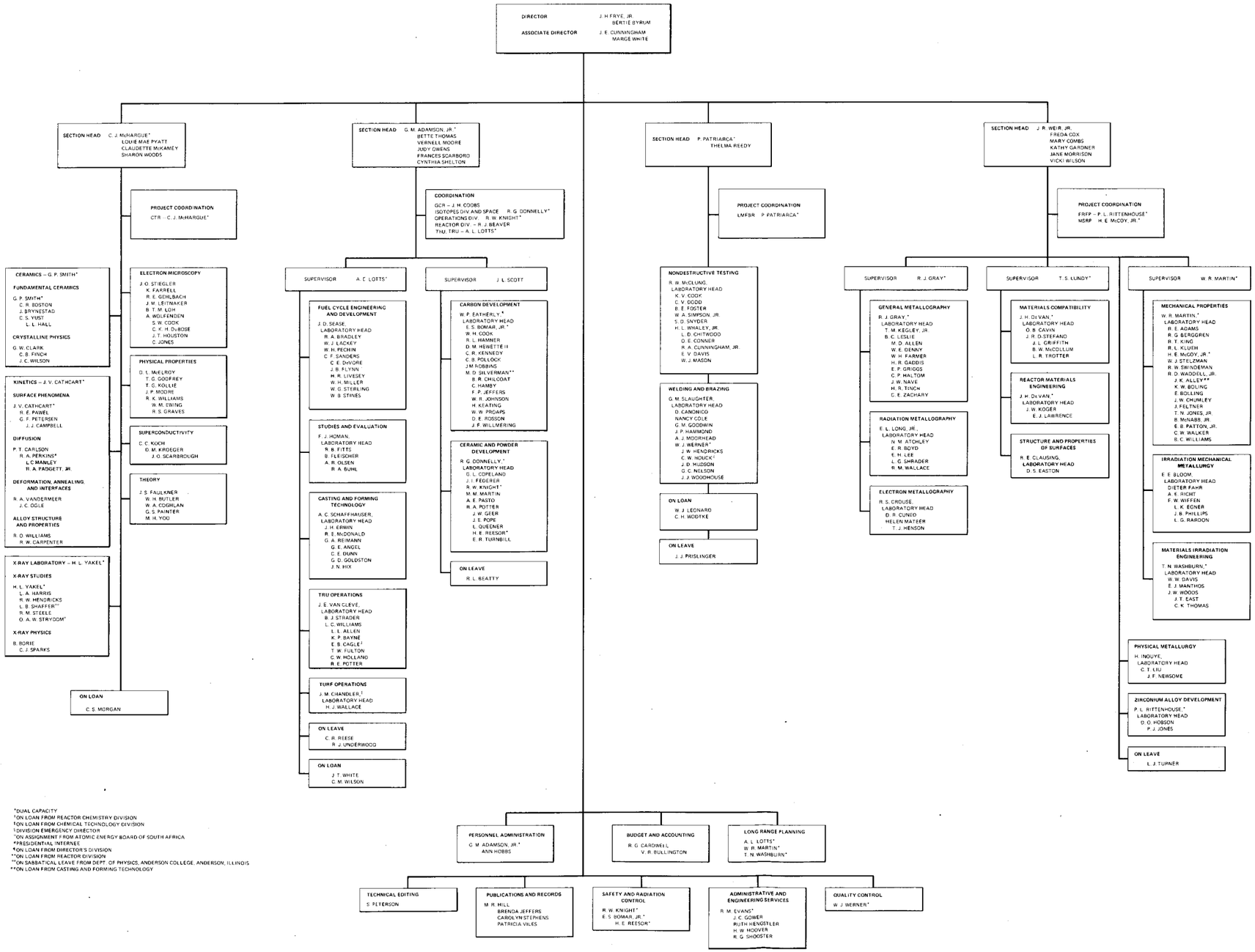

*DUAL CAPACITY
†ON LOAN FROM REACTOR CHEMISTRY DIVISION
‡ON LOAN FROM CHEMICAL TECHNOLOGY DIVISION
§DIVISION EMERGENCY DIRECTOR
¶ON ASSIGNMENT FROM ATOMIC ENERGY BOARD OF SOUTH AFRICA
#PRESIDENTIAL INTERNEE
¶ON LOAN FROM DIRECTOR'S DIVISION
**ON LOAN FROM REACTOR DIVISION
***ON SABBATICAL LEAVE FROM DEPT. OF PHYSICS, ANDERSON COLLEGE, ANDERSON, ILLINOIS
**ON LOAN FROM CASTING AND FORMING TECHNOLOGY

INTERNAL DISTRIBUTION

1–2. Central Research Library
3–4. ORNL – Y-12 Technical Library
Document Reference Section
5–59. Laboratory Records Department
60. Laboratory Records, ORNL R.C.
61. MIT Practice School
62. ORNL Patent Office
63. Laboratory Shift Supervisor
64. R. E. Adams
65. G. M. Adamson, Jr.
66. H. I. Adler
67. S. I. Auerbach
68. R. L. Beatty
69. S. E. Beall
70. R. J. Beaver
71. M. Bender
72. L. L. Bennett
73. R. G. Berggren
74. D. S. Billington
75. E. E. Bloom
76. E. S. Bomar
77. A. L. Boch
78. B. S. Borie
79. C. J. Borkowski
80. C. R. Boston
81. G. E. Boyd
82. R. A. Bradley
83. R. B. Briggs
84. W. E. Browning, Jr.
85. J. Brynestad
86. F. R. Bruce
87. W. H. Butler
88. D. A. Canonico
89. P. T. Carlson
90. R. W. Carpenter
91. J. M. Case (Y-12)
92. J. V. Cathcart
93. O. B. Cavin
94. J. M. Chandler
95. G. W. Clark
96. R. E. Clausing
97. W. A. Coghlan
98. N. C. Cole
99. W. C. Colwell
100. J. H. Coobs
101. K. V. Cook
102. W. H. Cook
103. G. L. Copeland
104. W. B. Cottrell
105. J. A. Cox
106. R. S. Crouse
107. F. L. Culler
108. J. E. Cunningham
109. W. W. Davis
110. J. H. DeVan
111. J. R. DiStefano
112. C. V. Dodd
113. R. G. Donnelly
114. D. S. Easton
115. J. H. Erwin
116. W. P. Eatherly
117. D. Fahr
118. K. Farrell
119. J. S. Faulkner
120. J. I. Federer
121. D. E. Ferguson
122. C. B. Finch
123. R. B. Fitts
124. B. Fleischer
125. B. E. Foster
126. A. P. Fraas
127. J. H Frye, Jr.
128. W. Fulkerson
129. R. E. Gehlbach
130. J. H. Gillette
131. T. G. Godfrey
132. G. M. Goodwin
133. R. J. Gray
134. Bill L. Greenstreet
135. W. R. Grimes
136. J. P. Hammond
137. R. L. Hamner
138. W. O. Harms
139. C. S. Harrill
140. L. A. Harris
141. R. F. Hibbs
142–156. M. R. Hill
157. R. W. Hendricks
158. D. M. Hewette II
159. D. O. Hobson
160. F. J. Homan
161. A. P. Huber (K-25)

162. H. Inouye
163. H. S. Isaacs
164. R. G. Jordan (K-25)
165. W. H. Jordan
166. P. R. Kasten
167. S. I. Kaplan
168. T. M. Kegley, Jr.
169. M. T. Kelley
170. C. R. Kennedy
171. E. M. King
172. R. T. King
173. R. L. Klueh
174. R. W. Knight
175. C. C. Koch
176. J. W. Koger
177. T. G. Kollie
178. D. M. Kroeger
179. W. J. Lackey
180. J. M. Leitnaker
181. W. J. Leonard
182. B. C. Leslie
183. T. B. Lindemer
184. C. Liu
185. J. L. Liverman
186. R. S. Livingston
187. B. T. M. Loh
188. E. L. Long, Jr.
189. A. L. Lotts
190. T. S. Lundy
191. E. J. Manthos
192. M. M. Martin
193. W. R. Martin
194. H. V. Mateer
195. R. W. McClung
196. H. E. McCoy
197. H. C. McCurdy
198. R. E. McDonald
199. H. F. McDuffie
200. D. L. McElroy
201. C. J. McHargue
202. J. P. Moore
203. A. J. Moorhead
204. C. S. Morgan
205. R. A. McNees
206. F. H. Neill
207. L. C. Oakes
208. J. C. Ogle
209. A. R. Olsen
210. G. S. Painter
211–212. R. B. Parker
213. A. E. Pasto
214. P. Patriarca
215. R. E. Pawel
216. W. H. Pechin
217. G. F. Petersen
218. S. Peterson
219. C. B. Pollock
220. H. Postma
221. R. A. Potter
222. J. J. Prislinger
223. G. A. Reimann
224. A. E. Richt
225. P. L. Rittenhouse
226. J M Robbins
227. M. W. Rosenthal
228. C. F. Sanders
229. A. C. Schaffhauser
230. J. L. Scott
231. H. E. Seagren
232. J. D. Sease
233. S. Siegel
234. M. D. Silverman
235. W. A. Simpson, Jr.
236. G. M. Slaughter
237. G. P. Smith, Jr.
238. A. H. Snell
239. S. D. Snyder
240. C. J. Sparks, Jr.
241. R. M. Steele
242. D. Steiner
243. W. J. Stelzman
244. J. O. Stiegler
245. G. M. Stocks
246. O. A. Strydom
247. D. A. Sundberg
248. R. W. Swindeman
249. D. B. Trauger
250. J. E. VanCleve, Jr.
251. R. A. Vandermeer
252. P. R. Vanstrum (Y-12)
253. R. D. Waddell, Jr.
254. T. N. Washburn
255. A. M. Weinberg
256. J. R. Weir, Jr.
257. W. J. Werner
258. H. L. Whaley
259. G. D. Whitman
260. F. W. Wiffen
261. R. K. Williams
262. R. O. Williams
263. J. C. Wilson
264. C. H. Wodtke
265. A. Wolfenden
266. J. W. Woods

267. H. L. Yakel, Jr.
268. M. H. Yoo
269. F. W. Young, Jr.
270. C. S. Yust
271. Walter Kohn (consultant)
272. G. V. Smith (consultant)
273. W. S. Williams (consultant)

EXTERNAL DISTRIBUTION

274. J. J. Flaherty, Assistant General Manager for Energy and Development Programs, AEC, Washington, DC 20545

275–279. Executive Secretary, Advisory Committee on Reactor Safeguards, AEC, Washington, DC 20545

Division of Applied Technology, AEC, Washington, DC 20545
280. G. W. Johnson, Director
281. E. E. Fowler
282. J. C. Bresee

Division of Controlled Thermonuclear Research, AEC, Washington, DC 20545
283. R. W. Hirsch, Director
284. W. C. Gough

Division of Military Applications, AEC, Washington, DC 20545
285. Major General Edward B. Giller (USAF), Director

Division of Naval Reactors, AEC Washington, DC 20545
286. R. H. Steele

Division of Physical Research, AEC, Washington, DC 20545
287. D. R. Miller, Acting Director
288. L. C. Ianniello
289. Dorothy Smith
290. D. K. Stevens

Division of Reactor Development and Technology, AEC, Washington, DC 20545
291. M. Shaw, Director
292. G. M. Anderson
293. LTC H. L. Arnold
294. M. Booth
295. J. W. Crawford, Jr.
296. G. W. Cunningham
297. R. P. Denise
298. M. D. Dubrow
299. A. P. D'Zmura
300. N. Grossman
301. P. A. Halpine
302. W. H. Hannum
303. P. L. Havenstein
304. K. E. Horton
305. J. R. Hunter
306. E. E. Kintner
307. R. E. Kosiba
308. E. C. Kovacic
309. W. H. Layman
310. J. E. McEwen

311. T. W. McIntosh
312. W. H. McVey
313. J. J. Morabito
314. E. C. Norman
315. R. E. Pahler
316. D. Pollock
317. A. J. Pressesky
318. D. R. Riley
319. M. A. Rosen
320. F. A. Ross
321–324. J. M. Simmons
325. E. E. Sinclair
326. J. F. Smith, Jr.
327. S. A. Szawlewicz
328. A. N. Tardiff
329. C. E. Weber
330. G. W. Wensch
331. M. J. Whitman
332. W. A. Williams, Jr.
333. J. G. Yevick

Division of Regulation, AEC, Washington, DC 20545

334. L. Manning Muntzing, Director
335. Richard Cunningham
336. A. Giambusso
337. Stephen Hanauer
338. J. M. Hendrie
339. J. A. Powers
340. L. R. Rogers

Division of Space Nuclear Systems, AEC, Washington, DC 20545

341. D. S. Gabriel, Director
342. R. E. Anderson
343. G. P. Dix
344. H. Jaffe
345. C. E. Johnson, Jr.
346. A. P. Litman
347. J. J. Lombardo
348. G. A. Newby
349. F. C. Schwenk

Division of Waste Management and Transportation, AEC, Washington, DC 20545

350. F. K. Pittman

351. Lazlo Adler, 4206 Taliluna Ave., Knoxville, TN 37919
352. G. M. Ault, NASA, Lewis Res. Center, 21000 Brookpark Rd., Cleveland, OH 44135
353. Lida K. Barrett, 7100 Downing Drive, Knoxville, TN 37919
354. H. R. Bungay, Division of Advanced Technical Applications, National Science Foundation, 1800 G St., NW, Washington, DC 20550
355. H. M. Burte, Chief, Metals and Ceramics Div., Air Force Materials Laboratory, Wright-Patterson AFB, Ohio 45433
356. W. T. Case, Mound Laboratory, P.O. Box 32, Miamisburg, OH 45342
357. A. T. Chapman, School of Ceramic Engineering, Georgia Institute of Technology, Atlanta, GA 30332
358. William Cooper, Teledyne Materials Research Corp., 303 Bare Hill Road, Waltham, MA 02154
359. D. F. Cope, RDT, SSR, AEC, Oak Ridge National Laboratory

360. E. C. Creutz, National Science Foundation, 1800 G St., Washington, DC 20550
361. R. M. Goldhoff, Metallurgy Applied Research, General Electric Company, One River Road, Schenectady, New York 12305
362. Claude Good, U.S. Bureau of Mines, Pittsburgh Mining and Safety Res. Center, 4800 Forbes Ave., Pittsburgh, PA 15213
363. F. B. Gurtner, U.S. Army Edgewood Arsenal, Edgewood Arsenal, MD 21010
364. O. C. Kopp, Department of Geology and Geography, University of Tennessee, Knoxville, TN 37916
365. Jan Korringa, Department of Physics, Ohio State University, 174 West 18th Ave., Columbus, OH 43210
366. Joseph R. Lane, National Materials Advisory Board, National Research Council, 2101 Constitution Avenue, Washington, DC 20418
367. J. J. Lynch, NASA, 1520 H Street, Washington, DC 20546
368. W. D. Manly, Stellite Division, Cabot Corp., 1020 Park Ave., Kokomo, IN 46901
369. Col. Whitfield A. Martin, Air Force Office of Scientific Research, 1400 Wilson Boulevard, Arlington, Virginia 22209
370. C. L. Matthews, RDT, OSR, AEC, Oak Ridge National Laboratory
371. R. R. Nash, NASA, Washington, DC 20546
372. W. J. O'Donnell, President, O'Donnell and Associates, Inc., 5100 Centre Ave., Pittsburgh, PA 15232
373. B. F. Oliver, 4211 Holston Hills Road, Knoxville, TN 37914
374. H. W. Paxton, National Science Foundation, 1800 G Street, Washington, DC 20550
375. N. E. Promisel, National Materials Advisory Board, National Research Council, 2101 Constitution Avenue, Washington, DC 20418
376. David Roberts, Gulf General Atomic, Inc., P.O. Box 608, San Diego, CA 92112
377. Neal Saunders, NASA, Lewis Research Center, 21000 Brookpark Road, Cleveland, OH 44135
378. Chester Sims, Materials Processing Laboratory, General Electric Company, One River Road, Schenectady, NY 12305
379. Richard Slember, Advanced Reactors Division, Westinghouse Electric Corp., P.O. Box 158, Madison, PA 15663
380. J. E. Spruiell, Department of Chemical and Metallurgical Engineering, University of Tennessee, Knoxville, TN 37916
381. E. E. Stansbury, Department of Chemical and Metallurgical Engineering, University of Tennessee, Knoxville, TN 37916
382. J. A. Swartout, Union Carbide Corporation, 270 Park Ave., New York, NY 10017
383. L. Young, Gulf General Atomic, P.O. Box 1111, San Diego, CA 92112
384. Research and Technical Support Division, AEC, ORO
385. Patent Office, AEC, ORO

386–578. Given distribution as shown in TID-4500 under Metals, Ceramics, and Materials category (25 copies – NTIS)